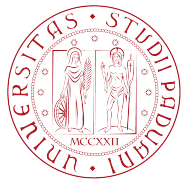

UNIVERSITÀ DEGLI STUDI DI PADOVA

Dipartimento di Fisica e Astronomia "Galileo Galilei"

Ph. D. in Physics

Cycle XXXVI

Gravitational Wave Background Anisotropies: Probing Early and Late Universe Cosmology with Interferometers

Coordinator: Giulio Monaco

Supervisor: Angelo Ricciardone

Co-Supervisor: Sabino Matarrese

Ph. D. student: Lorenzo Valbusa Dall'Armi

Contents

Abstract

With the advent of precision cosmology, it is possible to test in an extremely accurate way a variety of theories which describe the history of our Universe. The *Planck* experiment has been able to detect with high significance the anisotropies of the Cosmic Microwave Background, measuring the parameters that characterize the Standard Model of Cosmology. However, a conclusive proof that inflation took place in the early Universe has not been found yet. The inflationary stochastic background, which would be a decisive evidence of the inflationary epoch, has not been discovered neither by looking at the polarization of the B-modes of the CMB or by a direct detection of a stochastic signal by the LIGO-Virgo-KAGRA collaboration. The recent observation of a stochastic background by the International Pulsar Timing Array collaboration raises the tantalizing hypothesis of a detection of a primordial signal, but the measurement is not precise enough to establish if this signal has a cosmological or astrophysical genesis. Future surveys of gravitational waves will improve the current sensitivities to stochastic backgrounds, therefore it is likely that in the incoming decades stochastic backgrounds will be detected in a very accurate way. Therefore, one one the main goals of theoretical cosmology and astrophysics is the characterization of stochastic backgrounds, in order to analyze properly the future data. Stochastic backgrounds are expected to be dominated by a homogeneous and isotropic contribution and to exhibit tiny anisotropies of the order $10^{-2} - 10^{-5}$. This is consistent with the Cosmological Principle, which states that the Universe is homogeneous and isotropic, when smoothed over sufficiently large scales. In this Thesis, we describe from a theoretical and observational perspective the anisotropies of cosmological and astrophysical background, characterizing their features, like the dependence on the frequency and angular scale considered, and forecasting their detectability.

In this dissertation, we compute the anisotropies of stochastic backgrounds for three sources of primordial gravitational waves: the quantum fluctuations of the metric during inflation, primordial black holes and phase transitions. All these mechanisms produce gravitational waves at energy scales much larger than the ones of particle experiments, therefore, because of the decoupling of gravitational interactions at early times, which makes the Universe transparent to gravitational waves, the cosmological background is a unique probe that keeps track of the physics at temperatures typical of Grand Unified Theories. The angular power spectrum of the cosmological background can be computed by introducing a distribution function for the primordial graviton and solving the Boltzmann equation in our perturbed Universe. The solution of this equation shows that the anisotropies are due

to the initial conditions on the distribution function and to the propagation of the gravitational waves through the large-scale perturbations of the metric encountered along their paths. We evaluate the initial conditions for the background generated by the quantum fluctuations during inflation, finding that a large amount of non-adiabatic initial conditions are present. This peculiar term generates an enhancement of the angular power spectrum by an order of magnitude, making easier the detection with future interferometers. For the case of a cosmological background generated by primordial black holes we find that a large amount of non-Gaussianity could also amplify the anisotropies by orders of magnitude. In this Thesis, we compute then the contribution to the angular power spectrum due to the propagation of gravitons through the perturbed Universe, obtaining the interesting result that it is sensitive to the fractional energy density of relativistic and decoupled species at the production. Since the production of cosmological signals takes place at temperatures much higher than the ones accessible by modern colliders, the distribution of gravitons in the sky could be used to test theories Beyond the Standard Model of Particle Physics. At large angular scales, gravitons and the photons of the Cosmic Microwave Background follow similar geodesics, therefore a large correlation between these two probes is expected. A computation of the angular power spectrum of the cross-correlation of these two signals shows that this is actually the case and the correlation is about 1 for the first ten multipoles. This close relation could be used in the future to test in a very robust way the large-scale structure of the Universe.

The Astrophysical Gravitational Wave Background considered in this work is generated by the superposition of the gravitational waves emitted by the black hole binaries in the sky which are too weak to be individually resolved. Its angular power spectrum contains three different sources of anisotropies: the intrinsic, the shot noise and the kinetic ones. The intrinsic anisotropies are due to pertubations of the number of sources in the sky and of the geodesics of gravitons. They can be estimated by using the *Cosmic Rulers* formalism, which accounts for all these effects by adopting gauge invariant quantities. The shot noise is induced by Poisson fluctuations in the discrete number of emitters of gravitational waves and it has a flat angular power spectrum. The kinetic anisotropies consist in a dipole generated by the relative velocity between the observer and the rest frame of the sources and it is typically and order of magnitude larger and smaller than the intrinsic anisotropies and the shot noise respectively. Although the homogeneous and isotropic contribution to the astrophysical background has zero circular polarization in General Relativity, because of the isotropic distribution of the inclination angle of the binaries, the shot noise fluctuations in the signal generate a non-vanishing V Stokes parameter which could be detected by the network Einstein Telescope and Cosmic Explorer with signal-to-noise ratio larger than 2 in one year of observations. We provide a characterization of this new signal, showing how its angular and frequency dependence could be very powerful tools to subtract it in order to measure a cosmological polarized background. The intrinsic, shot noise and kinetic anisotropies exhibit different frequency dependences above 100 Hz, because at each frequency binaries in distinct stages of the evolution and at separate distances contribute, weighting (in redshift) differently the three contributions to the anisotropies. The specific scalings with the frequency of the intrinsic, kinetic e shot noise anisotropies could be used to

separate the individual components from the total angular power spectrum. In particular, the kinetic dipole could be reconstructed with signal-to-noise ratio larger than three in ten years of observation, giving better constraints on our peculiar motion than other probes, such as galaxy surveys.

The impressing progresses that could be done in theoretical physics and in the comprehension of the early and late Universe through the characterization of the anisotropies of cosmological and astrophysical backgrounds of gravitational waves indicate that this field could be one of the most important to increase our knowledge in the future.

List of papers

1. L. Valbusa Dall'Armi, A. Ricciardone, N. Bartolo, D. Bertacca and S. Matarrese, "*Imprint of relativistic particles on the anisotropies of the stochastic gravitational-wave background*", **Phys. Rev. D 103 (2021) no.2, 023522**

2. A. Ricciardone, L. V. Dall'Armi, N. Bartolo, D. Bertacca, M. Liguori and S. Matarrese, "*Cross-Correlating Astrophysical and Cosmological Gravitational Wave Backgrounds with the Cosmic Microwave Background*", **Phys. Rev. Lett. 127 (2021) no.27, 271301**

3. L. Valbusa Dall'Armi, A. Ricciardone and D. Bertacca, "*The dipole of the astrophysical gravitational-wave background*", **JCAP 11 (2022), 040**

4. L. Valbusa Dall'Armi, A. Nishizawa, A. Ricciardone and S. Matarrese, "*Circular Polarization of the Astrophysical Gravitational Wave Background*", **Phys. Rev. Lett. 131 (2023) no.4, 041401**

5. F. Schulze, L. Valbusa Dall'Armi, J. Lesgourgues, A. Ricciardone, N. Bartolo, D. Bertacca, C. Fidler and S. Matarrese, "*GW_CLASS: Cosmological Gravitational Wave Background in the Cosmic Linear Anisotropy Solving System*", **Accepted by JCAP**

6. L. Valbusa Dall'Armi, A. Mierna, S. Matarrese and A. Ricciardone, "*Adiabatic or Non-Adiabatic? Unraveling the Nature of Initial Conditions in the Cosmological Gravitational Wave Background*", **Submitted to arXiv**

Preface

This Thesis collects the results of the research activity conducted during the three years of my Ph. D. at the Department of Physics and Astronomy "Galileo Galilei", University of Padova, Italy, under the supervision of Prof. Angelo Ricciardone.

In Chapter 1 we have carried out a survey of stochastic backgrounds of gravitational waves, showing the main statistical properties of these signals and the current detection strategies, providing also the most recent constraints at different frequencies.
In Chapter 2 we have outlined the main characteristics of the ΛCDM model, summarizing the features of the particle content and of the geometry of the Universe, focusing in particular on their departure from homogeneity and isotropy.
In Chapter 3 we have introduced the Boltzmann approach to compute the anisotropies of the SGWB of cosmological origin, providing also a description of the primary candidates which can source a primordial signal. During my visiting at the Institute for Theoretical Particle Physics and Cosmology, RWTH Aachen University, Germany, we have developed an optimized code `GW_CLASS`, presented in [1], to compute the anisotropies of cosmological backgrounds.
In Chapter 4 we have computed the initial conditions for any inflationary gravitational wave background. These calculations are based on the results I have obtained in [2]. We have provided also a shorter computation of the initial conditions for other sources of cosmological backgrounds, according to what has been done in [1].
In Chapter 5 we have presented the first numerical predictions of the angular power spectrum of the cosmological background we have found in [3], where we have investigated also the impact of relativistic and decoupled degrees of freedom at high temperatures on the anisotropies of gravitons. In this chapter, we have extended the numerical computation of [3] by using the optimized code `GW_CLASS` developed in [1].
In Chapter 6 we have explored the cross-correlation between the cosmological backgrounds and the Cosmic Microwave Background, utilizing the outcomes of the *letter* [4].
In Chapter 7 we have overviewed the stochastic background of astrophysical origin. In this chapter we have listed the most important features of a code authored by me to compute the homogeneous and isotropic part and the anisotropies of astrophysical backgrounds, which will be extensively used in the next two chapters.
In Chapter 8 we have recapped the outcomes about the circular polarization of the astrophysical background achieved in the *letter* [5], written during the period I spent at the

Research Center for the Early Universe, University of Tokyo, Japan.
In Chapter 9 we have studied the dipole of the astrophysical background, following [6]. In this chapter we have described also the first, in the context of the anisotropies of stochastic gravitational wave backgrounds, component separation technique based on the different frequency dependence of the contributions to the angular power spectrum. We have adopted this method to reconstruct, with high accuracy, our peculiar motion.

Introduction

In less than ten years from the first direct detection of a gravitational wave (GW) signal by the LIGO-Virgo-KAGRA (LVK) collaboration [7], substantial improvements have been achieved. After the third observing run (O3), the LVK collaboration has been able to detect more than 90 GW signals generated by the merging of binary black hole (BBH), binary neutron star (BNS) and black hole-neutron star systems (BHNS) [8], supplying information about the population of astrophysical binaries and General Relativity (GR). Furthermore, the recent detection of a stochastic background of GWs (SGWB) in the nHz band by the Pulsar Timing Array (PTA) collaboration [9, 10, 11, 12], confirmed the power of GW observatories to understand our universe in a very unique fashion. In addition, many ground- and space-based detectors are planned to be built in the incoming decades. The third-generation interferometers Einstein Telescope (ET) [13] and Cosmic Explorer (CE) [14] are expected to detect around $10^5 - 10^6$ mergers of compact objects of stellar masses in the deca-Hertz frequency band, while space-based missions like LISA [15] and Taiji [16] will search for GWs in the mHz band. The most advanced and futuristic detectors BBO [17] and DECIGO [18], which operates in the dHz range, are presumed to be sensitive to the weakest gravitational signals from the very early Universe. The increasing in sensitivity requires at the same time an exhaustive characterization of the SGWBs, therefore it is crucial to have a theoretical understanding of the sources and of the properties of stochastic backgrounds that could be inspected by these future surveys.

Different mechanisms which take place in the early Universe, such as inflation [19], phase transitions [20], cosmic strings [21, 22], second-order scalar perturbations [23] or vector fields [24], can generate a stochastic background of cosmological origin (CGWB) with amplitudes large enough to be detected by future interferometers. The peculiar frequency spectra of the waves sourced by these different phenomena, could help the comprehension of the physics operating at very high energy scales, allowing to distinguish the epoch of the production of the background and the features of the processes which originate the CGWBs. For instance, the detection of an inflationary CGWB would be a conclusive proof of inflation. On the other hand, waves from phase transitions or cosmic strings would improve our knowledge of the content of the Universe and of the fundamental interactions at energies larger than the ones accessible by modern colliders, sheding light on the physics Beyond the Standard Model. The different frequency bands spanned by the future earth- and space-based interferometers will allow to constrain the models which could source the CGWBs. Since these primordial GWs started propagating at early times, the observed

spectra are not just related to the properties of the sources, but also to the chronology of the Universe, making clear that there is a deep connection between study of SGWB (and GWs in general) and cosmology. The deep relation between these two branches of physics implies automatically that SGWBs could be used as an additional observable to gain information on the unsolved problems in the description of our Universe.

Since the detection of the Cosmic Microwave Background (CMB) in 1965 [25], enormous theoretical and experimental progresses have been made in cosmology, which has led to the formulation of the ΛCDM model. This model represents, nowadays, the most accurate description of the content and expansion history of our Universe. One of the main pillars of the Standard Model of Cosmology is the assumption that the Universe is homogeneous and isotropic on large angular scales, exhibiting anisotropies of approximately 1 part in 10^5. CMB observations have supported these hypotheses [26], although some anomalies have been noticed in the WMAP [27] and *Planck* [28] data on large scales. On the other hand, the cosmic history of the Universe is well explained by the Hot Big Bang Model [29], which describes the evolution over time of the abundance of cosmological relics in terms of the physics of the fundamental interactions and General Relativity. Nevertheless, this model alone cannot account for the homogeneity, isotropy and flatness of our Universe. Therefore inflation, a period of accelerated expansion that occurred in the very early times, was introduced [30, 31, 32, 33]. The great flexibility of the inflationary paradigm makes it extremely challenging to confirm (or falsify) inflation. As a result, numerous attempts have been made to validate the most exciting theory of the last century. For instance, upper limits on the amplitude of inflationary CGWBs have been set by the non-observation of the B-mode polarization of the CMB [34] and could also be put by the direct measurement of the SGWB by future interferometers.

The homogeneity and isotropy of the Universe on large scales is reflected also in the spatial features of CGWBs, which are presumed to display a dominant term (i.e., the monopole), which depends just on the frequency, and small anisotropies which are suppressed by a factor $10^{-3} - 10^{-5}$ w.r.t. the leading contribution. The amount of anisotropies is quantified by the excess in the intensity (or in any other Stokes parameter) along a given direction of observation w.r.t. the value averaged over the whole celestial sphere. The frequency f of the GWs considered stays within the band of PTA, ground- and space-based detectors, $f \in [10^{-9}, 10^{3}]$ Hz, while the inhomogeneities considered are generated in regions separated by distances of the order of $r_0 \Delta\Omega$, with the distance between the observer and the surface of production of the background and the angular scales of the anisotropies equal to $r_0 \approx 10^4$ Mpc and $\Delta\Omega \approx \pi/\ell$, with ℓ the multipole of the angular power spectrum. Since $2\pi c/r_0\Delta\Omega \ll f$, in our framework we are considering the anisotropies of GWs of small wavelenghts, generated by perturbations of the spacetime on much larger scales. The most convenient technique to compute the angular power spectrum of CGWB anisotropies is to introduce a distribution function for the stochastic GWs, which can be treated, in the limit of high frequencies, as collisionless and massless particles (gravitons) [35, 36, 37], and to solve the Boltzmann equation in the perturbed Universe [38, 39, 40]. As it happens for the CMB [41, 42], the anisotropies of the CGWB are imprinted at the production, due to spatial inhomogeneities in the energy density at that time, and during the free-streaming,

as a consequence of the redshift of gravitons due to the potential wells encountered along their geodesics. In Chapter 3 we will discuss the definition of the graviton distribution function, the initial time of propagation and the Boltzmann equation.

The initial overdensity of GWs at the time of the cosmological background production strongly depends on the source. For adiabatic perturbations, the computation is similar to the CMB case [42], up to a factor which depends on the spectral tilt of the CGWB at the pivot frequency at which the anisotropies are computed. The adiabatic initial conditions for cosmological gravitons have been inspected in [4, 1] and presented in this Thesis in Chapter 4. Unlike many other cosmological relics, the initial conditions of the CGWB originated by the quantum fluctuations of the metric during inflation are not adiabatic, because they are not generated by the same field which produces photons, baryons, neutrinos and, eventually, Cold Dark Matter (CDM). The computation of these non-adiabatic initial conditions has been performed in [5], adopting the original approach of evaluating the overdensity of gravitons at early times starting from the perturbed energy-momentum tensor of the gravitational field. These results will also be presented in Chapter 4, where we will show how this peculiar contribution could increase the angular power spectrum of the CGWB by an order of magnitude. A small section of this chapter is dedicated to quantifying the initial conditions for scalar-induced GWs in the case of non-Gaussian perturbations, following [23].

The anisotropies due to the propagation of gravitons through a perturbed Universe consist in the standard Sachs-Wolfe (SW) and Integrated Sachs-Wolfe (ISW) terms [43], which are the redshifts experienced by gravitons at their production and during their free-streaming respectively. An interesting aspect is that the decoupling of gravitational interactions at early times [37] allows to test the content of the Universe at much earlier times than the CMB, baryons and neutrinos, which were tightly coupled until recombination, thus any trace of early-times physics has been erased by the scatterings [42]. In Chapter 5, details on the numerical computation of these two effects for the primordial GWs have been reported, showing that the angular power spectrum of the CGWB is sensitive to the particle content of the Universe at energy scales larger than 10^{12} GeV. The results, derived for the first time in [3], have been improved by optimizing the Boltzmann solver Cosmic Linear Anisotropy Solving System (`CLASS`) [44, 45] in the branch `GW_CLASS` presented in [1][1]. The sensitivity of the CGWB to other parameters (e.g., the equation of state of the Universe) which affect the evolution of the perturbations of the Universe at early times has been studied in [46].

Gravitons and photons propagate along null geodesics, thus it is natural to expect that a large correlation is present between (the sky maps of the) two signals, since, at large angular scales, the paths followed by light and GWs are the same. Under adiabatic initial conditions, the correlation between the CMB and the CGWB is almost one, up to $\ell = 10$ [4]. Such a strong correlation implies that, by using the observed CMB maps, it is possible to predict the expected CGWB uniquely through constrained realizations [4]. Such constrained maps are extremely useful for testing foregrounds or systematic contaminations

[1]The branch is available under the name `GW_CLASS` at https://github.com/lesgourg/class_public/tree/GW_CLASS.

in future data. Chapter 6 provides all the contributions to the cross-correlation, and the physical interpretation.

The CGWB is intrinsically stochastic, but it is not the only non-deterministic superposition of GWs which could be observed at interferometers. For instance, the GWs emitted by the individual binaries which are too weak to be resolved or overlap in time in such a way they become indistinguishable, generate a stochasic background of astrophysical origin (AGWB) [47, 48]. The possible sources of an AGWB could be rotating neutron stars [49, 50], core collapse supernovae [51, 52] or massive stars [53, 54], magnetars [55, 56], compact binary systems of black holes (BBH), neutron stars (BNS) or black hole and neutron stars (BHNS) [57, 58, 59, 60, 61, 62, 63]. According to the latest constraints by the LVK collaboration on the population of GW sources [8], the most promising candidates are expect to be BBH binaries and in this Thesis we have focused just on the amplitude of their AGWB. The population of binary systems of stellar mass and the expected monopole have been computed in detail in Chapter 7. As the CGWB, also the AGWB is homogeneous and isotropic at the leading order, and it is characterized by anisotropies due to the fluctuation in the number of discrete events which contribute to the total signal (shot noise) [64, 65, 66], to the peculiar velocity of the observer w.r.t. the rest frame of the emitters (kinetic dipole) [67, 6, 68], and to the inhomogeneities in the distribution of the sources, because of the cosmological perturbations (intrinsic anisotropies) [69, 70, 71, 72, 73, 74, 75].

In GR, the AGWB is supposed to be unpolarized at the leading order, because of the isotropic distribution of the inclination angle of the binaries. This property could be used to disentangle astrophysical and cosmological backgrounds, which reveal a large amount of circular polarization in the case of violations of parity in the mechanism which generates the CGWB [24, 76, 77, 78, 79, 80, 81, 82]. However, at the anisotropic level, the shot noise fluctuations in the number of astrophysical sources generates a non-negligible amount of circular and linear polarization [2]. This polarized AGWB could represent a troublesome foreground that has to be subtracted in order to measure the circular polarization of cosmological backgrounds. In Chapter 8 we show that the amount of circular polarization could be detected by the network of interferometers ET+CE in one year of observations. Moreover we show that a cosmological background could be distinguished from the astrophysical one by exploiting the different angular and frequency dependence. A similar analysis has been performed for PTA in [83, 84].

The AGWB keeps also track of the peculiar velocity of the observer w.r.t. the rest frame of the sources, which generates a large dipole that dominates the intrinsic anisotropies [6]. The same peculiar velocity of the Large-Scale Structure (LSS) should impact the distribution of radio sources [85, 86, 87, 88, 89, 90] and quasars [91, 92], and, in the ΛCDM model, the CMB maps [93]. However, discrepancies in the estimates of our peculiar velocity by using LSS and CMB probes have been found [94, 90], thus a third additional, independent, probe should be used to shed light on this "tension". In Chapter 9 we show that detecting the AGWB it is possible to reconstruct the kinetic dipole with high precision, by using a multi-frequency analysis of the anisotropies, which allows to disentangle the intrinsic, the kinetic and the shot noise dipole [6].

The different fields involved in this Thesis, from theoretical physics and cosmology

to astrophysics, statistics and GW interferometry, demonstrate that the anisotropies of SGWBs are an extremely complex subject that should be understood in depth, because it could contain a plethora of new information about different aspects of Nature.

Chapter 1

Stochastic Gravitational Wave Backgrounds

1.1 Radiative degrees of freedom of the gravitational field

General Relativity (GR) accurately describes the relationship between the geometry of spacetime and the energy densityof the Universe's contents through the Einstein equations,

$$G_{\mu\nu}(x) = 8\pi G\, T_{\mu\nu}(x)\,, \tag{1.1}$$

where $G_{\mu\nu}$ is the Einstein tensor, which can be written as a function of the derivatives of the metric, and $T_{\mu\nu}$ is the total energy-momentum tensor in the region of space and time around the four-vector x. In analogy with electromagnetism (EM), a natural question to ask is whether the Einstein equations admit waves as solutions. Since GR is invariant under diffeomorphisms, in order to properly define GWs it is crucial to show that each solution of the wave equation carries physical information and it is not an artifact due to a particular choice of the coordinates [95]. It has indeed been shown [96] that in GR some plane waves could be merely sinuosities in the coordinate system their velocity changes under diffeomorphisms. In some cases, they can even exhibit superluminal behaviour and thus violating special relativity. In [96], it was also demonstrated that plane waves, specifically those that are transverse-traceless [97], propagate at the speed of light in all reference frames, defining the true radiative degrees of freedom of the system. Given the complexity introduced by the nonlinearity of the Einstein equations, we begin by defining gravitational waves in a flat spacetime and subsequently explore their propagation in a curved spacetime as a second step.

1.1.1 Wave solutions in Linearized Theory

We consider the simplest case in which there is no source of energy and momentum in the Universe, $T_{\mu\nu} = 0$, and the there is a tiny perturbation $h_{\mu\nu}$ on top of a flat (Minkowski) geometry. The natural definition of GWs is simply then

$$h_{\mu\nu}(x) \equiv g_{\mu\nu}(x) - \eta_{\mu\nu}\,, \tag{1.2}$$

where $|h_{\mu\nu}(x)| \ll 1$. By introducing a coordinate transformation

$$x^\mu \to x'^\mu = x^\mu + \xi^\mu(x), \tag{1.3}$$

with $\xi^\mu(x)$ an infinitesimal vector field, the metric transforms as

$$g'_{\mu\nu}(x') = \frac{\partial x^\alpha}{\partial x'^\mu}\frac{\partial x^\beta}{\partial x'^\nu} g_{\alpha\beta}(x) = g_{\mu\nu} - \partial_\mu \xi_\nu - \partial_\nu \xi_\mu \to h'_{\mu\nu}(x') = h_{\mu\nu}(x) - \partial_\mu \xi_\nu - \partial_\nu \xi_\mu \,. \tag{1.4}$$

In order to preserve the condition of having a weak gravitational field that perturbs a flat spacetime, we impose the additional constraint

$$|\partial_\alpha \xi(x)| \leq |h_{\mu\nu}(x)| \,. \tag{1.5}$$

The Christoffel symbols in the presence of a small perturbations around a Minkowski spacetime are

$$\begin{aligned} \Gamma^\mu_{\nu\rho} \equiv & \frac{1}{2} g^{\mu\alpha}(\partial_\nu g_{\alpha\rho} + \partial_\rho g_{\nu\alpha} - \partial_\alpha g_{\nu\rho}) = \frac{1}{2}\Big(\eta^{\mu\alpha} + h^{\mu\alpha}\Big)(\partial_\nu h_{\alpha\rho} + \partial_\rho h_{\alpha\nu} - \partial_\alpha h_{\nu\rho}) = \\ = & \frac{1}{2}(\partial_\nu h^\mu_\rho + \partial_\rho h^\mu_\nu - \partial^\mu h_{\nu\rho}) \,. \end{aligned} \tag{1.6}$$

The Riemann tensor at first order in the perturbation of the metric assumes the simple form

$$\begin{aligned} R^\rho_{\mu\sigma\nu} = & \partial_\sigma \Gamma^\rho_{\nu\mu} - \partial_\nu \Gamma^\rho_{\sigma\mu} + \Gamma^\rho_{\sigma\lambda}\Gamma^\lambda_{\nu\mu} - \Gamma^\rho_{\nu\lambda}\Gamma^\lambda_{\sigma\mu} = \partial_\sigma \Gamma^\rho_{\nu\mu} - \partial_\nu \Gamma^\rho_{\sigma\mu} = \\ = & \frac{1}{2}\big[\partial_\sigma\partial_\nu h^\rho_\mu + \partial_\sigma\partial_\mu h^\rho_\nu - \partial_\sigma\partial^\rho h_{\nu\mu} - \big(\partial_\nu\partial_\sigma h^\rho_\mu + \partial_\nu\partial_\mu h^\rho_\sigma - \partial_\nu\partial^\rho h_{\sigma\mu}\big)\big] = \\ = & \frac{1}{2}(\partial_\sigma\partial_\mu h^\rho_\nu + \partial_\nu\partial^\rho h_{\sigma\mu} - \partial_\nu\partial_\mu h^\rho_\sigma - \partial_\sigma\partial^\rho h_{\nu\mu}) \,, \end{aligned} \tag{1.7}$$

while the Ricci tensor and the Ricci scalar are

$$\begin{aligned} R_{\mu\nu} \equiv & R^\rho_{\mu\rho\nu} = \frac{1}{2}(\partial_\mu\partial_\rho h^\rho_\nu + \partial_\nu\partial^\rho h_{\rho\mu} - \partial_\nu\partial_\mu h^\rho_\rho - \Box h_{\mu\nu}) \,, \\ R \equiv & R^\mu_\mu = \partial^\mu\partial_\rho h^\rho_\mu - \Box h^\mu_\mu \,. \end{aligned} \tag{1.8}$$

The Einstein tensor at the leading order in $h_{\mu\nu}$ is given by

$$\begin{aligned} G_{\mu\nu} \equiv & R_{\mu\nu} - \frac{1}{2} R g_{\mu\nu} = \\ = & \frac{1}{2}\big[\partial_\mu\partial_\rho h^\rho_\nu + \partial_\nu\partial^\rho h_{\rho\mu} - \partial_\nu\partial_\mu h^\rho_\rho - \Box h_{\mu\nu} - \eta_{\mu\nu}(\partial^\mu\partial_\rho h^\rho_\mu - \Box h^\mu_\mu)\big] \,. \end{aligned} \tag{1.9}$$

In order to extract the physical degrees of freedom from the solution of the Einstein equations, $G_{\mu\nu} = 0$, we need to remove any spurious information carried by the gauge transformation w.r.t. ξ^μ. Therefore we fix the gauge by imposing the conditions

$$\partial^\mu \left(h_{\mu\nu} - \frac{1}{2}\eta_{\mu\nu} h^\rho_\rho\right) = 0 \,, \qquad h^\mu_\mu = 0 \,, \qquad h_{0i} = 0 \,. \tag{1.10}$$

It is easy to check indeed that in order to go from a gauge $h'_{\mu\nu}$ to the gauge $h_{\mu\nu}$ we need to apply to Eq. (1.4) the transformations

$$\Box\xi^\mu = -\partial^\mu\left(h'_{\mu\nu} - \frac{1}{2}\eta_{\mu\nu}h^{\rho\prime}_{\rho}\right), \qquad \partial^\mu\xi_\mu = -\frac{1}{2}h^{\mu\prime}_{\mu}, \qquad \partial_0\xi_i + \partial_i\xi_0 = -h'_{0i}, \tag{1.11}$$

which completely saturate any residual gauge in ξ^μ. In this gauge, the Einstein tensor given in Eq. (1.9) has a much less complicate expression and the Einstein equations do indeed take the form of wave equations,

$$\Box h_{\mu\nu} = 0 \to \Box h_{ij} = 0\,. \tag{1.12}$$

It is also possible to show that, in this gauge, h_{00} is not a dynamical quantity, but depends solely on the spatial coordinates. It represents the Newtonian gravitational potential, which is zero in the vacuum since there is no source of energy and momentum. In these few steps we have shown that there is a gauge-independent perturbation of the metric which evolves according to the wave equation. From the 10 initial degrees of freedom of the perturbation of the metric $h_{\mu\nu}$ only two of them carry physical information. These two degrees of freedom can be interpreted as the two polarization states of the propagating radiation.

When a tiny source of energy is present, it is possible to write the perturbations of the energy-momentum tensor by using

$$\begin{aligned} T_{00} =& \delta\rho\,, \\ T_{0i} =& v_i^\perp + \partial_i v\,, \\ T_{ij} =& \delta_{ij}\delta P + \pi_{ij} + \partial_{(i}\pi_{j)}^\perp + \left(\partial_i\partial_j - \frac{1}{3}\delta_{ij}\nabla^2\right)\pi\,, \end{aligned} \tag{1.13}$$

where we have defined with the round parentheses the symmetrization of tensors w.r.t. the indices within the parentheses. $\delta\rho$ is the energy density, δP the pressure, $\pi_i^\perp$ a transverse vector field, while π_{ij} is the anisotropic stress (a transverse-traceless tensor field). The velocity v_i has been decomposed into a scalar and solenoidal contributions, v and $v_i^\perp$ respectively. Four of these degrees of freedom are constrained by the conservation of the energy-momentum tensor,

$$\partial^\mu T_{\mu\nu} = 0\,. \tag{1.14}$$

It is possible to write the metric perturbation according to the same decomposition,

$$\begin{aligned} h_{00} =& -2A\,, \\ h_{0i} =& -B_i^\perp - \partial_i B\,, \\ h_{ij} =& 2D\,\delta_{ij} + \partial_{(i}F_{j)}^\perp + \left(\partial_i\partial_j - \frac{1}{3}\delta_{ij}\nabla^2\right)F + H_{ij}\,, \end{aligned} \tag{1.15}$$

with $B_i^\perp$, $F_i^\perp$ solenoidal vectors, while H_{ij} is a transverse-traceless tensor. We will provide additional details on the decomposition of the energy-momentum tensor and of the metric

in Appendix A.1 and in Section 2.4.1. In order to show that there are physical degrees of freedom that also in this case obey the wave equation, we define the following gauge invariant variables (denoted by the subscripts "GI")[1] which are combination of the metric perturbations,

$$\begin{aligned}\Phi_{\rm GI} \equiv& A - \partial_0 B - \frac{1}{2}\partial_0^2 F\,,\\ \Theta_{\rm GI} \equiv& 2D - \frac{1}{3}\nabla^2 F\,,\\ \Xi_{\rm GI} \equiv& - B_i^{\perp} - \partial_0 F_i^{\perp}\,.\end{aligned} \tag{1.16}$$

The transverse-traceless perturbation H_{ij} are gauge invariant and, as we will see in Section 2.4.1, the Einstein equations can be recasted in the following form

$$\begin{aligned}\nabla^2\Theta_{\rm GI} =& - 8\pi G\,\delta\rho,\\ \nabla^2\Phi_{\rm GI} =& 4\pi G\Big(\delta\rho + 3\delta P - 3\,\partial_0 v\Big),\\ \nabla^2\Xi_{\rm GI} =& - 16\pi G\,v,\\ \Box H_{ij}^{TT} =& - 16\pi G\,\sigma_{ij}.\end{aligned} \tag{1.17}$$

We conclude therefore that also in this case the transverse-traceless perturbations of the metric propagate according to the wave equation and that their dynamics does not depend on the gauge choice. The r.h.s. of the equation of motion of the GWs shows that any transverse-traceless contribution in the energy-momentum tensor would act as a source term in the Einstein equations, amplifying or damping the propagation of GWs.

In the next section, we will extend this result to scenarios where the background geometry of the Universe is not flat. We will demonstrate that it remains possible to provide a meaningful definition for the concept of radiative degrees of freedom of the gravitational field.

1.1.2 High frequency expansion and linearized Einstein equations

In this Thesis, we characterize SGWBs in the high-frequency limit or shortwave approximation [98, 35, 36, 37], in which the GWs have a small amplitude and their wavelengths are much smaller than the typical scales over which the background varies. As we will see in more detail in Sections 1.4.1, 1.5, the former hypothesis is well motivated by the fact that only a tiny fraction of the enegy density of the Universe is expected to be in form of GWs, since all the known sources studied here emit weak GWs. The latter assumption is justified by the comparison between the frequencies of the GWs observed at interferometers and the distance between the emitters and the observer for the angular scales of the anisotropies considered (related to the size of the region over which the background changes significantly), see e.g. Section 3.1 for a more quantitative estimate of the separation of these

[1] The gauge invariance can be proved by applying the gauge transformations defined in Appendix A.1, keeping in mind that in this case the background spacetime is a Minkowski spacetime, therefore the terms proportional to $\mathcal{H}$ in the gauge transformations have to be neglected.

scales. Therefore, the underlying idea of this *shortwave approximation* is that it is possible to distinguish in the metric the slowly varying background from the oscillating GWs,

$$g_{\mu\nu}(x) = g^{(B)}_{\mu\nu}(x) + \gamma^{(\mathrm{GW})}_{\mu\nu}(x)\,, \tag{1.18}$$

where the background and the waves change on scales k and q respectively,

$$\begin{aligned} \partial_\alpha g^{(B)}_{\mu\nu}(x) &\sim k\ \mathcal{O}\left[g_{\mu\nu}(x)\right]\,, \\ \partial_\alpha \gamma^{(\mathrm{GW})}_{\mu\nu}(x) &\sim q\ \mathcal{O}\left[\gamma^{(\mathrm{GW})}_{\mu\nu}(x)\right]\,. \end{aligned} \tag{1.19}$$

When the weak field limit is hold, $|\gamma^{(\mathrm{GW})}_{\mu\nu}(x)| \ll 1$, and the frequency of the GWs is much larger than the inverse of the timescales over which the background varies, $q \gg k$, the waves can be thought as small ripples that propagate through a spacetime that curves very slowly compared to them. According to the splitting into high- and low- frequency modes defined in Eq. (1.18), the Ricci tensor can be expanded into terms of order zero, linear, quadratic and cubic in $\gamma^{(\mathrm{GW})}_{\mu\nu}$,

$$R_{\mu\nu}(x) = R^{(0)}_{\mu\nu}(x) + R^{(1)}_{\mu\nu}(x) + R^{(2)}_{\mu\nu}(x) + R^{(3)}_{\mu\nu}(x)\,. \tag{1.20}$$

The linear and the quadratic terms in $\gamma^{(\mathrm{GW})}_{\mu\nu}$ can be written as[2] the following combinations of covariant derivatives,

$$\begin{aligned} R^{(1)}_{\mu\nu} \equiv& \frac{1}{2}\Big(-\mathcal{D}_\nu\mathcal{D}_\mu\gamma^{(\mathrm{GW})\,\alpha}_{\alpha} - \mathcal{D}^\alpha\mathcal{D}_\alpha\gamma^{(\mathrm{GW})}_{\mu\nu} + \mathcal{D}^\alpha\mathcal{D}_\nu\gamma^{(\mathrm{GW})}_{\mu\alpha} + \mathcal{D}^\alpha\mathcal{D}_\mu\gamma^{(\mathrm{GW})}_{\alpha\nu}\Big)\,, \\ R^{(2)}_{\mu\nu} \equiv& \frac{1}{2}\Big[\frac{1}{2}\mathcal{D}_\mu\gamma^{(\mathrm{GW})}_{\alpha\beta}\mathcal{D}_\nu\gamma^{(\mathrm{GW})\,\alpha\beta} \\ &+ \gamma^{(\mathrm{GW})\,\alpha\beta}\Big(\mathcal{D}_\mu\mathcal{D}_\nu\gamma^{(\mathrm{GW})}_{\alpha\beta} + \mathcal{D}_\alpha\mathcal{D}_\beta\gamma^{(\mathrm{GW})}_{\mu\nu} - \mathcal{D}_\nu\mathcal{D}_\beta\gamma^{(\mathrm{GW})}_{\alpha\mu} - \mathcal{D}_\mu\mathcal{D}_\beta\gamma^{(\mathrm{GW})}_{\alpha\nu}\Big) \\ &+ \mathcal{D}^\beta\gamma^{(\mathrm{GW})\,\alpha}_{\nu}\Big(\mathcal{D}_\beta\gamma^{(\mathrm{GW})}_{\alpha\mu} - \mathcal{D}_\alpha\gamma^{(\mathrm{GW})}_{\beta\mu}\Big) \\ &+ \Big(\frac{1}{2}\mathcal{D}^\alpha\gamma^{(\mathrm{GW})\,\beta}_{\beta} - \mathcal{D}_\beta\gamma^{(\mathrm{GW})\,\alpha\beta}\Big)\Big(\mathcal{D}_\nu\gamma^{(\mathrm{GW})}_{\alpha\mu} + \mathcal{D}_\mu\gamma^{(\mathrm{GW})}_{\alpha\nu} - \mathcal{D}_\alpha\gamma^{(\mathrm{GW})}_{\mu\nu}\Big)\Big]\,, \end{aligned} \tag{1.21}$$

where the covariant derivative for a tensor of mixed covariant and contravariant indices is defined by

$$\mathcal{D}_\rho T^\mu_\nu \equiv \partial_\rho T^\mu_\nu + \Gamma^\mu_{\rho\sigma}T^\sigma_\nu - \Gamma^\sigma_{\rho\nu}T^\mu_\sigma\,, \tag{1.22}$$

with $\Gamma^\alpha_{\beta\gamma}$ the Christoffel symbols that, in this framework, are computed w.r.t. the background metric. A similar expansion can be done for the Riemann tensor and for the Ricci scalar, and it is easy to show [35, 36] that their contributions related to the high-frequency waves are non-vanishing and gauge invariant. Since these two quantities carry the physical information of the system and remain independent of the coordinate choice, it precisely confirms that GWs are physical degrees of freedom of the gravitational field, as one would

[2] An easy way to compute these terms is to evaluate the Ricci tensor around a flat spacetime and to substitute the partial derivatives that appear with covariant derivatives.

expect from the generalization of the results obtained in the previous section. According to Eq. (1.20), the Einstein equations in vacuum give

$$G_{\mu\nu} = 0 \to R_{\mu\nu} = 0 \to R^{(B)}_{\mu\nu} + R^{(1)}_{\mu\nu}(x) + R^{(2)}_{\mu\nu}(x) + \mathcal{O}\left[\left(\gamma^{(\mathrm{GW})}_{\mu\nu}(x)\right)^3\right] = 0\,, \tag{1.23}$$

where we have considered just terms of order zero, one and two in $\gamma^{(\mathrm{GW})}_{\mu\nu}$, neglecting the corrections due to contributions at third order. In the shortwave approximation, it is possible to solve the Einstein equations by separating the high- and the low-frequency modes, with the introduction of an averaging scheme over the small scales [35, 36]. More specifically, we introduce the Brill-Hartle average [98], which consists on an average in a region of size L_{BH}, with $1/k \gg L_{\mathrm{BH}} \gg 1/q$. In this way, the contribution of the GWs to the background, i.e., the averaged one, is disentangled from the rapidly-oscillating one, whose average goes to zero. Intuitively, we expect indeed that terms independent of $\gamma^{(\mathrm{GW})}_{\mu\nu}$ are invariant under the average, while objects linear in the GWs have zero average, and terms quadratic in the rapidly-oscillating waves could have both negligible or non-negligible averages. A formal definition of this averaging scheme and of its rules have been given in Appendix B, where we show also which kind of tensors quadratic in the GWs have negligible averages. It is possible then to solve separately Eq. (1.23) for the part whose average gives zero and for the high-frequency contribution,

$$\begin{aligned} R^{(0)}_{\mu\nu}(x) &= -\left\langle R^{(2)}_{\mu\nu}(x)\right\rangle_{\mathrm{BH}}\,, \\ R^{(1)}_{\mu\nu} &= -R^{(2)}_{\mu\nu} + \left\langle R^{(2)}_{\mu\nu}(x)\right\rangle_{\mathrm{BH}}\,. \end{aligned} \tag{1.24}$$

By looking at the expression of the Ricci tensor linear in the GW degrees of freedom, the first row of Eq. (1.21), it is clear the the Einstein equation for the high-frequency modes corresponds to the the wave equation for $\gamma^{(\mathrm{GW})}_{\mu\nu}$ in GR, including nonlinear corrections sourced by terms quadratic in the GWs. For instance, if we consider the Lorentz gauge in which

$$\mathcal{D}^\alpha \gamma^{(\mathrm{GW})}_{\mu\alpha}(x) = 0\,, \tag{1.25}$$

and we define

$$\bar{\gamma}^{(\mathrm{GW})}_{\mu\nu}(x) \equiv \gamma^{(\mathrm{GW})}_{\mu\nu}(x) - \frac{1}{2}\gamma^{(\mathrm{GW})\,\alpha}_{\alpha} g^{(B)}_{\mu\nu}(x)\,, \tag{1.26}$$

the equation of motion of the radiative degrees of freedom becomes

$$\mathcal{D}_\alpha \mathcal{D}^\alpha \bar{\gamma}^{(\mathrm{GW})}_{\mu\nu}(x) + 2R^{(B)}_{\alpha\mu\beta\nu}\bar{\gamma}^{(\mathrm{GW})\,\alpha\beta}(x) = \mathcal{O}\left[\left(\gamma^{(\mathrm{GW})}_{\mu\nu}\right)^3\right]\,, \tag{1.27}$$

with $R^{(B)}_{\alpha\mu\beta\nu}$ the Riemann tensor evaluated w.r.t. the background metric. The averaged part of the Einstein equations, given by the first row of Eq. (1.24), determines the structure of the energy-momentum tensor of the gravitational field, as we will discuss in detail in the next section. The r.h.s. of Eq. (1.27) represents the corrections to the equation of motion of the GWs due to the nonlinear nature of gravitation and they could be thought

as an interaction between the GWs while they propagate. Nevertheless, in this work, we will focus just on terms linear (in the equation of motion) and quadratic (in the energy-momentum tensor) in the small-scale waves, neglecting the higher-order contributions, which are expected to be suppressed by the large separation between the scales k and q.

1.1.3 Energy-momentum tensor of the GWs

According to the equivalence principle, any gravitational field can be transformed locally by a diffeomorphism, thus one could argue whether the GWs defined in the previous section really carry energy and momentum. Intuitively, the r.h.s. of the first row of Eqs. (1.24) looks like the standard energy-momentum tensor [35, 36] that appears in r.h.s. of the Einstein equations, Eq. (1.1),

$$T^{(\mathrm{GW})}_{\mu\nu}(x) \equiv -\frac{1}{8\pi G}\left\langle R^{(2)}_{\mu\nu}(x)\right\rangle_{\mathrm{BH}} . \tag{1.28}$$

The interpretation of this result is that the curvature of spacetime at large-scales could be generated by the smoothed small-scale fluctuations of the metric, which act as a source of energy and momentum. The averaging procedure is a crucial step in the definition of the energy-momentum tensor, because it makes clear that is possible to define an energy-momentum tensor for the gravitational field only when we pass from a "microscopic" description of the metric, in which $g^{(B)}_{\mu\nu}$ and $\gamma^{(\mathrm{GW})}_{\mu\nu}$ are indistinguishable, to a coarse-grained, "macroscopic", description [99]. By exploiting some properties of the Brill-Hartle average, discussed in Appendix B, it is possible to show that, despite the complicated form of the Ricci tensor generated by terms quadratic in the GWs, defined in Eq. 1.21, the Einstein tensor for the gravitational field, defined in Eq. 1.28, reduces [35, 36, 37] to a very simple expression given in terms of the covariant derivatives of the radiative degrees of freedom of the metric,

$$T^{(\mathrm{GW})}_{\mu\nu}(x) = \frac{1}{32\pi G}\left\langle \mathcal{D}_\mu \gamma^{(\mathrm{GW})}_{\alpha\beta}(x)\mathcal{D}_\nu \gamma^{(\mathrm{GW})\,\alpha\beta}(x)\right\rangle . \tag{1.29}$$

It is possible to show that, up to negligible terms in the shortwave approximation, the energy-momentum tensor of the GWs is conserved,

$$\mathcal{D}^\mu T^{(\mathrm{GW})}_{\mu\nu}(x) = 0 . \tag{1.30}$$

It is important to stress that the definition of the energy momentum tensor given in Eq. (1.28) is valid just in the shortwave approximation, while there are ambiguities in the general definition of the energy density, pressure and anisotropic stress of the GWs when $q \approx k$, because it is not possible to define a gauge-invariant energy-momentum tensor [100]. This could be also interpreted as the difficulty in distinguishing the background from its perturbations, thus generating issues in discriminating the source of curvature with the curvature itself. Alternative definitions of $T^{(\mathrm{GW})}_{\mu\nu}$ have been given for instance in [101], where the conservation law of the total momentum of the gravitational field and matter has been imposed, or in [102, 103], where the Einstein-Hilbert action has been perturbed at second order in the GW amplitude, while in [104], gravity has been treated as a nonlinear

tensor field in a flat spacetime. Although all these ambiguities in the definition of GWs of "low frequencies", in this Thesis we will introduce the concept of energy density of GWs only when the shortwave approximation is valid, thus we will use just the energy-momentum tensor defined by Eq. (1.28), which converges, for $q \ll k$, to the other definitions mentioned in this paragraph.

1.2 Stochastic signals

In Section 1.1, we have provided a formal characterization of the GWs and of their energy-momentum tensor, independently on the nature of the sources and on the properties of the gravitational signal itself. Currently, all the GWs signal which have been detected at the interferometers [7, 105, 106, 107, 108, 8] have been generated by isolated resolved astrophysical sources. As we will discuss in more detail in Sections 7.3, these GWs are characterized by known waveforms that depend on few parameters of the emitters. Therefore the evolution of the waves in time (or, equivalently, in frequency) is quite well understood. However, recently, the Pulsar Timing Array (PTA) collaboration (i.e., NANOGrav, EPTA/InPTA, PPTA, and CPTA [9, 10, 11, 12]) has claimed a detection of GWs produced by a stochastic process, for which the shape of the waveform is aleatory and unpredictable. In this Thesis, we will focus only on this second type of GWs, which, as we will see, is extremely interesting for many reasons that we will explain in the next chapters.

An SGWB is a random signal $h_{ij}(t, \mathbf{x})$ that can be characterized only in terms of its statistical properties, for instance by its probability density function (PDF), $\mathcal{P}[h_{ij}]$. Such a PDF depends on the values of the tensor perturbations of the metric at different locations and times[3], $h_{ij}(t_n, \mathbf{x}_n)$, with n that goes from one to N. In this case, the observables that carry physical information about the mechanism that produced the GWs are the moments of the distribution,

$$\left\langle \prod_{m=1}^{M} h_{ij}(t_m, \mathbf{x}_m) \right\rangle \equiv \int \prod_{n=1}^{N} \mathrm{d}h_{ij}(t_n, \mathbf{x}_n) \prod_{m=1}^{M} \mathrm{d}h_{ij}(t_m, \mathbf{x}_m)\, \mathcal{P}[h_{ij}] \,. \tag{1.31}$$

For instance, when $M = 0$, the normalization condition on the PDF gives $\left\langle (h_{ij}(t, \mathbf{x}))^0 \right\rangle = 1$, while for $M = 1$, $M = 2$, $M = 3$, $M = 4$, the moments of the distribution are equal to the mean, the covariance, the skewness and the kurtosis respectively.

Although this definition of SGWBs is very intuitive and clear, we would like to provide some practical criteria which ensure that the data collected at interferometers reflect the stochastic nature of the incoming GWs. From an observational point of view, a signal is stochastic if a probabilistic description of the evolution in space and time of the waves is preferred to any other deterministic waveform predicted by the theory [109, 110]. In a Bayesian context, this is equivalent to state that the model selection computation prefers a SGWB to any other causal GW [110]. More formally, we describe a model in which

[3] In this case, we discretize the spacetime in order to write down the PDF of h_{ij} as a joint PDF of many (correlated) random variables. We avoid in this Section the formal discussion of the limit $N \to \infty$, in which the PDF can be written in a slightly more complicated expression.

the signal is stochastic as $\mathcal{M}_{\rm SGWB}\left(\mathcal{P}, \boldsymbol{\theta}_{\rm SGWB}\right)$, with $\boldsymbol{\theta}_{\rm SGWB}$ the moments that univocally determine the distribution of h_{ij}. Given some observed data $\mathbf{d}$, the PDF of the parameters $\boldsymbol{\theta}_{\rm SGWB}$ associated to the model $\mathcal{M}_{\rm SGWB}$ is computed by using Bayes' theorem [111],

$$p\left(\boldsymbol{\theta}_{\rm SGWB}|\mathcal{P};\mathbf{d}\right) = \frac{\mathcal{L}\left(\mathbf{d}|\boldsymbol{\theta},\mathcal{P}\right)\pi\left(\boldsymbol{\theta}_{\rm SGWB}\right)}{p\left(\mathbf{d}\right)}\,, \tag{1.32}$$

where $\mathcal{L}$ is the likelihood of the data given the SGWB model and a specific experiment, $\pi\left(\boldsymbol{\theta}_{\rm SGWB}\right)$ is the prior that keeps into account our degree of belief on the PDF of the parameters $\boldsymbol{\theta}_{\rm SGWB}$ before the experiment, and $p\left(\mathbf{d}\right)$ is the evidence, which represents the total probability that the data are distributed according to the measurements, keeping into account for all the possible models,

$$p\left(\mathbf{d}\right) \equiv \int \mathrm{d}\mathcal{M} \int \mathrm{d}\boldsymbol{\theta}_{\mathcal{M}}\, \mathcal{L}\left(\mathbf{d}|\boldsymbol{\theta}_{\mathcal{M}},\mathcal{M}\right)\, \pi\left(\boldsymbol{\theta}_{\mathcal{M}}\right)\,. \tag{1.33}$$

The probability associated to the SGWB model given the data is computed by marginalizing the posterior of the parameters, w.r.t. all the possible values of the parameters,

$$p\left(\mathcal{M}_{\rm SGWB}|\mathbf{d}\right) = \int \mathrm{d}\boldsymbol{\theta}_{\rm SGWB}\; p\left(\boldsymbol{\theta}_{\rm SGWB}|\mathcal{P};\mathbf{d}\right)\,, \tag{1.34}$$

which can be written according to Bayes' theorem as

$$p\left(\mathcal{M}_{\rm SGWB}|\mathbf{d}\right) = \frac{p\left(\mathbf{d}|\mathcal{M}_{\rm SGWB}\right)\pi\left(\mathcal{M}_{\rm SGWB}\right)}{p\left(\mathbf{d}\right)}\,. \tag{1.35}$$

In Bayesian analysis, we compare two models by looking at the Bayes factor between a model in which there is a stochastic background and the ones in which the GWs come from deterministic processes,

$$\mathcal{B}_{\rm SGWB-det} \equiv \frac{p\left(\mathbf{d}|\mathcal{M}_{\rm SGWB}\right)}{p\left(\mathbf{d}|\mathcal{M}_{\rm det}\right)}\,, \tag{1.36}$$

where the deterministic model has been defined by its own parameters $\boldsymbol{\theta}_{\rm det}$ and by an ensemble of different known waveform models $\mathbf{h}_{ij}^{\rm det}$,

$$p\left(\mathbf{d}|\mathcal{M}_{\rm det}\right) \equiv \int \mathrm{d}\mathbf{h}_{ij}^{\rm det} \int \mathrm{d}\boldsymbol{\theta}_{\rm det}\, \mathcal{L}\left(\mathbf{d}|\boldsymbol{\theta}_{\rm det},\mathbf{h}_{ij}^{\rm det}\right)\, \pi\left(\boldsymbol{\theta}_{\mathcal{M}},\mathbf{h}_{ij}^{\rm det}\right)\,. \tag{1.37}$$

A large Bayes factor supports the model for the SGWB more than the ones for deterministic sources, with an evidence than increases with $\mathcal{B}_{\rm SGWB-det}$. For instance, for $\mathcal{B}_{\rm SGWB-det} \geq 12$, the evidence for SGWB relative to causal waves is strong [109, 110].

In the discussion up to now, we did not care about the origin of the stochasticity of the gravitational field, but we have just considered a generic PDF with some non-vanishing moments. It is important however to discriminate between SGWBs that are intrinsically stochastic, because of the nature of their sources, or "observationally stochastic", because they are generated by the superposition of many deterministic signals that are too weak to be detected or that overlap in time in such a way that they cannot be decomposed

into individual GWs. We discuss the former case in Section 1.4.1, illustrating the example of SGWBs produced during inflation, phase transitions (PTs) and primordial black holes (PBHs) [112, 113, 114, 115], while we list some examples of the latter in Section 1.4.2, focusing in particular on the background generated by the superposition of the waves emitted by binary astrophysical systems [48]. We stress that the PDF of the second kind of SGWB could depend on the detector considered, since with larger sensitivities it would be possible to resolve more individual sources and to reduce the amplitude of the moments of the distribution of the background.

As we will show in Section 1.3, it is useful to characterize the SGWB in the frequency domain, by Fourier transforming the incoming signal in time. According to the standard plane-wave expansion [99], we can write[4] the SGWB as

$$h_{ij}(t,\mathbf{x}) = \int_{-\infty}^{+\infty} \mathrm{d}f \int \mathrm{d}\hat{n} \sum_{\alpha} h_{\alpha}(\hat{n},f) e^{\alpha}_{ij}(\hat{n}) e^{-2\pi i f(t-\hat{n}\cdot\mathbf{x})}\,, \tag{1.38}$$

where $\hat{n}$ is the direction of observation, $e^{\alpha}_{ij}(\hat{n})$ is the polarization tensor of the GWs in the direction of observation $\hat{n}$ for the polarization α, while h_{α} is the (stochastic) amplitude of the GW background that we are typically interested in. In the most general scenario, to fully characterize the PDF of the SGWB, it is necessary to know an infinite number of moments of the distribution, defined in Eq. (1.31). In Fourier space, these moments are univocally related to the M-point correlators

$$\left\langle \prod_{u=1}^{M} h_{\alpha_u}(\hat{n}_u, f_u) \right\rangle\,, \tag{1.39}$$

with M that goes from one to infinity. In most of the cases of interest, it is possible to assume that the amplitude of the SGWB is a Gaussian random variable with zero mean and covariance given by

$$\left\langle h_{\alpha}(\hat{n},f) h^{*}_{\alpha'}(\hat{n}',f') \right\rangle \equiv \mathcal{C}_{h}^{\alpha\alpha'}(\hat{n},f;\hat{n}',f')\,. \tag{1.40}$$

In Sections 1.4.1 and 1.4.2, we show that the Gaussian approximation for the SGWB is almost always valid, and we specify the limits in which the Gaussian limit does not hold. For example, if the source of the SGWB keeps track of some primordial non-Gaussianity, the statistics of the background could be more complicated. In the case of an AGWB generated by the superposition of many unresolved GWs, the Gaussian limit is guaranteed by the fact that the number of discrete events which source the AGWB is very large and it is possible to apply the Central Limit Theorem (CLT), finding that $\mathcal{P}[h_{ij}]$ approaches a Gaussian distribution. Another assumption that is usually done in the SGWB context is that the stochastic background is stationary, which means that its statistical properties are invariant under the time shift $t \to t+\tau$. This assumption is motivated by the fact that the timescales over which the correlators of h_{ij} could change are much larger than

[4] With a little abuse of notation, we refer to h in real space and in Fourier space with the same symbol, writing explicitly the dependence of h case by case.

the times over which observations are performed. For instance, as we will see in further sections, GWs propagate through an expanding Universe, which means that the energy density of stochastic backgrounds decreases with time. However, the characteristic time of the evolution of the Universe, given in terms of the Hubble constant at the present epoch by $\tau_0 \equiv 1/H_0 \approx 5 \times 10^{10}\,\mathrm{yr}$, is much larger that the duration of our observations, $T_{\mathrm{obs}} \approx 1 - 10\,\mathrm{yr}$. Therefore it is possible to assume that the SGWB is stationary. The stationarity condition is equivalent to say that the distribution of $h_{ij}(t, \mathbf{x})$ and $h_{kl}(t', \mathbf{x}')$ should depend only on $|t - t'|$, which is equivalent, in the simplified case of a Gaussian background, to the condition

$$\mathcal{C}_h^{\alpha\alpha'}(\hat{n}, f; \hat{n}', f') \sim \delta(f - f')\,. \tag{1.41}$$

Furthermore, it is reasonable to assume that the GWs produced in the points $(t, t\hat{n})$ and $(t', t\hat{n}')$ are uncorrelated, which implies that

$$\mathcal{C}_h^{\alpha\alpha'}(\hat{n}, f; \hat{n}', f') \sim \delta(\hat{n} - \hat{n}')\,. \tag{1.42}$$

Any violation of this relation would imply that statistical isotropy is broken, generating a coupling between different frequencies that should be studied in a different framework w.r.t. the one introduced here. Since statistical isotropy is conserved for all the cosmological and astrophysical sources of stochastic backgrounds considered in this Thesis, from now on we will use just Eq. (1.42) as a condition on the covariance between two GWs from different directions in the sky. Under these assumptions, it is possible to connect the two-point correlation functions for different polarizations to the Stokes parameters I, V, Q and U, used, for example, in the CMB context [116]. They represent the intensity, the circular polarization and the two orthogonal modes of linear polarization respectively. In the $+$, $\times$ polarization basis, defined in detail in Appendix C.1, we get the following relations

$$\begin{aligned}
\langle h_+(\hat{n}, f)\, h_+^*(\hat{n}', f')\rangle \equiv& \frac{\delta(f - f')\delta(\hat{n} - \hat{n}')}{4\pi} \frac{S_I(\hat{n}, f) + S_Q(\hat{n}, f)}{2}\,,\\
\langle h_+(\hat{n}, f)\, h_\times^*(\hat{n}', f')\rangle \equiv& \frac{\delta(f - f')\delta(\hat{n} - \hat{n}')}{4\pi} \frac{-iS_V(\hat{n}, f) + S_U(\hat{n}, f)}{2}\,,\\
\langle h_\times(\hat{n}, f)\, h_+^*(\hat{n}', f')\rangle \equiv& \frac{\delta(f - f')\delta(\hat{n} - \hat{n}')}{4\pi} \frac{iS_V(\hat{n}, f) + S_U(\hat{n}, f)}{2}\,,\\
\langle h_\times(\hat{n}, f)\, h_\times^*(\hat{n}', f')\rangle \equiv& \frac{\delta(f - f')\delta(\hat{n} - \hat{n}')}{4\pi} \frac{S_I(\hat{n}, f) - S_Q(\hat{n}, f)}{2}\,.
\end{aligned} \tag{1.43}$$

In this Thesis, we will rescale the Stokes parameters, characterizing the two-point correlation function of the amplitudes of stochastic backgrounds in terms of the adimensional parameters

$$\Omega_{\mathrm{SGWB}}^{\alpha}(\hat{n}, f) \equiv \frac{4\pi^2 f^3}{3H_0^2} S_\alpha(\hat{n}, f)\,, \tag{1.44}$$

where H_0 is the Hubble factor at the present time. These parameters are equivalent to the energy density (associated to the Stokes parameter α) per logarithmic frequency, normalized to the critical energy density of the Universe today,

$$\Omega_{\mathrm{SGWB}}^{\alpha}(\hat{n}, f) = \frac{1}{\rho_{\mathrm{crit}}} \frac{\mathrm{d}\rho_{\mathrm{SGWB}}^{\alpha}}{\mathrm{d}\ln f}(\hat{n}, f)\,, \tag{1.45}$$

with

$$\rho_{\rm crit} \equiv \frac{3}{8\pi G} H_0^2 \,. \tag{1.46}$$

In the case of unpolarized backgrounds, $\Omega^{\alpha}_{\rm SGWB} = 0$ for $\alpha \neq I$. The dependence of the expectation value of the covariance of h on the direction of observation implies that the stochastic background is not isotropic and that the energy density could change for GWs propagating in different directions in the sky. The main target of this Thesis is the detailed discussion of the angular dependence of the GW signals for different polarization states, showing that deviations from statistical homogeneity and isotropy would carry important physical information that could be useful to discriminate between stochastic backgrounds and to gain a deeper understanding of the large-scale perturbations of the Universe. The violation of statistical isotropy could be large or small, depending on the mechanism that generated it. More formally, we define the homogeneous and isotropic contribution to the SGWB (the monopole) as

$$\bar{\Omega}^{\alpha}_{\rm SGWB}(f) \equiv \frac{1}{4\pi} \int {\rm d}\hat{n}\, \Omega^{\alpha}_{\rm SGWB}(\hat{n}, f) \,, \tag{1.47}$$

where the frequency dependence of the monopole could be encoded in the form of a tilt defined by

$$n_{\rm gwb}(f) \equiv \frac{\partial \ln \bar{\Omega}^{\alpha}_{\rm SGWB}(f)}{\partial \ln f} \,. \tag{1.48}$$

We describe the fluctuations in different directions in the sky with

$$\delta^{\alpha}_{\rm SGWB}(\hat{n}, f) \equiv \frac{\Omega^{\alpha}_{\rm SGWB}(\hat{n}, f) - \bar{\Omega}^{\alpha}_{\rm SGWB}(f)}{\bar{\Omega}^{\alpha}_{\rm SGWB}(f)} \,. \tag{1.49}$$

When the amount of anisotropy is very small, as it is the case of cosmological backgrounds [117, 38, 39, 40, 3] or of the astrophysical background generate by BBH, BNS and BHNS [74, 75], the relative overdensity of GWs assumes values in the range $10^{-2} - 10^{-5}$, depending on the properties of the source [1]. On the other hand, it is possible that the dominant contribution to the background is anisotropic, as it happens for the signals emitted by compact galactic binaries which comes just from the Milky Way and not from the whole celestial sphere [118, 119, 120]. In the next sections we will enter more into the detail, discussing different sources of stochastic backgrounds, showing that in most of the cases the isotropy is broken just in a soft way.

The averages introduced in Eqs. (1.31), (1.40), (1.43) represent ensemble averages, which correspond to averages over an infinite number of realizations of the system. Even if it is not possible to compute exactly these expectation values, because we do not have access to all the possible realizations of the system, it is still achievable to define an unbiased estimator for the energy density of SGWBs, by making use of the ergodic hypothesis. The ergodic hypothesis states that in a sufficiently long period of time a system explores all the phase space, with the amount of time spent in a given point proportional to the PDF associated to such a configuration [121]. This implies that we could estimate the expectation values of the ensemble average by using temporal averages, having a clear connection between the theoretical correlators we are interested in and the quantities that can be measured at GW detectors.

1.3 Detectability of isotropic stochastic backgrounds

Over the last few decades, numerous experiments have been proposed to detect stochastic backgrounds, utilizing various techniques to constrain the amplitude of SGWBs at different frequencies. The stochastic backgrounds of cosmological origin, characterized by the longest wavelengths accessible, have been subject to constraints by the Planck collaboration [122, 123, 34, 124], which looked for a contribution to the B-mode of the polarization of the CMB due to the CGWB [125, 116, 126]. These observations have been able to put only an upper bound on the tensor-to-scalar perturbation ratio, or, equivalently, to the amplitude of the tensor perturbations, around the scale $10^{-2}\,\mathrm{Mpc}^{-1}$, which corresponds to frequencies of the order $10^{-17}\,\mathrm{Hz}$. The upper limit obtained by combining *Planck* and BICEP/Keck[127] is $r < 0.032$ at 95% CL [128]. SGWBs with frequencies in the nHz band can be probed by pulsar timing arrays (PTA) experiments, which look for variations in the orbital periods of many pulsars due to the presence of a SGWB. It is known indeed that pulsars are expected to exhibit highly regular spin periods, emitting subsequent pulses at regular times. Thus any GW that perturbs the propagation of the signals between the emitters and the observer would generate time residuals in the pulses that could be correlated to get information about the waves [129, 130, 131]. Recently, NANOGrav [132] found a strong evidence for a stochastic process modeled as a power law in frequency [133], which only few months ago, thanks to the joint effort of the PTA collaborations NANOGrav, EPTA/InPTA, PPTA, and CPTA have been confirmed to correspond to a SGWB [9, 10, 11, 12]. The amplitude of the background has been estimated to be of the order of 10^{-8} around $10^{-8}\,\mathrm{Hz}$, see Eqs. (1.91), (1.92) for more details. In the past years, GW observations did non focus only on the monopole of SGWBs, but also on the anisotropies of these signals. For example, the LVK collaboration found the maximum value of the angular power spectrum of SGWB between 20 and 1726 Hz. The most recent upper bound given by terrestrial detectors is $C_\ell \lesssim 3.6$ for $1 \leq \ell \leq 4$ and $n_{\mathrm{gwb}} = 2/3$ [134]. Searches for anisotropic SGWBs have been done recently also at PTA, finding $C_\ell \lesssim 10^{-2} - 10^{-1}$ in the nHz band [135]. As we will see in the next chapters, these bounds are few orders of magnitude larger than the anisotropies expected for cosmological and astrophysical backgrounds, therefore the most promising candidate to provide information about the sky maps of SGWBs are the ground-based interferometers ET [13], CE [14] and the space-based missions LISA [15], BBO [17] and DECIGO [18]. In the next sections, we will discuss the main techniques adopted in GW interferometry to detect isotropic SGWBs, discussing also the specifics of these future ground- and space-based interferometers.

1.3.1 Response of interferometers to the signal

In Section 1.1.2, we have defined the GWs as small perturbations of the metric with high frequency, $h_{ij}(t, \mathbf{x})$. It is therefore possible to investigate the presence of GWs in a given region of space by looking at geodesic deviations w.r.t. the case in which the background geometry is unperturbed. The data can be written as the sum of the signals, which is proportional to the amplitude of the GW, plus some noise which depends on the specifics

of the interferometers under consideration,

$$d_A(t) = \int \mathrm{d}\hat{n}\, D_A^{ij}(t)\, h_{ij}(t,\hat{n}) + n_A(t)\,, \tag{1.50}$$

where we have introduced the detector tensor D_A^{ij} that can be obtained by computing the response of the instrument to a GW passing through it or, equivalently, by computing the effect induced by a GW on the observable [99]. The detector tensor takes into account the length of the arms of the detector, the orientation and the type of interferometry used. We compute it for a generic network of interferometers in Appendix C.2. The noise of the detector is in general a random variable that can be characterized by its PDF $\mathcal{P}[n]$, as the stochastic background, and its PDF could be non-Gaussian and non-stationary [99] in some particular cases that will be mentioned later on. In this work we assume that $n(t)$ is stationary and Gaussian, with zero mean, thus fully characterized by its covariance. As mentioned in the previous section, in GW data analysis we divide the data stream in many time segments of duration $T_{\rm seg}$ and we perform the Fourier transform of the signal in this time interval, obtaining a resolution $\Delta f \equiv 1/T_{\rm seg}$. For a discrete time interval, the Fourier transform of a variable $x(t)$ is defined by

$$x(f) \equiv \int_{t-T_{\rm seg}/2}^{t+T_{\rm seg}/2} \mathrm{d}\tilde{t}\, e^{-2\pi i f \tilde{t}}\, x(t)\,, \tag{1.51}$$

which implies that the Dirac delta does not diverge in zero, $\delta(0) = T_{\rm seg}$. The noise is characterized by its power spectral density (PSD)[5], defined by

$$\left\langle n_A(f)\, n_B^*(f')\right\rangle \equiv \frac{1}{2}\delta(f-f')N_{AB}(f)\,. \tag{1.52}$$

As we will discuss in Section 1.3.3, the noises between two different interferometers could be correlated, as it happens for instance in LISA [15]. In 1.3.3 we will also discuss the PSD of the noise for LVK, ET, CE, LISA, BBO and DECIGO, providing analytical formulas for computing them and discussing the source of noise. The Fourier transform of the data taken at interferometers in a time segment of duration $T_{\rm seg}$ is

$$d_A(f) = \int \mathrm{d}\hat{n} \sum_\alpha F_A^\alpha(\hat{n},f) h_\alpha(\hat{n},f) + n_A(f)\,, \tag{1.53}$$

where the detector pattern function for the polarization α is defined by

$$F_A^\alpha(\hat{n},f) \equiv d_A^{ij}(\hat{n},f)\, e_{ij}^\alpha(\hat{n})\,, \tag{1.54}$$

with $d_A^{ij}(\hat{n},f)$ that depends on the detector tensor and on the transfer function of the signal at the interferometers. More details on the computation of d_A^{ij} can be found in Appendix C.2.

[5] In the literature the strain sensitivity $\sqrt{N_{AB}(f)}$ is also used, but in this Thesis we will consider only the PSD.

1.3.2 Estimator of an homogeneous and isotropic background

In this section, we discuss the detectability of the Stokes parameters of a homogeneous and isotropic stochastic background, characterized by $\bar{\Omega}^{\alpha}_{\rm SGWB}(f)$, defined in Eqs. (1.43), (1.44) and (1.47). In order to quantify the capability of measuring a SGWB, we would like to define some estimators for the Stokes parameters, denoted by $\hat{\bar{\Omega}}^{\alpha}_{\rm SGWB}(f)$, to compute the error bars associated to them and to evaluate the signal-to-noise ratio (SNR). The SNR is directly related to the significance that the data observed at interferometers are not generated by random fluctuations of the noise, but by a SGWB. The choice of the SNR to claim a detection depends on the significance required in rejecting a false alarm; for instance, in the context of resolved GW sources, the SNR should be greater than the the value that gives a false alarm probability equal to 2.5×10^{-15} [99]. In general, we would like to estimate together the amplitude of the background and its scaling with the frequency, but in this first example we will work under the hypothesis that we have a full knowledge of the frequency shape of the background and we are interested in constraining just its amplitude. The Stokes parameters of the SGWB in this case can be written then as a product of a frequency template, that encodes the scaling of the SGWB with the frequency, and of the amplitude we are interested in,

$$\bar{\Omega}^{\alpha}_{\rm SGWB}(f) = A_{\alpha}\, \mathcal{E}^{\alpha}_{p}(f)\,, \tag{1.55}$$

where p identifies the pivot frequency $f_{\rm p}$ at which we estimate the amplitude A_{α}. Since the energy density of the CGWB is quadratic in the metric perturbations h_{ij}, it is natural to build an estimator which is quadratic in the data. To understand better this, we look at the following expectation values of the data,

$$\begin{aligned} \langle d_A(f) \rangle =& 0\,, \\ \left\langle d_A(f) d^*_B(f') \right\rangle =& \int \mathrm{d}\hat{n} \sum_{\alpha,\beta} F^{\alpha}_A(\hat{n}, f) F^{\beta\,*}_B(\hat{n}, f) \left\langle h_{\alpha}(f) h^*_{\beta}(f) \right\rangle + \frac{1}{2} N_{AB}(f) \delta(f - f') \end{aligned} \tag{1.56}$$

and we note that the second expression contains the amplitudes A_{α} we want to constrain. By using the relations given in Eq. (1.43) and exploiting the fact that the background is homogeneous and isotropic, it is possible to recast the two-point correlation function in the following way,

$$\left\langle d_A(f) d^*_B(f') \right\rangle = \left[\frac{3H_0^2}{4\pi^2 f^3} \sum_{\alpha} \gamma^{\alpha}_{AB}(f) A_{\alpha}\, \mathcal{E}^{\alpha}_{p}(f) + \frac{1}{2} N_{AB}(f) \right] \delta(f - f')\,, \tag{1.57}$$

where we have defined the overlap reduction functions (ORFs)

$$\begin{aligned}
\gamma^I_{AB}(f) &\equiv \int \frac{\mathrm{d}\hat{n}}{8\pi} \left(F^+_A F^{+\,*}_B + F^\times_A F^{\times\,*}_B\right) , \\
\gamma^V_{AB}(f) &\equiv \int \frac{\mathrm{d}\hat{n}}{8\pi}\, i\, \left(F^+_A F^{\times\,*}_B - F^\times_A F^{+\,*}_B\right) , \\
\gamma^U_{AB}(f) &\equiv \int \frac{\mathrm{d}\hat{n}}{8\pi} \left(F^+_A F^{\times\,*}_B + F^\times_A F^{+\,*}_B\right) , \\
\gamma^Q_{AB}(f) &\equiv \int \frac{\mathrm{d}\hat{n}}{8\pi}\, \left(F^+_A F^{+\,*}_B - F^\times_A F^{\times\,*}_B\right) .
\end{aligned} \tag{1.58}$$

The most natural estimator of the amplitude of the Stokes parameters of the SGWB at the pivot frequency f_p is therefore a linear combination (in frequency and in the detector space) of objects quadratic in the data,

$$\hat{A}_\alpha \equiv \int \mathrm{d}f \sum_{A,B} d_A(f) E^\alpha_{AB}(f) d^*_B(f) - b^\alpha \,, \tag{1.59}$$

where the bias b^α and the weights E^α_{AB} have to be determined by requiring that the estimator is unbiased and by minimizing its covariance. The unbiasedness condition is

$$\left\langle \hat{A}_\alpha \right\rangle = A_\alpha \,, \tag{1.60}$$

which gives the following constraints on the bias and on the weights,

$$\begin{aligned}
b^\alpha &= \frac{T_{\rm seg}}{2} \int \mathrm{d}f \sum_{A,B} E^\alpha_{AB}(f)\, N_{AB}(f) \,, \\
T_{\rm seg} \int \mathrm{d}f\, \frac{3H_0^2}{4\pi^2 f^3} \sum_{A,B} \gamma^\alpha_{AB}(f) E^\alpha_{AB}(f) \mathcal{E}_p(f) &= 1 \,,
\end{aligned} \tag{1.61}$$

where $T_{\rm seg}$ comes from the Dirac delta evaluated in zero. For simplicity we work in the case in which the SGWB could have just one non-vanishing Stokes parameter, thus there is no contamination of different polarizations in the maps. The covariance for the estimator we have defined is then computed by using

$$\begin{aligned}
\mathcal{C}_{\hat{A}_\alpha} &\equiv \left\langle \left(\hat{A}_\alpha - A_\alpha\right)^2 \right\rangle = \left\langle \left(\hat{A}_\alpha\right)^2 \right\rangle - (A_\alpha)^2 = \\
&= \sum_{A,B,C,D} \left\langle \int \mathrm{d}f\, \mathrm{d}f' E^\alpha_{AB}(f)\, E^\alpha_{CD}(f')\, d_A(f) d^*_B(f) d_C(f') d^*_D(f') \right\rangle - (A_\alpha)^2 \,.
\end{aligned} \tag{1.62}$$

The four-point correlation function in the data can be decomposed, in the Gaussian limit, into two-point correlation functions, for all the three possible combinations. It is immediate to see that the $(A,B)-(C,D)$ combination cancels with the $(A_\alpha)^2$ term and that the

$(A,D)-(B,C)$ combination is equivalent to the $(A,C)-(B,D)$, because of the symmetry of the weights, therefore we get

$$\begin{aligned}\mathcal{C}_{\hat{A}_\alpha} = 2\,T_{\rm seg}\int \mathrm{d}f\left(\frac{3H_0^2}{4\pi^2 f^3}\right)^2 \sum_{A,B,C,D} E^\alpha_{AB}(f)E^\alpha_{CD}(f) \\ \Big[\gamma^\alpha_{AD}(f)\gamma^\alpha_{CD}(f)\,(A_\alpha)^2\,\mathcal{E}_p(f)\mathcal{E}_p(f) \\ +\frac{1}{4}N_{AD}(f)N_{BC}(f)\Big]\,.\end{aligned} \tag{1.63}$$

In most of the cases considered, it is possible to work in the low-SNR regime, in which $A_\alpha \ll N_{AB}(f)$, therefore we can neglect the terms proportional to the amplitude of the signal in the computation of the covariance,

$$\mathcal{C}_{\hat{A}_\alpha} = 2\,T_{\rm seg}\int \mathrm{d}f\left(\frac{3H_0^2}{4\pi^2 f^3}\right)^2 \sum_{A,B,C,D} E^\alpha_{AB}(f)E^\alpha_{CD}(f)\frac{1}{4}N_{AD}(f)N_{BC}(f)\,. \tag{1.64}$$

Note however that the contribution to the covariance provided by the monopole of the SGWB in general is not negligible and, as shown in [136, 137], it corresponds to an intrinsic variance term, which could play a crucial role in the estimate of the anisotropies of the SGWB. The weights E^α_{AB} are computed by minimizing the covariance, under the condition that the estimator is unbiased, Eq. (1.61). The simplest way to do this is by introducing a Lagrangian function

$$\mathcal{L} = \mathcal{C}_{\hat{A}_\alpha} + \lambda\left[T_{\rm seg}\int \mathrm{d}f\,\frac{3H_0^2}{4\pi^2 f^3}\sum_{A,B}\gamma^\alpha_{AB}(f)E^\alpha_{AB}(f)\mathcal{E}_p(f) - 1\right]\,, \tag{1.65}$$

and by minimizing it w.r.t. the weights and the Lagrange multiplier,

$$\frac{\delta}{\delta E^\alpha_{AB}(f)}\mathcal{L} = \frac{\partial}{\partial\lambda}\mathcal{L} = 0\,. \tag{1.66}$$

The derivative w.r.t. λ gives the unbiasedness condition on $E^\alpha_{AB}(f)$, while the functional derivative w.r.t. the weights gives

$$\left(\frac{3H_0^2}{4\pi^2 f^3}\right)^2\frac{1}{4}\sum_{C,D}E^\alpha_{CD}(f)N_{AD}(f)N_{CB}(f) + \lambda\frac{3H_0^2}{4\pi^2 f^3}\,\gamma^\alpha_{AB}(f)\mathcal{E}_p(f) = 0\,. \tag{1.67}$$

We can isolate in this expression the contribution coming from the weights, by using the inverse matrix of the noise PSD,

$$\frac{3H_0^2}{4\pi^2 f^3}\mathcal{E}_p(f)\frac{1}{4}E^\alpha_{AB}(f) + \lambda\,[\mathcal{E}_p(f)]^2\sum_{C,D}N^{-1}_{AC}(f)\gamma^\alpha_{CD}(f)N^{-1}_{DB}(f) = 0\,. \tag{1.68}$$

By multiplying this equation by $T_{\rm seg}\,\gamma^{\alpha}_{AB}(f)$, summing over A, B and integrating over the frequency we get

$$\lambda = -\frac{1}{4T_{\rm seg}}\frac{1}{\int \mathrm{d}f\,[\mathcal{E}_p(f)]^2\,\sum_{A,B,C,D}\gamma^{\alpha}_{AB}(f)N^{-1}_{BC}(f)\gamma^{\alpha}_{CD}(f)N^{-1}_{DA}(f)}\,. \tag{1.69}$$

The weights are then given by

$$E^{\alpha}_{AB}(f) = \frac{1}{T_{\rm seg}}\frac{4\pi^2 f^3}{3H_0^2}\mathcal{E}_p(f)\frac{\sum_{C,D}N^{-1}_{AC}(f)\gamma^{\alpha}_{CD}(f)N^{-1}_{DB}(f)}{\int \mathrm{d}f\,[\mathcal{E}_p(f)]^2\,\sum_{A,B,C,D}\gamma^{\alpha}_{AB}(f)N^{-1}_{BC}(f)\gamma^{\alpha}_{CD}(f)N^{-1}_{DA}(f)}\,. \tag{1.70}$$

The covariance of the estimator can be computed by plugging (1.70) into (1.63), finding

$$\mathcal{C}_{\hat{A}_\alpha} = \frac{1}{T_{\rm seg}}\frac{2}{\int \mathrm{d}f\,[\mathcal{E}_p(f)]^2\,\sum_{A,B,C,D}\gamma^{\alpha}_{AB}(f)N^{-1}_{BC}(f)\gamma^{\alpha}_{CD}(f)N^{-1}_{DA}(f)}\,. \tag{1.71}$$

The result shows that the covariance in a single time segment is inversely proportional to the duration of the time segment. Since the measurements in several time segments are independent in the case of a stationary background, the covariance in an observing time $T_{\rm obs}$ will be just

$$\mathcal{C}_{\hat{A}_\alpha} = \frac{1}{T_{\rm obs}}\frac{2}{\int \mathrm{d}f\,[\mathcal{E}_p(f)]^2\,\sum_{A,B,C,D}\gamma^{\alpha}_{AB}(f)N^{-1}_{BC}(f)\gamma^{\alpha}_{CD}(f)N^{-1}_{DA}(f)}\,. \tag{1.72}$$

The SNR is defined by the ratio between the signal and the noise, thus we get

$$\mathrm{SNR} = \frac{\hat{A}_\alpha}{\sqrt{\mathcal{C}_{\hat{A}_\alpha}}}\,. \tag{1.73}$$

The value of the observed SNR depends on the realization of the signal and of the noise, that could be larger or smaller than their expected amplitudes, but, on averge, we expect that the SNR is equal to

$$\langle \mathrm{SNR}\rangle = \frac{\left\langle \hat{A}_\alpha \right\rangle}{\sqrt{\mathcal{C}_{\hat{A}_\alpha}}} = \frac{A_\alpha}{\sqrt{\mathcal{C}_{\hat{A}^\alpha}}}\,. \tag{1.74}$$

In this simple scenario, the SNR depends on the ORFs, on the PSD of the interferometers, on the observing time, on the amplitude of the signal and on $\mathcal{E}_p(f)$. In particular, we stress that the different scaling of the signal and of the noise in frequency, $\mathcal{E}_p(f)$ and $N_{AB}(f)/N_{AB}(f_p)$ respectively, allows to disentangle a tiny SGWB from a random noise that could be several orders of magnitude larger. This is possible because, thanks to the large number of frequencies accessible at interferometers, one could choose a filter on the data (the weights E^{α}_{AB}), to select just the components which vary with the frequency like $\mathcal{E}_p(f)$. This is a sort of generalization of the Internal Linear Combination (ILC) technique presented in [138, 139] and used to do component separation in the CMB context.

Since the quantity that represents the detectability of a homogeneous and isotropic SGWB is the average SNR computed in Eq. (1.74), it would be useful to give a pictorial representation of the sensitivity of a network of interferometers to an incoming signal. When $\mathcal{E}_p(f)$ is a power law of tilt $n_{\rm gwb}$, it is possible to construct the power-law sensitivity curve (PLS) [140], which contains all the information about the SNR. The PLS, defined here as $\bar{\Omega}^{\alpha\ \rm PLS}_{\rm SGWB}(f)$, is constructed in a way that it constitutes a threshold for the amplitude of a SGWB to get an SNR larger than $\rm SNR^{SGWB}_{thr}$ for an observing time $T_{\rm obs}$. More specifically, if we have that at some frequency f

$$\bar{\Omega}^{\alpha}_{\rm SGWB}(f) \geq \bar{\Omega}^{\alpha\ \rm PLS}_{\rm SGWB}(f) \tag{1.75}$$

then we have that for $T_{\rm obs}$

$$\rm SNR \geq SNR^{SGWB}_{thr}\,. \tag{1.76}$$

To construct the PLS of a detector network it is sufficient to do the following steps:

1. compute the amplitude $A^{\rm thr}_{\alpha}(n_{\rm gwb})$ that gives $\langle \rm SNR\rangle = \rm SNR^{SGWB}_{thr}$ for $T_{\rm obs}$ for different values of $n_{\rm gwb}(f)$. Typically we use $n_{\rm gwb} \in [-10, 10]$;

2. at each frequency find the tensor tilt $n^{\rm min}_{\rm gwb}(f)$ which minimizes the amplitude of the background,

$$n^{\rm min}_{\rm gwb}(f) = \log_{f/f_p}\left\{\frac{1}{A^{\rm thr}_{\alpha}(n_{\rm gwb})}\min\left[A^{\rm thr}_{\alpha}(n_{\rm gwb})(f/f_p)^{n_{\rm gwb}}\right]\right\}\,;$$

3. the PLS at the frequency f is equal to

$$\bar{\Omega}^{\alpha\ \rm PLS}_{\rm SGWB}(f) = A^{\rm thr}_{\alpha}\left(n^{\rm min}_{\rm gwb}(f)\right)\left(\frac{f}{f_p}\right)^{n^{\rm min}_{\rm gwb}(f)}\,. \tag{1.77}$$

The PLS is a particularly intuitive and useful graphical representation of the SNR, because it encodes automatically the constraints given by the integration over all the frequencies accesible to interferometers. A different way to quantify the detectability of SGWB is the sensitivity in a single bin,

$$\bar{\Omega}^{\alpha\ \rm SSB}_{\rm SGWB}(f) \equiv \frac{4\pi^2 f^3}{3H_0^2}\frac{1}{2}N_{AB}(f)\,, \tag{1.78}$$

which does not rely on template fitting and thus it provides less stringent upper bounds in the single bins. In Figure 1.1 we plot the PSD and the PLS for all the detectors considered in this work, for $\rm SNR^{SGWB}_{thr} = 1$ and $T_{\rm obs} = 1\,\rm yr$.

The analogous computation of the optimal estimator for an anisotropic SGWB will be done in Sections 8.3, 8.4 and 9.6.

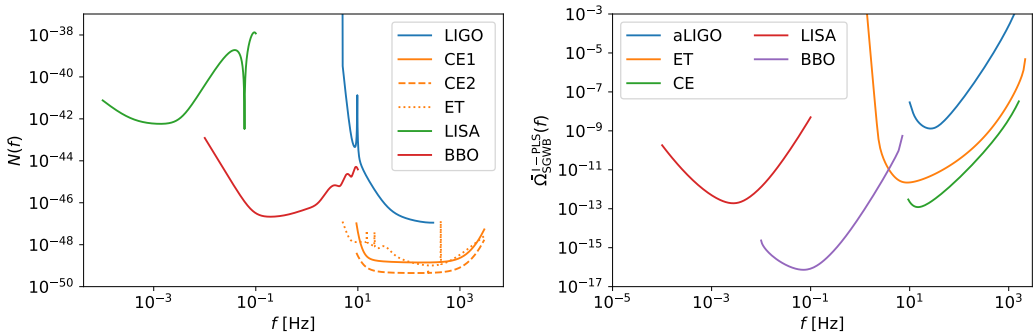

Figure 1.1: Plot of the PSD (left) and of the PLS (right) for different detectors.

1.3.3 GW Interferometers

Reference frames

The computation of the covariance of the optimal estimator for the amplitude of an isotropic SGWB found in Eq. (1.72) does not rely on the choice of the basis through which we characterize the orientation of the arms of the interferometers. In this section we will therefore introduce a coordinate system which will be used to describe univocally $\hat{n}$, $F_A^\alpha(\hat{n}, f)$ for all the networks of interferometers considered in this Thesis.

The positions of the objects in the celestial sphere have been evaluated in the heliocentric and ecliptic coordinate system, in which the Sun occupies the position $(0, 0, 0)$, $\hat{z}$ is perpendicular to the ecliptic plane and $\hat{x}$ points towards the vernal equinox. It is possible then to introduce the galactic longitude and latitude[6], which parametrize the position in the components parallel and perpendicular to the ecliptic plane respectively,

$$\mathbf{x} = r \begin{pmatrix} \cos(\vartheta)\cos(\varphi) & \cos(\vartheta)\sin(\varphi) & \sin(\vartheta) \end{pmatrix} . \tag{1.79}$$

Since we are considering sources very far from the Solar System, we assume that for any detector the direction of observation [7] coincides with

$$\hat{n} = \begin{pmatrix} \cos(\vartheta)\cos(\varphi) & \cos(\vartheta)\sin(\varphi) & \sin(\vartheta) \end{pmatrix} . \tag{1.80}$$

The position of the center of mass of the Earth orbiting around the Sun as a function of time is then just

$$\mathbf{x}_{\rm E}^{\rm com} = r_{\rm E}^{\rm com} \begin{pmatrix} \cos\left(\frac{2\pi}{T_{\rm E-S}} t\right) & \sin\left(\frac{2\pi}{T_{\rm E-S}} t\right) & 0 \end{pmatrix} , \tag{1.81}$$

with $T_{\rm E-S} = 1\,{\rm yr}$ and $R_{\rm Eart-Sun} \equiv 1\,{\rm AU} = 1.5 \times 10^8\,{\rm km} = 4.8 \times 10^{-6}\,{\rm pc}$. In Eq. (1.81), we have set to zero the eccentricity of the orbit of the revolution of the Earth around the Sun, since it provides negligible effects in the estimate of the anisotropies of SGWBs [141]. We describe the position of an object co-rotating with the Earth by a reference frame with

[6] By definition, the latitude is defined in the range $[-\pi/2, +\pi/2]$.

[7] With a little abuse of notation, the latitude ϑ defined here coincides with $\pi/2 - \theta$, where θ is the polar angle used in the rest of this Thesis.

the $z_{\rm E}$ axis oriented along the axis of Earth's rotation and we use as angular coordinates the declination δ_E and the right ascension α_E.

$$\mathbf{x}_{\rm E} = r_{\rm E} \begin{pmatrix} \cos(\vartheta_E)\cos(\alpha_E) & \cos(\delta_E)\sin(\alpha_E) & \sin(\delta_E) \end{pmatrix} . \tag{1.82}$$

Following [142], we connect the ecliptic coordinates to the equatorial coordinates by using

$$\begin{aligned} \sin\vartheta &= \sin(\delta_E)\cos(\epsilon_D) - \cos(\delta_E)\sin(\epsilon_D)\sin\left(\alpha_E - \alpha_{E,0} + \frac{2\pi}{T_{\rm E}}t\right) , \\ \cos(\varphi-\varphi_0) &= \cos\left(\alpha_E - \alpha_{E,0} + \frac{2\pi}{T_{\rm E}}t\right)\frac{\cos(\delta_E)}{\cos(\vartheta)} , \\ \sin(\varphi-\varphi_0) &= \sin(\delta_E)\sin(\epsilon_D) + \cos(\delta_E)\cos(\epsilon_D)\frac{\sin\left(\alpha_E - \alpha_{E,0} + \frac{2\pi}{T_{\rm E}}t\right)}{\cos(\vartheta)} , \end{aligned} \tag{1.83}$$

where we have used $T_{\rm E} = 1\,\mathrm{d}$. The angle ϵ_D is the obliquity of the ecliptic and, neglecting effects due to precession and nutation, it is roughly equal 23.4°. The angles φ_0, α_0 are fixed at a given epoch and represent just a normalization factor. For instance, in 1950 [142], $\varphi_0 = 32.93°$ and $\alpha_{E,0} = 282.86°$.

In the next sections, we list the main detector networks considered in this Thesis, mentioning all the specifics needed to evaluate the detectability of the anisotropies of SGWBs.

Einstein Telescope

ET is a proposed third-generation GW detector that will probably start collecting data in the middle of 2030s [13]. Thanks to an increase in the length of the arms and to new technologies, such as a cryogenic system to cool some of the main optics and new quantum technologies to reduce the fluctuations of the light [143, 13, 144], ET is expected to achieve a better sensitivity than at least one order of magnitude than the current ground-based interferometers LIGO, Virgo and KAGRA. The location of the ET could be in the Sos Enattos site in Sardinia or in the Meuse-Rhine region at the border of Germany, Belgium and the Netherlands [145]. In this work we will consider the case where ET is located in Sardinia, for which we take the following coordinates

$$\begin{pmatrix} \delta_E & \alpha_E \end{pmatrix} = \begin{pmatrix} 40°\,31' & 9°\,25' \end{pmatrix} . \tag{1.84}$$

Among the possible different configurations, we consider a triangular detector with 10 km arms [145], with ET-D sensitivity [146]. Although the PSD of the cross-correlation between two channels of ET has not been clarified, in this work we consider as an example $N_{XY} = -N_{XX}/2$.

Cosmic Explorer

As ET, CE is future third-generation GW detector, planned to start collecting data in the 2030s [147, 14]. Different number of L-shaped interferometers have been considered for

the CE, such as one single 40 km interferometer, one 20 km interferometer, combinations of two interferometers 40 or 20 km long. In this Thesis, we will consider one CE of 40 km, combined with a 20 km CE, located in Hanford and Livingston as the LIGO detectors. A more realistic choice for the 20 km interferometer would be Australia, but we expect that the choice of the location will not alter too much the results. The locations for the detectors in Hanford and Livingston are therefore

$$\begin{aligned}\left(\delta_E^{(H)} \quad \alpha_E^{(H)}\right) &= \left(46°24' \quad 119°24'\right) \,, \\ \left(\delta_E^{(L)} \quad \alpha_E^{(L)}\right) &= \left(30°33' \quad 90°46'\right) \,.\end{aligned} \tag{1.85}$$

The CE project will be divided in two stages. During the first one, it is expected to used the improved sensitivity of LIGO "A+", scaled up to a 40 km detector with improved sensitivity. In the second stage, new technologies will be used to reduce the quantum and the thermal noise of the interferometer. The sensitivity we have used for the two CE can be found in [146].

LISA

LISA is a future space-based interferometer that is scheduled to be launched in the early 2030s [15]. LISA will consists of three spacecrafts in an Earth-trailing heliocentric orbit, with a separation angle of $19-23°$ from the Earth (w.r.t. the Sun). In this work we consider this separation equal to $20°$, consistently with [148, 115, 149]. The three spacecraft are arranged in an equilateral triangular configuration, with a separation $L = 2.5 \times 10^6$ km. The plane containing this triangle will be tilted of $60°$ w.r.t. the ecliptic plane. The PSD has been computed by accounting for the presence of acceleration noise, which accounts for random displacements of the test masses, and the "Interferometry Metrology System" (IMS), which includes also the shot noise in the laser beams. The parametrization for these two terms can be found in [150, 151, 152, 148], and it depends on two parameters A, P,

$$\begin{aligned}P_{\rm acc}(f,A) =& A^2 \frac{\rm fm^2}{s^4 \rm Hz}\left[1+\left(\frac{0.4\,\rm mHz}{f}\right)^2\right]\left[1+\left(\frac{f}{8\,\rm mHz}\right)^2\right]\left(\frac{1}{2\pi f}\right)^4\left(\frac{2\pi f}{c}\right)^2 \,, \\ P_{\rm IMS}(f,P) =& P^2 \frac{\rm pm^2}{\rm Hz}\left[1+\left(\frac{2\rm mHz}{f}\right)^4\right]\left(\frac{2\pi f}{c}\right)^2 \,.\end{aligned} \tag{1.86}$$

The PSD of the noise, defined in Eq. (1.52), is evaluated for the auto- and cross-channel following [152, 148],

$$\begin{aligned}N_{XX}(f,A,P) =& 16\sin^2\left(\frac{2\pi f L}{c}\right)\left\{\left[3+\cos\left(\frac{4\pi f L}{c}\right)\right]P_{\rm acc}(f,A)+P_{\rm IMS}(f,P)\right\} \,, \\ N_{XY}(f,A,P) =& -8\sin^2\left(\frac{2\pi f L}{c}\right)\cos\left(\frac{2\pi f L}{c}\right)+\left[4P_{\rm acc}(f,A)+P_{\rm IMS}(f,P)\right] \,.\end{aligned} \tag{1.87}$$

In this Thesis we adopt $P = 15$ and $A = 3$.

DECIGO

DECIGO consists of four clusters observatories placed in heliocentric orbit. Each of them is made of three spacecrafts, as LISA, which form three interferometers. The spacecrafts are separated by 60° in the heliocentric plane, while the fourth one is placed in the same location of one of them, forming a Star of David configuration [153, 18, 154]. The arm length is expected to be $L = 10^3\,\mathrm{km}$ and the sensitivity should increase by an order of magnitude w.r.t. LISA around 0.1 Hz. The PSD of DECIGO is given following [155, 156, 157], including the acceleration and IMS noise in analogy with LISA,

$$\begin{aligned} P_{\rm acc}(f) =& 6.2\times 10^{-49}\,\frac{1}{s^4\,\mathrm{Hz}}\left(\frac{1}{2\pi f}\right)^4, \\ P_{\rm IMS}(f) =& 4.48\times 10^{-48}\,\frac{1}{\mathrm{Hz}}\left(\frac{7.5\,\mathrm{Hz}}{f}\right)^2\frac{1}{1+\left(\frac{7.5\,\mathrm{Hz}}{f}\right)^2}. \end{aligned} \tag{1.88}$$

The PSD of the auto- and cross-channels are computed by plugging $P_{\rm acc}$ and $P_{\rm IMS}$ in Eq. (1.87).

Big Bang Observer

BBO is a mission similar to DECIGO, with small differences in the sensitivity and in the design. It is constituted by the same configuration of interferometers in clusters as DECIGO, but with length of the arm equal to $5\times 10^4\,\mathrm{km}$ [158, 159, 17, 140]. In the same fashion of DECIGO, the acceleration and the IMS noise of BBO are

$$\begin{aligned} P_{\rm acc}(f) =& 6.0\times 10^{-49}\,\frac{1}{s^4\,\mathrm{Hz}}\left(\frac{1}{2\pi f}\right)^4, \\ P_{\rm IMS}(f) =& 5.8\times 10^{-48}\,\frac{1}{\mathrm{Hz}}\left(\frac{0.15\,\mathrm{Hz}}{f}\right)^2\frac{1}{1+\left(\frac{0.15\,\mathrm{Hz}}{f}\right)^2}. \end{aligned} \tag{1.89}$$

1.4 Sources of SGWB

1.4.1 Primordial sources

Gravitational interactions decouple at the Planck scale [37], $T^{\rm GW}_{\rm dec}\sim 1/M_{\rm Pl}\approx 10^{19}\,\mathrm{GeV}$, therefore the scattering of GWs can be considered an extremely subdominant process, since we consider the generation (and the propagation) of SGWBs during or after the inflationary epoch, which took place at energy scales $T_{\rm infl}\lesssim 10^{16}\,\mathrm{GeV}$ [160, 161, 34]. Since the CGWB is generated by the superposition of many non-interacting waves, it keeps track of the features of the mechanisms that sourced it at early times. For other particle species, like photon and neutrino, the energy spectrum is thermal, because of the tight electromagnetic and weak interactions that were present from production until decoupling of these two particle species [42]. This peculiarity of the CGWB strongly motivates future

GW experiments to look for it, because it would provide a unique probe of the physics operating at very high energy scales, which are not reachable to other signals, because of the tight coupling between the Standard Model particles. In this Thesis, we say that a background is cosmological if it has been produced in the early Universe, before the decoupling of the weak interactions that occurs at $T^{\nu}_{\rm dec} \approx 1\,\text{MeV}$. In the most recent reviews [162, 113, 163, 114] (see also [164, 165, 166]), a plethora of primordial sources has been considered.

Inflationary CGWB

The most important cosmological background is the one produced by quantum fluctuations of the metric during inflation. During this hypothetical early stage of accelerated expansion of the Universe, the fluctuations of the metric, generated by the quantum nature of gravity, are enhanced [167] and they could produce a signal observable by future ground- and space-based interferometers. The amplitude and the shape in frequency of this primordial signal depends on the model of inflation considered. For instance, the energy scale of the background depends on the potential of the inflaton field and on the number of fields which contributed to the dynamics of the background during inflation [113]. The computation of the expected monopole and inhomogeneities of inflationary CGWBs will be done in Sections 2.3.3 and 4.2 respectively.

Scalar Induced GWs

Another relevant mechanism which could source GWs in the early Universe is the classical production of a stochastic background by scalar perturbations. Scalar Induced GWs (SIGWs) could be generated when scalar fields have a non-negligible anisotropic stress which acts as a source in the transverse-traceless tensor part of the Einstein equations [168, 169, 170, 171, 172, 173, 174]. This classical production could take place during inflation or during the radiation-dominated era, approximately around the time at which the scalar perturbations re-enter the causal horizon. More specifically, scalar perturbations which re-enter the horizon during the radiation epoch could source CGWBs in the frequency band of interferometers. Although the SIGWs in the case of single-field inflation [8] are suppressed [174], several different inflationary models could amplify more the scalar perturbations at small scales, generating a CGWB with larger energy densities. Typical examples are given by the curvaton scenario [175], in which an additional field, the curvaton, does not alter the dynamics of the background during inflation, but modifies the amplitude of the perturbations at small scales, increasing the production of GWs [176, 177, 178]. Other possibilities are given, for instance, by the presence of spectator fields during inflation [179, 180, 181] or by the coupling of the inflaton with a spectator scalar field [182]. In this Thesis we will focus on secondary GWs induced by scalar perturbations which exhibit a peak in the power spectrum at small scales [173, 23], which could enhance also the formation of PBHs in the ealy Universe. The computation of the production of the

[8] To obtain these constraints, the estimate of the scalar power spectrum obtained at CMB scales are applied to the scalar power spectrum at interferometric scales, which differ of 20 orders of magnitude.

monopole and the inhomogeneities of this kind of background will be done in detail in Sections 3.4.2, 4.3.

Particle Production

When the inflaton is coupled to other scalar or gauge fields, it is possible that the inflaton energy is transferred to the other fields, which could provide a large amount of anisotropic stress that sources GWs. This could happen for instance during axion inflation, when the axion is coupled to a vector boson [24, 76, 77, 78, 79]. Interesting aspects of the GWs generated during axion inflation are the circular polarization and the blue tilt of the spectrum. These features could increase the possibility of a dection of this CGWB by future interferometers.

Phase Transition

In many extensions of the Standard Model, it is possible that second-order phase transitions (PTs) take place. In these transitions, the configuration of minimal energy changes with the temperature, therefore it is possible that it is forbidden to go from the false (UV) to the true vacuum in a smooth way. This process leads to the nucleation of bubbles [183], which could produce GWs through different processes [20, 184, 145], such as the collision of the bubbles [185, 186, 187, 188, 189], the sound waves generated by the field which undergoes through the PT [190, 191, 192], or turbolence phenomena [193, 194]. We will comment in more detail the features of the spectrum from PT in Section 3.4.3.

1.4.2 Astrophysical sources

The astrophysical background is generated by the superposition of many unresolved astrophysical sources [47, 48]. An unresolved signal corresponds to a GW that cannot be associated with sufficiently high significance to a deterministic waveform, which means that the signal-to-noise ratio (or the Bayes factor defined in Eq. (1.36)) is smaller (or larger) than a certain threshold. The choice of such a threshold depends on the information we would like to extract from the resolved GWs, for instance it could depend on the accuracy required in the estimate of the parameters that characterize the binary. In Section 7.1.1 we will specify the threshold chosen for the purposes of this work. A stochastic background could also be generated by astrophysical sources which emit GWs with large amplitudes, but which also overlap in time in such a way that it is not possible to distinguish with sufficient significance the single components [195, 196, 197]. When we talk about astrophysical sources, we refer to any kind of process that occur in the late Universe, $z \lesssim 20$, after the first population of star formed [198, 199, 200]. Among the several astrophysical sources of GWs there are rotating neutron stars [49, 50], core collapse supernovae [51, 52] or massive stars [53, 54], magnetars [55, 56], compact binary systems of black holes (BBH), neutron stars (BNS) or black hole and neutron stars (BHNS) [57, 58, 59, 60, 61, 62, 63] (see also [99, 201, 112]). Another possibility is that the GWs that cannot be individually resolved are originated by binary systems of primordial black holes (PBH), that interact

among themselves (DPBH) [202, 203, 204] or with ABH (PBHABH) [205]. In this Thesis, we will focus just on BBHs of stellar mass, which are the most promising candidates to produce an astrophysical background detectable by future ground-based interferometers, according to the information inferred about their population by recent LVK measurements [107, 108, 8]. Note also that the AGWB is at the same time a foreground for the detection of the CGWB and a complementary source of information, because it sensitive to the content and geometry of the Universe during the late stages of its evolution. In Chapter 8 and 9, we will explore these two aspects, showing how the circular polarization of the AGWB could worsen measurements of the Stokes parameters of CGWBs and how the dipole of the astrophysical background could be important to get a precise measurement of our peculiar velocity.

1.5 Current bounds on stochastic backgrounds

The presence of GWs in our Universe can be tested directly, by detecting them at interferometers and PTA, or indirectly, by looking at their imprint on the cosmological observables, like the CMB or the abundance of light elements.

At the smallest accessible frequencies, the amplitude of the CGWB produced during inflation is constrained by Planck [122, 123, 34]. The B-mode polarization of the CMB is indeed sensitive to the presence of primordial tensor perturbations. By combining the Planck measurements with the ones of BICEP/KEK [124], it is possible to get, assuming the standard single-field inflation scenario,

$$\bar{A}_I^{\rm CGWB}(f = 3.1 \times 10^{-15}) \leq 2.9 \times 10^{-16}\,, \tag{1.90}$$

where we have used the parametrization of SGWBs given in Eq. (1.55).

The observations done by the PTA collaboration [9] in the nHz band gave the first direct measurement of a SGWB. The current sensitivity of PTA does not allow to discriminate between a signal generated by supermassive black hole binaries (SMBHB) [206] and cosmological sources, although primordial signals have larger Bayes factors and are slightly preferred [207]. The constraints on the amplitudes and the tilt for the SMBH model [9] is

$$\bar{A}_I^{\rm SMBHB}(f = 3.2 \times 10^{-8}\,{\rm Hz}) = 8.1^{+4.7}_{-4.0} \times 10^{-9}\,. \tag{1.91}$$

If a more general parametrization is used, the joint contraints on the amplitude and on the tensor tilt are

$$\bar{A}_I^{\rm SGWB}(f = 3.2 \times 10^{-8}\,{\rm Hz}) = 5.8^{+7.6}_{-4.8} \times 10^{-8}\,, \qquad n_{\rm gwb} = 1.8 \pm 0.6\,. \tag{1.92}$$

[9] In [9], the scaling with the frequency of the SGWB is quantified by the tilt of the characteristic strain α, which is connected to the tilt $n_{\rm gwb}$ used in this Thesis by $n_{\rm gwb} = 2 + 2\alpha$. The relation between our tilt and the one of the energy density of the SGWB also used in [9] is then $n_{\rm gwb} = 5 - \gamma$. The value of the amplitude of the characteristic strained used by the PTA collaboration $\bar{A}_I^{\rm PTA}$ is connected to our value by

$$\bar{A}_I = \frac{\pi}{4}\frac{1}{G\,\rho_{\rm crit}} f^2 \left(\frac{f}{f_p}\right)^{2\alpha} |\bar{A}_I^{\rm PTA}|^2\,.$$

Additional investigations on the interpretation of the nature of the SGWB measured by the PTA collaboration can be found for instance in [208].

The LVK collaboration gave an upper bound on the amplitude of an isotropic SGWB in [209]. According to the procedure introduced in Section 1.3.2, the SGWB has been parametrized, as in Eq. 1.55, by a power law, which amplitude at a pivot frequency has been estimated marginalizing over the tensor tilt of the signal. At 95% credible level, the LVK collaboration found that

$$\bar{A}_I \equiv \bar{\Omega}^I_{\rm SGWB}(f = 25\,{\rm Hz}) \leq \begin{cases} 5.8 \times 10^{-9} & n_{\rm gwb} = 0 \\ 3.4 \times 10^{-9} & n_{\rm gwb} = 2/3 \\ 3.9 \times 10^{-10} & n_{\rm gwb} = 3 \end{cases} \tag{1.93}$$

A scale-invariant GW spectrum reflects many properties of cosmological backgrounds from single-field inflation or cosmic strings [113, 114], while $n_{\rm gwb} = 2/3$ and $n_{\rm gwb} = 3$ are the tensor tilts expected from the astrophysical background generate by binary systems during the inspiral stage [47] and by supernovae [55]. These constraints are applied in the frequency range $20 - 77$ Hz for $n_{\rm gwb} = 0$, $20 - 90$ Hz for $n_{\rm gwb} = 2/3$ or $20 - 230$ Hz for $n_{\rm gwb} = 3$. In [209], upper limits on the amplitude of the SGWB have been combined with information about the population of BBH, BNS and BHNS obtained in [108], to constrain the maximum energy density of the background produced by these three different sources in the frequency band of LVK,

$$\bar{A}_I \equiv \bar{\Omega}^I_{\rm SGWB}(f = 25\,{\rm Hz}) \leq \begin{cases} 5.0^{+1.7}_{-1.4} \times 10^{-10} & \text{BBH} \\ 2.1^{+2.9}_{-1.6} \times 10^{-10} & \text{BNS} \\ 8.4 \times 10^{-10} & \text{BHNS} \end{cases} \tag{1.94}$$

In [210], the *Planck* and LVK bounds on the inflationary CGWB has been combined[10], finding a smaller upper limit on the amplitude of the cosmological background

$$\bar{A}^{\rm CGWB}_I(f = 3.1 \times 10^{-15}) \leq 2.5 \times 10^{-16}\ . \tag{1.95}$$

At frequencies larger than 1 kHz, less string bounds have been set by resonant-mass detectors like AURIGA [211], EXPLORER and NAUTILUS [212], but they will not be considered in this Thesis.

An additional upper limit on the total energy density of primordial GWs can be obtained by observations of the abundance of light elements. Big-Bang Nucleosynthesis provides indeed an upper bound on the number of relativistic and decoupled degrees of freedom (including therefore also CGWBs) at temperatures larger than few MeV. We will discuss in more details these constraints in Section 2.2.

[10] This relies on the assumption that the inflationary CGWB has the same spectral index at the *Planck* and LVK frequencies.

Chapter 2

Review of the Standard Model of Cosmology

The cosmological observations of the last century seem to suggest that the ΛCDM model [213, 167, 29, 19, 42, 214, 215] gives the most accurate description of the expansion history of the Universe. According to the Standard Model of Cosmology, the energy density of the Universe is widely dominated by dark energy (DE) (70%), which drives the current accelerated expansion, while non-relativistic matter is mainly made of cold dark matter (CDM) (roughly 30%), while baryons (3%) and neutrinos (less than 1%) are subdominant contribution. Nowadays, the only relativistic component of the Universe is made by photon (CMB) [25], which presents a blackbody spectrum with temperature $T_{\rm CMB,0} \approx 2.7\,\mathrm{K}$, contributing to the energy density of the Universe for less than 1%, and GWs, whose energy density is subdominant. The Hot Big Bang model is able to explain with high accuracy the abundance of the Standard Model particles in our Universe, providing all the details of the thermal history of the Universe in terms of GR, high-energy physics and statistical mechanics. However, although the Universe is homogeneous and isotropic when smoothed over sufficiently large scales, small perturbations exist, giving rise to the structures we observe nowadays [216]. Also CMB observations throughout the years revealed that there are tiny fluctuations in the temperature of the homogeneous and isotropic blackbody spectrum [217, 27, 218, 219, 220, 26]. The most natural explanation for the presence of these inhomogeneities and anisotropies in the Universe, which justifies also the homogeneity and the flatness of the Universe, has been found in inflation [30, 31, 32, 33]. It is a short period of exponential expansion that occurred during the first stage of the evolution of the Universe. The inflationary paradigm, because of its great flexibility, is difficult to falsify, which makes at the same time difficult to prove the validity of the theory. One of the most important predictions of inflation is the production of a CGWB, because of the enhancement of the tensor fluctuations of the metric during this hypothetical accelerated expansion. Therefore, a detection of this primordial signal would be the "smoking gun of inflation".

In this Chapter, we review the main pillars of the ΛCDM model, illustrating the main features of the geometry of spacetime, the thermal history of the content of the Universe,

the dynamics of the background and of the perturbations.

2.1 Homogeneous and isotropic Universe

The Cosmological Principle states that the Universe is homogeneous and isotropic when smoothed on sufficiently large scales [213, 167, 29, 19, 42, 214, 215]. This assumption is justified by the observed blackbody spectrum of the CMB, which is the same in all the directions of the sky [217, 27, 218, 219, 220, 26], up to tiny fluctuations, smaller than 10^{-4}. In addition, the distribution of matter seems to be uniform for scales larger than $200\,h\,\mathrm{Mpc}^{-1}$ [221, 222, 223, 224, 225], where $h \approx 0.67$. In GR, this highly-symmetric spacetime is described by the Friedmann-Lemaître-Robertson-Walker metric (FLRW),

$$ds^2 = -\mathrm{d}t^2 + a^2(t)\left[\frac{\mathrm{d}r^2}{1-Kr^2} + r^2\left(\mathrm{d}\theta^2 + \sin^2\theta\mathrm{d}\phi^2\right)\right], \tag{2.1}$$

where K is the curvature parameter and a is the scale factor that keeps into account for the expansion of the Universe in time. The curvature indicates deviations from an Euclidean spatial geometry, while when $K = 0$ the Universe is flat. The expansion of the Universe determines a redshift in the radiation observed at the time t_0 w.r.t. the emitted one at t,

$$z \equiv \frac{a_0}{a} - 1\,, \tag{2.2}$$

with $a_0 \equiv a(t_0)$, which is arbitrarily set to one in our conventions. It is useful to parametrize the time coordinate in terms of a conformal time η, which is connected to the cosmic time t by the relation

$$\mathrm{d}\eta \equiv \frac{\mathrm{d}t}{a(t)} \to \eta = \int_0^t \frac{\mathrm{d}t}{a(t)}\,, \tag{2.3}$$

where we have set by convention $\eta(0) = 0$. The conformal time represents the comoving distance that could have been travelled by particles propagating at the speed of light from $t = 0$ to t, thus, according to Special Relativity, it represents the size of the spherical region at t which has been in causal contact since $t = 0$. When the comoving distance between two points is larger than η, there is no way in which these two signsls could have exchanged radiation and, equivalently, information, thus the regions are causally disconnected. By using the conformal time, we see that the FLRW line element is conformal to the Minkowski line element,

$$ds^2 = a^2(\eta)\left[-\mathrm{d}\eta^2 + \frac{\mathrm{d}r^2}{1-Kr^2} + r^2\left(\mathrm{d}\theta^2 + \sin^2\theta\mathrm{d}\phi^2\right)\right]. \tag{2.4}$$

The homogeneity and the isotropy of the Universe implies that radiation and matter are perfect fluids, thus their energy-momentum tensor has the simple form

$$T_{\mu\nu} = (\rho + P)\,u_\mu u_\nu - P g_{\mu\nu}\,, \tag{2.5}$$

with u^μ the four-velocity of the fluid, while ρ and P the energy density and the pressure that are related via the equation of state

$$P = w\rho\,, \tag{2.6}$$

where $w = 0$ for non-relativistic matter, $w = 1/3$ for radiation and $w = -1$ for a cosmological constant. The Einstein equations in this spacetime are

$$\begin{aligned} H^2 \equiv \left(\frac{1}{a}\frac{\mathrm{d}a}{\mathrm{d}t}\right)^2 &= \frac{8\pi}{3}G\rho - \frac{K}{a^2}\,, \\ \frac{1}{a}\frac{\mathrm{d}^2 a}{\mathrm{d}t^2} &= -\frac{4\pi G}{3}(\rho + 3P)\,. \end{aligned} \tag{2.7}$$

The conservation of the energy-momentum tensor of the fluid gives an additional equation to determine the evolution of the background,

$$\mathcal{D}^\mu T_{\mu\nu} = 0 \rightarrow \frac{\mathrm{d}\rho}{\mathrm{d}t} = -3H(\rho + P)\,, \tag{2.8}$$

with $\mathcal{D}^\mu = g^{\mu\nu}\mathcal{D}_\nu$, where the covariant derivative has been defined in Eq. (1.22). If we introduce the conformal Hubble parameter

$$\mathcal{H} \equiv \frac{a'}{a}\,, \tag{2.9}$$

which is related to the standard Hubble parameter by

$$\mathcal{H} = aH\,, \qquad \mathcal{H}' = \mathcal{H}^2 + a^2\frac{\mathrm{d}H}{\mathrm{d}t}\,, \tag{2.10}$$

we can write the set of equations by using

$$\begin{aligned} \mathcal{H}^2 &= \frac{8\pi}{3}G\rho a^2 - K\,, \\ \mathcal{H}' &= -\frac{4\pi}{3}G(\rho + 3P)\,, \\ \rho' &= -3\mathcal{H}(\rho + P)\,. \end{aligned} \tag{2.11}$$

When the equation of state of the fluid is fixed, it is easy to derive the scaling of the energy density with the scale factor,

$$\frac{\mathrm{d}\ln\rho}{\mathrm{d}\eta} = -3(1+w)\frac{\mathrm{d}\ln a}{\mathrm{d}\eta} \rightarrow \rho = \rho_0\, a^{-3(1+w)} = \rho_0 \begin{cases} a^{-3} & \text{Matter} \\ a^{-4} & \text{Radiation} \\ 1 & \text{Dark Energy} \end{cases}\,. \tag{2.12}$$

These relations show that the energy density for non-relativistic matter decreases in time as a^{-3}, since the number density is diluted by the particle content of the Universe, while the energy of relativistic species goes like a^{-4}, because the number of particles is diluted and the energy density (frequency) of the individual particle is redshifted too, while for a cosmological constant the energy density does not change in time. In a flat Universe, since

H_0 $\left[\mathrm{km\,s^{-1}\ Mpc^{-1}}\right]$	67.66 ± 0.42
$\Omega_{b,0}h^2$	0.02242 ± 0.00014
$\Omega_{c,0}h^2$	0.11933 ± 0.00091
τ_{reio}	0.0561 ± 0.0071
$\ln 10 A_s$	3.047 ± 0.014
n_s	0.9665 ± 0.0038
Ω_Λ	0.679 ± 0.013
Ω_K	0.044 ± 0.033

Table 2.1: Cosmological parameters constrained at 68% credible intervals by Planck [26]. These constraints have been obtained by combining the TT,TE,EE+lowE+lensing+BAO measurements.

$K = 0$, it is easy to get very simple expressions for the evolution of the scale factor as a function of the conformal time,

$$\frac{\mathrm{d}a}{\mathrm{d}\eta} = \sqrt{\frac{8\pi}{3}G\rho_0}a^{-(1+3w)/2} \rightarrow a = a_0 \begin{cases} \eta^{\frac{2}{1+3w}} & w \neq 1 \\ e^{-\eta} & w = 1 \end{cases} = a_0 \begin{cases} \eta^2 & \text{Matter} \\ \eta & \text{Radiation} \\ e^{-\eta} & \text{Dark Energy} \end{cases} . \tag{2.13}$$

It is possible then to normalize the energy density of the content of the Universe w.r.t. the critical energy density of the Universe today defined in Eq. (1.46)[1], introducing the parameters

$$\Omega_{i,0} \equiv \frac{\rho_i(\eta_0)}{\rho_{\mathrm{crit}}} . \tag{2.14}$$

In this Thesis, we use the parameters constrained by Planck [26] written in Table 2.1. These constraints exploit the maps of temperature, polarization, lensing and the measurements of Baryon Acoustic Oscillations (BAO) done by BOSS [226]. According to Eq. (2.13), the evolution of the scale factor in time depends on which is the source that provides the dominant contribution to the energy density of the Universe. Since the energy densities for radiation, non-relativistic matter and dark energy scale in time as described in Eq. (2.12), it is reasonable to expect that the Universe crosses different stages of evolution in which radiation, non-relativistic matter and dark energy dominate. To compute the redshift at which radiation and matter or matter and dark energy have the same energy density, z_{eq}, $z_{\mathrm{eq},\,\Lambda}$ respectively, it is just sufficient to impose $\rho_m = \rho_r$ and $\rho_m = \rho_{\mathrm{DE}}$ and evolve the

[1]Notice that this definition is slightly different w.r.t. Eq. (1.45), which refers to the energy density in a single logarithmic frequency bin.

present energy densities, constrained by experiments, backward in time, finding

$$\begin{aligned}(1+z_{\rm eq})^3\,\Omega_{m,0} =&(1+z_{\rm eq})^4\,\Omega_{r,0} \to z_{\rm eq} = \frac{\Omega_{m,0}}{\Omega_{r,0}} - 1 \approx 3400\,,\\ (1+z_{{\rm eq},\,\Lambda})^3\,\Omega_{m,0} =&\Omega_\Lambda \to z_{{\rm eq},\,\Lambda} = \left(\frac{\Omega_\Lambda}{\Omega_{m,0}}\right)^{1/3} - 1 \approx 0.32\,.\end{aligned} \tag{2.15}$$

In the next section, we will enter into the details of the particle species that contribute to the energy density at different epochs, specifying how their abundance changed in time, looking for their imprint on the evolution of the background geometry of the Universe.

2.2 Thermal history of the Universe

Thermodynamics of relativistic and non-relativistic particles

When an ensemble of particles originates from a thermal process or it is strongly interacting, it is possible to quantify its statistical properties in terms of the temperature of the system and the mass of the particles. For relativistic particles, the number density and the energy density are just given by

$$n(T) = g\frac{\zeta(3)}{\pi^2}T^3\begin{cases}1 & \text{bosons}\\ \frac{3}{4} & \text{fermions}\end{cases} \qquad \rho(T) = g\frac{\pi^2}{30}T^4\begin{cases}1 & \text{bosons}\\ \frac{7}{8} & \text{fermions}\end{cases} \tag{2.16}$$

with ζ the Riemann function and g the intrinsic degrees of freedom of the particles, that keep into account, e.g., for the helicity stases. When non-relativistic particles are considered, the statistics of bosons and fermions is just given by a Maxwell-Boltzmann distribution,

$$n(T) = g\left(\frac{m}{2\pi}\right)^{3/2} e^{-m/T}\,, \qquad \rho(T) = m\,n(T)\,. \tag{2.17}$$

If more than ore species is considered, the total energy density and entropy of the relativistic particles can be computed in terms of some effective degrees of freedom,

$$\begin{aligned}\rho(T) &= \frac{\pi^2}{30}T^4 g_*(T)\,,\\ s(T) &= \frac{4}{3}\frac{\pi^2}{30}T^3 g_{*,s}(T)\,,\end{aligned} \tag{2.18}$$

with T the temperature of photons and where we have defined the effective degrees of freedom as

$$\begin{aligned}g_*(T) &\equiv \sum_{\alpha={\rm bosons}} g_\alpha\left(\frac{T_\alpha}{T}\right)^4 + \frac{7}{8}\sum_{\beta={\rm fermions}} g_\beta\left(\frac{T_\beta}{T}\right)^4\,,\\ g_{*,s}(T) &\equiv \sum_{\alpha={\rm bosons}} g_\alpha\left(\frac{T_\alpha}{T}\right)^3 + \frac{7}{8}\sum_{\beta={\rm fermions}} g_\beta\left(\frac{T_\beta}{T}\right)^3\,.\end{aligned} \tag{2.19}$$

In a Universe dominated by radiation, it is easy to see that the temperature decreases with time, because $T \sim \rho^{1/4} \sim 1/a$. When a particle at thermal equilibrium becomes non-relativistic, its number density is suppressed by the exponential factor that appears in Eq. (2.17), therefore its abundance in the Universe becomes negligible w.r.t. the other relativistic species. Since the entropy of the Universe is conserved in this transition, the temperature of the thermal bath increases in order to balance the entropy. Physically, this increase is due to the fact that the heavy particle decays into non-relativistic ones, injecting energy and increasing the temperature. In the next section, we will provide a detailed description of g_*, keeping into account for the presence of relativistic and non-relativistic particles. A non-trivial change in g_* and $g_{*,s}$ occurs when electron and positrons become non-relativistic. At that time, both photons and neutrinos are relativistic, but, since neutrinos are decoupled from the thermal bath, they are not affected by changes in the number of degrees of freedom that contribute to the entropy. Before and after electron and positrons become non relativistic, the effective degrees of freedom of the entropy are equal to

$$\begin{aligned} g_{*,s}(T > 0.5\,\mathrm{MeV}) =& 2 + \frac{7}{8} \times 4 = \frac{11}{2}\,, \\ g_{*,s}(T < 0.5\,\mathrm{MeV}) =& 2\,. \end{aligned} \tag{2.20}$$

According to the conservation of entropy, the temperature of photon is heated by a factor $(11/4)^{1/3}$ compared to neutrinos, therefore the effective degrees of freedom are

$$g_*(T < 0.5\,\mathrm{MeV}) = 2 + \frac{7}{8}\,6\,\left(\frac{4}{11}\right)^{4/3} = 3.4\,. \tag{2.21}$$

Chronology of the relativistic degrees of freedom of the Universe

We consider the thermal bath made by Standard Model particles, from energy scales of the order of 1 TeV to the current temperature of CMB photon, $T = 2.73\,K \approx 2.3 \times 10^{-4}$eV. The intrinsic degrees of freedom from the lower temperature to the highest one are given in Table 2.2, which is consistent to the one provided by [227]. The effective degrees of freedom increase every time a particle like neutrinos, electrons and positrons, muons, pions, many of the quarks and taons become relativistic. Since these species are all at thermal equilibrium, at every time $g_* = g_{*,s}$, with the only exception of the time at which electron and positrons are non-relativistic and neutrinos are still relativistic. At around $T = 175\,\mathrm{MeV}$ there is the phase transition of quantum chromodynamics (QCD), therefore the degrees of freedom given by u, d, s quarks and the gluons, which are all relativistic at that temperature, start contributing at the same time to the total effective degrees of freedom.

Constraints on the number of effective degrees of freedom

At low temperatures, the effective degrees of freedom are parametrized by deviations from the expect numer of neutrino species,

$$g_*(T) = 2 + \frac{7}{4}\left(\bar{N}_{\mathrm{eff}} + \Delta N_{\mathrm{eff}}\right)\,. \tag{2.22}$$

Particle/Process	Mass/Energy Scale [MeV]	Intrinsic d.o.f.	$g_*(T)$	$g_{*,s}(T)$
γ	0	2	2	2
ν, $\bar{\nu}$	?	6	3.4	2
e^+, e^-	0.51	4	10.75	5.5
ν Decoupling	1		10.75	10.75
μ^+, μ^-	106	4	14.25	14.25
π^+, π^-	135	2	16.25	16.25
π^0	140	1	17.25	17.25
gluon	0	16		
u, $\bar{u}$	5	12		
d, $\bar{d}$	9	12		
s, $\bar{s}$	115	12		
QCD PT	175		61.75	61.75
c, $\bar{c}$	1.3×10^3	12	72.25	72.25
τ^+,τ^-	1.8×10^3	4	75.75	75.75
b, $\bar{b}$	4.4×10^3	12	86.25	86.25
W^+, W^-	80×10^3	6	92.25	92.25
Z	91×10^3	3	95.25	95.25
H	114×10^3	1	96.25	96.25
t, $\bar{t}$	174×10^3	12	106.75	106.75

Table 2.2: Evolution of the relativistic degrees of freedom of the Standard Model particles.

If only neutrinos are present, $\bar{N}_{\rm eff} = 3.045$, where the correction w.r.t. the standard value of three neutrino generations comes from non-instantaneous neutrino decoupling [228, 229] and QED effects [230] (see also [231] for a joint discussion). The parameter $N_{\rm eff}$ can be constrained by the CMB [26] or by BBN [232]. A recent analysis that combine CMB and BBN measurements [233, 234] shows that $\Delta N_{\rm eff} = -0.14 \pm 0.15$, indicating deviations from the presence of just standard neutrinos in the early Universe. As mentioned in Section 1.5, since GWs are relativistic degrees of freedom, measurements of $\Delta N_{\rm eff}$ constitutes an indirect upper bound on the amplitude of CGWB produced before BBN. Following [114], it is possible to show that the upper bound on the energy density of the CGWB at the time η is

$$\frac{\rho_{\rm CGWB}(\eta, \mathbf{x})}{\rho_{\rm crit}} \leq \Omega_{\gamma,0} \left(\frac{g_*(T_{\rm rec})}{g_{*,s}(T(\eta))} \right)^{4/3} \frac{7}{8} \Delta N_{\rm eff} \,, \tag{2.23}$$

with $T_{\rm rec} \approx 0.3$ the temperature of recombination of photons.

2.3 Inflation

2.3.1 Shortcomings of the Hot Big Bang model

Inflation was motivated by different puzzles regarding the statistical properties of the Universe and the geometry of the spacetime which were impossible to solve in the framework provided by the Hot Big-Bang Model.

The first enigma which emerges in the standard description of the Universe is the "horizon problem", which consists in the fact that the observed homogeneity and isotropy of the structures and of the CMB at large angular scales cannot be justified by assuming that regions which exhibit similar properties interacted efficiently throughout cosmic history. By looking at the definition of conformal time, Eq. (2.3), we notice that the region of causal contact described by η, increases during the radiation and the matter epoch, while it diminuishes during the period dominated by DE, see, e.g., Eq. (2.13). This indicates that the maximum region of causal connection was at $\eta(z_{\rm eq,\Lambda})$ defined in Eq. (2.15), thus two regions whose separation is larger than this conformal time would have never been able to communicate. This lack of causal contact would require a fine tuning in the initial conditions in order to reflect the current observations.

A second issue is the "flatness problem", related to the very tiny value of the curvature of the Universe measured today. Since the contribution of the curvature to the expansion of the Universe increases in time, at very early times the Universe should have approached to a flat Universe, up to corrections of the order 10^{-60}.

Additional problems, like the "entropy problem", consisting in an extremely large entropy of the Universe, and the "monopole problem", keeping into account for the presence of unwanted heavy relics, have also been considered [167].

A natural solution to all these inconsistencies, which requires no fine-tuning in the initial conditions, is the introduction of an accelerated phase of expansion of the Universe at early times, which reduces the value of the conformal time w.r.t. the one expected by the Hot Big-Bang Model and at the same time drives the curvature of the Universe to

extremely small values. In the next sections we will show that inflation permits to have a dynamical mechanism, which is not affected by any choice of the initial conditions, which solves al these tensions. Furthermore, inflation would be able to explain also the presence of the small perturbations of a homogeneous and isotropic background.

2.3.2 Inflationary paradigm

In the simplest scenario of inflation, it is assumed that a single scalar field φ dominates the energy density of the Universe at early times. The total action assumes then the form

$$S = \frac{1}{16\pi G}\int \mathrm{d}^4x\sqrt{-g}\left(R + \mathcal{L}_\varphi[\varphi, g_{\mu\nu}]\right) , \tag{2.24}$$

where the determinant of the metric has been defined by $g \equiv g^\mu_\mu$. According to the Cosmological Principle, we consider a FLRW spacetime, whose metric is given in Eq. (2.1), up to small perturbations which will be discussed later. In full generality, the Lagrangian density of the inflaton can be written as the sum of a kinetic term and an interaction potential,

$$\mathcal{L}_\varphi = -\frac{1}{2}g^{\mu\nu}\mathcal{D}_\mu\varphi\mathcal{D}_\nu\varphi - V(\varphi) . \tag{2.25}$$

The energy-momentum tensor associated to the inflaton is simply evaluated by using

$$T^\varphi_{\mu\nu} \equiv -\frac{2}{\sqrt{-g}}\frac{\delta S_\varphi[\varphi, g_{\mu\nu}]}{\delta g^{\mu\nu}} = \mathcal{D}_\mu\varphi\mathcal{D}_\nu\varphi - g_{\mu\nu}\left[\frac{1}{2}g^{\alpha\beta}\mathcal{D}_\alpha\varphi\mathcal{D}_\beta\varphi + V(\varphi)\right] . \tag{2.26}$$

According to the homogeneity and isotropy of the Universe, it is possible to assume that the field is dominated by an homogeneous and isotropic contribution and that exhibits tiny perturbations, which vary in space and time,

$$\varphi(t, \mathbf{x}) = \varphi_0(t) + \delta\varphi(t, \mathbf{x}) . \tag{2.27}$$

At the zero order in the perturbations, the energy and the pressure associated to this field are

$$\bar{\rho}_\varphi = -\bar{T}^0_0 = \frac{1}{2}\dot{\varphi}_0^2 + V(\varphi_0) , \qquad \bar{P}_\varphi = \frac{1}{3}\delta^i_j\bar{T}^j_i = \frac{1}{2}\dot{\varphi}_0^2 - V(\varphi_0) . \tag{2.28}$$

By looking at Eq. (2.7), we note that an accelerated expansion occurs when the evolution of the Universe is governed by contents with equation of state with $w < -1/3$. If we assume, for simplicity, that $w = -1$, we see that this is equivalent to require that

$$V(\varphi_0) \gg \frac{1}{2}\dot{\varphi}_0^2 . \tag{2.29}$$

This condition implies that the inflaton is slowly rolling to the minimum of the potential, since the its kinetic energy is a subdominant contribution. An additional condition that needs to be imposed to solve the horizon and the flatness problem is that inflation lasted for a sufficiently long enough period, in such a way that the accelerated expansion put in causal contact all the regions observed in the Universe today with analog features. The

equation of motion for the leading order contribution to the inflation field is computed by using

$$\frac{\delta S_\varphi[\varphi, g_{\mu\nu}]}{\delta\varphi} = 0 \rightarrow g^{\mu\nu}\mathcal{D}_\mu\mathcal{D}_\nu\varphi - \frac{\partial V}{\partial\varphi}(\varphi) = 0\,. \tag{2.30}$$

This conditions gives

$$\ddot{\varphi}_0 + 3H\dot{\varphi}_0 + \frac{\partial V}{\partial\varphi_0}(\varphi_0) = 0\,, \tag{2.31}$$

therefore we require that the acceleration of the inflaton field is much smaller than the friction term due to the expansion of the Universe,

$$|\ddot{\varphi}_0| \ll |3H\dot{\varphi}_0|\,. \tag{2.32}$$

Under these two assumptions, it is possible to show that inflation is able to produce an attractor solution to the initial conditions required to solve the problems of the Hot Big-Bang Model. The two requirements imposed can be summarized by demanding that two slow roll parameters, defined by

$$\begin{aligned} \epsilon_V \equiv & \frac{1}{16\pi G}\left(\frac{\frac{\partial V}{\partial\varphi_0}(\varphi_0)}{V(\varphi_0)}\right)^2\,, \\ \eta_V \equiv & \frac{1}{8\pi G}\frac{\frac{\partial^2 V}{\partial\varphi_0^2}(\varphi_0)}{V(\varphi_0)}\,, \end{aligned} \tag{2.33}$$

are much smaller than one, $\epsilon_V \ll 1$, $\eta_V \ll 1$. By using the Friedmann equations, Eq. (2.7), we notice that the Hubble factor during inflation is equal to

$$H^2 = \frac{8}{3}\pi G\left(\frac{1}{2}\dot{\varphi}_0^2 + V(\varphi_0)\right)\,. \tag{2.34}$$

The derivative w.r.t. the cosmic time of the Hubble factor is

$$\dot{H} = \frac{1}{H}\frac{8}{3}\pi G\left(\dot{\varphi}_0\ddot{\varphi}_0 + \frac{\partial V}{\partial\varphi_0}(\varphi_0)\dot{\varphi}_0\right) = -8\pi G\dot{\varphi}_0^2 = -\frac{8\pi G}{9H^2}\left(\frac{\partial V}{\partial\varphi_0}(\varphi_0)\right)^2 = -\frac{2\left[8\pi G\,V(\varphi_0)\right]^2}{9H^2}\epsilon_V\,, \tag{2.35}$$

where we have used twice the equation of motion of the inflaton, Eq. (2.30), the slow roll condition given by Eq. 2.32, and the definition of the slow roll parameter provided by Eq. (2.33). From this equation we see that the Hubble factor is constant, up to linear contributions in the slow roll parameters, as we would expect from Eq. (2.12) for a stage of accelerated expansion. The evolution of the scale factor at first order in the slow roll parameter is computed by using

$$\frac{\dot{H}}{H^2} = -\epsilon_V \rightarrow H = H_i(1 - \epsilon_V\, t)\,, \tag{2.36}$$

with H_i the initial condition. The scale factor grows exponentially, because

$$\frac{\dot{a}}{a} = H \rightarrow a = a_i e^{H_i t}\left(1 - \frac{1}{2}\epsilon_V\, H_i^2 t^2\right)\,. \tag{2.37}$$

The relation between the conformal time and the scale factor is then

$$\eta = \int_0^t \mathrm{d}\tilde{t} \frac{1}{a(\tilde{t})} = -\frac{1}{a(t)H(t)(1-\epsilon_V)}\,. \tag{2.38}$$

2.3.3 Quantum fluctuations during inflation

Fluctuations of the inflaton

In Eq. (2.27) we have assumed that the inflaton field is dominated by a homogeneous and isotropic component, while small fluctuations, which depend on time and space, appear because of the quantum nature of the field. In a similar way, the metric is perturbed around a FLRW spacetime and, in the Poisson gauge, we can write it according to

$$ds^2 = a^2(\eta)\Big\{-\mathrm{d}\eta^2\,(1+2\Phi) + \mathrm{d}x^i\mathrm{d}x^j\,[\delta_{ij}\,(1-2\Psi) + H_{ij}]\Big\}\,, \tag{2.39}$$

with H_{ij} transverse-traceless perturbations. In Appendix A.1 and in Section 2.4.1, additional details will be provided about the choice of the gauge and the decomposition of the metric in terms of scalar, vector and tensor fields. By using Eq. (2.30), we find that the evolution of the perturbation of the inflaton is given by

$$\delta\varphi'' + 2\mathcal{H}\delta\varphi' - \nabla^2\delta\varphi + \frac{\partial^2 V}{\partial\varphi_0^2}(\varphi_0)\delta\varphi - 2\varphi_0''\Phi - \mathcal{H}\varphi_0'\left(4\Phi + \Phi'\right) = 0\,. \tag{2.40}$$

If we neglect the impact of the perturbations of the metric on the evolution of φ, we get

$$\delta\varphi'' + 2\mathcal{H}\delta\varphi' - \nabla^2\delta\varphi + \frac{\partial^2 V}{\partial\varphi_0^2}(\varphi_0)\delta\varphi = 0\,. \tag{2.41}$$

In Fourier space, this equation becomes

$$\delta\varphi'' + 2\mathcal{H}\delta\varphi' + k^2\delta\varphi + \frac{\partial^2 V}{\partial\varphi_0^2}(\varphi_0)\delta\varphi = 0\,. \tag{2.42}$$

Since the fluctuations of the inflaton field have a quantum nature, the perturbations $\delta\varphi$ is not a real scalar field, but a scalar operator $\delta\hat{\varphi}$ which acts on a Hilbert space. The quantization of a scalar field in a FLRW spacetime is done by observing that the field $\delta\hat{\varphi}/a$ behaves like a real scalar quantum field in Minkowski. The quantization of such a field is done by decomposing $\delta\hat{\varphi}$ in creation and annihilation operators,

$$\delta\hat{\varphi}(\eta,\mathbf{x}) = \int \frac{\mathrm{d}^3k}{(2\pi)^3}\left[e^{i\mathbf{k}\cdot\mathbf{x}}\frac{u_k(\eta)}{a}\hat{a}_{\mathbf{k}} + e^{-i\mathbf{k}\cdot\mathbf{x}}\frac{u_k^*(\eta)}{a}\hat{a}_{\mathbf{k}}^\dagger\right]\,, \tag{2.43}$$

where the operators act on the vacuum in such a way that

$$\hat{a}_{\mathbf{k}}\,|0\rangle = 0 \qquad \langle 0|\,\hat{a}_{\mathbf{k}}^\dagger = 0\,. \tag{2.44}$$

The commutation relation of the operators and of the fields are

$$\begin{aligned}[\hat{a}^\dagger_{\mathbf{k}}, \hat{a}_{\mathbf{k}'}] &= -\hbar\,\delta(\mathbf{k}-\mathbf{k}')\,, \\ \left[\delta\hat{\varphi}(\eta,\mathbf{x}'), \partial_0\delta\hat{\varphi}(\eta,\mathbf{x}')\right] &= i\hbar\,\delta(\mathbf{x}-\mathbf{x}')\,.\end{aligned} \tag{2.45}$$

The combination of these two relations gives also a condition on the wave functions,

$$u_k\, u_k^{*\prime} - u_k'\, u_k^* = i\,. \tag{2.46}$$

The differential equation of the quantum operator reduces to a classical equation of motion of the wave function,

$$u_k'' + \left(k^2 - \frac{a''}{a} + \frac{\partial^2 V}{\partial\varphi^2}(\varphi)a^2\right) u_k = 0\,. \tag{2.47}$$

To find the solution of this differential equation, we need to express the scale factor and its derivatives in terms of the conformal time. By using Eq. (2.38), the conformal time is related to the conformal Hubble factor by

$$\eta = -\frac{1}{\mathcal{H}(1-\epsilon_V)}\,, \tag{2.48}$$

therefore the derivatives of a are connected to η by

$$\frac{a''}{a} = \frac{2}{\eta^2}\left(1 + \frac{3}{2}\epsilon_V\right)\,. \tag{2.49}$$

If we define $\nu^2 \equiv 9/4 + 3\epsilon_V$, the equation for the wave function becomes

$$u_k'' + \left[k^2 - \left(\nu^2 - \frac{1}{4}\right)\frac{1}{\eta^2}\right] u_k = 0\,. \tag{2.50}$$

This equation is a Bessel equation and the solution is

$$u_k(\eta) = \sqrt{-\eta}c_1(k)\, H_\nu^{(1)}(-k\eta) + c_2(k)\, H_\nu^{(2)}(-k\eta)\,, \tag{2.51}$$

where $H^{(1)}$, $H^{(2)}$ are the Hankel functions of the first and second kind, while c_1 and c_2 are initial conditions that need to be specified. To find them, match the general solution to the solutions obtained in the limits $k\eta \ll 1$ and $k\eta \gg 1$. For sub-horizon scales the solution coincides with the De Sitter result,

$$u_k = \frac{e^{-ik\eta}}{\sqrt{2k}}\,, \tag{2.52}$$

while for super-horizon scales the wave function is just proportional to the scale factor.

$$u_k = B(k)a(\eta)\,. \tag{2.53}$$

In order to satisfy these two limits, the coefficients of Eq. (2.51) have to be equal to

$$c_1(k) = \frac{\sqrt{\pi}}{2}e^{i\left(\nu+\frac{1}{2}\right)\frac{\pi}{2}}\,, \qquad c_2(k) = 0\,. \tag{2.54}$$

The solution of the wave function is then

$$u_k(\eta) = \frac{\sqrt{\pi}}{2} e^{i\left(\nu+\frac{1}{2}\right)\frac{\pi}{2}} \sqrt{-\eta} H_\nu^{(1)}(-k\eta)\,. \tag{2.55}$$

In the limit of super-horizon scales we get

$$u_k(\eta) = e^{i\left(\nu+\frac{1}{2}\right)\frac{\pi}{2}} 2^{\nu-3/2} \frac{\Gamma(\nu)}{\Gamma(3/2)} (-k\eta)^{1/2-\nu} \frac{1}{\sqrt{2k}}\,, \tag{2.56}$$

which means that the amplitude of the perturbations is

$$|\delta\varphi(\eta,k)| \simeq 2^{\nu-3/2} \frac{\Gamma(\nu)}{\Gamma(3/2)} \frac{H}{\sqrt{2k^3}} \left(\frac{k}{aH}\right)^{3/2-\nu}\,. \tag{2.57}$$

Fluctuations of the metric

The action of the gravitational field is given by

$$S_{H_{ij}} = \frac{1}{64\pi G} \int \mathrm{d}\eta\, \mathrm{d}^3x\, a^2(\eta) \left(H'_{ij}(\eta,\mathbf{x}) H^{ij\,\prime}(\eta,\mathbf{x}) - \boldsymbol{\nabla} H_{ij}(\eta,\mathbf{x}) \cdot \boldsymbol{\nabla} H^{ij}(\eta,\mathbf{x})\right)\,, \tag{2.58}$$

where the tensor perturbation of the metric can be written in Fourier space by using

$$H_{ij}(\eta,\mathbf{x}) = \int \frac{\mathrm{d}^3k}{(2\pi)^3} \sum_{\lambda=+,\times} e^{i\mathbf{k}\cdot\mathbf{x}}\, H_\lambda(\eta,\mathbf{k})\, e^\lambda_{ij}(\mathbf{k})\,. \tag{2.59}$$

It is clear that for the combination

$$\tilde{H}_\lambda(\eta,\mathbf{k}) \equiv \frac{a}{4\sqrt{\pi G}} H_\lambda(\eta,\mathbf{k})\,, \tag{2.60}$$

the action is the same of a real scalar field around Minkowski. In this way, it is possible to quantize the amplitude of the tensor perturbations in analogy with what has been done for the inflaton,

$$\hat{\tilde{H}}_\lambda(\eta,\mathbf{x}) = \int \frac{\mathrm{d}^3k}{(2\pi)^3} \left[e^{i\mathbf{k}\cdot\mathbf{x}} v_{k,\lambda}(\eta) \hat{b}_{\mathbf{k},\lambda} + e^{-i\mathbf{k}\cdot\mathbf{x}} v^*_{k,\lambda}(\eta) \hat{b}^\dagger_{\mathbf{k},\lambda}\right]\,, \tag{2.61}$$

where $\hat{b}_{\mathbf{k},\lambda}$, $\hat{b}^\dagger_{\mathbf{k},\lambda}$ are the creation and annihilation operators which acts on the Hilbert space as $\hat{b}_{\mathbf{k},\lambda}\,|0\rangle = 0$ and $\langle 0|\,\hat{b}^\dagger_{\mathbf{k},\lambda} = 0$. The commutation relations in this case are

$$\begin{aligned} [\hat{b}^\dagger_{\mathbf{k},\lambda}, \hat{b}_{\mathbf{k}',\lambda'}] &= -\,\hbar\,\delta_{\lambda\lambda'}\delta(\mathbf{k}-\mathbf{k}')\,, \\ \left[\delta\hat{\tilde{H}}_\lambda(\eta,\mathbf{x}'), \partial_0\delta\hat{\tilde{H}}_{\lambda'}(\eta,\mathbf{x}')\right] &= i\hbar\,\delta_{\lambda\lambda'}\,\delta(\mathbf{x}-\mathbf{x}')\,. \end{aligned} \tag{2.62}$$

Also in this case, the normalization of the wave function is given with a condition analogous to Eq. (2.46),

$$v_{k,\lambda} v^{*\prime}_{k,\lambda} - v^*_{k,\lambda} v'_{k,\lambda} = i\,. \tag{2.63}$$

The equation of motion of the tensor perturbations is obtained by the action or by looking at the transverse-traceless part of the Einstein equations, Eq. (2.108). The anisotropic stress of the inflaton field in this case is negligible, because it is a term quadratic in $\delta\varphi$, therefore the equation of motion of the tensor perturbations is just

$$H_{ij}''(\eta,\mathbf{x}) + 2\mathcal{H}(\eta)H_{ij}'(\eta,\mathbf{x}) - \nabla^2 H_{ij}(\eta,\mathbf{x}) = 0\,. \tag{2.64}$$

The equation of motion of the wave functions is then

$$v_{k,\lambda}'' + \left(k^2 - \frac{a''}{a}\right)v_{k,\lambda} = 0\,. \tag{2.65}$$

This equation is identical in form to the one of the scalar perturbations, therefore the solution is

$$v_{k,\lambda}(\eta) = \frac{\sqrt{\pi}}{2}e^{i(\nu+1/2)\pi/2}\sqrt{-\eta}H_\nu^{(1)}(-k\eta)\,, \tag{2.66}$$

whose limit on super-horizon scales is equal to

$$v_k(\eta) = e^{i(\nu-1/2)\pi/2}2^{\nu-3/2}\frac{\Gamma(\nu)}{\Gamma(3/2)}\frac{1}{\sqrt{2k}}(-k\eta)^{1/2-\nu}\,. \tag{2.67}$$

The amplitude of the tensor fluctuations is then

$$|H_\lambda(\eta,\mathbf{k})| = \sqrt{32\pi G}\,2^{\nu-3/2}\frac{\Gamma(\nu)}{\Gamma(3/2)}\frac{H}{\sqrt{2k^3}}\left(\frac{k}{aH}\right)^{3/2-\nu}\,. \tag{2.68}$$

Primordial Power Spectra

According to Appendix A.1, the perturbations of the inflaton field and of the metric are not gauge invariant and transform under changes of the coordinates. Because of this reason, it would be useful to descibe the amount of perturbations produced during inflation in terms of gauge-invariant quantities. For the scalar perturbations, we define the gauge-invariant curvature perturbation

$$\zeta(\eta,k) \equiv -\left[-D(\eta,k) + \frac{1}{6}F(\eta,k)\right] - \mathcal{H}(\eta)\frac{\delta\rho(\eta,k)}{\bar{\rho}(\eta)}\,, \tag{2.69}$$

where the perturbations of the metric have been defined in a generic gauge in Eq. (A.2). An interesting property of this object is that it is conserved on super-horizon scales, therefore we will use from now on the notation $\zeta(k) \equiv \zeta(\eta,k)|_{aH=k}$. The primordial power spectra of the scalar and tensor perturbations are defined by

$$\begin{aligned}\langle 0|\,\zeta(\mathbf{k})\zeta^*(\mathbf{k}')\,|0\rangle \equiv& \frac{2\pi^2}{k^3}P_\zeta(k)\,,\\ \langle 0|\,\hat{H}_{ij,\lambda}(\eta,\mathbf{k})\,\hat{H}^{ij\,*}_{\lambda'}(\eta,\mathbf{k}')\,|0\rangle \equiv& \frac{2\pi^2}{k^3}\delta_{\lambda\lambda'}\delta(\mathbf{k}-\mathbf{k}')P^{(\lambda)}(\eta,k)\,.\end{aligned} \tag{2.70}$$

By using Eqs. (2.57), (2.68) it is possible to get

$$\begin{aligned} P_\zeta(k) =& \frac{2\pi G H^2}{k^3 \epsilon_V}\Big|_{aH=k}\,, \\ P^{(\lambda)}(k) =& \frac{64\pi G}{k^3}\Big|_{aH=k}\,, \end{aligned} \tag{2.71}$$

where we have used the fact that the power spectrum of the tensor perturbation for the two polarization is conserved for super-horizon scales. It is possible also to introduce also the total tensor spectrum, which accounts for the total tensor perturbations produced during inflation,

$$P_T(k) \equiv \sum_\lambda P^{(\lambda)}(k)\,. \tag{2.72}$$

The tensor-to-scalar ratio quantifies the difference in amplitude of the tensor and the scalar perturbations and it is defined by

$$r \equiv \frac{P_T(k)}{P_\zeta(k)} = 16\epsilon_V\,. \tag{2.73}$$

2.4 Cosmological Perturbations

In the previous sections, we have shown that inflation provides a justification for the homogeneity and the isotropy of the Universe on large scales and it keeps into account also for the presence of tiny perturbations, which exhibit spatial and angular correlations which can be measured by looking at different cosmological observables. In this section, we focus on the description of the perturbation of the geometry and of the energy density of the Universe, discussing the structure of the Einstein and the Boltzmann equations that govern the evolution of the Universe.

2.4.1 Perturbations of the metric

Poisson gauge

When a tiny amount of inhomogeneity is considered, the most general extension of the line element in FLRW, defined in Eq. (2.1), is given by

$$\begin{aligned} ds^2 = a^2(\eta)\Big\{ &-\mathrm{d}\eta^2\,(1+2A) - \left(\partial_i B + B_i^\perp\right)\mathrm{d}x^i\mathrm{d}\eta \\ &+ \mathrm{d}x^i\mathrm{d}x^j\left[\delta_{ij}\,(1+2D) + \left(\partial_i\partial_j - \frac{1}{3}\delta_{ij}\nabla^2\right)F + \partial_i F_j^\perp + \partial_j F_i^\perp + H_{ij}\right]\Big\}\,, \end{aligned} \tag{2.74}$$

where $\perp$ denotes solenoidal vector fields, $\partial^i X_i^\perp = 0$, while H_{ij} are transverse-traceless perturbations of the metric. This decomposition in terms of scalar, vector and tensor degrees of freedom [235, 236] reflects the transformation properties of the perturbations under spatial rotations. All the perturbations of the metric have to be thought as linear

terms in the expansion in the small parameter ϵ, while higher-order terms have been neglected here, since they will produce subdominant effects for the observables considered in this Thesis. The computation of the cosmological perturbations at second order has been done for instance in [171, 237] and some applications to the CMB have been presented in [238, 239, 240]. Thanks to the decomposition theorem, it can be shown that the scalar, the vector and the tensor degrees of freedom evolve independently at first order in perturbation theory. As shown in Section 1.1.1, not all these degrees of freedom are physical, thus a natural way to deal with the problem of the choice of the gauge would be to work with gauge invariant variables or to fix the gauge. In this Thesis, for simplicity, we will work in the Poisson gauge, defined by setting

$$B = 0\,, \qquad F = 0\,, \qquad F_j^{\perp} = 0\,, \tag{2.75}$$

and relabelling the scalar perturbations $\Phi = A$, $\Psi = -D$. The gauge fixing we have done saturates all the spurious degrees of freedom of associated to the coordinate transformations, ending up with just six degrees of freedom. However, it is possible to show that the solenoidal vector field $B_i^{\perp}$ in this gauge the vorticity is suppressed by the expansion of the Universe [241], therefore we can neglect such a contribution, since in the model of inflation considered here we do not expect the presence of primordial solenoidal vector fields. The line element we will consider from now on is therefore

$$ds^2 = a^2(\eta)\Big\{ -\mathrm{d}\eta^2\,(1+2\Phi) + \mathrm{d}x^i\mathrm{d}x^j\,[\delta_{ij}\,(1-2\Psi) + H_{ij}]\Big\}\,, \tag{2.76}$$

The metric and its inverse at first order in the perturbations are just

$$\begin{aligned} g_{\mu\nu} =& a^2 \begin{pmatrix} -(1+2\Phi) & 0 \\ 0 & \delta_{ij}(1-2\Psi) + H_{ij} \end{pmatrix}\,, \\ g^{\mu\nu} =& \frac{1}{a^2} \begin{pmatrix} -(1-2\Phi) & 0 \\ 0 & \delta^{ij}(1+2\Psi) - H^{ij} \end{pmatrix}\,, \end{aligned} \tag{2.77}$$

where the indices of the tensor perturbation are raised by the Kronecker delta, $H^{ij} = \delta^{ij}H_{ij}$.

Perturbations of the Einstein tensor

The Christoffel symbols are defined in terms of the derivatives of the metric by

$$\Gamma^{\mu}_{\nu\rho} \equiv \frac{1}{2} g^{\mu\alpha}\left(\partial_\rho g_{\nu\alpha} + \partial_\nu g_{\alpha\rho} - \partial_\alpha g_{\rho\nu}\right)\,. \tag{2.78}$$

The computation of the affine connection in the Poisson gauge gives the result

$$\begin{aligned}
\Gamma^0_{00} =& \mathcal{H} + \Phi' \,, \\
\Gamma^0_{0i} =& \partial_i \Phi \,, \\
\Gamma^0_{ij} =& [\mathcal{H}(1 - 2\Phi - 2\Psi) - \Psi']\delta_{ij} + \frac{1}{2} H'_{ij} + \mathcal{H} H_{ij} \,, \\
\Gamma^i_{00} =& \partial^i \Phi \,, \\
\Gamma^i_{j0} =& \left(\mathcal{H} - \Psi'\right) \delta^i_j + \frac{1}{2} H^{i\,\prime}_j \,, \\
\Gamma^i_{jk} =& \partial^i \Psi \delta_{jk} - \partial_j \Psi \delta^i_k - \partial_k \Psi \delta^i_j + \frac{1}{2} \left(\partial_j H^i_k + \partial_k H^i_j - \partial^i H_{jk}\right) \,.
\end{aligned} \tag{2.79}$$

The Riemann tensor is then computed by using

$$R^\rho_{\mu\sigma\nu} = \partial_\sigma \Gamma^\rho_{\nu\mu} - \partial_\nu \Gamma^\rho_{\sigma\mu} + \Gamma^\rho_{\sigma\lambda} \Gamma^\lambda_{\nu\mu} - \Gamma^\rho_{\nu\lambda} \Gamma^\lambda_{\sigma\mu} \,. \tag{2.80}$$

The Ricci tensor is given by

$$R_{\mu\nu} = R^\sigma_{\mu\sigma\nu} \,, \tag{2.81}$$

therefore its components are

$$\begin{aligned}
R_{00} =& 3\mathcal{H}^2 - 3\frac{a''}{a} + \nabla^2 \Phi + 3\mathcal{H}\left(\Phi' + \Psi'\right) \,, \\
R_{0i} =& 2\partial_i \Psi' + 2\mathcal{H}\partial_i \Phi \,, \\
R_{ij} =& \left[\left(\frac{a''}{a} + \mathcal{H}^2\right)(1 - 2\Psi - 2\Phi) - \mathcal{H}(5\Psi' + \Phi') - \Psi'' + \nabla^2 \Psi\right] \delta_{ij} + \partial_i \partial_j \left(\Psi - \Phi\right) \\
& + \frac{1}{2} H''_{ij} + \mathcal{H} H'_{ij} - \frac{1}{2a^2} \nabla^2 H_{ij} + \left(\mathcal{H}' + 2\mathcal{H}^2\right) H_{ij} \,.
\end{aligned} \tag{2.82}$$

The Einstein tensor is defined by

$$G_{\mu\nu} \equiv R_{\mu\nu} - \frac{1}{2} g_{\mu\nu} R \,, \tag{2.83}$$

where the Ricci scalar is

$$R \equiv g^{\mu\alpha} R_{\mu\alpha} \,. \tag{2.84}$$

The components of the Einstein tensor are therefore

$$\begin{aligned}
G^0_0 =& \frac{1}{a^2}\left[\mathcal{H}^2(6\Phi - 3) + 6\mathcal{H}\Psi' - 2\nabla^2 \Psi\right] \,, \\
G^0_i =& -\frac{2}{a^2}\left(\mathcal{H}\partial_i \Phi + \partial_i \Psi'\right) \,, \\
G^i_0 =& \frac{2}{a^2}\left(\partial^i \Psi' + \mathcal{H}\partial^i \Phi\right) \,, \\
G^i_j =& \frac{1}{a^2}\left\{\left[-2\frac{a''}{a}(1 - 2\Phi) + \mathcal{H}^2(1 - 2\Phi) + 2\mathcal{H}(\Phi' + 2\Psi') + 2\Psi'' - \nabla^2(\Psi - \Phi)\right]\delta_{ij}\right. \\
& \left. + \partial^i \partial_j (\Psi - \Phi) + H^{i\,\prime\prime}_j + 2\mathcal{H} H^{i\,\prime}_j - \frac{1}{a^2}\nabla^2 H^i_j\right\} \,.
\end{aligned} \tag{2.85}$$

Distribution function

As discussed in Section 2.2, the energy density of the Universe is mainly provided by photons, neutrinos, baryons, CDM and dark energy. It is possible to characterize the abundance of these species by introducing a distribution function $f(\eta, \mathbf{x}, \mathbf{p})$ in such a way that the quantity $\mathrm{d}^3\mathbf{x}\,\mathrm{d}^3\mathbf{p}\,f(\eta, \mathbf{x}, \mathbf{p})$ corresponds to the number of particles that at η occupy the volume of the phase space $\mathrm{d}^3\mathbf{x}\,\mathrm{d}^3\mathbf{p}$ surrounding $\mathbf{x}$ and $\mathbf{p}$, with $\mathbf{p}$ the canonical conjugate variable of the position. The momentum in GR is defined by

$$p^\mu \equiv \frac{\mathrm{d}x^\mu}{\mathrm{d}\lambda}(\lambda)\,, \tag{2.86}$$

where λ is the affine parameter of the geodesic. Additional details on the physical and on the comoving momentum will be given in Section 3.2. Consistently with the cosmological principle, the distribution function can be decomposed into a homogeneous and isotropic part, plus a tiny fluctuation, which depends on the position and on the direction of the momentum,

$$f(\eta, \mathbf{x}, \mathbf{q}) = \bar{f}(\eta, q) + \delta f(\eta, \mathbf{x}, q)\,. \tag{2.87}$$

where q is the comoving momentum associated to $\mathbf{p}$. In the literature [42], the perturbations of the distribution function of photons and neutrinos are often rescaled into

$$\begin{aligned} \delta f_\gamma(\eta, \mathbf{x}, \mathbf{q}) &= -\frac{\partial \bar{f}_\gamma(\eta, q)}{\partial q}\Theta(\eta, \mathbf{x}, \hat{n})\,, \\ \delta f_\nu(\eta, \mathbf{x}, \mathbf{q}) &= -\frac{\partial \bar{f}_\nu(\eta, q)}{\partial q}\mathcal{N}(\eta, \mathbf{x}, \hat{n})\,. \end{aligned} \tag{2.88}$$

In the CMB case, the spectrum of photon is a blackbody, therefore it is characterized just by the temperature,

$$f(\eta, \mathbf{x}, \mathbf{q}) = \left\{ \exp \frac{q}{T(\eta)\left[1 + \frac{\delta T}{T}(\eta, \mathbf{x}, \hat{n})\right]} - 1 \right\}^{-1}\,, \tag{2.89}$$

where it is straightforward to see that

$$\frac{\delta T}{T}(\eta, \mathbf{x}, \hat{n}) = \Theta(\eta, \mathbf{x}, \hat{n})\,. \tag{2.90}$$

Perturbation of the energy-momentum tensor

In the same philosophy of what has been done for the perturbations of the metric in the previous sections, we would like to find the most general form of the energy-momentum tensor of a perfect fluid in terms of scalar, vector and tensor perturbations. In [236], it has been shown that it is possible to write

$$T^\mu_\nu = (\rho + P)u^\mu u_\nu + \delta^\mu_\nu P + \pi^\mu_\nu\,, \tag{2.91}$$

where π^{μ}_{ν} is connected to the anisotropic stress/viscosity of the fluid and it is a term of first order in the perturbations. The velocity and the pressure can be expanded in terms of their background contributions, which depend just on the conformal time, and of small fluctuations which are inhomogeneous,

$$\rho(\eta,\mathbf{x}) = \bar{\rho}(\eta) + \delta\rho(\eta,\mathbf{x})\,, \qquad P(\eta,\mathbf{x}) = \bar{P}(\eta) + \delta P(\eta,\mathbf{x})\,. \tag{2.92}$$

The four-velocity is computed in perturbation theory by using the condition $u^2 = -1$ and by noticing that its spatial component should vanish at zero order in the perturbations, $u^i = v^i/a$,

$$u^{\mu}u_{\mu} = -1 \rightarrow g_{\mu\nu}u^{\mu}u^{\nu} = -1 \rightarrow a^2\left[-(1+2\Phi)\left(u^{(0)}\right)^2 + 2u^{(0)}u^{(1)}\right] = -1\,, \tag{2.93}$$

therefore we conclude that

$$u^{\mu} = \frac{1}{a}\left(1-\Phi \quad v^i\right)\,, \qquad u_{\mu} = a\left(-(1+\Phi) \quad v_i\right)\,. \tag{2.94}$$

The components of the energy-momentum tensor are then

$$T^0_0 = -\bar{\rho} - \delta\rho\,, \qquad T^0_i = (\bar{\rho}+\bar{P})v_i\,, \qquad T^i_0 = (\bar{\rho}+\bar{P})v^i \qquad T^i_j = \delta^i_j(\bar{P}+\delta P) + \pi^i_j\,. \tag{2.95}$$

In order to connect the energy-momentum tensor, which plays a crucial role in the Einstein equation, to the distribution function of a given species, whose evolution is computed by using the Boltzmann equation, we write the energy-momentum as an integral over the phase space of the distribution function. The stress-energy tensor for a species α is defined [236] according to

$$T^{\mu}_{\nu,\alpha}(\eta,\mathbf{x}) = \frac{g_{\alpha}}{\sqrt{-g}}\int \frac{\mathrm{d}p_1\mathrm{d}p_2\mathrm{d}p_3\mathbf{p}}{(2\pi)^3}\frac{p^{\mu}p_{\nu}}{p^0}f_{\alpha}(\eta,\mathbf{x},\mathbf{p})\,, \tag{2.96}$$

where g_{α} are the intrinsic degrees of freedom of the species considered. As it will be explicitly shown in Section 3.2, for a particle of mass m, the physical momentum is equal to

$$\begin{aligned} p^{\mu} =& \frac{1}{a}\left(e^{-\Phi}E \quad p\,\hat{n}^i e^{\Psi}\left(1-\tfrac{1}{2}H_{jk}\hat{n}^j\hat{n}^k\right)\right)\,, \\ p_{\mu} =& a\left(e^{\Phi}E \quad p\,\hat{n}_i\, e^{-\Psi}\left(1+\tfrac{1}{2}H_{jk}\hat{n}^j\hat{n}^k\right)\,.\right) \end{aligned} \tag{2.97}$$

with $E \equiv \sqrt{m^2+p^2}$ the energy density of a particle, $p^2 \equiv \delta_{ij}p^ip^j$. It is possible to show that, by introducing a comoving momentum $q^{\mu} = a\,p\,\hat{n}^{\mu}$, the energy-momentum tensor can be written according to

$$T^{\mu}_{\nu,\,\alpha}(\eta,\mathbf{x}) = g_{\alpha}\int \frac{\mathrm{d}^3\mathbf{q}}{(2\pi)^3}e^{\Phi}\frac{p^{\mu}p_{\nu}}{p^0}f_{\alpha}(\eta,\mathbf{x},\mathbf{q})\,, \tag{2.98}$$

where the integral is now a standard integral over spherical coordinates. We characterize photons in terms of the perturbations of their distribution function,

$$f_{\gamma} = \bar{f}_{\gamma} - q\frac{\partial\bar{f}_{\gamma}}{\partial q}\Theta\,. \tag{2.99}$$

It is useful to compute the energy-momentum tensor in Fourier space, denoted by $\mathbf{k}$, instead of real space, and it is useful to decompose the distribution function in terms of Legendre polynomials of argument $\mu \equiv \hat{k} \cdot \hat{n}$,

$$\Theta(\eta, \mathbf{k}, \hat{n}) = \sum_{\ell} \mathcal{P}_{\ell}(\mu) \Theta_{\ell}(\eta, \mathbf{k}) \,. \tag{2.100}$$

In this way, the $(0,0)$ component of the energy-momentum tensor is

$$T^{0}_{0,\gamma}(\eta, \mathbf{k}) = -\bar{\rho}_{\gamma}(\eta)[1 + \delta_{\gamma}(\eta, \mathbf{k})] = -\bar{\rho}_{\alpha}(\eta)[1 + 4\Theta_{0}(\eta, \mathbf{k})] \,, \tag{2.101}$$

where the background energy density is defined by

$$\bar{\rho}_{\gamma}(\eta) \equiv 2 \int \frac{\mathrm{d}^{3} q}{(2\pi)^{3}} \, q \bar{f}_{\gamma}(\eta) \,. \tag{2.102}$$

In a similar fashion it can be shown that

$$\begin{aligned} \hat{k}^{i} \, T^{0}_{i,\gamma}(\eta, \mathbf{k}) =& 4\bar{\rho}_{\alpha}(\eta) \Theta_{1}(\eta, \mathbf{k}) \,, \\ \left(\hat{k}^{j} \hat{k}_{i} - \frac{1}{3} \delta^{j}_{i} \right) \, T^{i}_{j,\gamma}(\eta, \mathbf{k}) =& -\frac{8}{3} \bar{\rho}_{\gamma}(\eta) \Theta_{2}(\eta, \mathbf{k}) \,. \end{aligned} \tag{2.103}$$

The same discussion holds for the perturbation of the distribution function of neutrinos, denoted by $\mathcal{N}$. For non-relativistic species, like CDM and baryons, we just use the velocity field and the density constrast

$$\delta_{\beta} \equiv \frac{\delta \rho_{\beta}}{\bar{\rho}_{\beta}} \,. \tag{2.104}$$

2.4.2 Boltzmann equation

The Universe is filled by matter and radiation, whose energy density and pressure present tiny anisotropies that influence the evolution of the metric perturbations. When some particle species that source the energy density of the Universe strongly interact, it is possible to assume that they are in thermodynamic equilibrium, studying the evolution of the system in terms of Eqs. (2.16), (2.17). On the other hand, when the interaction rate decreases, coming closer to the expansion rate of the Universe, the evolution of the system should be studied by mean of the Boltzmann equation, which is the most powerful tool to characterize non-equilibrium processes [242, 243]. The Boltzmann equation describes the evolution in time of the distribution function as a function of the properties of the spacetime, of the scattering processes involved and of the presence of external sources that could inject particles in the system,

$$\mathcal{L}[f] = \mathcal{C}[f] + \mathcal{J}[f] \,, \tag{2.105}$$

where the collision and the source operators depend on the specific environment considered, while the Liouville operator is equal to

$$\mathcal{L}[f] \equiv p^{\mu} \frac{\partial}{\partial x^{\mu}} - \Gamma^{\mu}_{\nu\rho} p^{\nu} p^{\rho} \frac{\partial}{\partial p^{\mu}} \,. \tag{2.106}$$

When the collision term is extremely large, the Boltzmann equation drives the distribution function to thermal equilibrium, while, when the collision term is subdominant, the Boltzmann equation computes the evolution of the distribution at each time in a nontrivial way. In Section 3.2, we show an example of the solution of the Boltzmann equation in the case of a CGWB, while in this chapter, we will just show the explicit results of the Boltzmann equation for the standard radiation and matter content of the Universe,

$$\begin{aligned}
\Theta' + ik\mu\Theta =& \psi' - ik\mu\Phi - \tau'\left[\Theta_0 - \Theta - \frac{1}{2}\mathcal{P}_2(\mu)\Theta_2\right] , \\
\delta_c' + ikv_c =& 3\Psi' , \\
v_c' + \mathcal{H}v_c =& - ik\Phi , \\
\mathcal{N}' + ik\mu\mathcal{N} =& \Psi' - ik\mu\Phi ,
\end{aligned} \tag{2.107}$$

where the term on the r.h.s. in the first equation comes from the interaction between photon and baryons.

2.4.3 Einstein equations in the Poisson gauge

According to the decomposition theorem, the equations of motion for the scalar, the vector and the tensor perturbations are decoupled at first order in the perturbations. This means that it is possible to characterize the evolution of H_{ij} independently on Φ and Ψ. By using the definition of the Einstein equations given by (1.1), we combine the Einstein tensor computed in Eq. (2.85) and the energy-momentum tensor defined in the previous section, obtaining

$$\begin{aligned}
H_{ij}'' + 2\mathcal{H}H_{ij}' - \frac{1}{a^2}\nabla^2 H_{ij} =& 16\pi G\pi_{ij}^{\mathrm{TT}} , \\
k^2\Psi + 3\mathcal{H}\left(\Psi' + \mathcal{H}\Phi\right) =& - 4\pi G a^2\left(\bar{\rho}_c\delta_c + \bar{\rho}_b\delta_b + \bar{\rho}_\gamma\Theta_{0,\gamma} + \bar{\rho}_\nu\Theta_{0,\nu}\right) , \\
k^2(\Phi - \Psi) =& - 32\pi G a^2\bar{\rho}_\nu\Theta_{2,\nu} ,
\end{aligned} \tag{2.108}$$

where π_{ij}^{TT} is the tensor component of the anisotropic stress. The system of the Einstein and the Boltzmann equations, Eqs. (2.108), (2.107) can be solved numerically, using for instance the numerical code CLASS [44, 45].

2.5 Current constraints

The most important constraints on the ΛCDM model have been provided by observations of the anisotropies of the CMB in the past decades, by the satellites COBE [217, 27], WMAP [218, 219] and Planck [220, 26]. The fluctuations in the CMB temperature along different directions of observation can be computed by solving the Boltzmann equation for Θ, analogously to what we will do for the CGWB in Chapter 3. At temperatures larger than 0.5 MeV, photons were tightly coupled to baryons via electromagnetic interaction, thus any imprint of the physics operating at large energy scales is washed out by the scattering processes [42]. Around 0.5 MeV, electrons and protons form bound systems in

form of hydrogen atoms. The evolution of the distribution function of the CMB photons is computed since this epoch, called recombination, which occurred approximately at $\eta_{\rm rec} \approx 280\,{\rm Mpc}$, until the present time, $\eta_0 \approx 10^4\,{\rm Mpc}$. To evaluate the amount of anisotropies, we typically expand the distribution function in spherical harmonics, where the coefficients of the expansion are defined by

$$\Theta_{\ell m}(\hat{n}, \eta_0) \equiv \int {\rm d}\hat{n} Y^*_{\ell m}(\hat{n})\, \Theta(\hat{n}, \eta_0)\,, \tag{2.109}$$

and we compute the angular power spectrum, defined as

$$\delta_{\ell\ell'}\delta_{mm'} C_\ell^{\rm CMB\times CMB} \equiv \langle \Theta_{\ell m}(\hat{n}, \eta_0)\Theta^*_{\ell' m'}(\hat{n}, \eta_0)\rangle\ , \tag{2.110}$$

The solution of the Boltzmann equation for the fluctuations of the temperature of the CMB, written in Eq. (6.3), shows that the angular power spectrum is sensitive to the inhomogeneities in the number of photons and in the gravitational potential at recombination (Sachs-Wolfe effect), to the variations of the potentials around the geodesics (Integrated Sachs-Wolfe), and to the velocity of photons at recombination (Doppler). An additional effect is provided by the lensing of photons by the massive structures they encountered. In the left panel of Figure 2.1, we plot these contribution to the angular power spectrum of the CMB, while to the right one we show the dependence of the spectrum to different cosmological parameters. The CMB spectrum is dominated by the SW, which exhibits a plateau at large angular scales, where the potentials and the number density of photons and baryons at recombination are constant. At smaller scales, the photon-baryon fluid behaves like an harmonic oscillator and the potential wells and the density of CMB photons oscillate. These acoustic oscillations translate in two a series of peaks in the SW contribution to the angular power spectrum of the CMB at high multipoles. At large angular scales, the ISW is dominated by variations of the metric perturbations at large angular scales (late-ISW), while at $\ell \approx 200$ by variations of the potentials around recombination (early-ISW). The strong constraining power of the CMB is due to the fact that varying different cosmological parameters determines very peculiar changes in the angular power spectrum:

- the overall amplitude of $C_\ell^{\rm CMB\times CMB}$ is fixed by $e^{-2\tau_{\rm reio}} A_s$, with $tau_{\rm reio}$ the optical depth of photons and A_s the amplitude of the power spectrum of the curvature perturbations at the pivot scale $0.05\,{\rm Mpc}^{-1}$,

$$A_s \equiv P_\zeta(k = 0.05\,{\rm Mpc}^{-1})\,; \tag{2.111}$$

- the Hubble parameter H_0 and the density of CDM $\bar{\Omega}_{\rm c,0}$ affect the late-ISW effect and the scale and the shape of the acoustic peaks;

- the overall scaling of the angular power spectrum of the CMB with ℓ depends on the tilt of the curvature perturbations n_s. The primordial power spectrum is parametrized in such a way that

$$P_\zeta(k) = A_s \left(\frac{k}{0.05\,{\rm Mpc}^{-1}}\right)^{n_s - 1}\ ; \tag{2.112}$$

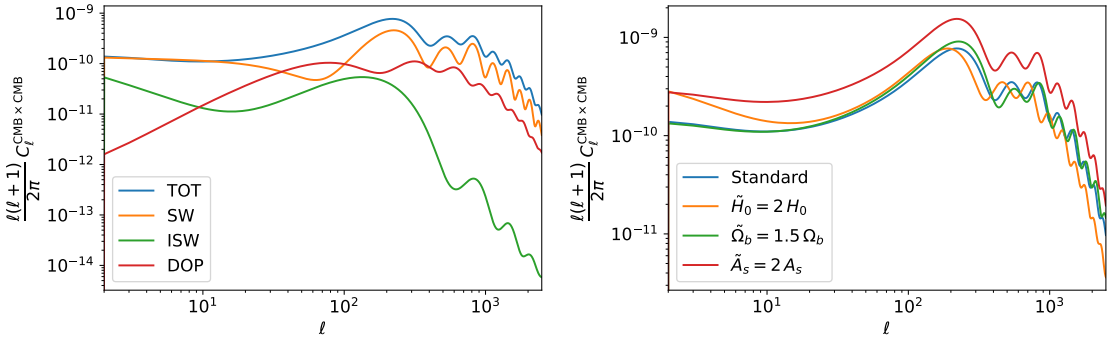

Figure 2.1: Left: plot of the contributions to the angular power spectrum of the CMB as a function of the multipole considered. Right: plot of the angular power spectrum of the CMB by varying one cosmological parameters, w.r.t. the standard value.

- variaton of $\Omega_{b,0}$ determine a lateral shift in the peaks of the CMB spectrum, because of the change of the sound horizon of the photon-baryon fluid at recombination. In addition, the baryon density affects the heights of the peaks;
- Ω_Λ regulates the variation of the potentials responsible for the early ISW effect, thus its variations could affect significantly the shape of the spectrum at large angular scales;
- the curvature of the Universe affects the geodesics of photon and could change the location of the acoustic peaks of the CMB.

In the right plot of Figure 2.1, we plot the angular power spectrum of the CMB by varying just one of the cosmological parameters previously mentioned, showing the effects of its variation on the angular power spectrum. Observations of the anisotropies of the temperature of the CMB allowed therefore to constrain several cosmological parameters. We report the results provided by *Planck* [26] in Table 2.1. Note however that the CMB spectrum is sensitive to other parameters, such as the effective number of neutrinos and their masses [244], not discussed in this section.

Chapter 3

Anisotropies of the CGWB

3.1 Geometric-optics limit

In this Thesis we consider CGWBs that could be detected by advanced PTA or by future space- and ground-based interferometers, having frequencies that lie within the range $10^{-12} - 10^{4}\,\mathrm{Hz}$. The relation between the comoving momentum and the frequency of the GWs is

$$q = \frac{2\pi}{\lambda} = \frac{2\pi}{c}\, f = 6 \times 10^{14}\, \frac{f}{\mathrm{Hz}}\ \mathrm{Mpc}^{-1}\,, \tag{3.1}$$

which means that in our case we are looking at momenta of the order $10^{3} - 10^{18}\,\mathrm{Mpc}^{-1}$. Typically, all the primordial gravitational signals start propagating long before the time of equality between matter and radiation, at a time η_{in} which is much smaller than the conformal time today, $\eta_0 \approx 10^{4}\,\mathrm{Mpc}$. This implies that when we look at the anisotropies of a signal that comes from a surface distant $\eta_0 - \eta_{\mathrm{in}} \approx \eta_0$, we are looking for cosmological perturbations that on such a sphere present hot and cold spots at a distance η_0/ℓ. The maximal amount of anisotropies is therefore given by the scales

$$k \approx \frac{\ell}{\eta_0}\,. \tag{3.2}$$

Since the multipoles that can be probed by future interferometers are quite small, $\ell_{\mathrm{max}} \lesssim 100$, the angular power spectrum of the CGWB is affected only by large-scale perturbations of the Universe, with comoving scales within the range $10^{-4} - 1\,\mathrm{Mpc}^{-1}$. This enormous separation of scales, $q \gg k$, permits to use the shortwave approximation introduced in Section 1.1.2, characterizing the GWs as small ripples that propagate through a slowly-varying background. More specifically, we consider the FLRW metric in the Poisson gauge introduced in Eq. (2.76),

$$ds^2 = a^2(\eta)\left\{-\mathrm{d}\eta^2\,(1 + 2\Phi(\eta,\mathbf{x})) + \mathrm{d}x^i \mathrm{d}x^j\,[\delta_{ij}\,(1 - 2\Psi(\eta,\mathbf{x})) + H_{ij}(\eta,\mathbf{x}) + h_{ij}(\eta,\mathbf{x})]\right\}\,, \tag{3.3}$$

where Φ, Ψ and H_{ij} are the large-scale perturbations of scale k, while h_{ij} is the rapidly-oscillating waves that compose the CGWB. As we will see in Appendix E.2, the propagation of the GWs through the Universe is modulated by the large-scale scalar and tensor

perturbations,

$$h''_{ij} + h'_{ij}\left(2\mathcal{H} - \Phi' + \Psi'\right) + h_{ij}\left(4\mathcal{H}\Psi' + 2\Psi''\right) - \nabla^2 h_{ij}\left(1 + 2\Phi + 2\Psi\right) + 2H^{kl}\partial_k\partial_l h_{ij} = 0\,. \tag{3.4}$$

However, since it is possible to show that in the shortwave approximation the geometric optics limit holds, we can describe the GWs as collisionless and massless particles that propagate through the geodesics computed by considering only the large-scale perturbations of the metric,

$$ds^2 = a^2(\eta)\left\{-\mathrm{d}\eta^2\left(1 + 2\Phi(\eta, \mathbf{x})\right) + \mathrm{d}x^i \mathrm{d}x^j\left[\delta_{ij}\left(1 - 2\Psi(\eta, \mathbf{x})\right) + H_{ij}(\eta, \mathbf{x})\right]\right\}\,. \tag{3.5}$$

In this way, we avoid a description of the CGWB in terms of the gravitational field, Eq. (3.4), but we use a simpler and more intuitive approach, which consists in the Boltzmann equation for the CGWB.

3.2 Boltzmann equation

Geodesics of graviton

In the geometric optics limit, we consider gravitons propagating along trajectories $x^\mu(\lambda)$ with physical momentum $p^\mu(\lambda)$, where λ is an affine parameter and the momentum is defined by

$$p^\mu(\lambda) \equiv \frac{\mathrm{d}x^\mu}{\mathrm{d}\lambda}(\lambda)\,. \tag{3.6}$$

The equation of motion is computed by recalling that massless particles propagate along null geodesics,

$$\frac{\mathrm{d}p^\mu}{\mathrm{d}\lambda} = -\Gamma^\mu_{\nu\rho}\, p^\nu p^\rho\,, \tag{3.7}$$

where the affine connection is evaluated w.r.t. the slowly-varying metric, Eq. (3.5). The full expression of the Christoffel symbols in the Poisson gauge has been given in Eq. 2.79. An intuitive way to parametrize the momentum of graviton is to write it in terms of its direction of propagation $\hat{n}$, which is a unit vector that satisfies $\delta_{ij}\,\hat{n}^i\hat{n}^j = 1$, and magnitude p, defined by

$$p^2 \equiv g_{ij}\, p^i p^j\,. \tag{3.8}$$

According to these definitions, it is straightforward to see that

$$p^i = \frac{p}{a}\,\hat{n}^i\, e^{\Psi}\left(1 - \frac{1}{2}H_{jk}\,\hat{n}^j\hat{n}^k\right)\,. \tag{3.9}$$

Since the physical momentum is redshifted, because of the expansion of the Universe, it would be useful to introduce the comoving momentum $q \equiv ap$, which gives

$$p^i = \frac{q}{a^2}\,\hat{n}^i\, e^{\Psi}\left(1 - \frac{1}{2}H_{jk}\,\hat{n}^j\hat{n}^k\right)\,. \tag{3.10}$$

By exploiting the condition on the momenutm for massless particles, $p^\mu p_\mu = 0$, we get an expression for the time component of the momentum of graviton, which also depends on the comoving momentum and on the scalar perturbations of the Universe,

$$p^0 = \frac{q}{a^2} e^{-\Phi} \,. \tag{3.11}$$

The evolution in time of the position of graviton is evaluated just by using the known expressions for the momentum,

$$\frac{\mathrm{d}x^i}{\mathrm{d}\eta}(\lambda) = \frac{\mathrm{d}\lambda}{\mathrm{d}\eta}\frac{\mathrm{d}x^i}{\mathrm{d}\lambda} = \frac{p^i}{p^0} = e^{\Phi+\Psi}\left(1 - \frac{1}{2}H_{jk}\,\hat{n}^j\hat{n}^k\right) \,. \tag{3.12}$$

The evolution in time of the magnitude of the comoving momentum, is computed then by combining the geodesics equation, Eq. (3.7), for $\mu = 0$,

$$\frac{\mathrm{d}p^0}{\mathrm{d}\lambda} = \frac{q^2}{a^4} e^{-2\Phi}\left(-2\mathcal{H} - \Phi' + \Psi' - 2\frac{\partial\Phi}{\partial x^i}\hat{n}^i - \frac{1}{2}H'_{lm}\hat{n}^l\hat{n}^m\right) \,, \tag{3.13}$$

with the derivative w.r.t. λ of Eq. (3.11),

$$\frac{\mathrm{d}p^0}{\mathrm{d}\lambda} = p^0\frac{\mathrm{d}p^0}{\mathrm{d}\eta} = \frac{q^2}{a^4} e^{-2\Phi}\left(-2\mathcal{H} + \frac{1}{q}\frac{\mathrm{d}q}{\mathrm{d}\eta} - \Phi' - \frac{\partial\Phi}{\partial x^i}\hat{n}^i\right) \,. \tag{3.14}$$

The result shows that the amplitude of the comoving momentum of the GWs changes in time, because the Universe is inhomogeneous,

$$\frac{\mathrm{d}q}{\mathrm{d}\eta} = q\left(\Psi' - \frac{\partial\Phi}{\partial x^i}\hat{n}^i - \frac{1}{2}H'_{lm}\hat{n}^l\hat{n}^m\right) \,. \tag{3.15}$$

A similar result, not interesting for our purposes, could be found for the derivative of the direction of propagation of gravitons, which, as q, is proportional to terms linear in the large-scale perturbations of the metric. The results we have found show that gravitons at the background level propagate through straight lines, with a redshift of the physical momentum due to the expansion of the Universe, while at first order in the perturbations the comoving momentum and the direction of propagation change in time, because of the scalar and tensor inhomogeneities in the Universe.

Distribution function of graviton and observables

We characterize the abundance of graviton of physical momentum $\mathbf{p}$ in a region of spacetime $(\eta, \mathbf{x})$ by introducing a distribution function $f_{\mathrm{CGWB}}(\eta, \mathbf{x}, \mathbf{q})$ as done in [117, 38, 39, 40]. The description of GWs in terms of a distribution function is possible only in the shortwave approximation, $q \gg k$ and $q\eta \gg 1$, because in this regime the propagation of the waves is given by geometric optics. We will give a more quantitative definition of the time at which the transition from the wave-optics and the geometrical-optics regimes occurs in

Section 3.3. According to Eqs. (2.95), (2.96), the connection between the energy density of graviton and the distribution function is given by

$$\rho_{\rm CGWB}(\eta,\mathbf{x}) = \int {\rm d}p_1{\rm d}p_2{\rm d}p_3\, p\, f_{\rm CGWB}(\eta,\mathbf{x},\mathbf{q}) = \frac{1}{a^4(\eta)}\int {\rm d}\hat{n}\int {\rm d}q\, q^3\, f_{\rm CGWB}(\eta,\mathbf{x},\mathbf{q})\,, \tag{3.16}$$

where we have used the change of variables between the physical momentum, over which the energy density is defined, and the comoving momentum, which is the argument of the distribution function we have adopted. The distribution function can be connected to the fractional energy density in GWs used in Eq. (1.45) by using

$$\Omega_{\rm CGWB}(\eta,\mathbf{x},\mathbf{q}) = \frac{1}{\rho_{\rm crit}}\left(\frac{q}{a}\right)^4 f_{\rm CGWB}(\eta,\mathbf{x},\mathbf{q})\,, \tag{3.17}$$

with $\rho_{\rm crit}$ the critical energy density of the Universe at the present epoch. By assuming then that the CGWB is produced isotropically, we expect that the distribution function shows a dominant homogeneous and isotropic contribution, $\bar{f}_{\rm CGWB}(\eta,q)$, and small inhomogeneities and anisotropies $\delta f_{\rm GW}(\eta,\mathbf{x},\mathbf{q})$, connected to the evolution of the inhomogeneities of the Universe in time. An useful way to write the perturbation of the distribution function of graviton is

$$\delta f_{\rm CGWB}(\eta,\mathbf{x},\mathbf{q}) \equiv -q\frac{\partial \bar{f}_{\rm CGWB}(\eta,q)}{\partial q}\Gamma(\eta,\mathbf{x},\mathbf{q})\,, \tag{3.18}$$

where Γ is the perturbation of the distribution function analogous to the one used for the CMB in Eq. (2.99). The perturbation of the energy density of the CGWB in a single frequency bin, defined in Eq. (1.49), is related to the perturbation of the distribution function by

$$\delta_{\rm CGWB}(\eta,\mathbf{x},\mathbf{q}) = \frac{1}{\rho_{\rm crit}}\left(\frac{q}{a}\right)^4\frac{\delta f_{\rm CGWB}(\eta,\mathbf{x},\mathbf{q})}{\bar{\Omega}_{\rm CGWB}(\eta,q)} = \frac{1}{\rho_{\rm crit}}\left(\frac{q}{a}\right)^4\frac{-q\frac{\partial \bar{f}_{\rm CGWB}(\eta,q)}{\partial q}\Gamma(\eta,\mathbf{x},\mathbf{q})}{\bar{\Omega}_{\rm CGWB}(\eta,q)}\,, \tag{3.19}$$

where the derivatives of the unperturbed part of the distribution function can be written as

$$-q\frac{\partial \bar{f}_{\rm CGWB}(\eta,q)}{\partial q} = \rho_{\rm crit}\left(\frac{a}{q}\right)^4\left(4-\frac{\partial\bar{\Omega}_{\rm CGWB}}{\partial\ln q}(\eta,q)\right)\,. \tag{3.20}$$

It is possible therefore to connect the perturbation of the distribution function Γ to perturbation of the energy density in a single frequency bin in terms the tensor tilt of the background, introduced in Eq. (1.48), via the simple relation

$$\delta_{\rm CGWB}(\eta,\mathbf{x},\mathbf{q}) = [4-n_{\rm gwb}(q)]\,\Gamma(\eta,\mathbf{x},\mathbf{q})\,. \tag{3.21}$$

The dependence on $\mathbf{x}$ of the distribution function means that in different regions in the Universe, the energy density of graviton could fluctuate, while the dependence on $\hat{n}$ implies the spectrum of the CGWB is anisotropic, since gravitons coming from different directions carry different energy.

Solution of the Boltzmann equation

Gravitational interactions decoupled at the Planck scale, therefore it is possible to neglect the collision term in the Boltzmann equation defined in Eq. (2.105). Since in this work we consider different sources of cosmological GWs separately, we write the emissivity terms in the Boltzmann equation as an initial condition for the abundance of graviton at the end of the production process, avoiding the complicated issue of solving the Boltzmann equation with a model-dependent source term [39, 40]. We will provide a more detailed explanation of the role played by the source term in Section 3.4.1, when we will define rigorously the initial time at which we compute the initial conditions of the Boltzmann equation in the case of GWs produced during inflation. The Boltzmann equation for collisionless particles is

$$\frac{\mathrm{d}}{\mathrm{d}\lambda} f_{\mathrm{CGWB}} = 0 \rightarrow \frac{1}{p^0}\frac{\mathrm{d}}{\mathrm{d}\eta} f_{\mathrm{CGWB}} = 0\,, \tag{3.22}$$

which is equivalent to

$$\frac{\partial}{\partial\eta} f_{\mathrm{CGWB}} + \frac{\mathrm{d}x^i}{\mathrm{d}\eta}\frac{\partial}{\partial x^i} f_{\mathrm{CGWB}} + \frac{\mathrm{d}q}{\mathrm{d}\eta}\frac{\partial}{\partial q} f_{\mathrm{CGWB}} + \frac{\mathrm{d}\hat{n}^i}{\mathrm{d}\eta}\frac{\partial}{\partial \hat{n}^i} f_{\mathrm{CGWB}} = 0\,. \tag{3.23}$$

The last term is the product of two terms linear in the scalar and the tensor perturbations, therefore it can be neglected in our linear approximation. By using the conditions found in Eqs. (3.12), (3.15), we get

$$\frac{\partial}{\partial\eta} f_{\mathrm{CGWB}} + \hat{n}^i\frac{\partial}{\partial x^i} f_{\mathrm{CGWB}} + q\frac{\partial}{\partial q} f_{\mathrm{CGWB}}\left(\Psi' - \frac{\partial\Phi}{\partial x^i}\hat{n}^i - \frac{1}{2}H'_{lm}\hat{n}^l\hat{n}^m\right) = 0\,. \tag{3.24}$$

By expanding the distribution function in perturbation theory, using the definition provided in Eq. (3.18), we find

$$\begin{aligned} \frac{\partial}{\partial\eta}\bar{f}_{\mathrm{CGWB}}(\eta, q) =& 0\,, \\ \Gamma'(\eta, \mathbf{x}, \mathbf{q}) + \hat{n}^i\frac{\partial}{\partial x^i}\Gamma(\eta, \mathbf{x}, \mathbf{q}) =& \Psi'(\eta, \mathbf{x}) - \hat{n}^i\frac{\partial}{\partial x^i}\Phi(\eta, \mathbf{x}) - \frac{1}{2}\hat{n}^l\hat{n}^m H'_{lm}(\eta, \mathbf{x})\,. \end{aligned} \tag{3.25}$$

The zero-order solution of the Boltzmann equation gives $\bar{f}_{\mathrm{CGWB}}(\eta, q) = \bar{f}_{\mathrm{CGWB}}(q)$, which means that the number density of graviton is diluted by the expansion of the Universe,

$$\bar{n}_{\mathrm{CGWB}}(\eta, q) \equiv \int \frac{d^3\mathbf{q}}{a^3(\eta)}\,\bar{f}_{\mathrm{CGWB}}(\eta, q) \sim \frac{1}{a^3(\eta)}\,, \tag{3.26}$$

while the energy density scales as standard radiation, $\bar{\rho}_{\mathrm{CGWB}}(\eta) \sim 1/a^4(\eta)$. The evolution of the perturbation of the energy density of the CGWB is governed, in Fouerier space, by

$$\Gamma'(\eta, \mathbf{k}, \mathbf{q}) + ik\mu\Gamma(\eta, \mathbf{k}, \mathbf{q}) = \Psi'(\eta, \mathbf{k}) - ik\mu\Phi(\eta, \mathbf{k}) - \frac{1}{2}\hat{n}^i\hat{n}^j H'_{ij}(\eta, \mathbf{k})\,, \tag{3.27}$$

with $\mu \equiv \hat{k}\cdot\hat{n}$. To solve analytically this equation, it is sufficient to recognize a partial derivative w.r.t. time on the left hand side,

$$\Gamma'(\eta, \mathbf{k}, \mathbf{q}) + ik\mu\Gamma(\eta, \mathbf{k}, \mathbf{q}) = e^{-ik\mu\eta}\frac{\partial}{\partial\eta}\left[\Gamma(\eta, \mathbf{k}, \mathbf{q})e^{ik\mu\eta}\right]\,, \tag{3.28}$$

therefore the solution of the Boltzmann equation is just

$$\Gamma(\tilde{\eta},\mathbf{k},\mathbf{q})e^{ik\mu\eta}\Big|_{\eta_{\rm in}}^{\eta}=\int_{\eta_{\rm in}}^{\eta}\mathrm{d}\tilde{\eta}\left[\Psi'(\tilde{\eta},\mathbf{k})-ik\mu\Phi(\tilde{\eta},\mathbf{k})-\frac{1}{2}\hat{n}^i\hat{n}^jH'_{ij}(\tilde{\eta},\mathbf{k})\right]e^{ik\mu\tilde{\eta}}\,. \tag{3.29}$$

If we use

$$-ik\mu\Phi(\tilde{\eta},\mathbf{k})e^{ik\mu\tilde{\eta}}=-\frac{\partial}{\partial\tilde{\eta}}\left[\Phi(\tilde{\eta},\mathbf{k})e^{ik\mu\tilde{\eta}}\right]+\Phi'(\tilde{\eta},\mathbf{k})e^{ik\mu\tilde{\eta}}\,, \tag{3.30}$$

we can write the solution of the Boltzmann equation in the form

$$\begin{aligned}\Gamma(\eta_0,\mathbf{k},\mathbf{q})=\Gamma(\eta_{\rm in},\mathbf{k},\mathbf{q})e^{ik\mu(\eta_{\rm in}-\eta_0)}+\Phi(\eta_{\rm in},\mathbf{k})e^{ik\mu(\eta_{\rm in}-\eta_0)}-\Phi(\eta_0,\mathbf{k})\\+\int_{\eta_{\rm in}}^{\eta_0}\mathrm{d}\tilde{\eta}\left[\Psi'(\tilde{\eta},\mathbf{k})+\Phi'(\tilde{\eta},\mathbf{k})-\frac{1}{2}\hat{n}^i\hat{n}^jH'_{ij}(\tilde{\eta},\mathbf{k})\right]e^{ik\mu\tilde{\eta}}\,.\end{aligned} \tag{3.31}$$

The first term represents the initial condition on the anisotropy of the CGWB and it keeps into account for any inhomogeneity given by the production mechanism, while the second term is the Sachs-Wolfe effect (SW), due to the redshift of graviton when it comes out from the potential wells at its production (w.r.t. the value of our local gravitational potential), while the last term is the Integrated Sachs-Wolfe (ISW), which keeps into account for the variation of the perturbations when gravitons are crossing them. The value of the local potential $\Phi(\eta_0,\mathbf{k})$ is unknown, but since this term contributes to the solution of the Boltzmann equation as an offset independent on $\hat{n}$, it would affect only the monopole, giving no physical effect on the angular power spectrum when $\ell\geq 1$. Note also that the energy spectrum of cosmological graviton is non-thermal, thence the perturbation of the distribution function is sensitive to the magnitude of the comoving momentum, because the distribution function cannot be recasted in the form of Eq. (2.89). We will discuss this difference in more detail in Section 4.1, where the perturbations in the energy density of the CGWB are computed in the adiabatic case and compared with those of thermalized species.

Spherical harmonics decomposition and angular power spectrum

The quantity we have access at future interferometers is the excess of energy density of the CGWB in a given frequency bin, defined in Eq. (1.49). This quantity is related to the perturbation of the distribution function by Eq. (3.21), where the distribution function is evaluated at the present time. In order to extract the information about the anisotropies in the map of the cosmological background, it would be useful to decompose the density field in spherical harmonics,

$$\delta_{\rm CGWB}(\eta_0,\mathbf{x}_0,\mathbf{q})=\sum_{\ell=0}^{+\infty}\sum_{m=-\ell}^{\ell}\delta_{{\rm CGWB},\ell m}(\eta_0,\mathbf{x}_0,q)Y_{\ell m}(\hat{n})\,, \tag{3.32}$$

where $\mathbf{x}_0$ are the coordinates of the observer. From now on, we set $\mathbf{x}_0=0$ and we will not write this dependence anymore. The solution of the Boltzmann equation at the present

time, Eq. (3.31) evaluated for $\eta = \eta_0$ and $\mathbf{x} = 0$, can be written as a the sum of "initial", scalar and tensor contributions,

$$\begin{aligned}
\delta_{\mathrm{GW},\ell m,I}(q) &= 4\pi(-i)^\ell[4 - n_{\mathrm{gwb}}(q)] \int \frac{d^3k}{(2\pi)^3} e^{i\mathbf{k}\cdot\mathbf{x}_0} Y^*_{\ell m}(\hat{k}) \Gamma(\eta_{\mathrm{in}}, \mathbf{k}, q) j_\ell[k(\eta_0 - \eta_{\mathrm{in}})] \,, \\
\delta_{\mathrm{GW},\ell m,S}(q) &= 4\pi(-i)^\ell[4 - n_{\mathrm{gwb}}(q)] \int \frac{d^3k}{(2\pi)^3} e^{i\mathbf{k}\cdot\mathbf{x}_0} Y^*_{\ell m}(\hat{k}) \zeta(\mathbf{k}) \Delta^S_\ell(k, \eta_0, \eta_{\mathrm{in}}) \,, \\
\delta_{\mathrm{GW},\ell m,T}(q) &= 4\pi(-i)^\ell[4 - n_{\mathrm{gwb}}(q)] \int \frac{d^3k}{(2\pi)^3} e^{i\mathbf{k}\cdot\mathbf{x}_0} \sum_{\lambda=\pm2} {}_{-\lambda}Y^*_{\ell m}(\hat{k}) H_\lambda(\mathbf{k}) \Delta^T_\ell(k, \eta_0, \eta_{\mathrm{in}}) \,,
\end{aligned} \tag{3.33}$$

where we have defined the scalar and the tensor source functions

$$\begin{aligned}
\Delta^S_\ell(k, \eta_0, \eta_{\mathrm{in}}) \equiv& T_\Phi(\eta_{\mathrm{in}}, k) j_\ell[k(\eta_0 - \eta_{\mathrm{in}})] + \int_{\eta_{\mathrm{in}}}^{\eta_0} \mathrm{d}\eta \left[T'_\Phi(\eta, k) + T'_\Psi(\eta, k)\right] j_\ell[k(\eta_0 - \eta)] \,, \\
\Delta^T_\ell(k, \eta_0, \eta_{\mathrm{in}}) \equiv& \sqrt{\frac{(\ell+2)!}{(\ell-2)!}} \frac{1}{4} \int_{\eta_{\mathrm{in}}}^{\eta_0} \mathrm{d}\eta T'_h(\eta, k) \frac{j_\ell[k(\eta_0 - \eta)]}{k^2(\eta_0 - \eta)^2} \,,
\end{aligned} \tag{3.34}$$

with the tensfer function of the scalar and the tensor perturbations defined by

$$\begin{aligned}
\Phi(\eta, \mathbf{k}) =& T_\Phi(\eta, k) \zeta(\mathbf{k}) \,, \\
\Psi(\eta, \mathbf{k}) =& T_\Psi(\eta, k) \zeta(\mathbf{k}) \,, \\
H_{ij}(\eta, \mathbf{k}) =& T_H(\eta, k) \sum_{\lambda=\pm2} e_{ij,\lambda}(\hat{k}) H_\lambda(\mathbf{k}) \,.
\end{aligned} \tag{3.35}$$

Additional details on the derivation of Eq. (3.33) have been provided in Appendix D. The source functions provided in Eq. (3.34) encode all the information related to the evolution of the perturbations in time, given by the transfer functions, and to the projection effects, associated to the spherical Bessel and their derivatives. The stochastic part of the anisotropies is factorized in the primordial stochastic fields ζ, which is the curvature perturbation defined in Eq. (2.69), and H_λ, which corresponds to the amplitude of the primordial tensor fluctuations during inflation, computed in Eq. (2.68). In our discussion, we have assumed that $\Gamma(\eta_{\mathrm{in}}, \mathbf{x}, q)$ does not depend on $\hat{n}$, allowing to use the spherical harmonics decomposition written above. In Section 4.2 we show an explicit example in which $\Gamma(\eta_{\mathrm{in}}, \mathbf{x}, q)$ depends on the direction of observation through the combination $(\hat{k} \cdot \hat{q})^2$, generating a quadrupole anisotropy in the initial conditions. A more general term in which the initial perturbation of the distribution function depends on the direction of propagation of gravitons alone could be generated by models that break statistical isotropy [245, 246, 247], although this is not the only possibility. In our work, however, we neglect this cases, leaving them for a future study. In some cases, the initial condition contribution, $\delta_{\mathrm{GW},\ell m,I}$, can be written by factorizing $\Gamma(\eta_{\mathrm{in}}, \mathbf{x}, q)$ as the product of a transfer function and a stochastic part, see, e.g., Eq. (3.39). In Eq. (3.33), we do not use such a

decomposition yet, in order to be as much general as possible.The angular power spectrum of the CGWB at two different frequencies is defined then by using

$$\delta_{\ell\ell'}\delta_{mm'}C_\ell^{\rm CGWB\times CGWB}(q_1,q_2)\equiv\left\langle\frac{\delta_{{\rm GW},\ell m}(q_1)\delta^*_{{\rm GW},\ell' m'}(q_2)+\delta_{{\rm GW},\ell m}(q_2)\delta^*_{{\rm GW},\ell' m'}(q_1)}{2}\right\rangle. \tag{3.36}$$

The angular power spectrum of the CGWB for two momenta q_1 and q_2 can be decomposed as the sum of an initial, a scalar, a tensor contribution plus the cross-correlation between the initial term and the scalar and the tensor ones,

$$\begin{aligned}C_\ell^{\rm CGWB\times CGWB}(q_1,q_2)=&4\pi\left[4-n_{\rm gwb}(q_1)\right]\left[4-n_{\rm gwb}(q_2)\right]\\&\int\frac{dk}{k}\Big[\left|\Delta^S_\ell(k,\eta_0,\eta_{\rm in})\right|^2P_\zeta(k)+\left|\Delta^T_\ell(k,\eta_0,\eta_{\rm in})\right|^2P_T(k)\\&+j^2_\ell[k(\eta_0-\eta_{\rm in})]P_\Gamma(k,q_1,q_2)\\&+\Delta^S_\ell(k,\eta_0,\eta_{\rm in})j_\ell[k(\eta_0-\eta_{\rm in})]\left(P_{\times,\zeta}(k,q_1)+P_{\times,\zeta}(k,q_2)\right)\\&+\Delta^T_\ell(k,\eta_0,\eta_{\rm in})j_\ell[k(\eta_0-\eta_{\rm in})]\left(P_{\times,T}(k,q_1)+P_{\times,T}(k,q_2)\right)\Big],\end{aligned} \tag{3.37}$$

where we have defined the following spectra, keeping into account for any possible correlation between the intial conditions with the scalar and the tensor perturbations,

$$\begin{aligned}\langle\zeta(\mathbf{k}_1)\zeta^*(\mathbf{k}_2)\rangle\equiv&\frac{2\pi^2}{k_1^3}(2\pi)^3P_\zeta(k_1)\delta(\mathbf{k}_1-\mathbf{k}_2),\\\left\langle H_{ij}(\mathbf{k}_1)H^{*\,ij}(\mathbf{k}_2)\right\rangle\equiv&\frac{2\pi^2}{k_1^3}(2\pi)^3P_T(k_1)\delta(\mathbf{k}_1-\mathbf{k}_2),\\\left\langle\frac{\Gamma(\eta_{\rm in},\mathbf{k}_1,q_1)\Gamma^*(\eta_{\rm in},\mathbf{k}_2,q_2)+{\rm c.c.}}{2}\right\rangle\equiv&\frac{2\pi^2}{k_1^3}(2\pi)^3P_\Gamma(k_1,q_1,q_2)\delta(\mathbf{k}_1-\mathbf{k}_2),\\\left\langle\frac{\Gamma(\eta_{\rm in},\mathbf{k}_1,q)\zeta^*(\mathbf{k}_2)+\Gamma^*(\eta_{\rm in},\mathbf{k}_1,q)\zeta(\mathbf{k}_2)}{2}\right\rangle\equiv&\frac{2\pi^2}{k_1^3}(2\pi)^3P_{\times,\zeta}(k_1,q)\delta(\mathbf{k}_1-\mathbf{k}_2),\\\left\langle\frac{\Gamma(\eta_{\rm in},\mathbf{k}_1,q)H^*(\mathbf{k}_2)+\Gamma^*(\eta_{\rm in},\mathbf{k}_1,q)H(\mathbf{k}_2)}{2}\right\rangle\equiv&\frac{2\pi^2}{k_1^3}(2\pi)^3P_{\times,T}(k_1,q)\delta(\mathbf{k}_1-\mathbf{k}_2).\end{aligned} \tag{3.38}$$

Eqs. (3.33), (3.37) account for the presence of extra random fields in the early Universe only in $\Gamma(\eta_{\rm in},\mathbf{k},q)$, because any source of isocurvature, that could affect the metric perturbations [41, 248, 249], has been constrained at lower energy scales by CMB measurements [122, 123, 34]. In the most general case it is clear that the frequency dependence of the angular power spectrum cannot be factorized out, but it depends on the convolution of the integral over k, generating different scalings of the angular power spectrum with the frequency at different multipoles [1]. In the case in which the tensor tilt of the CGWB does not depend on the frequency, $n_{\rm gwb}(q)\simeq$ const., and the initial condition does not depend on the frequency and is proportional to the curvature that sources the scalar perturbations,

$$\Gamma(\eta_{\rm in},\mathbf{k})j_\ell[k(\eta_0-\eta_{\rm in})]=\Delta^I_\ell(k,\eta_0,\eta_{\rm in})\,\zeta(\mathbf{k}), \tag{3.39}$$

we can write the angular power spectrum by in the simple form

$$\frac{C_\ell^{\mathrm{CGWB}\times\mathrm{CGWB}}}{4\pi(4-n_{\mathrm{gwb}})^2} = \int \frac{dk}{k}\left[\left|\Delta_\ell^I(k,\eta_0,\eta_{\mathrm{in}}) + \Delta_\ell^S(k,\eta_0,\eta_{\mathrm{in}})\right|^2 P_\zeta(k) + \left|\Delta_\ell^T(k,\eta_0,\eta_{\mathrm{in}})\right|^2 P_T(k)\right]. \tag{3.40}$$

3.3 Initial time and source term

The evolution of the distribution function of the cosmological gravitons is computed by using the Boltzmann equation, starting from an initial time η_{in} until the present time at which observations are perfomed, η_0. The choice of the time at which the initial conditions are set is different w.r.t. the CMB case. Photons are indeed tightly coupled to baryons until recombination, therefore it is sufficient to choose any initial time for which the smallest observable scales in the CMB are larger than the causal horizon. This is due to the fact that any effect in the evolution of the Universe before that time is washed out by the tight coupling of photons with baryons. On the other hand, since the CGWB decouples at the Planck epoch, it allows to probe much earlier times in the cosmic history, thus a more rigorous definition of the initial time, from whom we start evolving the distribution function by using the Boltzmann equation, is needed. In this Thesis, we consider a CGWB of frequency f generated at the time η_{prod} and decoupled afterwards. If at η_{prod} the GWs are inside the horizon, it is possible to use the approach described in Section 1.1.2 and 3.1, by using geometric optics and introducing a distribution function for graviton, setting $\eta_{\mathrm{in}} = \eta_{\mathrm{prod}}$. On the other hand, if the shortwave approximation is no longer valid, it is not possible to describe the CGWB as an ensemble of massless particles, because, for example, the energy density of the gravitational field is not well defined. In the case in which the GWs produced at η_{prod} are super-horizon, the initial conditions are set at $\eta_{\mathrm{in}} = 150\,\eta_{\mathrm{h.c.}}$, where

$$\frac{q}{\mathcal{H}(\eta_{\mathrm{h.c.}})} = 1 \to \eta_{\mathrm{h.c.}} = \begin{cases} 1/q & \text{Radiation Domination} \\ 2/q & \text{Matter Domination} \end{cases} \tag{3.41}$$

with $\mathcal{H}$ the conformal Hubble rate. The factor 150 implies that the modes are deeply inside the horizon, ensuring the validity of the shortwave approximation. In full generality, it is possible to compute the initial time as

$$\eta_{\mathrm{in}}(f) = \max\left[\eta_{\mathrm{prod}},\, 100\,\eta_{\mathrm{h.c.}}(f)\right]. \tag{3.42}$$

The vast majority of the primordial mechanisms that source a primordial background generate GWs within the causal horizon, therefore the case $\eta_{\mathrm{in}}(f) = 150\eta_{\mathrm{h.c.}}(f)$ would apply just to few cases that are basically related to inflation. We will show an explicit example in Section 3.4.1. The frequency dependence of the initial time implies that the anisotropies of the CGWB at different frequencies are sensitive to the geometry of the Universe at different times, as we will discuss in detail also in the next chapters.

3.4 Cosmological Gravitational-Wave Background Sources

The physical observable that we can measure with interferometers is the CGWB density contrast [39, 40, 149], defined in Eqs. (1.49), and it is related to the perturbation of the distribution function, defined in (3.18), by Eq. (3.21). In order to connect the solution of the Boltzmann equation to the observable, it is necessary to know the spectral tilt of the monopole of the CGWB, defined in Eq. (1.48). Since this tilt is model dependent, we need to know the underlying source of GWs to properly characterize the amplitude and the shape of the angular power spectrum. In this section we enumerate the most promising sources of GWs, because they relate to different aspects of early universe models: inflation with a blue tilt, first-order phase transitions, and second-order-induced GWs. In this section we will focus just on the monopole contribution of the different sources, although differences in the initial conditions could emerge. We will go through these additional differences in Chapter 4.

3.4.1 Quantum fluctuations of the metric during inflation

During inflation, the quantum fluctuations of the scalar and tensor perturbations of the metric could be amplified by the accelerated expansion of the Universe [167]. The amplitude of the fluctuations of plane waves of frequency $\mathbf{k}$ and $\mathbf{q}$, when $k\eta \approx 1$, gets frozen to the value

$$\left\langle h_{ij}^{\rm inf}(\mathbf{k}) h^{{\rm inf}\, ij\, *}(\mathbf{q}) \right\rangle = \frac{2\pi^2}{k^3} (2\pi)^3 \, P_T(k) \, \delta(\mathbf{k}-\mathbf{q}) \,, \tag{3.43}$$

where $P_T(k)$ is the primordial tensor spectrum. In canonical model of inflation, it is computed by using

$$P_T(k) \simeq \frac{2}{\pi^2} \frac{H_k^2}{M_{\rm Pl}^2} \,, \tag{3.44}$$

for $k = aH$. The amplitude of the primordial tensor spectrum at the pivot scale $k_* = 0.01\,{\rm Mpc}^{-1}$ is connected to the amplitude of the scalar power spectrum by the tensor-to-scalar ratio,

$$P_T\left(k_*\right) \equiv r \, P_\zeta\left(k_*\right) \,, \tag{3.45}$$

while the evolution in frequency is typically determined by the tensor tilt n_t,

$$P_T(k) = P_T(k_*) \left(\frac{k}{k_*} \right)^{n_t} \,. \tag{3.46}$$

The most recent bound on (r, n_t), obtained in [210], contraints $r < 0.98$ and $n_t \in [-1.37, 0.42]$ at 95% confidence level. These constraints have been obtained by combining measurements of the polarization of the CMB maps, from Planck (considering also the intensity) [26, 250, 34] and BICEP/*Kek* [251], with the current limit on the direct detection of SGWBs provided by LVK [209]. The analysis done in [210] constrains an inflationary CGWB parametrized by Eqs. (3.45), (3.46) (see, e.g., [128] for constraints on r by fixing n_t to the value predicted by single-field inflation), without considering the most general

case in which there could be a running on the tensor tilt, that becomes frequency dependent. In this Thesis, we will also focus just on the case of an inflationary CGWB with a null running of the tensor tilt. The inflationary spectrum of the CGWB can be simply connected to the observed background by evaluating the propagation of the GWs across the cosmic history. By comparing the definition of fractional energy density of the CGWB per frequency bin, given in Eq. (1.45), with the expression for the energy density of the GWs, Eq. (2.95), where the energy-momentum tensor can be computed by using (1.28), it is possible to show that the energy density of the primordial background is

$$\bar{\Omega}_{\rm CGWB}(\eta, q) = \frac{1}{12H_0^2} P_T(q) \frac{1}{a^2(\eta)} \langle \left[T_h'(\eta, q)\right]^2 \rangle \,. \tag{3.47}$$

The transfer function T_h has been defined in Eq. (3.35) and its analytic expression will be written explicitly in Eq. (F.33). The average of the square of the time derivative of the transfer function is the corrispective the Brill-Hartle average that appears in the definition of the energy-momentum tensor of the GWs. It is possible to show that when $\eta \to \eta_0$, the energy density of the GWs becomes

$$\bar{\Omega}_{\rm CGWB}(\eta, q) = \frac{1}{12H^2(\eta)a^2(\eta)} \frac{\eta_{\rm eq}^2}{\eta^4} P_T(q) \,, \tag{3.48}$$

where $\eta_{\rm eq}$ is the conformal time at the equality between matter and radiation. This relation takes into account the evolution of the tensor modes that re-entered the Hubble scale during radiation domination [227], taking into account the evolution of GWs during radiation and matter domination, while the effects due to the propagation of tensor modes during dark energy domination are negligible. Besides, Eq. (3.48) neglects the damping of tensor modes propagating in a Universe with non-zero anisotropic stress [252, 253, 254], amplified for instance by free-streaming particles. When the damping is due only to active neutrinos, this effect is close to 0.8^2, while in general it is proportional to the fractional energy density of relativistic and decoupled particle species at the time at which the tensor perturbations start oscillating, $\eta \approx 1/q$. We provide additional details on the derivation of Eq. (3.48) in Section 5.2. In this prescription, the quantity P_T in Eq. (3.48) is the same power spectrum, evaluated at a different scale, that generates the tensor contribution to the ISW of the CMB and of the CGWB, defined in Eq. (3.40).

In this scenario, the production time of the CGWB corresponds to inflation, during which the tensor fluctuations are amplified. However, once the GWs cross the Hubble horizon, they are frozen and do not oscillate in space and time, thus it is difficult to define properly the energy density of the CGWB. This problem is analogous to the definition of the energy-momentum tensor when the shortwave approximation is not valid, see Section 1.1.3. As debated in Section 3.3, to compute the anisotropies of gravitons, it is crucial to define time $\eta_{\rm in}$ at which we evaluate the initial conditions on the distribution function. Considering that at $\eta_{\rm prod}$ the tensor modes are outside the causal horizon, we should define the minimum time at which the shortwave approximation holds. By construction, $q \gg k$, therefore we should chose a value of $q\eta$ large enough in such a way that GWs could be considered an ensemble of collisionless and massless particles. To do this, we look at the

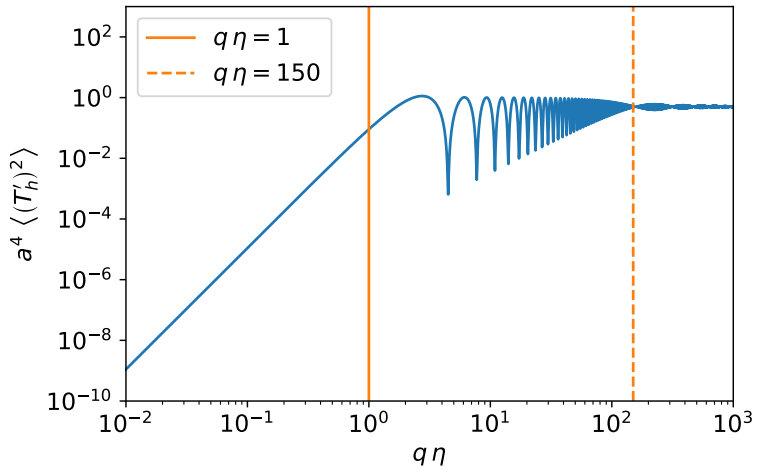

Figure 3.1: Plot of the transfer function of the energy density of the CGWB, multiplied by a^4. When $q\eta \approx 150$, the energy density scales like a^{-4}, thus the CGWB behaves like a standard radiation fluid.

evolution of the energy density of the GWs, Eq. (3.47), during the radiation dominated epoch. As we will see in Eq. (F.33), the transfer function of the tensor perturbations that re-enter the horizon during the radiation epoch is

$$T_h(\eta, q) = j_0(q\eta)\,, \tag{3.49}$$

therefore the energy density of the primordial background is

$$\bar{\Omega}_{\rm CGWB}(\eta, q) = \frac{1}{12H_0^2} P_T(q) \frac{1}{a^2(\eta)} \langle \left[j_0'(q\eta) \right]^2 \rangle\,, \tag{3.50}$$

Note that when $q\eta \gg 1$, it is possible to use $\langle \sin^2(q\eta) \rangle = \langle \cos^2(q\eta) \rangle = 1/2$ and $\langle \sin(q\eta) \rangle = \langle \cos(q\eta) \rangle 0$. In Figure 3.1, we plot $a^4 \left\langle (T_h')^2 \right\rangle$ as a function of $q\eta$. We note that when $q\eta \approx 150$, $a^4 \bar{\Omega}_{\rm CGWB} \sim$ const., thus the energy density of the CGWB scales like standard radiation. In this case, we define $\eta_{\rm in} = 150/q$, because at this time gravitons can be described as a radiation fluid. From $\eta_{\rm prod}$ up to $150/q$, the evolution of the CGWB should be characterized by the transfer function of the tensor perturbations, keeping into account, eventually, for any kind of wave-optics effect in the propagation [255].

3.4.2 Primordial Black Holes

GR is a nonlinear theory, therefore, although at linear order the evolutions of scalar and tensor modes are decoupled, secondary GWs could be produced by quadratic contributions in the scalar perturbations, which act as a source in the transverse and traceless part of the Einstein equations [168, 169, 170, 171, 172, 173, 174] (see [256] for a recent review). In [174] it has been shown indeed that if the scalar power spectrum used to compute the perturbations of the CMB is assumed, the amplitude of the cosmological background is

expected to be subdominant, $\bar{\Omega}_{\rm CGWB} \simeq 10^{-22}\,(f/1\,{\rm Hz})^{-0.1}$. Consequently, to produce a notable amount of GWs, it is necessary to have an enhancement in the scalar power spectrum, at the frequencies of the CGWB, compared to the inflationary predictions. Deviations from scale invariance [257] happens for instance in an ultra-slow-roll phase [258, 259, 260], or in multi-field models [261, 262, 263]. The magnification of P_ζ at small scales implies that a big number of regions with large density fluctuations is present in the early Universe. When the density fluctuations of these regions are larger than a critical value, they collapse forming PBHs [264, 265, 202]. The mass range of these PBH are of the order $\sim (0.001 - 1000) M_\odot$, which enclose the actual mass range probed by current detectors. The peak in the scalar power spectrum could augment the production of PBHs in such a way their abundance could be constrained by future observations[1]. The CGWB associated to the secondary-GWs has been computed for different shapes of the primordial power spectrum [266]. In the monochromatic case, with a primordial scalar spectrum featuring a Dirac delta-function, $\mathcal{P}_{\zeta_s}(q) = A_*\, q_*\, \delta\,(q - q_*)$, the SGWB energy density can be computed analytically and results [267, 23][2]

$$\bar{\Omega}_{\rm CGWB}(\eta_0, f) = \frac{1}{a_0^2 H_0^2 \eta_0^2}\frac{A_*^2}{15552}\frac{f^2}{f_*^2}\left[\frac{4f_*^2}{f^2} - 1\right]^2 \theta_H\,(2f_* - f)\;\mathcal{I}^2\left(\frac{f_*}{f}, \frac{f_*}{f}\right) \tag{3.51}$$

where θ_H is the Heaviside step function, and

$$\begin{aligned}&\mathcal{I}^2\left(\frac{f_*}{f}, \frac{f_*}{f}\right)\\ &= \frac{729}{16}\left(\frac{f}{f_*}\right)^{12}\left(3 - \frac{2f_*^2}{f^2}\right)^4\left\{\left[4\left(2 - 3\frac{f^2}{f_*^2}\right)^{-1} - \log\left(\left|1 - \frac{4f_*^2}{3f^2}\right|\right)\right]^2 + \pi^2\theta_H\left(\frac{2f_*}{\sqrt{3}f} - 1\right)\right\}.\end{aligned} \tag{3.52}$$

The peak GW frequency f_* is related to the spike scale q_* by

$$f_* = \frac{c}{2\pi a_0}\, q_*\,. \tag{3.53}$$

3.4.3 Phase Transition

When a PT takes place, the Universe goes from a metastable to a stable state, which represent the configurations of minimal potential energy at high and low temperatures respectively. If latent heat is involved, the PT is of the first order and the phases of the Universe are converted from the false to the true vacuum in a discontinuous way, through the nucleation of bubbles [183]. Such first order PTs can happen in many extensions of the Standard Model (e.g., with additional scalar singlet or doublet, spontaneously broken conformal symmetry, or phase transitions in a hidden sector). In [20], it has been realized

[1] Together with the secondary GWs, an additional SGWB could be produced by the merging of binary systems of PBHs. This SGWB would have a similar shape in frequency of the AGWB discussed in Section 7 and could be constrained by space- and earth-based interferometers, depending on the mass of the PBHs.

[2] This expression is valid during radiation domination.

for the first time that a large CGWB could be produced during a first-order PT and this is potentially detectable by present and future GW interferometers [184, 145]. In general, three main mechanisms contribute to the generation of GWs [114], by acting as a source in the transverse-traceless part of the Einstein equations:

- **Bubble wall collisions** creating distortions in the plasma. Their action is usually accounted with a method called *envelope approximation* [185, 186, 187, 188, 189], consisting in approximating the bubble motion with an infinitesimally thin spherical layer. This is the backbone of the scalar field ϕ contribution to the SGWB signal.
- **Sound waves** generated by the coupling of the scalar field to the plasma during the expansion of the bubbles. These compressional modes constitute an important source of GWs also long after the collision of the bubbles [190, 191, 192].
- **Turbulence phenomena** after the bubble collision, which generate vortices in the fluid with a non-vanishing quadrupole moment. The amount of GWs sourced by these eddies from Magneto-Hydro-Dynamics (MHD) turbulence has been computed for instance in [193, 194].

As a consequence, the density of GWs generated by phase transitions can be split into three contributions,

$$\bar{\Omega}_{\rm GW}(f) = \bar{\Omega}_{\phi}(f) + \bar{\Omega}_{\rm sw}(f) + \bar{\Omega}_{\rm turb}(f)\,. \tag{3.54}$$

Broken Power-law

Each of these three contributions can be well described by a broken power law (BPL) spectrum. In CLASSGW we use the same parametrization as in the LIGO analysis of Ref. [268],

$$\bar{\Omega}^{\rm BPL}_{\rm GW}(f) = \bar{\Omega}_* \left(\frac{f}{f_*}\right)^{n_1} \left[1 + \left(\frac{f}{f_*}\right)^{\Delta}\right]^{\frac{n_2-n_1}{\Delta}} \tag{3.55}$$

with $n_1 = 3$ to account causality, n_2 takes the value -4 (resp. -1) for sound waves (resp. bubble collisions), and the contribution from turbulence (MHD) is neglected.

Chapter 4

Initial conditions of the CGWB

The non-thermal nature of gravitons poses a significant challenge in setting the initial conditions. In the case of CMB photons, the tight coupling of the photon-baryon fluid leads to the evolution of any initial distribution in phase space toward the Maxwell-Boltzmann distribution, as defined in Eq. (2.89). The effects of inhomogeneities in the electromagnetic field at early times, occurring well before the thermalization of photons, remain unobservable due to the opacity of the Universe during these earlier epochs, long before recombination. On the other hand, the CGWB decouples when energy scales fall below the Planck scale, denoted as $T_{\rm Pl} = 1.22 \times 10^{19}, \text{GeV}$ [37]. Consequently, the spectrum of its monopole and anisotropies contains valuable information about the mechanism responsible for its generation or, equivalently, about the initial conditions. In this section we quantify the amount of initial inhomogeneities in the energy density of CGWB from different sources, keeping track of adiabatic and non-adiabatic contributions. The approach we employ in this chapter is general and can be extended to compute the initial conditions of any stochastic background of primordial origin. We begin by illustrating the simplest scenario in which the initial conditions of the CGWB are assumed to be adiabatic. This initial examination reveals significant differences between the CGWB and other cosmological relics, such as the CMB. In subsequent sections, we compute the initial conditions for non-adiabatic perturbations, including those generated by the quantum fluctuations of the metric during inflation or SIGW.

4.1 Adiabatic initial conditions

If the Universe is filled with many different particle species, the adiabatic initial condition imposes that the relative entropy between two different particles, defined by

$$S_{\alpha\beta} \equiv -\frac{1}{1+w_i}\delta_i + \frac{1}{1+w_j}\delta_j \,, \tag{4.1}$$

is equal to zero. We recall that we have defined, consistently with Eq. (2.104), the density contrast of the species i,

$$\delta_i \equiv \frac{\delta\rho_i}{\bar{\rho}_i} \,. \tag{4.2}$$

Under this assumption, the density contrast of different perturbations are just rescaled by their equation of state parameters,

$$\delta_i = \frac{1+w_i}{1+w_j}\delta_j\,. \tag{4.3}$$

When the perturbations are adiabatic, it is immediate to get a relation between δ_i and the metric perturbations, and thus the curvature perturbation ζ. The $(0,0)$ component of the Einstein equation given in Eq. (2.108), if we use Eq. (4.3), assuming that all the species involved are relativistic, gives

$$\delta(\eta_{\rm in},\mathbf{k}) = -\frac{2}{\mathcal{H}}\Psi'(\eta_{\rm in},\mathbf{k}) - 2\Phi(\eta_{\rm in},\mathbf{k})\,, \tag{4.4}$$

where we have neglected the term proportional to $k^2\Psi$ in the Einstein equations, because we set the initial conditions when the modes are super-horizon, $k\eta \approx k/\mathcal{H} \ll 1$. In Section 5.1, a more precise derivation of the initial conditions will be done and we will also show that Ψ' is negligible at early times, because the variations of the scalar potentials are suppressed by the expansion of the Universe. In the CMB case, the spectrum is thermal and, as we have shown in Eq. (2.101), the perturbation of the distribution function is just

$$\Theta_0(\eta_{\rm in},\mathbf{k}) = \frac{1}{4}\delta_{\rm CMB}(\eta_{\rm in},\mathbf{k}) = -\frac{1}{2}\Phi(\eta_{\rm in},\mathbf{k})\,. \tag{4.5}$$

The graviton spectrum is non-thermal, therefore the density contrast is not $\delta_{\rm CGWB}$ defined in Eq. (1.49), but a bolometric quantity, integrated over the frequency of gravitons,

$$\delta^{\rm bol}_{\rm CGWB}(\eta,\mathbf{k}) \equiv \frac{\delta\rho_{\rm CGWB}(\eta,\mathbf{k})}{\bar{\rho}_{\rm CGWB}(\eta)} = \frac{\int \frac{d^3q}{(2\pi)^3}\, q\, \bar{f}(q)\,[1+(4-n_{\rm gwb}(q))\Gamma(\eta,\mathbf{k},\mathbf{q})]}{\int \frac{d^3q}{(2\pi)^3}\, q\, \bar{f}(q)}\,. \tag{4.6}$$

In the graviton case, the adiabatic initial condition corresponds to

$$\delta^{\rm bol}_{\rm CGWB}(\eta,\mathbf{k}) = -2\Phi(\eta,\mathbf{k})\,, \tag{4.7}$$

which is an integral equation for $\Gamma(\eta,\mathbf{k},\mathbf{q})$ that needs a further assumption to be solved. The generalization of the adiabatic initial condition we make consists in considering gravitons in each bin as many independent and decoupled species and for each of them we apply the adiabatic initial condition. In a mathematical language, we assume that

$$\delta_{\rm CGWB}(\eta,\mathbf{k},\mathbf{q}) = \delta_{\rm CGWB}(\eta,\mathbf{k}) = \delta^{\rm bol}_{\rm GW}(\eta,\mathbf{k}) \to \Gamma(\eta,\mathbf{k},q) = -\frac{2}{4-n_{\rm gwb}(q)}\Phi(\eta,\mathbf{k})\,, \tag{4.8}$$

where the density contrast has been defined in Eq. (3.21). This condition can be obtained by requiring that the adiabatic initial condition has to be true for any $\bar{f}(q)$,

$$\int \frac{\mathrm{d}^3q}{(2\pi)^3}\bar{f}(q)\,[2\Phi(\eta,\mathbf{k}) + (4-n_{\rm gwb}(q))\,\Gamma(\eta,\mathbf{k},q)] = 0\,, \qquad \forall\ \bar{f}(q)\,, \tag{4.9}$$

thus the integrand over q has to be always zero and we get the adiabatic initial condition

$$\Gamma(\eta, \mathbf{k}, q) = \Gamma_0^{\rm AD}(\eta, \mathbf{k}, q) = -\frac{2}{4 - n_{\rm gwb}(q)}\Phi(\eta, \mathbf{k})\,. \tag{4.10}$$

The subscript 0 clarifies that in the adiabatic case the initial condition is a monopole term, while higher multipoles are suppressed. To see explicitly this, it is sufficient to notice that, by combining the $(0,0)$ and the $(0,i)$ Einstein equations, see e.g. Eq. (2.108), one would get

$$\Gamma_1^{\rm AD}(\eta_{\rm in}, \mathbf{k}, q) = -\frac{1}{4 - n_{\rm gwb}(q)}\frac{k}{6\mathcal{H}(\eta_{\rm in})}\left[\frac{\Psi'(\eta_{\rm in}, \mathbf{k})}{\mathcal{H}(\eta_{\rm in})} + \Phi(\eta_{\rm in}, \mathbf{k})\right], \tag{4.11}$$

from which we conclude that

$$\left|\Gamma_1^{\rm AD}(\eta_{\rm in}, \mathbf{k}, q)\right| \ll \left|\frac{1}{4 - n_{\rm gwb}(q)}\Phi(\eta_{\rm in}, \mathbf{k})\right|. \tag{4.12}$$

In analogy with CMB photons, we can assume that higher multipoles are also suppressed, because of some tight coupling regime between GW modes at the production. Furthermore, at the initial time $\eta_{\rm in}$, the structure of the Boltzmann hierarchy[1] requires $\Gamma_\ell(\eta_{\rm in}, k, q) \approx k\eta_{\rm in}\,\Gamma_{\ell-1}(\eta_{\rm in}, k, q)$, therefore the ℓ contribution is suppressed w.r.t. the $\ell - 1$ one, since $k\eta_{\rm in} \ll 1$. The substantial difference between the CMB and the CGWB case is encoded in the factor $4 - n_{\rm gwb}$, which reflects the contrast between photons, which are thermalized and the perturbation of their distribution function Θ does not depend on the frequency, and gravitons, whose initial condition is set by requiring that the perturbation of the energy density in a given frequency bin $\delta_{\rm CGWB}$ does not depend on the frequency.

Behind the idea of adiabatic initial conditions, there is the assumption that any kind of perturbation in the Universe is generated by a single-clock during inflation. The conjecture relies on the fact that there exists a time-shifting function $\delta\eta(\mathbf{x})$ such that the perturbation of any homogeneous and isotropic field $\bar{X}$ can be written according to

$$\delta X(\eta, \mathbf{x}) = \bar{X}\left(\eta + \delta\eta(\mathbf{x})\right) = \bar{X}'(\eta)\delta\eta(\mathbf{x}) \to \delta_X(\eta, \mathbf{x}) \equiv \frac{\delta X(\eta, \mathbf{x})}{\bar{X}(\eta)} = -3\mathcal{H}(\eta)(1 + w_X)\delta\eta(\mathbf{x})\,. \tag{4.13}$$

The time shifting function is the same for all the fields, thus it is immediate to get the condition provided in Eq. (4.3). Adiabatic initial conditions are therefore typically generated when in the early Universe there is just a single source of energy and momentum that produces other cosmic relics at later times. To prove this, suppose for instance that i particles are present during reheating and are originated by one single-clock. The continuity equations at the background and at the perturbed level are

$$\begin{aligned} \bar{\rho}_i' + 3\mathcal{H}(1 + w_i)\bar{\rho}_i &= \bar{Q}_i\,, \\ \delta\rho_i' + 3\mathcal{H}(1 + w_i)\delta\rho_i - 3\Psi'(1 + w_i)\bar{\rho}_i &= \delta Q_i\,, \end{aligned} \tag{4.14}$$

where the energy transfer rate is subjected to the constraint $\sum_i Q_i = 0$. For instance, i could run over the inflaton, standard radiation, and the CGWB. It is possible to show [269]

[1] A detailed discussion of the Boltzmann hierarchy will be done in Section 5.1.

that, in the case of single-field inflation, for the species i sourced by the above continuity equations, the initial conditions are adiabatic. On the other hand, if other fields are present in the early Universe or if non-Gaussianity is taken into account, the initial conditions could be non-adiabatic (NAD). It would be useful, for convenience, to express the initial condition as the sum of an adiabatic and a non-adiabatic term,

$$\Gamma(\eta_{\rm in}, \mathbf{k}, \mathbf{q}) = \Gamma_0^{\rm AD}(\eta_{\rm in}, \mathbf{k}, q) + \Gamma^{\rm NAD}(\eta_{\rm in}, \mathbf{k}, \mathbf{q}) \tag{4.15}$$

In the subsequent sections, we will discuss the initial conditions for the sources of cosmological backgrounds presented in Section 3.4, illustrating mainly the features of the non-adiabatic contribution (if present).

4.2 Initial conditions in single-field inflation

Non-adiabaticity of the primordial GWs

During single-field inflation, the scalar and the two tensor degrees of freedom fluctuate independently, since we assume no interaction between these fields in the most vanilla scenario. The most important consequence of this fact is that it is no longer possible to assume apriori the adiabatic initial condition,

$$\delta_i \neq \delta_j \frac{1+w_i}{1+w_j}\,, \tag{4.16}$$

because the "separate universe" condition is unvalidated by the existence of more than one clock in the early Universe. Furthermore, the energy density of a cosmological background is supposed to be much smaller than the energy density of standard radiation, $\bar{\rho}_{\rm CGWB}(\eta_{\rm in}) \ll \bar{\rho}_{\rm rad}(\eta_{\rm in})$, according to BBN+Planck constraints discussed in Section 1.5. This means that the Einstein equations give no direct relation between $\delta_{\rm CGWB}$ and $\delta_{\rm rad}$,

$$\frac{2}{3\mathcal{H}}k^2\Psi + 2\left(\Psi' + \mathcal{H}\Phi\right) = -\frac{1}{\bar{\rho}_{\rm rad} + \bar{\rho}_{\rm CGWB}}\left(\bar{\rho}_{\rm rad}\Theta_{0,\rm rad} + \bar{\rho}_{\rm CGWB}\delta^{\rm bol}_{\rm CGWB}\right) \approx -\Theta_{0,\rm rad}\,, \tag{4.17}$$

where we have used the definition of the "bolometric" energy density of the CGWB, Eq. (4.6). An alternative way to say this is that the metric perturbations are not sensitive to the inhomogeneities in the distribution of gravitons at early times, because such a contribution is suppressed by the little input that the primordial GWs provide to the total energy budget of the Universe.

Therefore, the only way possible to compute the energy-momentum tensor of the CGWB is directly from the gravitational field. The main reason for this is that we have equations that characterize for the magnitude of the fluctuations and the evolution of the tensor modes, thus there are no further assumptions (like the adiabatic one) we should make to evaluate the energy density. In this way, we can connect the only source of information we have access (the microphysics involving h_{ij}), to the macroscopic properties of the system (the smoothed energy density $\rho_{\rm CGWB}$).

Energy-momentum tensor of the CGWB

We recall that in this work we are considering the line element in the Poisson gauge given in Eq. (3.3), which is

$$ds^2 = a^2(\eta)\left\{-\mathrm{d}\eta^2\left(1+2\Phi(\eta,\mathbf{x})\right)+\mathrm{d}x^i\mathrm{d}x^j\left[\delta_{ij}\left(1-2\Psi(\eta,\mathbf{x})\right)+H_{ij}(\eta,\mathbf{x})+h_{ij}(\eta,\mathbf{x})\right]\right\}. \tag{4.18}$$

According to the prescription of [35, 36], explored in Section 1.1.2, the GWs are defined as the high-frequency part of the metric,

$$\begin{aligned}\gamma^{\mathrm{GW}}_{ij}(\eta,\mathbf{x}) \equiv& a^2(\eta)h_{ij}(\eta,\mathbf{x})\,,\\ \gamma^{\mathrm{GW}\,ij}(\eta,\mathbf{x}) =& g^{ik}(\eta,\mathbf{x})g^{jl}(\eta,\mathbf{x})\gamma^{\mathrm{GW}}_{kl}(\eta,\mathbf{x}) = -\frac{1}{a^2}\left[(1+4\Psi)h^{ij}+H^{k(i}h^{j)}_{k}\right],\end{aligned} \tag{4.19}$$

where the metric and its inverse considered have been defined in Eqs. (2.77) and does not contain the rapidly-oscillating waves. In the shortwave approximation, the energy-momentum tensor is defined by Eq. (1.28), and it corresponds to

$$T^{(\mathrm{GW})}_{\mu\nu}(x) = \frac{1}{32\pi G}\left\langle \mathcal{D}_\mu\gamma^{(\mathrm{GW})}_{\alpha\beta}(x)\mathcal{D}_\nu\gamma^{(\mathrm{GW})\,\alpha\beta}(x)\right\rangle. \tag{4.20}$$

Since in the shortwave approximation $q\eta \gg 1$ and $q/k \gg 1$, it possible to neglect any containing temporal and spatial derivatives of the metric, because they are subdominant compared to variations of the GWs, which are proportional to q. The covariant derivatives of the radiative degrees of freedom of the metric are

$$\begin{aligned}\mathcal{D}_0\left(\gamma^{\mathrm{GW}}_{ij}\right) =& a^2h'_{ij}\,,\\ \mathcal{D}_k\left(\gamma^{\mathrm{GW}}_{ij}\right) =& a^2\partial_k h_{ij}\,,\\ \mathcal{D}_0\left(\gamma^{\mathrm{GW}\,\mathrm{ij}}\right) =& -\frac{(1+4\Psi)h^{ij\,\prime}-H^{k(i}h^{j)\,\prime}_{k}}{a^2}\,,\\ \mathcal{D}_k\left(\gamma^{\mathrm{GW}\,\mathrm{ij}}\right) =& -\frac{(1+4\Psi)\partial_k h^{ij}-H^{l(i}\partial_k h^{j)}_{l}}{a^2}\,,\end{aligned} \tag{4.21}$$

which means that the components of the energy-momentum tensor are

$$\begin{aligned}
\rho_{\rm GW} =& -T_0^{0\,\rm GW} = \frac{1}{32\pi G a^2}\left\langle \left(h'_{ij}h^{ij\,\prime}(1-2\Phi+4\Psi) - 2h'_{ij}h_k^{j\,\prime}H^{ik}\right)\right\rangle ,\\
P_{\rm CGWB} =& \delta_i^j\, T_j^{i\,\rm GW} = \frac{1}{32\pi G a^2}\frac{1}{3}\left\langle \partial_r h_{ij}\partial^k h^{ij}\left[(1+6\Psi)\delta_k^r + H_k^r\right] + H^{rl}\partial^s h_r^m \partial_s h_{lm}\right\rangle ,\\
v_{i\,\rm CGWB} =& \frac{T_i^{0\,\rm GW}}{\bar\rho_{\rm CGWB}+\bar P_{\rm CGWB}} = \frac{3}{4\left\langle h^{ij\,\prime}h'_{ij}\right\rangle}\left\langle (1-2\Phi)\left[(1+4\Psi)h^{ij\,\prime} - 2H^{ki}h_k^{j\,\prime}\right]\partial_k h_{ij}\right\rangle ,\\
\pi^i_{j\,\rm CGWB} =& \frac{1}{32\pi G a^2}\Bigg\langle (1+6\Psi)\left(\partial^i h^{lm}\partial_j h_{lm} - \frac{1}{3}\delta^i_j \partial^k h^{lm}\partial_k h_{lm}\right)\\
&+\left(H^{ik}\partial_k h^{lm}\partial_j h_{lm} - \frac{1}{3}\delta^i_j H^{rk}\partial_k h^{lm}\partial_r h_{lm}\right)\\
&+\left(H^{rl}\partial^i h_r^m \partial_j h_{lm} - \frac{1}{3}\delta^i_j H^{rl}\partial^s h_r^m\partial_s h_{lm}\right)\Bigg\rangle .
\end{aligned} \tag{4.22}$$

As discussed in Appendix B, in the shortwave approximation, tensors of the form $\mathcal{D}_\rho S^\rho_{\mu\nu}$, with $S^\rho_{\mu\nu}$ quadratic in $\gamma_{ij}^{\rm GW}$, can be dropped under averages. It is possible to see that, up to a four-divergence $\mathcal{G}$ defined in Eq. E.8, the contributions to the energy-momentum tensor become

$$\begin{aligned}
\rho_{\rm GW} =& \frac{1}{32\pi G a^2}\left\langle \left(h'_{ij}h^{ij\,\prime}(1-2\Phi+4\Psi) - 2h'_{ij}h_k^{j\,\prime}H^{ik}\right)\right\rangle ,\\
P_{\rm CGWB} =& \frac{1}{32\pi G a^2}\frac{1}{3}\left\langle h'_{ij}h^{ij\,\prime}(1-2\Phi+4\Psi) + H^{rl}\partial^s h_r^m\partial_s h_{lm}\right\rangle ,\\
v_{i\,\rm CGWB} \ll& \delta\rho_{\rm GW} ,\\
\pi^i_{j\,\rm CGWB} =& \frac{1}{32\pi G a^2}\Bigg\langle \left(H^{ik}\partial_k h^{lm}\partial_j h_{lm} - \frac{1}{3}\delta^i_j H^{rk}\partial_k h^{lm}\partial_r h_{lm}\right)\\
&+\left(H^{rl}\partial^i h_r^m\partial_j h_{lm} - \frac{1}{3}\delta^i_j H^{rl}\partial^s h_r^m\partial_s h_{lm}\right)\Bigg\rangle .
\end{aligned} \tag{4.23}$$

In this way we have shown explicitly that the equation of state of the CGWB is still the one of standard radiation, $P_{\rm CGWB} = \rho_{\rm CGWB}/3$.

Initial condition on the distribution function in single-field inflation

The energy density, the pressure, the velocity and the anisotropic stress of the CGWB evaluated in Eq. (4.23) are "bolometric" quantities, evaluated integrating over all the frequency spectrum of the CGWB, because the GWs considered $h_{ij}(\eta,\mathbf{x})$ are the superposition of many small-scale GWs of frequencies q. It is possible then to use the expansion of the GWs introduced in Eq. (1.38), decomposing the CGWB into many plane waves,

$$h_{ij}(\eta,\mathbf{x}) = \int \frac{d^3q}{(2\pi)^3}\sum_\lambda e^{i\mathbf{q}\cdot\mathbf{x}}\, e_{ij}^\lambda(\hat q) h_\lambda^{\rm prim}(\eta,\mathbf{q}) T_h(\eta,q) , \tag{4.24}$$

where $T_h(\eta, q)$ is the transfer function of the tensor perturbations of momentum q at the time η, introduced in Eq. (3.35) for the large-scale tensor perturbation H_{ij}. The two-point correlation function of the GWs at a generic time after inflation is given by

$$\left\langle h_\lambda(\eta, \mathbf{q}) h_{\lambda'}(\eta, \mathbf{q}') \right\rangle = \frac{1}{2} \frac{8\pi^5}{q^3} P_T(q)\, \delta_{\lambda\lambda'}\, \delta(\mathbf{q} - \mathbf{q}')\, \left[T_h(\eta, q)\right]^2 , \tag{4.25}$$

where the tensor power spectrum from inflation has been defined in Eq. (3.43). In this way, by using the normalization condition

$$e^{\lambda}_{ij}(\hat{q}) e^{ij\,\lambda'}(\hat{q}) = \delta_{\lambda\lambda'} , \tag{4.26}$$

we get that the energy density of the CGWB is equal to

$$\begin{aligned} \rho_{\rm CGWB} =& \frac{1}{32\pi G a^2} \int \frac{d^3q}{(2\pi)^3} \frac{2\pi^2}{q^3} P_T(q) \left\langle \left[T_h'(\eta, q)\right]^2 \right\rangle \\ & \left[1 - 2\Phi(\eta, \mathbf{x}) + 4\Psi(\eta, \mathbf{x}) - 2H^{ij}(\eta, \mathbf{x}) \sum_\lambda e^{\lambda}_{ik}(\hat{q}) e^{k\,\lambda}_{j}(\hat{q}) \right] . \end{aligned} \tag{4.27}$$

It is also possible to show that the polarization tensors obey

$$\sum_\lambda e^{\lambda}_{ik}(\hat{q}) e^{k\,\lambda}_{j}(\hat{q}) = \delta_{ij} - \hat{q}_i \hat{q}_j , \tag{4.28}$$

which means that the perturbation in the energy density of the CGWB is

$$\begin{aligned} \rho_{\rm CGWB} =& \frac{1}{32\pi G a^2} \int \frac{d^3q}{(2\pi)^3} \frac{2\pi^2}{q^3} P_T(q) \left\langle \left[T_h'(\eta, q)\right]^2 \right\rangle \\ & \left[1 - 2\Phi(\eta, \mathbf{x}) + 4\Psi(\eta, \mathbf{x}) + 2H^{ij}(\eta, \mathbf{x}) \hat{q}_i \hat{q}_j \right] . \end{aligned} \tag{4.29}$$

In order to connect the perturbation of the energy density to the perturbation of the distribution function, we recall that the energy density of the CGWB can be written in terms of the distribution function by combining Eqs. (3.16) and Eq. (3.18), we write the energy density as

$$\rho_{\rm CGWB} = \int \frac{d^3q}{(2\pi)^3} \bar{f}(q) \left[1 - \frac{q}{\bar{f}(q)} \frac{d\bar{f}}{dq}(q) \Gamma(\eta, \mathbf{x}, \mathbf{q}) \right] , \tag{4.30}$$

which makes possible to connect the unperturbed distribution function of gravitons to the primordial tensor power spectrum,

$$\bar{f}(q) = \frac{\pi}{16 G a^2 q^3} P_T(q) \left\langle \left[T_h'(\eta, q)\right]^2 \right\rangle , \tag{4.31}$$

in agreement with Eqs. (3.17), (3.48). The perturbation of the distribution function of graviton is then

$$\Gamma(\eta, \mathbf{x}, \mathbf{q}) = \frac{1}{4 - n_{\rm gwb}(q)} \left[-2\Phi(\eta, \mathbf{x}) + 4\Psi(\eta, \mathbf{x}) + 2H^{ij}(\eta, \mathbf{x}) \hat{q}_i \hat{q}_j \right] . \tag{4.32}$$

The Fourier transform this expression at $\eta_{\rm in}$ gives the initial conditions in the case of single-field inflation,

$$\Gamma(\eta_{\rm in},\mathbf{k},\mathbf{q}) = \frac{1}{4-n_{\rm gwb}(q)}\left[-2\Phi(\eta_{\rm in},\mathbf{k})+4\Psi(\eta_{\rm in},\mathbf{k})+2\sum_{\lambda}H_{\lambda}(\eta_{\rm in},\mathbf{k})e^{ij}(\hat{k})\hat{q}_i\hat{q}_j\right]. \tag{4.33}$$

By assuming that the primordial tensor modes are unpolarized we can use Eq. (4.28), finding

$$\Gamma(\eta,\mathbf{k},\mathbf{q}) = \frac{1}{4-n_{\rm gwb}(q)}\left\{-2\Phi(\eta,\mathbf{k})+4\Psi(\eta,\mathbf{k})+2H(\eta,\mathbf{k})\left[1-\left(\hat{k}\cdot\hat{q}\right)^2\right]\right\}. \tag{4.34}$$

We recognize in this equation the adiabatic contribution, Eq. (4.10), plus non-adiabatic terms which reads

$$\Gamma^{\rm NAD}(\eta,\mathbf{k},\mathbf{q}) = \frac{1}{4-n_{\rm gwb}(q)}\left\{4\Psi(\eta,\mathbf{k})+2H(\eta,\mathbf{k})\left[1-\left(\hat{k}\cdot\hat{q}\right)^2\right]\right\} \tag{4.35}$$

By recalling that the first Legendre polynomials are

$$\mathcal{P}_0(\mu)=1\,,\qquad \mathcal{P}_1(\mu)=\mu\,,\qquad \mathcal{P}_2(\mu)=\frac{1}{2}(3x^2-1)\,, \tag{4.36}$$

where $\mu\equiv\hat{k}\cdot\hat{q}$, we get that the initial anisotropy of the CGWB is the sum of a monopole and a quadrupole,

$$\begin{aligned}
\Gamma_0(\eta_{\rm in},\mathbf{k},q) =& \frac{1}{4-n_{\rm gwb}(q)}\left[-2\Phi(\eta_{\rm in},\mathbf{k})+4\Psi(\eta_{\rm in},\mathbf{k})+\frac{2}{3}H(\eta_{\rm in},\mathbf{k})\right],\\
\Gamma_1(\eta_{\rm in},\mathbf{k},q) =& 0\,,\\
\Gamma_2(\eta_{\rm in},\mathbf{k},q) =& -\frac{1}{4-n_{\rm gwb}(q)}\frac{2}{3}H(\eta_{\rm in},\mathbf{k})\,.
\end{aligned} \tag{4.37}$$

In this interesting case, the initial condition does not consist of just a monopole term proportional to the primordial scalar perturbations, but it includes also a quadrupole related to the large-scale tensor modes. The source functions associated to this peculiar initial conditions are similar to the ones defined in Eq. (3.34) and it can be decomposed into a scalar and a tensor contribution,

$$\begin{aligned}
\Delta_\ell^{I-S} =& \frac{1}{4-n_{\rm gwb}(q)}\left[-2T_\Phi(\eta_{\rm in},k)+4T_\Psi(\eta_{\rm in},k)\right]j_\ell[k(\eta_0-\eta_{\rm in})]\,,\\
\Delta_\ell^{I-T} =& -\frac{1}{4-n_{\rm gwb}(q)}T_H(\eta_{\rm in},k)\frac{1}{2}\sqrt{\frac{(\ell+2)!}{(\ell-2)!}}\frac{j_\ell[k(\eta_0-\eta_{\rm in})]}{k^2(\eta_0-\eta_{\rm in})^2}\,.
\end{aligned} \tag{4.38}$$

If the monopole of the CGWB does not depend on the frequency, the angular power spectrum can be computed by using

$$\frac{C_\ell^{\rm CGWB}}{4\pi(4-n_{\rm gwb})^2} = \int\frac{dk}{k}\left[P_{\mathcal{R}}(k)\left(\Delta_\ell^{I-S}+\Delta_\ell^{\rm S}\right)^2+P_T(k)\left(\Delta_\ell^{I-T}+\Delta_\ell^{T}\right)^2\right]. \tag{4.39}$$

4.3 Initial conditions in presence of primordial non-Gaussianity

In this section, we evaluate the initial conditions of the CGWB sources by second-order scalar perturbations discussed in Section 3.4.2. In this case the CGWB is originated by scalar perturbations which are adiabatic, therefore the presence of the adiabatic initial condition, Eq. (4.10), is unavoidable. However, in [23] it is shown that if some (local) underlying non-Gaussianity is present in the primordial curvature perturbation, an additional intrinsic primordial GW inhomogeneity is produced. We parametrize the curvature perturbation as in [23],

$$\zeta(\mathbf{k}) = \zeta_g(\mathbf{k}) + \frac{3}{5} f_{\rm NL} \int \frac{d^3p}{(2\pi)^3} \zeta_g(\mathbf{p})\, \zeta_g(\mathbf{k}-\mathbf{p})\,, \tag{4.40}$$

where the subscript g identifies the Gaussian part of the perturbations. The $f_{\rm NL}$ parameter is assumed here to be scale-independent. In this case, on top of the adiabatic contribution, the CGWB energy density exhibits an additional inhomogeneities proportional to the non-Gaussian term. The total energy density reads

$$\Omega_{\rm CGWB}(\eta, \mathbf{x}, q) = \bar{\Omega}_{\rm CGWB}(\eta,\, q) \left[1 - \frac{2}{4 - n_{\rm gwb}(q)} \Phi(\eta, \mathbf{k}) + \frac{24}{5} f_{\rm NL} \int \frac{d^3k}{(2\pi)^3} \mathrm{e}^{i\mathbf{k}\cdot\mathbf{x}}\, \zeta_g(\mathbf{k})\right], \tag{4.41}$$

where the monopole has been computed in (3.51). The additional perturbations to the energy density in a given frequency bin, proportional to $f_{\rm NL}$, do not depend on $\mathbf{q}$, thus we conclude that also in this case the non-adiabatic initial condition is a monopole,

$$\Gamma_0^{\rm NAD}(\eta_{\rm in}, \mathbf{x}, q) = \frac{1}{4 - n_{\rm gwb}(q)} \frac{24}{5} f_{\rm NL} \int \frac{d^3k}{(2\pi)^3} \mathrm{e}^{i\mathbf{k}\cdot\mathbf{x}}\, \zeta_g(\mathbf{k})\,. \tag{4.42}$$

In Fourier space, this initial condition reads

$$\Gamma_0^{\rm NAD}(\eta_{\rm in}, \mathbf{k}, q) = \frac{1}{4 - n_{\rm gwb}(q)} \frac{24}{5} f_{\rm NL}\, \zeta_g(\mathbf{k})\,, \tag{4.43}$$

where $\zeta_g(\mathbf{k})$ represents the Gaussian curvature perturbation on large (cosmological) scales, whose power spectrum is given by $P_\zeta(k)$ in the notations of previous sections. In this case the non-adiabatic contribution exactly correlates with the adiabatic and the scalar ones, while the correlation with the tensor perturbations is zero.

Chapter 5

Imprint of relativistic and decoupled species on the anisotropies of the CGWB

The angular power spectrum of the CGWB depends on the initial conditions, $\Gamma(\eta_{\rm in}, \mathbf{k}, \mathbf{q})$, and on the evolution of the large-scale scalar and tensor perturbations of the metric, $\Phi(\eta, \mathbf{k})$, $\Psi(\eta, \mathbf{k})$ and $H_{ij}(\eta, \mathbf{k})$. Since the energy density and the anisotropic stress of the CGWB are subdominant w.r.t. the other particle content of the Universe, the dynamics of the metric perturbations during cosmic history is univocally determined by the combined Einstein and Boltzmann equation for radiation, matter and dark energy, Eqs. (2.107), (2.108). In this Chapter, we review the evolution of the metric perturbations at different times and for different scales, discussing their impact on the angular power spectrum of the CGWB. As discussed in Section 3.3, the angular power spectrum of the CGWB is sensitive to the geometry of the Universe at very early times, because there is no tight coupling that could wash out this contribution. This is the reason why a lot of attention will be devoted to discuss the initial conditions of the scalar perturbations at $\eta_{\rm in}$.

5.1 Initial conditions for the scalar perturbations of the metric

We consider the Universe at early times populated by some relativistic tight-coupled particles with energy density $\rho_{\rm coup}$ and by relativistic decoupled species with energy density $\rho_{\rm dec}$. We consider the CGWB as an independent decoupled species whose energy density is subdominant, $\rho_{\rm CGWB} \ll \rho_{\rm coup}$. Most of the mechanisms that could produce a CGWB occur at energy scales much larger than 100 GeV, therefore it is reasonable to assume that all the Standard Model particles are coupled via the electroweak and the strong interactions, while the decoupled degrees of freedom could emerge because of some physics Beyond Standard Model, such as Supersymmetry [227]. The relativistic degrees of freedom are characterized by the perturbations of the distribution functions $\Theta_{\rm coup}$ and $\Theta_{\rm dec}$,

introduced for the CMB analog in Section 2.4. The distribution function for the tight-coupled particles consists just in a monopole and in a dipole term, because the remaining contributions are suppressed by the large number of interactions, while for the decoupled species one could use the collisionless Boltzmann equation to understand the behaviour of the distribution function [42],

$$\Theta'_{\rm dec}(\eta,\mathbf{k},\hat{n})+ik\mu\Theta_{\rm dec}(\eta,\mathbf{k},\hat{n})=\Psi'(\eta,\mathbf{k})-ik\mu\Phi(\eta,\mathbf{k})\,. \tag{5.1}$$

By expanding the distribution function in Legendre polynomials,

$$\Theta_{\rm dec}(\eta,\mathbf{k},\hat{n})=\sum_{\ell}(2\ell+1)\mathcal{P}_{\ell}(\mu)\Theta_{{\rm dec},\ell}(\eta,\mathbf{k})\,, \tag{5.2}$$

we can derive an hierarchy of Boltzmann equations for the ℓ-coefficient of the multipole expansion of the perturbation of the distribution function,

$$\int\frac{{\rm d}\mu}{2}\frac{\mathcal{P}_{\ell}(\mu)}{(-i)^{\ell}}\left[\Theta'_{\rm dec}(\eta,\mathbf{k},\hat{n})+ik\mu\Theta_{\rm dec}(\eta,\mathbf{k},\hat{n})-\mathcal{P}_0(\mu)\Psi'(\eta,\mathbf{k})+ik\mathcal{P}_1(\mu)\Phi(\eta,\mathbf{k})\right]=0\,, \tag{5.3}$$

which leads to

$$\begin{aligned}
\Theta'_{{\rm dec},0}(\eta,k)+k\Theta_{{\rm dec},1}(\eta,\mathbf{k})=&\Psi'(\eta,\mathbf{k})\,,\\
\Theta'_{{\rm dec},1}(\eta,\mathbf{k})-\frac{1}{3}k\Theta_{{\rm dec},0}(\eta,\mathbf{k})+\frac{2}{3}k\Theta_{{\rm dec},2}(\eta,\mathbf{k})=&\frac{k}{3}\Phi(\eta,\mathbf{k})\,,\\
\Theta'_{{\rm dec},2}(\eta,\mathbf{k})-\frac{2}{5}k\Theta_{{\rm dec},1}(\eta,\mathbf{k})+\frac{3}{5}k\Theta_{{\rm dec},3}(\eta,\mathbf{k})=&0\,,\\
\Theta'_{{\rm dec},\ell}(\eta,\mathbf{k})-\frac{k\ell}{2\ell+1}\Theta_{{\rm dec},\ell-1}(\eta,\mathbf{k})+\frac{k(\ell+1)}{2\ell+1}\Theta_{{\rm dec},\ell+1}(\eta,\mathbf{k})=&0\,,
\end{aligned} \tag{5.4}$$

where the last equation holds for $\ell>2$ and we have used the relation

$$\mu\mathcal{P}_{\ell}(\mu)=\frac{1}{2\ell+1}\left[(\ell+1)\mathcal{P}_{\ell+1}(\mu)+\ell\mathcal{P}_{\ell-1}(\mu)\right]\,. \tag{5.5}$$

From the last equation it is clear to see that, when $k\eta\ll1$ and $\ell\geq3$, we have

$$\Theta_{{\rm dec},\ell}\sim k\eta\,\Theta_{{\rm dec},\ell-1}\to\Theta_{{\rm dec},\ell}\ll\Theta_{{\rm dec},\ell-1}\,, \tag{5.6}$$

therefore we are allowed to neglect all the multipoles above the quadrupole. Then, the hierarchy of the Boltzmann equation for the coupled species is

$$\begin{aligned}
\Theta'_{{\rm coup},0}(\eta,\mathbf{k})+k\Theta_{{\rm coup},1}(\eta,\mathbf{k})=&\Psi'(\eta,\mathbf{k})\,,\\
\Theta'_{{\rm coup},1}(\eta,\mathbf{k})-\frac{1}{3}k\Theta_{{\rm coup},0}(\eta,\mathbf{k})=&\frac{k}{3}\Phi(\eta,\mathbf{k})\,,
\end{aligned} \tag{5.7}$$

where all the multipoles above the dipole are zero. If we assume to be in radiation domination, the scalar and the transverse-traceless part of the Einstein equations, given in (2.108), read

$$\begin{aligned}
k^2\Psi+\frac{1}{\eta}\left(\Psi'+\frac{1}{\eta}\Phi\right)=&-\frac{2}{\eta^2}\left[(1-f_{\rm dec})\,\Theta_{{\rm coup},0}+f_{\rm dec}\Theta_{{\rm dec},0}\right]\,,\\
k^2\left(\Phi-\Psi\right)=&-\frac{12}{\eta^2}f_{\rm dec}\Theta_{{\rm dec},2}\,,
\end{aligned} \tag{5.8}$$

where we have introduced the fractional energy density of relativistic and decoupled particle species

$$f_{\rm dec}(\eta) \equiv \frac{\bar{\rho}_{\rm dec}(\eta)}{\bar{\rho}_{\rm dec}(\eta) + \bar{\rho}_{\rm coup}(\eta) + \bar{\rho}_{\rm CGWB}(\eta)}\,, \tag{5.9}$$

where $\rho_{\rm CGWB}$ has been written for completeness, but it is negligible compare to the other two energy components. When $k\eta \ll 1$, the first equation of the Boltzmann hierarchy gives

$$\Theta'_{\rm coup,0} = \Theta'_{\rm dec,0} = \Psi'\,. \tag{5.10}$$

If we combine this relation with the derivative w.r.t. the conformal time of the $(0,0)$ Einstein equation we get

$$\eta\Psi'' + 3\Psi' + \Phi' = 0\,, \tag{5.11}$$

where we have neglected the $k^2\Psi$ term that appears in the Einstein equations. These equation has a constant solution and another one, which goes as η^{-4},that is suppressed by the expansion of the Universe. It is therefore legitimate to consider just the constant solution and, by neglecting the temporal derivatives of Ψ in the $(0,0)$ Einstein equations, the initial condition for the monopole of the perturbation of the distribution function reads

$$\Phi = -\frac{2}{\eta^2}\left[(1 - f_{\rm dec})\,\Theta_{\rm coup,0} + f_{\rm dec}\Theta_{\rm dec,0}\right]\,. \tag{5.12}$$

If the initial conditions are adiabatic, $\Theta_{\rm coup,0} = \Theta_{\rm dec,0}$ and we find the initial condition used for the CMB [42], which simply connects the perturbation of the energy density to the Newtonian potential,

$$\Theta_{\rm coup,0} = -\frac{1}{2}\Phi\,. \tag{5.13}$$

It is possible then to find a relation between Φ and Ψ by combining the transverse-traceless part of the Einstein equations and the Boltzmann hierarchy of the distribution function of the decoupled degrees of freedom. By taking two times the derivative w.r.t. the conformal time of the transverse-traceless part of the Einstein equations, neglecting the derivatives w.r.t. the scalar perturbations, we get

$$\Theta''_{\rm dec,0} = -\frac{k^2}{6\,f_{\rm dec}}(\Phi - \Psi)\,. \tag{5.14}$$

By plugging this expression in the derivative w.r.t. conformal time of the equation for the evolution of the quadrupole in the Boltzmann hierarchy we get

$$\Theta''_{\rm dec,2} = \frac{2}{5}k\,\Theta'_{\rm dec,2} \to -\frac{k^2}{6\,f_{\rm dec}}(\Phi - \Psi) = \frac{2}{5}k^2\left(\frac{1}{3}\Theta_{\rm dec,0} - \frac{2}{3}\Theta_{\rm dec,2} + \frac{1}{3}\Phi\right)\,. \tag{5.15}$$

By expressing $\Theta_{\rm dec,0}$ by using the adiabatic initial condition, Eq. (5.13), and $\Theta_{\rm dec,2}$ through the transverse-traceless part of the Einstein equations, we get a relation between the two scalar perturbations as a function of the fractional energy density of relativistic and decoupled species, defined in Eq. (5.9),

$$\Psi(\eta, \mathbf{k}) = \left[1 + \frac{2}{5}f_{\rm dec}(\eta)\right]\Phi(\eta, \mathbf{k})\,. \tag{5.16}$$

It is useful to write the initial condition as a function of the primordial stochastic fields sourced during inflation, in particular as a function over the primordial curvature perturbation ζ defined in Eq. (2.69). This quantity, which is gauge invariant and constant on super-horizon scales, is defined in terms of the line element given in Eq. (2.74) by

$$\zeta(\mathbf{k}) \equiv -\left[D(\eta,\mathbf{k}) + \frac{1}{6}k^2 F(\eta,\mathbf{k})\right] - \mathcal{H}\frac{\delta\rho(\eta,\mathbf{k})}{\bar{\rho}'(\eta)}\,. \tag{5.17}$$

In the Poisson gauge $D = -\Psi$ and $F = 0$, while under adiabatic initial conditions and in a Universe dominated by radiation the second term, which corresponds to the total fractional density perturbations, simplifies to

$$\frac{\delta\rho}{\bar{\rho}'} \equiv \sum_{\alpha}\frac{\delta\rho_{\alpha}}{\bar{\rho}_{\alpha}} = -\sum_{\alpha}\frac{\delta\rho_{\alpha}}{-3\mathcal{H}(1+w_{\alpha})\bar{\rho}_{\alpha}} = -\frac{2}{\mathcal{H}}\Phi\sum_{\alpha}\frac{1}{1+w_{\alpha}}\frac{\bar{\rho}}{\bar{\rho}_{\alpha}}\,. \tag{5.18}$$

In the case in which all the particles are relativistic, we set $w_{\alpha} = 1/3$, finding the initial conditions on the scalar perturbations

$$\begin{aligned}
\Phi(\eta,\mathbf{k}) &= -\frac{2}{3}\left[1 + \frac{4}{15}f_{\rm dec}(\eta)\right]^{-1}\zeta(\mathbf{k})\,,\\
\Psi(\eta,\mathbf{k}) &= -\frac{2}{3}\left[1 + \frac{2}{5}f_{\rm dec}(\eta)\right]\left[1 + \frac{4}{15}f_{\rm dec}(\eta)\right]^{-1}\zeta(\mathbf{k})\,.
\end{aligned} \tag{5.19}$$

These expressions are consistent with the result found in [270, 271] for relativistic neutrinos at much lower temperatures, which could produce interesting signatures in other relics, like the CMB. Note also that, as realized in [46], the transfer function of the scalar potentials at high energies is sensitive also the equation of state of the Universe, $P = w\rho$. For instance, if we suppose that there are no decoupled species that contribute to the energy density of the Universe, which is dominated by a fluid with an equation of state of parameter w, under adiabatic initial conditions, we can write Eq. (2.69), according to the expression found in (5.18), by using

$$\zeta = -\Psi - \frac{2}{3(1+w)}\Phi \to \Phi = -\frac{3(1+w)}{5+3w}\zeta\,. \tag{5.20}$$

As we will see in Section 5.3, the initial conditions given by Eqs. (5.19), (5.20) play an important role in the computation of the angular power spectrum of the CGWB, by enhancing/damping the anisotropies, depending on the amount of relativistic and decoupled species and on the equation of state of the Universe at early times.

5.2 Transfer function of the metric perturbations

Once the initial conditions on the metric fluctuations have been determined, it is crucial to evaluate the evolution of the scalar and tensor perturbations in order to compute the line-of-sight integrals, Eqs. (3.33), that allow to predict the CGWB amount of anisotropies.

The transfer functions introduced in Eqs. (3.35) are obtained by solving the system of the Boltzmann and Einstein equations, Eqs. (2.107), (2.108), by numerical integration. In this Thesis we have modified the Boltzmann solver code CLASS [44, 45] to compute the angular power spectrum of the CGWB at early times in order to keep into account also for relativistic and decoupled species and for an exotic equation of state $w \neq 1/3$ at $\eta_{\rm in}$. In this section we will comment on the main analytical and numerical features of the computation of the transfer functions of the metric perturbations, in order to justify the shape of the angular power spectrum of the CGWB we will obtain. Since the evolution of Φ, Ψ and H_{ij} depends on the nature of the mode (scalar and tensor) and of the wavelength of the perturbations, we will discuss separately the properties of the scalar and the tensor transfer functions.

Transfer function of scalar perturbations

As discussed in the previous section, when $k\eta \ll 1$ and the equation of state of the Universe is constant, Eq. (5.19) regulates the evolution of the scalar perturbations in time. The only source of variation of Φ and Ψ is the change in the fractional energy density of relativistic and decoupled species, which stays between zero and one, while any other variation is suppressed by the fact that the wavelength of the perturbations is larger than the causal horizon. As discussed in Section 2.2, the fractional energy density of relativistic and decoupled species, defined in Eq. (5.9), is constrained by BBN [232, 272] and CMB [26] observations. Therefore after $\eta_{\rm min} \approx 0.1\,{\rm Mpc}$, variations in $f_{\rm dec}(\eta)$ due to anisotropic stresses are known and can be computed numerically (see, e.g., Section 2.2). In this section we discuss the evolution of the scalar perturbations from $\eta_{\rm min}$ to η_0, while the transition from $\eta_{\rm in}$ and $\eta_{\rm min}$, which depends on the history of the Universe at energy scales not probed by current experiments, will be examined in detail in Section 5.3.

In the literature [42], the evolution of the scalar transfer function is divided into three cases, depending on the scale of the perturbation considered. We define the scale of the modes that re-enter the horizon at the equality between matter and radiation by

$$k_{\rm eq} \equiv \frac{1}{\eta_{\rm eq}(z_{\rm eq})} \approx 0.08\,{\rm Mpc}^{-1}\,, \tag{5.21}$$

where the redshift of the equality has been defined in Eq. (2.15).

When $k \ll k_{\rm eq}$, the transfer function is constant during the radiation dominated epoch, because of the solution for Φ and Ψ of Eq. (5.11), when the fractional energy density of relativistic and decoupled particles is constant. Around $z_{\rm eq}$, the equation of state of the Universe is changing and the scalar potentials experience a smooth transition from the end of the radiation dominated era to the beginning of the matter dominated epoch. In absence of decoupled particles, it is possible to show [42] that the transfer function of the scalar potentials through $z_{\rm eq}$ can be expressed as an analytic function,

$$T_\Phi(\eta,k) = T_\psi(\eta,k) = \frac{1}{10y^3}\left(16\sqrt{1+y(\eta)} + 9y^3(\eta) + 2y^2(\eta) - 8y(\eta) - 16\right)\Psi(\eta_{\rm min},k)\,, \tag{5.22}$$

where we have defined the parameter

$$y(\eta) \equiv \frac{1+z_{\rm eq}}{1+z(\eta)}\,. \tag{5.23}$$

If $f_{\rm dec}(\eta) \neq 0$ and $\Psi \neq \Phi$, it is still possible to show that the solutions still converge to

$$T_\Phi(\eta, k \ll k_{\rm eq}) = T_\Psi(\eta \gg \eta_{\rm eq}, k \ll k_{\rm eq}) = -\frac{3}{5}\,. \tag{5.24}$$

During the matter dominated epoch, the transfer function remains constant, because non-relativistic matter has not enough kinetic energy to escape from the potential wells and to reduce their depth. On the other hand, T_Φ, T_Ψ decay exponentially during the dark energy era, where the accelerated expansion of the Universe dilutes the amplitude of the metric perturbations.

If $k \gg k_{\rm eq}$, the potential starts a decaying before $\eta_{\rm eq}$, because of the high kinetic energy of relativistic particles that damps the metric perturbations. Also in this case, when no decoupled particles are present, and thus $\Phi = \Psi$, it is possible to find an analytic solution [42] for the scalar perturbations during the radiation epoch,

$$T_\Phi(\eta, k) = T_\Psi(\eta, k) = j_1\left(\frac{k\eta}{\sqrt{3}}\right) = 3\frac{\sin\frac{k\eta}{\sqrt{3}} - \frac{k\eta}{\sqrt{3}}\cos\frac{k\eta}{\sqrt{3}}}{\left(\frac{k\eta}{\sqrt{3}}\right)^2}\,. \tag{5.25}$$

The evolution of these perturbations at times $\eta \gtrsim \eta_{\rm eq}$ is not important, because around the equality epoch these fields have already undergone over many oscillations, therefore Φ and Ψ at $z_{\rm eq}$ evolution after the equality produces no effects on the CMB and the CGWB.

For $k \approx k_{\rm eq}$, a smooth transition around $z_{\rm eq}$ occurs, but with larger damping than the one computed in Eq. (5.24). During the matter dominated epoch, also these perturbations remain constant and then decay when $z \leq z_{\rm eq-\Lambda}$.

In Figure 5.1, we plot the transfer functions T_Ψ (solid) and T_Φ (dashed) for $k \ll k_{\rm eq}$ (red), $k \approx k_{\rm eq}$ (blue) and $k \gg k_{\rm eq}$ (green).

Transfer function of tensor perturbations

Because of the decomposition theorem, the tensor transfer function at linear order can be computed neglecting the presence of the scalar perturbations in the Universe. This assumption, combined with the fact that in GR the equation of motion for the two polarizations of the tensor modes are decoupled, simplifies a lot the computation of $T_H(\eta, k)$, which can be evaluated analytically in most of the cases of interest. According to [227], it is possible to find the following solutions for the equation of motion of the tensor perturbations, given by the first row of Eq. (2.108). When the anisotropic stress is zero, the transfer functions of tensors are then

$$\begin{aligned} T_H(\eta < \eta_{\rm eq}, k > k_{\rm eq}) =& j_0(k\eta)\,, \\ T_H(\eta > \eta_{\rm eq}, k > k_{\rm eq}) =& \frac{\eta_{\rm eq}}{\eta}\left[A(k) j_1(k\eta) + B(k) y_1(k\eta)\right]\,, \\ T_H(\eta, k < k_{\rm eq}) =& \frac{j_1(k\eta)}{k\eta}\,, \end{aligned} \tag{5.26}$$

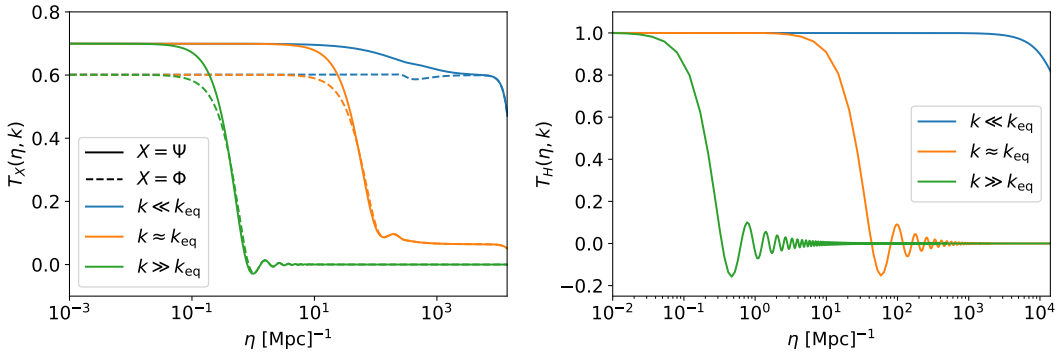

Figure 5.1: Left: plot of the transfer function of the scalar perturbation Ψ (solid) and Φ (dashed). Right: Plot of the transfer function of the tensor perturbations H_{ij}. In both plots, we have considered the case in which $k \ll k_{\rm eq}$ (red), $k \approx k_{\rm eq}$ (blue) and $k \gg k_{\rm eq}$ (green).

where j_ℓ and y_ℓ are the spherical Bessel function of the first and second kind, while the coefficients A and B come from the matching of the solution during the radiation dominated era with the one evaluated during the matter dominated era at the equality,

$$\begin{aligned} A(k) \equiv & \frac{3}{2k\eta_{\rm eq}} - \frac{\cos(2k\eta_{\rm eq})}{2k\eta_{\rm eq}} + \frac{\sin(2k\eta_{\rm eq})}{(k\eta_{\rm eq})^2}\,, \\ B(k) \equiv & -1 + \frac{1}{(k\eta_{\rm eq})^2} - \frac{\cos(2k\eta_{\rm eq})}{(k\eta_{\rm eq})^2} - \frac{\sin(2k\eta_{\rm eq})}{2k\eta_{\rm eq}}\,. \end{aligned} \tag{5.27}$$

In the case of tensor perturbations, the transfer function is just constant when $k\eta \ll 1$, independently on $f_{\rm dec}$ and w, while it starts an oscillating and damping behaviour for $k\eta \gtrsim 1$. The main difference between tensor modes that re-entered the horizon during the radiation and the matter dominated epochs are the oscillating parts in the transfer function, which consist in different combinations of the spherical Bessel functions. When a source of anisotropic stress which contributes considerably to the energy density of the Universe is present, the evolution of the tensor modes around the time $k\eta \approx 1$ slightly differ from (F.33). In [252, 253] it has been shown that the anisotropic stress of neutrinos reduces the squared amplitude of tensor modes by 35.6 % when $k \gg k_{\rm eq}$, while the effect is smaller when $k \lesssim k_{\rm eq}$, because the contribution of neutrinos to the energy density of the Universe at $\eta \lesssim 1/k_{\rm eq}$ is smaller. As a rule of thumb, we could say that the transfer function of tensor modes is sensitive to the decoupled degrees of freedom at the time corresponding to the horizon crossing, i.e., when the GWs start oscillating.

5.3 Scalar contribution to the angular power spectrum of the CGWB

One of the most important contribution to the anisotropies of the CGWB is due to the propagation of gravitons through the large-scale scalar perturbations of the Universe Φ and Ψ. Eqs. (3.33), (3.34) show that the angular power spectrum of the CGWB depends

on the source function

$$\Delta_\ell^S(k,\eta_0,\eta_{\rm in}) \equiv T_\Phi(\eta_{\rm in},k) j_\ell[k(\eta_0-\eta_{\rm in})] + \int_{\eta_{\rm in}}^{\eta_0} {\rm d}\eta \left[T'_\Phi(\eta,k) + T'_\Psi(\eta,k)\right] j_\ell[k(\eta_0-\eta)]\,, \quad (5.28)$$

where the two terms represent the SW and ISW contributions, introduced for the first time in the CMB context [43]. The main difference w.r.t. the CMB case is given by the fact that the SW and the ISW are sensitive to the physics operating at $\eta_{\rm in}$, while for photons the Universe is opaque before $\eta_{\rm rec}$, because of the tight coupling of the CMB with baryons. In this section we will explore the main features of these two effects, discussing the scaling of the angular power spectrum with the multipole and the sensitivity to additional parameters that govern the evolution of the metric perturbations in the early Universe, such as $f_{\rm dec}(\eta_{\rm in})$ or $w(\eta_{\rm in})$.

Sachs-Wolfe of the CGWB

The SW is the redshift experienced by a graviton when crossing a potential well at its production, which enhances/reduces the energy density, depending if the background has been produced in an underdense/overdense region. A peculiarity of the CGWB is that the background is generated at early times, when all the perturbations of interest were inside the causal horizon, since scales that are comparable to the horizon at $\eta_{\rm in}$ would affect the angular power spectrum[1] at multipoles much larger than the ones that could be detected by future interferometers,

$$\ell \approx k\eta_0 \approx \frac{\eta_0}{\eta_{\rm in}} \approx 10^7 - 10^{22}\,, \quad (5.29)$$

where we have used the frequencies of the CGWB discussed in Section 3.1. If the initial time, computed by using Eq. (3.42), does not depend on q, the potentials at $\eta_{\rm in}$ are constant, thus the transfer function of the scalar modes at $\eta_{\rm in}$ is independent on k, q and it is equal to

$$T_\Phi(\eta_{\rm in}) = -\frac{2}{3}\left[1+\frac{4}{15}f_{\rm dec}(\eta_{\rm in})\right]^{-1}\,, \quad (5.30)$$

which makes clear that the presence of relativistic and decoupled species at the production of the background generates a damping in the SW contribution to the angular power spectrum. In the case of a power-law dependence of the scalar power spectrum, it is possible to provide an analytic formula of the SW of the CGWB,

$$\begin{aligned} C_\ell^{\rm SW\times SW} =& 4\pi\,\frac{4}{9}\left[1+\frac{4}{15}f_{\rm dec}(\eta_{\rm in})\right]^{-2}\int\frac{dk}{k}\,A_s\left(\frac{k}{k_p}\right)^{n_s-1} j_\ell^2[k(\eta_0-\eta_{\rm in})] = \\ =& \frac{8\pi^2 A_s}{9[k_p(\eta_0-\eta_{\rm in})]^{n_s-1}}\left[1+\frac{4}{15}f_{\rm dec}(\eta_{\rm in})\right]^{-2}\int_0^\infty {\rm d}x\, x^{n_s-3} J^2_{\ell+1/2}(x)\,, \end{aligned} \quad (5.31)$$

where the relation between the Bessel and the spherical Bessel functions is given by

$$j_\ell(x) = \sqrt{\frac{\pi}{2x}}J_{\ell+1/2}(x)\,. \quad (5.32)$$

[1] Note also that in this case the shortwave approximation is no more valid.

A derivation of the solution of the integral over x has been given in Eq. (G.3) and we get

$$C_\ell^{\mathrm{SW}\times\mathrm{SW}} = \frac{2^{n_s}\,\pi^2 A_s}{9[k_p(\eta_0-\eta_{\rm in})]^{n_s-1}}\left[1+\frac{4}{15}f_{\rm dec}(\eta_{\rm in})\right]^{-2}\frac{\Gamma(3-n_s)\Gamma\left(\frac{2\ell-1+n_s}{2}\right)}{\Gamma^2\left(\frac{4-n_s}{2}\right)\Gamma\left(\frac{2\ell+5-n_s}{2}\right)}\,. \tag{5.33}$$

In the limit $n_s \to 1$, the SW contribution to the angular power specturm of the CGWB is

$$C_\ell^{\mathrm{SW}\times\mathrm{SW}} = \frac{8}{9}A_s\left[1+\frac{4}{15}f_{\rm dec}(\eta_{\rm in})\right]^{-2}\frac{1}{\ell(\ell+1)}\,, \tag{5.34}$$

where we have used $\Gamma(n) = (n-1)!$, $\Gamma(3/2) = \sqrt{\pi}/2$. According to the constraints given by Planck [34, 26], at the scales of interest $n_s = 0.96$, therefore the angular power spectrum of the CGWB scales approximately like $\ell(\ell+1)$, with a small decrease in ℓ, due to the fact that the primordial scalar spectrum is red tilted. From theses analytic results, it is clear that when $f_{\rm dec}(\eta_{\rm in})$ increases, the SW contribution to the angular power spectrum of the CGWB is suppressed, thus the angular power spectrum is sensitive to the particle content of the Universe at early times. The same result holds of course for the equation of state parameter of the Universe at $\eta_{\rm in}$, which affects the initial conditions for the scalar potentials, and consequently the SW, via Eq. (5.20). In Figure 5.2, we plot the SW contribution to the angular power spectrum of the CGWB for $n_{\rm gwb} = 0.35$ and for $f_{\rm dec}(\eta_{\rm in})$ equal to zero and one respectively. In our plot, we assume that at $\eta_{\rm in}$ the Universe is filled by radiation, thus we impose $w(\eta_{\rm in}) = 1/3$, neglecting the degeneracy between w and $f_{\rm dec}$ for simplicity.

Integrated Sachs-Wolfe of the CGWB

The ISW is the redshift of graviton when they cross metric perturbations that change their amplitude in time. The ISW generates a net amount of anisotropies when the length of the perturbations is much smaller than the time required to the particles to cross them; in this way the GWs experience a coherent damping/amplification due to variations of the potentials. On the other hand, when $k\eta \gg 1$, gravitons are redshifted by each of the many potential wells crossed, but since the crossing time is very small, the overall effect is a net cancellation (incoherent amplification) and the ISW gives zero anisotropies [41]. As we have discussed in Section 5.2, the evolution in time of the potentials from $\eta_{\rm in}$ to $\eta_{\rm min}$ is governed just by the evolution of $f_{\rm dec}(\eta)$, while from $\eta_{\rm min}$ to η_0, the time dependence is the standard one depicted in Figure 5.1. Because of this reason, we divide the computation of the ISW into a primordial-ISW (p-ISW), that is model dependent and can be computed analytically, and into a standard ISW, which depends on the constraints on the cosmological parameters provided by other independent observations.

The p-ISW depdends on the particle physics model one would choose to describe the content of the Universe at energy scales much larger than the ones that can be probed by present colliders, that is strongly model dependent. However, it is straightforward to notice that the spherical Bessel function $j_\ell[k(\eta_0-\eta)]$ is almost constant in the interval in which we compute this effect, since $k\eta_0 \ll 1$ and $\eta_0 \gg \eta_{\rm min} \gg \eta_{\rm in}$. It is possible then to

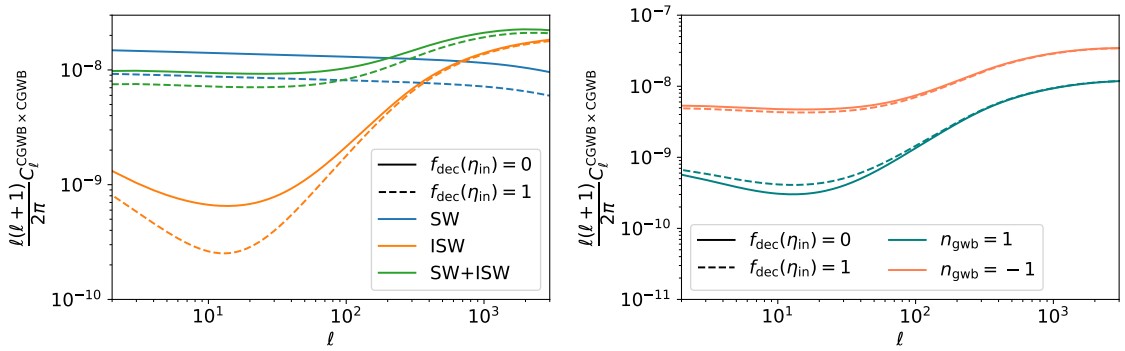

Figure 5.2: Left: plot of the SW, the ISW and the SW+ISW contribution to the angular power spectrum of the CGWB, for $f_{\rm dec}(\eta_{\rm in})$ equal to zero and one. In this plot, a constant tensor tilt, $n_{\rm gwb} = 0.35$ has been assumed. Right: plot of the total contribution to the angular power spectrum of the CGWB for adiabatic initial conditions, for $f_{\rm dec}(\eta_{\rm in})$ equal to zero and one and $n_{\rm gwb} = \pm 1$.

compute analytically the p-ISW [3, 46, 1], showing that it is function just of the value of the fractional relativistic and decoupled species from $\eta_{\rm in}$ to $\eta_{\rm min}$,

$$\begin{aligned}\Delta_\ell^{\rm p-ISW} &\equiv \int_{\eta_{\rm in}}^{\eta_{\rm min}} d\eta\, j_\ell[k(\eta_0-\eta)]\,\left[T'_\Psi(\eta,k)+T'_\Phi(\eta,k)\right]\\ &\simeq j_\ell[k(\eta_0-\eta_{\rm in})]\left[T_\Psi(\eta,k)+T_\Phi(\eta,k)\right]_{\eta_{\rm in}}^{\eta_{\rm min}}\\ &= j_\ell[k(\eta_0-\eta_{\rm in})]\frac{2}{15}\frac{f_{\rm dec}(\eta_{\rm in})-f_{\rm dec}(\eta_{\rm min})}{1+\frac{4}{15}f_{\rm dec}(\eta_{\rm min})}T_\Phi(\eta_{\rm in},k)\,.\end{aligned} \tag{5.35}$$

For the standard ISW, we can understand the impact of variations of the potentials on the angular power spectrum by looking at the transfer functions for different scales at different times plotted in Figure 5.1. At large angular scales, the CGWB is sensitive to the ISW due to the variations of the scalar perturbations that re-enter the horizon during the matter dominated era, therefore to the transition of the potentials around $z_{\rm eq}$ (early-ISW) and to the decay of these potentials after $z_{\rm eq-\Lambda}$ (late-ISW). At small angular scales, the ISW is sensitive to the variations of the potentials that re-enter the horizon during the radiation dominated era. As it can be seen in Figure 5.1, the variations of these potentials are larger, because these potentials decays almost completely, so the ISW increases at small scales. This is the opposite of the CMB case, in which everything is computed around recombination, where the variations of the potentials in the radiation-dominated era do not play any role, since the angular power spectrum of the CMB is basically integrated from recombination, $\eta_{\rm rec} > \eta_{\rm eq}$. At small angular scales, the ISW is dominated by the early-ISW from $\eta_{\rm min}$ to η_0, therefore the sensitivity to $f_{\rm dec}(\eta_{\rm in})$ due to the p-ISW is reduced, thus one could not see the impact of relativistic and decoupled species on the ISW by looking at the angular power spectrum only at small angular scales, where the late-ISW from $\eta_{\rm min}$ to η_0 has a much smaller impact on the anisotropies and is not able to hid the p-ISW contribution.

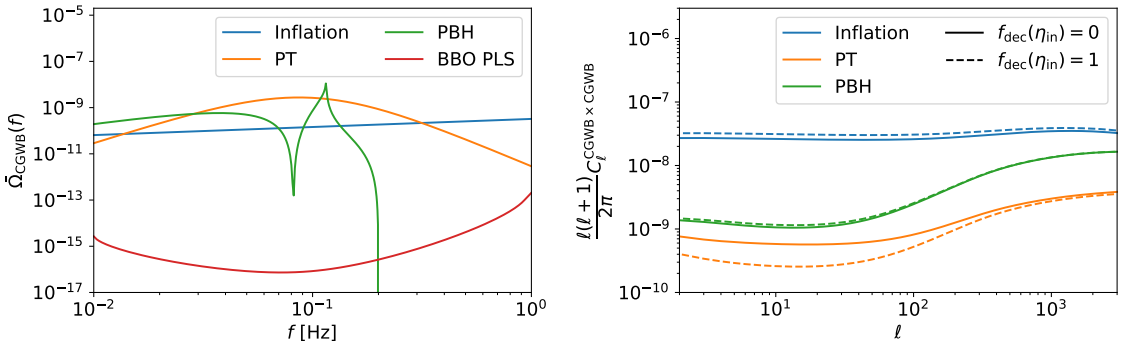

Figure 5.3: Left: plot of the monopoles of the CGWB from inflation, PT and PBH. Right: plot of the angular power spectra for these three sources.

5.4 Sensitivity of the spectrum to relativistic particles for adiabatic initial conditions

The dominant contribution to the angular power spectrum of the CGWB at large angular scales is the sum of the IC, SW and p-ISW. Each of these terms depend on $f_{\rm dec}(\eta_{\rm in})$ and $w(\eta_{\rm in})$ through the transfer functions of the scalar perturbations, Eq. (5.19) and (5.20). All these effects are proportional to $j_\ell[\eta_0 - \eta_{\rm in}]$, therefore it would be natural to ask whether a cancellation among them could appear in such a way that the angular power spectrum is no more sensitive to the two early Universe parameters discussed in this Section. Under adiabatic initial conditions, defined by Eq. (4.10), it is possible to see that, by summing the source functions of the SW and of the p-ISW, the total spectrum is proportional to

$$\Delta_\ell^{\rm AD} + \Delta_\ell^S \sim \frac{\frac{6-n_{\rm gwb}(q)}{4-n_{\rm gwb}(q)} + \frac{2}{5} f_{\rm dec}(\eta_{\rm in})}{1 + \frac{4}{15} f_{\rm dec}(\eta_{\rm in})}\,, \tag{5.36}$$

which implies that when $n_{\rm gwb}(q) = 0$ the spectrum does not vary with $f_{\rm dec}(\eta_{\rm in})$. In the right panel of Figure 5.2 we plot the total angular power spectrum of the CGWB with $n_{\rm gwb} = \pm 1$ for adiabatic initial conditions, showing that the spectrum is indeed sensitive to the presence of relativistic and decoupled degrees of freedom when the tensor spectrum is not scale invariant. Note also that the case of adiabatic initial conditions and $n_{\rm gwb} = 0$ seems to be quite unrealistic, because many physical models generate non-adiabatic initial conditions, see, e.g., Eq. (4.35) for single-field inflation and Eq. (4.43) for the scalar-induced GWs with non-Gaussianity. Furthermore, most of the monopoles considered in this Thesis scale with the frequency, thus the cancellation given by Eq. (5.36) does not occur.

5.5 Total angular power spectrum for different initial conditions

Eqs. (4.10), (4.35) and (4.43) show that the initial conditions could be very different, depending on the source of CGWB considered. In this section, we compare three angular

power spectra for three different mechanisms that generate GWs detectable by the future space-based interferometers BBO/DECIGO:

- PT with adiabatic initial conditions. For the phase transitions we choose the following parameters that characterize the GW monopole, given in Eq. (3.55),

$$\bar{\Omega}_* = 3.0 \times 10^{-8}\,, \qquad f_* = 0.1\,\mathrm{Hz}\,, \qquad n_1 = 3.0\,, \qquad n_2 = -4.0\,, \qquad \Delta = 2.0\,. \tag{5.37}$$

- PBH with AD+NAD initial conditions given by Eq. (4.43). The parameters that describe the monopole, Eq. (3.51), and the anisotropies are

$$A_* = 1.3 \times 10^{-4}\,, \qquad f_* = 0.1\,\mathrm{Hz}\,, \qquad f_{\rm NL} = 0.01\,. \tag{5.38}$$

- inflationary background, with AD+NAD initial conditions given by (4.35). To characterize the monopole we use

$$r = 0.30\,, \qquad n_T = 0.35\,. \tag{5.39}$$

In the left panel of Figure 5.3, we plot the monopoles of the CGWB for the three sources we have chosen and the PLS of BBO, defined in Section 1.3, for $T_{\rm obs} = 1\,\mathrm{yr}$. In the right panel, we plot the angular power spectra for these three models for $f_{\rm dec}(\eta_{\rm in}) = 0$ and $f_{\rm dec}(\eta_{\rm in}) = 1$, at the frequency $f_p = 3 \times 10^{-2}\,\mathrm{Hz}$.

The amplitude and the scalings with the multipoles of the three spectra can be explained in terms of the initial conditions and of the tensor tilt of the CGWB at the pivot frequency [1]. At low multipoles, the angular power spectra are sensitive mainly to the combination of the initial conditions and the SW, therefore the spectra would scale like

$$C_\ell^{\rm CGWB\times CGWB} \sim [4 - n_{\rm gwb}(f_p)]^2 \left[\left(1 - \frac{2}{4 - n_{\rm gwb}(f_p)}\right) T_\Phi(\eta_{\rm in}, k) + \Gamma^{\rm NAD}(\eta_{\rm in}, k, f_p)\right]^2 . \tag{5.40}$$

At $f_p = 3 \times 10^{-2}\,\mathrm{Hz}$, the spectral tilt of the three backgrounds are

$$n_{\rm gwb}^{\rm Inflation}(f_p) = 0.35\,, \qquad n_{\rm gwb}(f_p)^{\rm PT} = 2.42\,, \qquad n_{\rm gwb}^{\rm PBH} = 0.48\,. \tag{5.41}$$

For the inflationary case, the NAD initial condition is given by Eq. (4.35), while for the PBH scenario by Eq. (4.43). In the case of $f_{\rm dec}(\eta_{\rm in}) = 0$, Eq. (5.40) predicts an enhancement of the CGWB from inflation w.r.t. the backgrounds from PT and PBH equal to

$$\frac{C_\ell^{\rm Inflation}}{C_\ell^{\rm PT}} = 1500\,, \qquad \frac{C_\ell^{\rm Inflation}}{C_\ell^{\rm PBH}} = 3.5\,. \tag{5.42}$$

These predictions differ with the numerical results of Figure 5.3, because they do not take into account for the early- and late-ISW contributions. More specifically, the early-ISW induced by changes of the potentials with $k \ll k_{\rm eq}$ around $\eta_{\rm eq}$, described in Eq. (5.22), contribute with a term of the same sign of the adiabatic initial conditions, reducing the enhancement expected from $\Gamma^{\rm NAD}$. In a similar fashion, it is possible to evaluate the

difference in amplitude of the angular power spectrum at low and high multipoles, defined by

$$\Delta C_\ell^{\rm peak} \equiv \frac{C_{3000}^{\rm CGWB\times CGWB}}{C_2^{\rm CGWB}} \frac{2(2+1)}{3000(3000+1)} \,. \tag{5.43}$$

This difference at low multipoles will be approximately given by the sum of AD+NAD+SW, while at large multipoles by AD+NAD+SW+ISW. At the smallest angular scales, the ISW is provided by variation of the potentials which enter the horizon during the radiation epoch and, by looking at Figure 5.1 it is clear that this ISW should be twice the SW. For the three CGWBs we expect something like

$$\begin{aligned}
\Delta C_\ell^{\rm peak-Inflation} &\sim \frac{\left[\left(1-\frac{2}{4-n_{\rm gwb}(f_p)}\right) T_\Phi(\eta_{\rm in},k) + 4T_\Phi(\eta_{\rm in},k)\right]^2 - [2T_\Phi(\eta_{\rm in},k)]^2}{\left[\left(1-\frac{2}{4-n_{\rm gwb}(f_p)}\right) T_\Phi(\eta_{\rm in},k) + 4T_\Phi(\eta_{\rm in},k)\right]^2} \sim 1.2\,, \\
\Delta C_\ell^{\rm peak-PT} &\sim \frac{\left[\left(1-\frac{2}{4-n_{\rm gwb}(f_p)}\right) T_\Phi(\eta_{\rm in},k)\right]^2 - [2T_\Phi(\eta_{\rm in},k)]^2}{\left[\left(1-\frac{2}{4-n_{\rm gwb}(f_p)}\right) T_\Phi(\eta_{\rm in},k)\right]^2} \sim 56\,, \\
\Delta C_\ell^{\rm peak-PBH} &\sim \frac{\left[\left(1-\frac{2}{4-n_{\rm gwb}(f_p)}\right) T_\Phi(\eta_{\rm in},k) + \frac{36}{5}\frac{f_{\rm NL}}{4-n_{\rm gwb}(f_p)} T_\Phi(\eta_{\rm in},k)\right]^2 - [2T_\Phi(\eta_{\rm in},k)]^2}{\left[\left(1-\frac{2}{4-n_{\rm gwb}(f_p)}\right) T_\Phi(\eta_{\rm in},k) + \frac{36}{5}\frac{f_{\rm NL}}{4-n_{\rm gwb}(f_p)} T_\Phi(\eta_{\rm in},k)\right]^2} \sim 1.6\,,
\end{aligned} \tag{5.44}$$

where we have assumed that the SW+AD+NAD and the ISW are uncorrelated, thus they can be summed in quadrature. In the case of the inflationary background, the difference in amplitude of the spectrum at high and low multipoles is explained by the fact that the NAD initial conditions has opposite sign w.r.t. SW+AD+ISW, therefore the spectrum does not grow. In an analogous way, it is possible to explain the scaling of the three spectra with $f_{\rm dec}(\eta_{\rm in})$, as already mentioned in Section 5.4.

5.6 ISW from tensor perturbations

The anisotropies generated by the ISW effect associated to the tensor perturbations, whose source function is Δ_ℓ^T defined in Eq. (3.34), are subdominant compared to the ones induced by the scalar perturbations. This happens because the tensor power spectrum is suppressed w.r.t. the scalar one by a factor $r \lesssim 0.035$. In the left panel of Figure 5.4, we plot the scalar, the tensor and the total contribution to the angular power spectrum of the CGWB, according to the latest constraints on the tensor-to-scalar ratio [247]. The CGWB has adiabatic initial condition and a tensor tilt $n_{\rm gwb} = 0.35$. In the right panel of Figure 5.4, we plot the tensor contribution for the case of single-field inflation, comparing the ISW and the NAD contribution, showing that these two terms sum, since they have the same sign. These coherent amplification enhances of a factor of 4 the tensor contribution, which is however still subdominant if compared to the scalar one.

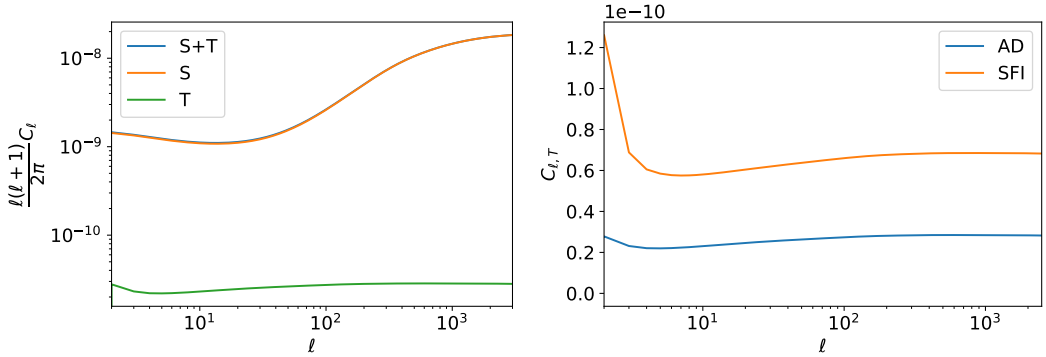

Figure 5.4: Left: Plot of the angular power specturm of the CGWB for scalar, tensor and scalar+tensor contributions, for adiabatic initial conditions and $n_{\rm gwb} = 0.35$. Right: plot of the tensor contribution to the angular power spectrum of the CGWB with adiabatic and NAD initial conditions from single-field inflation.

Chapter 6

Cross-correlation between the CMB and the CGWB

6.1 Correlation of cosmological signals produced at different epochs

Photons and gravitons start their free streaming at $\eta_{\rm rec} \approx 280\,{\rm Mpc}$, $\eta_{\rm in} \lesssim 10^{-10}\,{\rm Mpc}$. The dominant contribution to the anisotropies typically comes from scales around $k \approx \ell/\eta_0$, which means that the ratio between the separation of the last-scattering surfaces of the CMB and CGWB and the wavelength that generates the angular power spectrum at a given multipole is

$$k(\eta_{\rm rec} - \eta_{\rm in}) \approx \ell \frac{\eta_{\rm rec} - \eta_{\rm in}}{\eta_0} \approx \ell \frac{\eta_{\rm rec}}{\eta_0} \approx \frac{\ell}{50}\,. \tag{6.1}$$

When $\ell \leq 10$, one would expect that the CMB and the CGWB are highly correlated, because the separation between the two surfaces is very low and the two signals share the same geodesics, which give rise to very similar SW and ISW effects. On the other hand, when $\ell \geq 50$, the difference between $\eta_{\rm rec}$ and $\eta_{\rm in}$ becomes important, because the length of the metric perturbations that generate the anisotropies is much smaller than the separation of the two surfaces, therefore the perturbations that produce the redshift of photons and gravitons are uncorrelated [4, 1]. A more mathematical interpretation of this result could be given in terms of projection effects. Suppose that at a given scale ℓ, the anisotropies of CMB and photons are generated by perturbations of scale k which are sharply peaked around η_1 and η_2. For the SW of CMB and graviton it is straightforward to have $\eta_1 = \eta_{\rm rec}$ and $\eta_2 = \eta_{\rm in}$. As a first approximation, the angular power spectrum of the cross-correlation between the CMB and the CGWB, which will be defined in Eq. (6.5) of next section, would depend (approximately) on the integral

$$I_\ell(\eta_1, \eta_2) \equiv \int \frac{{\rm d}k}{k} j_\ell[k(\eta_0 - \eta_1)] j_\ell[k(\eta_0 - \eta_2)] \sim \frac{1}{\sqrt{\ell}\left(\ell + \frac{1}{2}\right)} e^{-\frac{\eta_1 - \eta_2}{\eta_0}\ell}\,, \tag{6.2}$$

where we have written the spherical Bessel as a Bessel function, Eq. (5.32), and then we have used the result obtained in Eq. (G.2). Eq. (6.2) is valid when $\eta_1 > \eta_2$ and shows that

when ℓ is sufficiently large, there is an exponential suppression of the signal, also in the case $\eta_1 - \eta_2 \ll \eta_0$. In the next section, we will define and compute numerically the angular power spectrum of the cross-correlation between the CMB and the CGWB, explaining the features (peaks, damping, etc.) in terms of a generalization of $I_\ell(\eta_1, \eta_2)$.

6.2 Angular power spectrum of the cross-correlation between CMB and CGWB

The solution of the Boltzmann equation of the CMB [42], gives the following coefficients of the spherical harmonics expansion of the perturbation of the distribution function of the CMB,

$$\begin{aligned} a_{\ell m} =& 4\pi\,(-i)^\ell \int \frac{d^3k}{(2\pi)^3}\, e^{i\vec{k}\cdot\vec{x}_0}\, Y^*_{\ell m}(\hat{k})\, \mathcal{R}(\vec{k})\, \Theta^S_\ell(k,\eta_0)\,, \\ \Theta^S_\ell(k,\eta_0) =& \int_{\eta_{\rm min}}^{\eta_0} d\eta \Big[g(\eta) \Big(T_{\Theta_0}(\eta,k) + T_\psi(\eta,k) \Big) j_\ell[k(\eta_0-\eta)] \\ &+ g(\eta)\; k^{-1} T_{\theta_b}(\eta,k) j'_\ell[k(\eta_0-\eta)] \\ &+ e^{-\kappa(\eta)}\; \frac{\partial[T_\psi(\eta,k)+T_\phi(\eta,k)]}{\partial\eta} j_\ell[k(\eta_0-\eta)] \Big]\,, \end{aligned} \tag{6.3}$$

where the visibility function $g(\eta)$ in the limit of instantaneous recombination is approximated by $\delta(\eta - \eta_{\rm rec})$, while the optical depth of photon $e^{-\kappa(\eta)}$ gives $\Theta_{\rm Heaviside}(\eta - \eta_{\rm rec})$. Also the CMB anisotropies are sensitive to the tensor perturbations of the metric through an ISW analogous to the CGWB one, but since it is expected to be subdominant, in this Chapter we will neglect it. In the CMB case there is also a Doppler term, proportional to the velocity of baryons, which does not appear in the CGWB with adiabatic initial conditions, because gravitons do not interact, see, e.g., Eq. (4.11) The CGWB is then computed by using Eqs. (3.33), (3.34),

$$\begin{aligned} \delta_{{\rm GW},\ell m}(q) =& 4\pi(-i)^\ell [(4 - n_{\rm gwb}(q)] \\ & \int \frac{{\rm d}^3k}{(2\pi)^3} Y^*_{\ell m}(k) \Big[\zeta(\mathbf{k}) \Delta^S_\ell(k,\eta_0,\eta_{\rm in}) + j_\ell[k(\eta_0-\eta_{\rm in})] \Gamma(\eta_{\rm in},\mathbf{k},q) \Big]\,. \end{aligned} \tag{6.4}$$

The angular power spectrum of the cross-correlation is defined by

$$\delta_{\ell\ell'}\delta_{mm'} C_\ell^{\rm CMB\times CGWB}(q) \equiv \frac{1}{2} \left\langle a^*_{\ell m} \delta_{{\rm GW},\ell m}(q) + a_{\ell m} \delta^*_{{\rm GW},\ell m}(q) \right\rangle\,. \tag{6.5}$$

To facilitate the interpretation of the features of the angular power spectrum, it is useful to decompose the spectrum as the sum of different contributions,

$$C_\ell^{\rm CMB\times CGWB} = C_\ell^{\rm SW\times SWI} + C_\ell^{\rm SW+ISW} + C_\ell^{\rm ISW\times SWI} + C_\ell^{\rm ISW\times ISW} + C_\ell^{\rm DOP\times SWI} + C_\ell^{\rm DOP\times ISW}\,, \tag{6.6}$$

where we have used the short notation SWI ≡ SW + IC for the CGWB. In the case of adiabatic initial conditions, these contributions are given by

$$
\begin{aligned}
\frac{C_\ell^{\mathrm{SW}\times\mathrm{SWI}}}{4-n_{\mathrm{gwb}}} =& 4\pi \int \frac{dk}{k} P_\zeta(k) j_\ell[k(\eta_0-\eta_*)] j_\ell[k(\eta_0-\eta_{\mathrm{in}})] \\
&\times \Big[T_{\Theta_0}(\eta_*,k)+T_\Phi(\eta_*,k)\Big]\left[T_\Gamma^{\mathrm{AD}}(\eta_{\mathrm{in}},k,q)+T_\Phi(\eta_{\mathrm{in}},k)\right] , \\
\frac{C_\ell^{\mathrm{SW}\times\mathrm{ISW}}}{4-n_{\mathrm{gwb}}} =& 4\pi \int \frac{dk}{k} P_\zeta(k) j_\ell[k(\eta_0-\eta_*)]\Big[T_{\Theta_0}(\eta_*,k)+T_\Phi(\eta_*,k)\Big] \\
&\times \int_{\eta_{\mathrm{in}}}^{\eta_0} d\eta \Big[T_\Phi'(\eta,k)+T_\Psi'(\eta,k)\Big] j_\ell[k(\eta_0-\eta)] , \\
\frac{C_\ell^{\mathrm{ISW}\times\mathrm{SWI}}}{4-n_{\mathrm{gwb}}} =& 4\pi \int \frac{dk}{k} P_\zeta(k) j_\ell[k(\eta_0-\eta_{\mathrm{in}})]\left[T_\Gamma^{\mathrm{AD}}(\eta_{\mathrm{in}},k,q)+T_\Phi(\eta_{\mathrm{in}},k)\right] \\
&\times \int_{\eta_*}^{\eta_0} d\eta \Big[T_\Phi'(\eta,k)+T_\Psi'(\eta,k)\Big] j_\ell[k(\eta_0-\eta)] , \\
\frac{C_\ell^{\mathrm{ISW}\times\mathrm{ISW}}}{4-n_{\mathrm{gwb}}} =& 4\pi \int \frac{dk}{k} P_\zeta(k) \int_{\eta_*}^{\eta_0} d\eta \Big[T_\Phi'(\eta,k)+T_\Psi'(\eta,k)\Big] j_\ell[k(\eta_0-\eta)] \\
&\times \int_{\eta_{\mathrm{in}}}^{\eta_0} d\tilde{\eta} \Big[T_\Phi'(\tilde{\eta},k)+T_\Psi'(\tilde{\eta},k)\Big] j_\ell[k(\eta_0-\tilde{\eta})] , \\
\frac{C_\ell^{\mathrm{DOP}\times\mathrm{SWI}}}{4-n_{\mathrm{gwb}}} =& 4\pi \int \frac{dk}{k} P_\zeta(k)\, j_\ell'[k(\eta_0-\eta_*)]\; j_\ell[k(\eta_0-\eta_{\mathrm{in}})] \\
&\times k^{-1} T_{\theta_b}(\eta_*,k)\left[T_\Gamma^{\mathrm{AD}}(\eta_{\mathrm{in}},k,q)+T_\Phi(\eta_{\mathrm{in}},k)\right] , \\
\frac{C_\ell^{\mathrm{DOP}\times\mathrm{ISW}}}{4-n_{\mathrm{gwb}}} =& 4\pi \int \frac{dk}{k} P_\zeta(k)\, j_\ell'[k(\eta_0-\eta_*)]\; k^{-1} T_{\theta_b}(\eta_*,k) \\
&\times \int_{\eta_{\mathrm{in}}}^{\eta_0} d\eta \Big[T_\Phi'(\eta,k)+T_\Psi'(\eta,k)\Big] j_\ell[k(\eta_0-\eta)] .
\end{aligned}
\tag{6.7}
$$

In Figure 6.1, we plot the contributions to the angular power spectrum of the cross-correlation for $f_{\mathrm{dec}}(\eta_{\mathrm{in}}) = 0$ and for $n_{\mathrm{gwb}} = 0.35$. As discussed in the previous sections, it is possible to give an explanation of the features of the spectra in terms of the overlap of the spherical Bessel functions for the different contributions.

SW × SWI **contribution**

If we assume instantaneous recombination, these the SW of the CMB and the SW+IC of the CGWB are sourced at η_{rec} and η_{in} respectively. According to Eqs. (6.1), (6.2), when $\ell(\eta_{\mathrm{rec}}-\eta_{\mathrm{in}})/\eta_0 \ll 1$, the primordial perturbations of that give the dominant contribution to the multipole ℓ imprint the same pattern to the CMB and CGWB, since the inhomogeneities that generate the anisotropies for the two signals are strongly correlated. On the other hand, when $\ell(\eta_{\mathrm{rec}}-\eta_{\mathrm{in}})/\eta_0 \gg 1$, the spectrum decreases exponentially, according to Eq. (6.2), thus there is no correlation between these two contributions. It is easy to check that, for $\eta_{\mathrm{rec}} \approx 280\,\mathrm{Mpc}$, this suppression starts around $\ell \approx 40$.

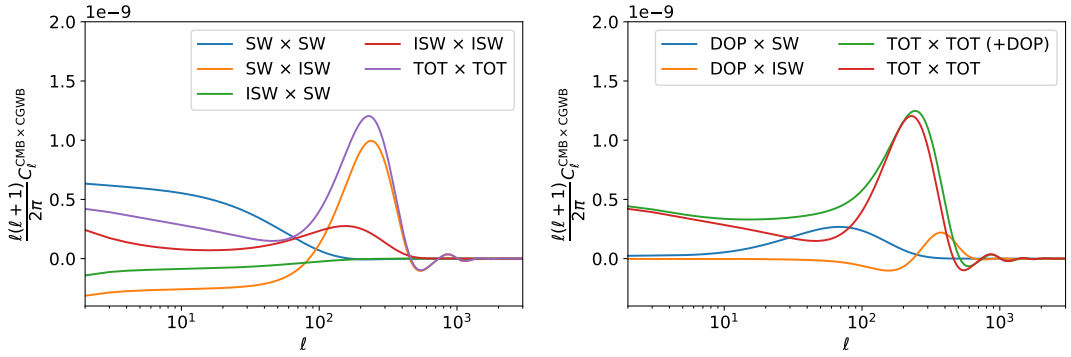

Figure 6.1: Plot of the contributions to the angular power specturm of the cross-correlation between the CMB and CGWB without the Doppler (left) and including the Doppler (right). For the CGWB we used $f_{\rm dec}(\eta_{\rm in}) = 0$ and $n_{\rm gwb} = 0.35$.

ISW × SWI **contribution**

The ISW of the CMB is made of a late-ISW term, which peaks in the dark energy dominated epoch, at times much larger than recombination, and of a early-ISW term, which is due to the variation of scalar perturbations that re-entered the horizon at $\eta_{\rm eq}$, of scales $k_{\rm eq} \approx 1/\eta_{\rm eq}$. The first contribution gives a tiny correlation, because of the large-separation between the times at which the late-ISW is operating and $\eta_{\rm in}$, while the latter is zero, because the early-ISW of the CMB peaks at $\eta_{\rm rec}$ and at angular scales $\ell \approx 200$, therefore, according to the suppression described by Eq. (6.2), is close to zero.

SW × ISW **contribution**

The ISW of the CGWB is made of a late-ISW term, identical to the CMB one, and by an early-ISW term that for scales $k \gtrsim k_{\rm eq}$ is peaked around $1/k$, while for scales $k \ll k_{\rm eq}$ is peaked around at the equality between matter and radiation. At large angular scales, the correlation of the late-ISW and the early-ISW of the CGWB gives a small correlation, comparable to the ISW × SWI contribution, while at large angular scales, where early-ISW of the CGWB is larger, the angular power spectrum is enhanced. According to Eq. (6.2), in order to have a correlation between the perturbations, at large angular scales the SW of the CMB and the ISW have to be sourced at the same time, therefore a peak is expected for the early-ISW generated by the perturbations that re-entered the horizon around recombination, $\ell \approx \eta_0/\eta_{\rm rec} \approx 200$.

ISW × ISW **contribution**

Since the ealy-ISW of CMB and CGWB are identical, at small angular scales we have an exact correlation between these two effect. At large angular scales, a smaller peak resembles the features discussed for the SW × ISW term.

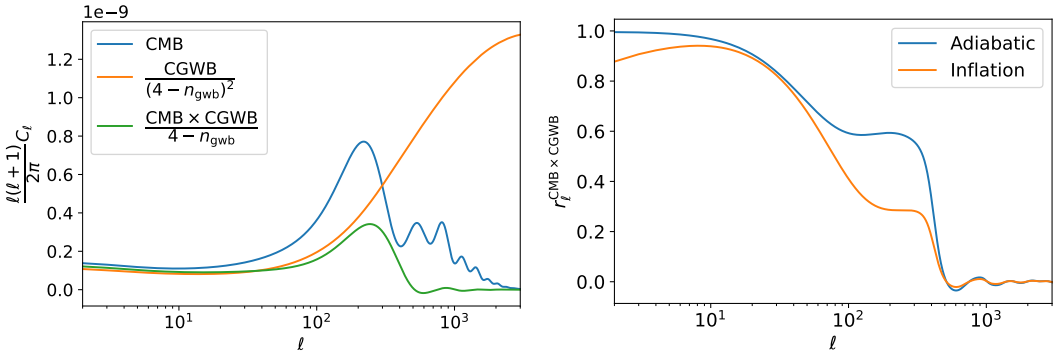

Figure 6.2: Left: plot of the angular power spectra of the auto-correlation of the CMB and CGWB and of the cross-correlation between the two for adiabatic initial conditions and $n_{\rm gwb} = 0.35$. Right: plot of the correlation between the CMB and CGWB for with $n_{\rm gwb} = 0.35$ for adiabatic initial conditions and NAD initial conditions from inflation.

DOP $\times$ SWI **contribution**

This discussion is very similar to the one done for the SW $\times$ SWI term, with the only expection that for super-horizon scales $T_{\theta_b}(\eta, k)$ vanishes, therefore the associate contribution to the Doppler term is null at small angular scales.

DOP $\times$ ISW **contribution**

In this case, analogous to the SW $\times$ ISW term, the spectrum presents two peaks due to pesks in the CMB spectrum with different phases. We should also notice that the peaks in the Doppler terms are slightly shifted compared to the ones associated to the SW of the CMB, because the time derivative of the Bessel function that appears in such contributions generated a tiny shift in the angular scales determined by Eq. (6.2).

6.3 Constrained realizations of the CGWB from the CMB map

At large angular scales, the angular power spectrum of the cross-correlation between the CMB and the CGWB is very large, therefore it is reasonable to expect that the maps of the anisotropies of photons and gravitons share similar features. It is possible to define the correlation between the CMB and the CGWB at the angular scale ℓ by

$$r_\ell^{\rm CMB\times CGWB}(q) \equiv \frac{C_\ell^{\rm CMB\times CGWB}(q)}{\sqrt{C_\ell^{\rm CMB\times CMB} C_\ell^{\rm CGWB\times CGWB}(q,q)}}\,. \tag{6.8}$$

In Figure 6.2, we plot the correlation between CMB and CGWB for a spectrum with $n_{\rm gwb} = 0.35$. We have considered a spectrum with adiabatic initial conditions and another one generated by the quantum fluctuations during inflation, when the non-adiabatic initial

conditions computed in Eq. (4.35) have to be taken into account. In the adiabatic case, the correlation is close to one at large angular scales, while for the inflationary spectrum the correlation is about 0.9, because of the NAD initial conditions. When the correlation is close to one, it means that fluctuations of a map univocally determine variations of the other one.To see more explicitly this, it is known that the CMB and the CGWB are Gaussian random variables with zero mean and covariance given by the angular power spectrum, therefore the distribution in the Universe follows a multivariate Gaussian of the form

$$\mathcal{L} = \prod_{\ell=0}^{\infty} \prod_{m=-\ell}^{\ell} \frac{\exp\left(-\frac{1}{2}\begin{pmatrix} a_{\ell m} & \delta_{\mathrm{GW},\ell m}\end{pmatrix}\begin{pmatrix} C_\ell^{\mathrm{CMB}\times\mathrm{CMB}} & C_\ell^{\mathrm{CMB}\times\mathrm{CGWB}} \\ C_\ell^{\mathrm{CMB}\times\mathrm{CGWB}} & C_\ell^{\mathrm{CGWB}\times\mathrm{CGWB}}\end{pmatrix}\begin{pmatrix} a_{\ell m} \\ \delta_{\mathrm{GW},\ell m}\end{pmatrix}\right)}{(2\pi)\left(C_\ell^{\mathrm{CMB}\times\mathrm{CMB}} C_\ell^{\mathrm{CGWB}\times\mathrm{CGWB}} - \left(C_\ell^{\mathrm{CMB}\times\mathrm{CGWB}}\right)^2\right)}\,, \tag{6.9}$$

where we have assumed that the frequency dependence of the anisotropies can be factorized out. The CMB map has been observed by the Planck collaboration, which means that it is possible to compute, starting from the likelihood $\mathcal{L}$, the PDF of conditioned map of the CGWB, given the observations of the CMB. It is known [**?**] that the conditioned distribution $\delta_{\mathrm{GW},\ell m}$, given $a_{\ell m}$ is a Gaussian distribution,

$$\mathcal{L}_{\mathrm{cond}} = \prod_{\ell=0}^{\infty} \prod_{m=-\ell}^{\ell} \frac{1}{\sqrt{2\pi} C_\ell^{\mathrm{constr}}} \exp\left[-\frac{1}{2}\left(\delta_{\mathrm{GW},\ell m} - \mu_{\mathrm{GW},\ell m}\right)\left(C_\ell^{\mathrm{constr}}\right)^{-1}\left(\delta_{\mathrm{GW},\ell m} - \mu_{\mathrm{GW},\ell m}\right)\right]\,, \tag{6.10}$$

where the mean and the covariance are given by

$$\begin{aligned} \mu_{\mathrm{GW},\ell m} \equiv & \frac{C_\ell^{\mathrm{CMB}\times\mathrm{CGWB}}}{C_\ell^{\mathrm{CMB}}} a_{\ell m}\,, \\ C_\ell^{\mathrm{constr}} = & C_\ell^{\mathrm{CGWB}\times\mathrm{CGWB}} - \frac{\left(C_\ell^{\mathrm{CMB}\times\mathrm{CGWB}}\right)^2}{C_\ell^{\mathrm{CMB}}} = C_\ell^{\mathrm{CGWB}\times\mathrm{CGWB}}\left[1 - \left(r_\ell^{\mathrm{CMB}\times\mathrm{CGWB}}\right)^2\right]\,. \end{aligned} \tag{6.11}$$

From the last row it is clear that the knowledge of the CMB map allows to predict deterministically the hot and the cold spot of the map of the CGWB when $r \to 1$, because the covariance of the condition Gaussian goes to zero, thanks to the large correlation of the two signals. As depicted in the right panel of Figure 6.2, the correlation at angular scales between the CMB and the CGWB is almost one, which is the map of the cosmological backgrounds exhibits the same seeds of the CMB one, just rescaled by the ratio of the angular power spectra that appears in the definition of $\mu_{\mathrm{GW},\ell m}$. At small scales, when $r_\ell^{\mathrm{CMB}\times\mathrm{CGWB}}$ deviates from one, the CGWB map presents fluctuations w.r.t. the CMB one, therefore the CGWB becomes another, independent, probe. In Figure 6.3, we show the example of a realization of the expected CGWB map, given the Planck SMICA map [273]. As already stressed, different realizations would change just the features of the map at small scales, that are affected by a source of uncertainty which goes like C_ℓ^{constr}. In

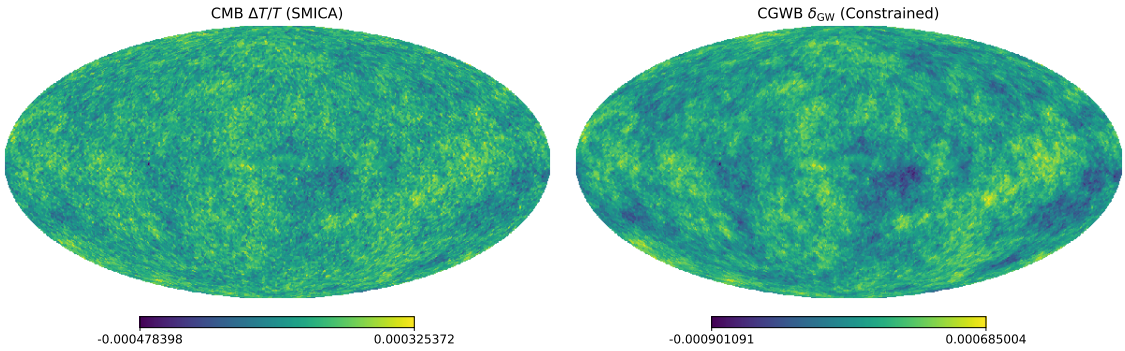

Figure 6.3: Left: plot of the CMB SMICA map for $\ell_{\rm max} = 200$. Right: plot of the constrained realization of the CGWB, for $n_{\rm gwb} = 0.35$, $f_{\rm dec}(\eta_{\rm in}) = 0$ and adiabatic initial conditions.

the next sections, we will show an application of these constrained realization that would be particularly useful to reconstruct the intrinsic dipole of the CMB, cleaning the signal from contaminations due to the kinetic dipole, by using a joint analysis of photons and gravitons.

6.4 Detectability of the anisotropies of the CGWB

6.4.1 The impact of Instrumental Noise

The main limitation in the detection of the anisotropies of CGWBs is due to the large instrumental noise at present and future interferometers. Intuitively, in order to measure fluctuations of the order of $10^{-3} - 10^{-5}$ in the energy density of stochastic Gws along different directions, one should be able to observe the monopole with SNR around $10^3 - 10^5$. The possibility of detecting a CGWB in the near future depends mainly on improvements in the sensitivity of the instruments and on the amplitude of the CGWB we are interested in. In Sections8.3 9.6 we will describe the state-of-the-art procedure to obtain the best unbiased estimator of the map of AGWB, while in this section we evaluate the detectability of the anisotropies in a different, but equivalent, way. Following [274], we assume that the observed coefficients of the spherical harmonics expansion at interferometers can be written as

$$\delta^{\rm obs}_{{\rm GW},\ell m} = \delta^{\rm obs}_{{\rm GW},\ell m} + n_{\ell m}\,, \tag{6.12}$$

where $n_{\ell m}$ are Gaussian random variables with zero mean and covariance described by the angular power spectrum of the noise

$$\langle n_{\ell m} n^*_{\ell' m'} \rangle \equiv \delta_{\ell\ell'}\delta_{mm'} N_\ell\,. \tag{6.13}$$

The N_ℓ has been computed by minimizing the covariance associated to the reconstruction of $\delta_{{\rm GW},\ell m}$, therefore it is sensitive to the scaling in frequency of the CGWB and on the

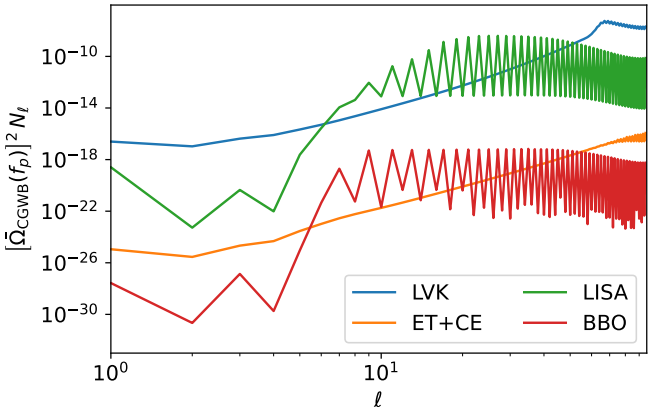

Figure 6.4: Plot of the angular power spectrum of the noise, normalized w.r.t. the amplitude of the CGWB, as a function of the multipole for different detectors.

amplitude of the monopole. The expression of the angular power spectrum of the noise is

$$N_\ell^{-1} = \frac{T_{\rm obs}}{2} \sum_{A,B,C,D} \int {\rm d}f \left[\frac{2}{5}\bar{\Omega}_{\rm CGWB}(f)\right]^2 N_{AB}^{-1}(f) N_{CD}^{-1}(f) \sum_m \frac{{\rm Re}\left[\mathcal{A}_{BC,\ell m}(f)\mathcal{A}^*_{DA,\ell m}(f)\right]}{2\ell+1}\,, \tag{6.14}$$

where the $\mathcal{A}_{AB,\ell m}$ is the coefficient of the spherical harmonics expansion of the antenna pattern, defined by

$$\mathcal{A}_{AB} \equiv \frac{5}{2}\tilde{B}^I_{AB} e^{-2\pi i f\,\hat{n}\cdot(\mathbf{x}_B - \mathbf{x}_A)}\,, \tag{6.15}$$

where the tensors $\tilde{B}$ have been defined in Eq. (8.20). The angular power spectrum of the noise decreases with the observing time and the amplitude of the monopole and it is sensitive to the different scaling in frequency of the CGWB. As already discussed in Section 1.3, the different frequency dependence of the cosmological signal and noise helps in disentangling the two contributions by using a Wiener filter. For simplicity, we consider a CGWB of the form

$$\bar{\Omega}_{\rm CGWB}(f) = \bar{\Omega}(f_p)\left(\frac{f}{f_p}\right)^{n_{\rm gwb}}\,, \tag{6.16}$$

with $n_{\rm gwb} = 0.35$ and in Figure 6.4 we plot $N_\ell/\bar{\Omega}_{\rm CGWB}(f_p)$ for different detectors. From this picture it is clear to see that detectors like BBO/DECIGO are much more sensitive than LISA or ET/CE to the anisotropies of CGWB and represent the most promising experiments to detect the angular power spectrum of the CGWB.

6.4.2 SNR of the anisotropies of the CGWB

The coefficients of the expansion in spherical harmonics of the maps of the CMB and of the CGWB are Gaussian random variables of zero mean and covariance given by the angular power spectra, therefore the likelihood takes the simple form given in Eq. (6.9). This result

can be generalized in the case in which the noises of the experiments are considered by replacing the

$$C_\ell^{\mathrm{CGWB}\times\mathrm{CGWB}} \to C_\ell^{\mathrm{CGWB}\times\mathrm{CGWB}} + N_\ell \,. \tag{6.17}$$

By using this substitution we have assumed that the noise of CMB and CGWB experiments are uncorrelated and that the noise associated to CMB measurements is negligible. This is a good approximation in the Planck case up to $\ell \approx 2500$. As shown in Eq (H.4), in order to estimate the angular power spectra we combine the observed maps in the following estimators,

$$\begin{aligned}
\hat{C}_\ell^{\mathrm{CMB}\times\mathrm{CMB}} \equiv& \frac{1}{2\ell+1}\sum_{m=-\ell}^{\ell} a_{\ell m} a_{\ell m}^* \,, \\
\hat{C}_\ell^{\mathrm{CGWB}\times\mathrm{CGWB}} \equiv& \frac{1}{2\ell+1}\sum_{m=-\ell}^{\ell} \delta_{\mathrm{GW},\ell m}\delta_{\mathrm{GW},\ell m}^* - N_\ell \,, \\
\hat{C}_\ell^{\mathrm{CMB}\times\mathrm{CGWB}} \equiv& \frac{1}{2\ell+1}\sum_{m=-\ell}^{\ell} \frac{a_{\ell m}\delta_{\mathrm{GW},\ell m}^* + \delta_{\mathrm{GW},\ell m} a_{\ell m}^*}{2} \,.
\end{aligned} \tag{6.18}$$

As explicitly proved in Appendix H, if we define the covariance between two estimators as

$$\mathcal{C}_\ell^{XY-WZ} \equiv \mathrm{cov}\left[C_\ell^{XY}, C_\ell^{WZ}\right] \,, \tag{6.19}$$

it is easy to find that

$$\begin{aligned}
\mathcal{C}_\ell^{\mathrm{CMB\,CMB}-\mathrm{CMB\,CMB}} =& \frac{2}{2\ell+1}\left(C_\ell^{\mathrm{CMB}\times\mathrm{CMB}}\right)^2 \,, \\
\mathcal{C}_\ell^{\mathrm{CGWB\,CGWB}-\mathrm{CGWB\,CGWB}} =& \frac{2}{2\ell+1}\left(C_\ell^{\mathrm{CGWB}\times\mathrm{CGWB}} + N_\ell\right)^2 \,, \\
\mathcal{C}_\ell^{\mathrm{CMB\,CGWB}-\mathrm{CMB\,CGWB}} =& \frac{1}{2\ell+1}\left[\left(C_\ell^{\mathrm{CMB}\times\mathrm{CGWB}}\right)^2 + C_\ell^{\mathrm{CMB}\times\mathrm{CMB}}\left(C_\ell^{\mathrm{CGWB}\times\mathrm{CGWB}} + N_\ell\right)\right] \,, \\
\mathcal{C}_\ell^{\mathrm{CMB\,CMB}-\mathrm{CGWB\,CGWB}} =& \frac{2}{2\ell+1}\left(C_\ell^{\mathrm{CMB}\times\mathrm{CGWB}}\right)^2 \,, \\
\mathcal{C}_\ell^{\mathrm{CMB\,CMB}-\mathrm{CMB\,CGWB}} =& \frac{2}{2\ell+1} C_\ell^{\mathrm{CMB}\times\mathrm{CMB}} C_\ell^{\mathrm{CMB}\times\mathrm{CGWB}} \,, \\
\mathcal{C}_\ell^{\mathrm{CGWB\,CGWB}-\mathrm{CMB\,CGWB}} =& \frac{2}{2\ell+1}\left(C_\ell^{\mathrm{CGWB}\times\mathrm{CGWB}} + N_\ell\right) C_\ell^{\mathrm{CMB}\times\mathrm{CGWB}} \,.
\end{aligned} \tag{6.20}$$

In order to provide an estimate for the detectability of the CGWB, we compute the SNR. If we define the total covariance matrix of the C_ℓs as

$$\Sigma_{C_\ell} \equiv \begin{pmatrix}
\mathcal{C}_\ell^{\mathrm{CMB\,CMB}-\mathrm{CMB\,CMB}} & \mathcal{C}_\ell^{\mathrm{CMB\,CMB}-\mathrm{CGWB\,CGWB}} & \mathcal{C}_\ell^{\mathrm{CMB\,CMB}-\mathrm{CMB\,CGWB}} \\
\mathcal{C}_\ell^{\mathrm{CMB\,CMB}-\mathrm{CGWB\,CGWB}} & \mathcal{C}_\ell^{\mathrm{CGWB\,CGWB}-\mathrm{CGWB\,CGWB}} & \mathcal{C}_\ell^{\mathrm{CGWB\,CGWB}-\mathrm{CMB\,CGWB}} \\
\mathcal{C}_\ell^{\mathrm{CMB\,CMB}-\mathrm{CMB\,CGWB}} & \mathcal{C}_\ell^{\mathrm{CGWB\,CGWB}-\mathrm{CMB\,CGWB}} & \mathcal{C}_\ell^{\mathrm{CMB\,CGWB}-\mathrm{CMB\,CGWB}}
\end{pmatrix} \,, \tag{6.21}$$

the square of the SNR is computed according to

$$\mathrm{SNR}^2 = \sum_{\ell=2}^{\ell_{\rm max}} \begin{pmatrix} C_\ell^{\rm CMB\times CMB} \\ C_\ell^{\rm CGWB\times CGWB} \\ C_\ell^{\rm CMB\times CGWB} \end{pmatrix}^T \Sigma_{C_\ell}^{-1} \begin{pmatrix} C_\ell^{\rm CMB\times CMB} \\ C_\ell^{\rm CGWB\times CGWB} \\ C_\ell^{\rm CMB\times CGWB} \end{pmatrix} . \tag{6.22}$$

Note however that the CMB experiments are mainly cosmic variance limited, therefore we should focus our analysis on the marginalized likelihood, withouth considering the contributions of the CMB auto-spectrum on the SNR. We define then

$$\tilde{\Sigma}_{C_\ell} \equiv \begin{pmatrix} \mathcal{C}_\ell^{\rm CGWB\,CGWB-CGWB\,CGWB} & \mathcal{C}_\ell^{\rm CGWB\,CGWB-CMB\,CGWB} \\ \mathcal{C}_\ell^{\rm CGWB\,CGWB-CMB\,CGWB} & \mathcal{C}_\ell^{\rm CMB\,CGWB-CMB\,CGWB} \end{pmatrix} \tag{6.23}$$

and we compute the SNR by using

$$\mathrm{SNR}^2_{\rm auto+cross} = \sum_{\ell=2}^{\ell_{\rm max}} \begin{pmatrix} C_\ell^{\rm CGWB\times CGWB} \\ C_\ell^{\rm CMB\times CGWB} \end{pmatrix}^T \tilde{\Sigma}_{C_\ell}^{-1} \begin{pmatrix} C_\ell^{\rm CGWB\times CGWB} \\ C_\ell^{\rm CMB\times CGWB} \end{pmatrix} . \tag{6.24}$$

We quantify the amount of information which comes from the auto- and cross-channels only by defining

$$\begin{aligned} \mathrm{SNR}^2_{\rm auto} &\equiv \sum_{\ell=2}^{\ell_{\rm max}} \frac{\left(C_\ell^{\rm CGWB\times CGWB}\right)^2}{\mathcal{C}_\ell^{\rm CGWB\,CGWB-CGWB\,CGWB}} , \\ \mathrm{SNR}^2_{\rm cross} &\equiv \sum_{\ell=2}^{\ell_{\rm max}} \frac{\left(C_\ell^{\rm CMB\times CGWB}\right)^2}{\mathcal{C}_\ell^{\rm CMB\,CGWB-CMB\,CGWB}} , \end{aligned} \tag{6.25}$$

In the definition of the SNR we stop to $\ell_{\rm max} = 100$, since it is the most reasonable target of future interferometers. In Figure 6.5, we plot the SNR of a signal parametrized by Eq. (6.16). In the left panel of Figure 6.5, we have plotted the SNR as a function of $\bar{\Omega}_{\rm CGWB}(f_p)$ for different interferometers, for one year of observations. Note that the pivot frequencies we have used have been chosen considering the sensitivities of the instruments and they are

$$f_p^{\rm LIGO} = 63\,{\rm Hz}\,, \qquad f_p^{\rm ET+CE} = 1\,{\rm Hz}\,, \qquad f_p^{\rm LISA} = 10^{-2}\,{\rm Hz}\,, \qquad f_p^{\rm BBO/DECIGO} = 0.5\,{\rm Hz}\,. \tag{6.26}$$

From this picture it is clear that BBO and DECIGO are the most promising candidates to detect the anisotropies of the CGWB, because of their larger sensitivity. In the right plot of Figure 6.5, we have shown the contributions to the SNR given by the auto- and cross-correlation for BBO/DECIGO in five years of observations.

6.4.3 Estimate of the number of relativistic and decoupled species with future detectors

The likelihood of the maps of the CMB and CGWB is a multivariate Gaussian, therefore the distribution of the estimators of the angular power spectra, the "pseudo-C_ℓs" defined in

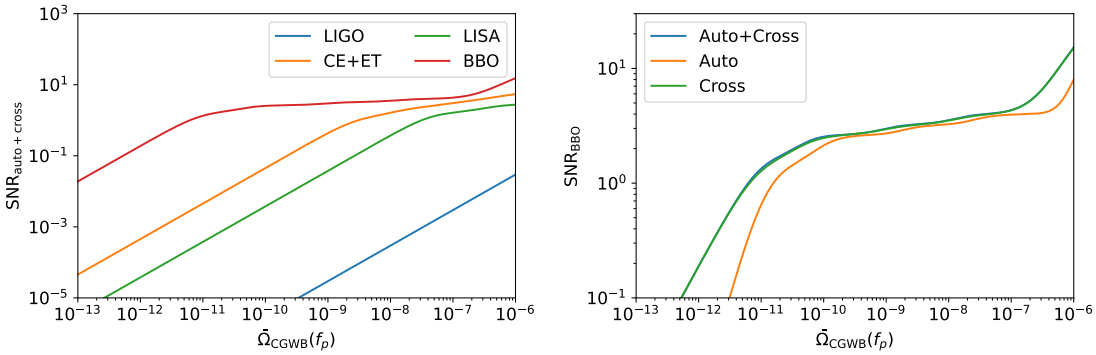

Figure 6.5: Left: plot of the SNR of auto- plus cross-correlation for different interferometers, as a function of the amplitude of the background at the pivot frequency f_p. The pivot frequency depends on the detector considered. Right: plot of the contributions to the SNR given by the auto- and cross-correlation for BBO.

Eq. (6.18) is a Wishart [275]. In Appendix H, a derivation of the likelihood of the angular power spectra has been done and the result is

$$-2\ln\mathcal{L}\left(\hat{C}_\ell^{XX},\hat{C}_\ell^{XY},\hat{C}_\ell^{YY}\middle|C_\ell^{XX},C_\ell^{XY},C_\ell^{YY}\right)=\sum_\ell(2\ell+1)\left[\frac{|D_\ell|}{|C_\ell|}+\ln\frac{|C_\ell|}{|\hat{C}_\ell|}-2\right]\,, \tag{6.27}$$

where we have defined the following determinants,

$$\begin{aligned}
|D_\ell| &\equiv \left(C_\ell^{XX}+N_\ell^{XX}\right)\left(\hat{C}_\ell^{YY}+N_\ell^{YY}\right)+\left(\hat{C}_\ell^{XX}+N_\ell^{XX}\right)\left(C_\ell^{YY}+N_\ell^{YY}\right)\\
&\quad -2\left(C_\ell^{XY}+N_\ell^{XY}\right)\left(\hat{C}_\ell^{XY}+N_\ell^{XY}\right)\,,\\
|C_\ell| &\equiv \left(C_\ell^{XX}+N_\ell^{XX}\right)\left(C_\ell^{YY}+N_\ell^{YY}\right)-\left(C_\ell^{XY}+N_\ell^{XY}\right)^2\,,\\
|\hat{C}_\ell| &\equiv \left(\hat{C}_\ell^{XX}+N_\ell^{XX}\right)\left(\hat{C}_\ell^{YY}+N_\ell^{YY}\right)-\left(\hat{C}_\ell^{XY}+N_\ell^{XY}\right)^2\,.
\end{aligned} \tag{6.28}$$

In this section, we forecast the sensitivity of future GW detectors to the cosmological parameters constrained by Planck and to the additional parameters introduced in this Thesis, such as $f_{\rm dec}(\eta_{\rm in})$ and $f_{\rm NL}$. Among the possible detectors introduced in Section 1.3.3, we focus on the network of ET+CE, even though space-based interferometers like BBO and DECIGO are expected to have a better angular resolution, see e.g. Figure 6.4. Following [276], we generate a mock likelihood of the form of Eq. (6.27), fitting mock data with a Markov-Chain-Monte-Carlo (MCMC) method. The MCMC analysis has been done by using the parameter inference package `MontePython` [277, 278]. Note that in this analysis we are assuming that the anisotropies of the CGWB scale in frequency as the monopole and we are approximating the noise of the detector by adopting the angular power spectrum N_ℓ. These assumptions could be useful to forecast the order of magnitude of the detectability of the anisotropies, although a more dedicated analysis should be done in the future.

We perform the analysis for the three CGWB discussed in Section 3.4, for the parameters discussed in Section 5.5. In order to compare the forecasts with detectors with

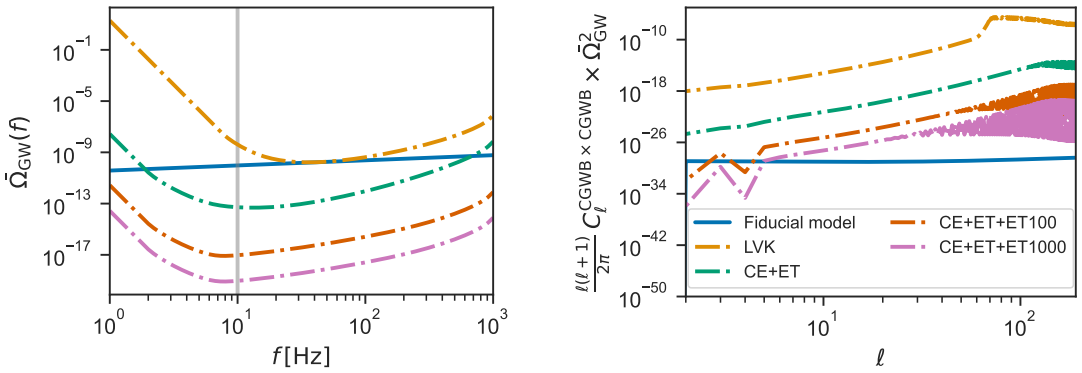

Figure 6.6: Left: plot of the fiducial monopole of the CGWB compared with the PLS of LVK, CE+ET, CE+ET+ET100, CE+ET+ET1000. Right: plot of the angular power spectrum of the CGWB and of the angular power spectrum of the noise of LVK, CE+ET, CE+ET+ET100, CE+ET+ET1000 for the fiducial monopole considered.

improved sensitivities, we introduce CE+ET+ET100 and CE+ET+ET1000 as two networks with the sensitivities of ET increased by a factor 100 and 1000 respectively. The posteriors of the cosmological parameters will be computed also for the cosmic variance (CV) limit, in which the instrumental noise of the detector is negligible.

Inflation with a blue tilt

We consider an inflationary CGWB with $r = 0.025$ and $n_{\rm gwb} = 0.4$, consistent with the Planck+Bicep+Keck bounds [128]. We assume then that the tensor spectrum follows a power-law scaling in frequency of a single $n_{\rm gwb}$, with no running. Under this assumption, the CGWB could have large amplitude at interferometric scales, thus allowing to detect the anisotropies with large SNR. However, any other background parametrized by a power law in the CE+ET frequency band would lead to similar results, therefore our assumption is not unrealistic. In order to be consistent with [1], in our forecasts we use adiabatic initial conditions for this CGWB, neglecting the NAD term computed in Eq. (4.35). In the left panel of Figure 6.6, we plot the monopole of the CGWB as a function of the frequency and the PLS for LVK, CE+ET, CE+ET+ET100, CE+ET+ET1000. In the right plot we show the angular power spectrum of the CGWB and the angular power spectrum of the noise for the three networks. From the picture it is clear that the anisotropies could be detected when the monopole is roughly $10^3 - 10^6$ times larger than the minimum of the PLS.

The parameters considered in our analysis, with uniform priors, are

$$\{h, \omega_m, \ln 10^{10} A_s, n_s, \tau_{\rm reio}, f_{\rm dec}(\eta_{\rm in})\}\,. \tag{6.29}$$

In this analysis we have neglected the impact of tensor fluctuations in the temperature of the CMB and on the overdensity of the CGWB, since we have found in Figure 5.4 that this contribution is negligible. In Table 6.1 we have written the fiducial values and

the priors on the parameter, discussing the error obtained by CMB and CGWB measurements. In Figure 6.7, we plot the posteriors for the parameters considered. As expected, realistic GW experiments like CE+ET or CE+ET+ET1000 will not be able to constrain the cosmological parameters better than Planck, because of the low SNR of the detection of the CGWB anisotropies. On the other hand, additional parameters like $f_{\rm dec}(\eta_{\rm in})$ could be measured just by observations of the anisotropies of the CGWB, therefore in the case CE+ET+ET1000 it is possible to significantly measure them. In the CV limit of measurements of the CGWB, up to $\ell_{\rm max} = 2500$, GW observations could help breaking the degeneracy in the CMB spectrum, such as the one between $\tau_{\rm reio}$ and A_s. This could be particularly useful to bring decisive information about the neutrino mass by removing these degeneracies [279, 280]. Figure 6.7 shows also that the amount of information on $\{h, \omega_m\}$ and ω_b are almost the same, while n_s could be constrained better since the CGWB spectrum is not affected by the Silk damping.

PBH in presence of primordial non-Gaussianity

We consider a CGWB parametrized by Eq. (3.51), with $A_* = 2 \times 10^{-5}$, $f_* = 100\,\text{Hz}$ and $f_{\rm NL} = 1$. In the left panel of Figure 6.8 we plot the monopole and the PLS of the detectors, while in the right plot one we show the angular power spectrum computed with `GW_CLASS` and the angular power spectrum of the noise. In this case, the SNR at the interferometers is much smaller than the ones produced during inflation considered in Fig. 6.6, thus no constraints can be put on $f_{\rm dec}(\eta_{\rm in})$. On the other hand, $f_{\rm NL}$ plays an important role in the amount of anisotropies, because the NAD initial condition, quantified by Eq. (4.43), could be very large. For a fiducial value $f_{\rm NL} = 1$, with CE+ET+ET1000 it is possible to constrain $|f_{\rm NL}| = 1$ efficiently, as shown in Figure 6.9. The sign of $f_{\rm NL}$ cannot be understood properly because the dominant contribution comes from the auto-correlation of the NAD term, which depends on $f_{\rm NL}^2$, while the terms which depend on the cross-correlation between the adiabatic modes and the NAD initial conditions (in the CGWB spectrum and in the cross-correlation between CMB and CGWB) are subdominant. An alternative way to constrain primordial non-Gaussianity is to look at the anisotropies of astrophysical backgrounds, as shown in [281].

PT with uncorrelated power-law NAD initial conditions

We consider as last example a CGWB produced by a PT with a spectrum parametrized by Eq. (3.55) with $n_1 = 3$, $n_2 = -4$, $\Delta = 2$ and $\Omega_* = 10^{-8}$. In Figure 6.10, we show that this monopole is consistent with the current LVK bounds and that it is potentially detectable by CE+ET. Also in this case, the anisotropies could e detected by the network CE+ET+ET1000. In this case, we consider, on top of adiabatic perturbations, an uncorrelated, non-adiabatic initial condition. Following Eq. (3.37), we parametrize this term by

$$P_\Gamma(k) = A_{\rm gwi}\,, \qquad P_{\times,\zeta}(k) = 0\,, P_{\times,T}(k) = 0\,, \tag{6.30}$$

with $A_{\rm gwi} = 10^{-10}$ or $A_{\rm gwi} = 10^{-7}$. We consider to cases to understand the differences when the NAD contribution dominates the angular power spectrum. The results are presented

Parameter	Fiducial	[Prior]	Planck + CE+ET+ET1000	Planck + CV($\ell_{\rm max} = 2500$)	Planck alone
h	0.6736	[0.5 - 0.8]	0.6741 ± 0.0096	0.6756 ± 0.0068	0.674 ± 0.010
ω_m	0.143	[0.1 - 0.2]	0.1429 ± 0.0020	0.1426 ± 0.0014	0.1429 ± 0.0021
$\ln 10^{10} A_s$	3.044	[1.7 - 5]	3.044 ± 0.015	3.0413 ± 0.0053	3.044 ± 0.016
n_s	0.965	[0.9 - 1]	0.9654 ± 0.0051	0.9662 ± 0.0028	$0.9653^{+0.0051}_{-0.0057}$
ω_b	0.02237	[0.02 - 0.025]	0.02238 ± 0.00020	0.02240 ± 0.00016	0.02238 ± 0.00022
$\tau_{\rm reio}$	0.0544	[0.02 - 0.08]	0.0547 ± 0.0071	0.0536 ± 0.0012	0.0545 ± 0.0073
$f_{\rm dec}(\eta_{\rm in})$	0	[0 - 1]	< 0.597	< 0.159	-

Table 6.1: Forecasted errors on parameters extracted from temperature anisotropy data from Planck, alone or in combination with mock GW anisotropy data.

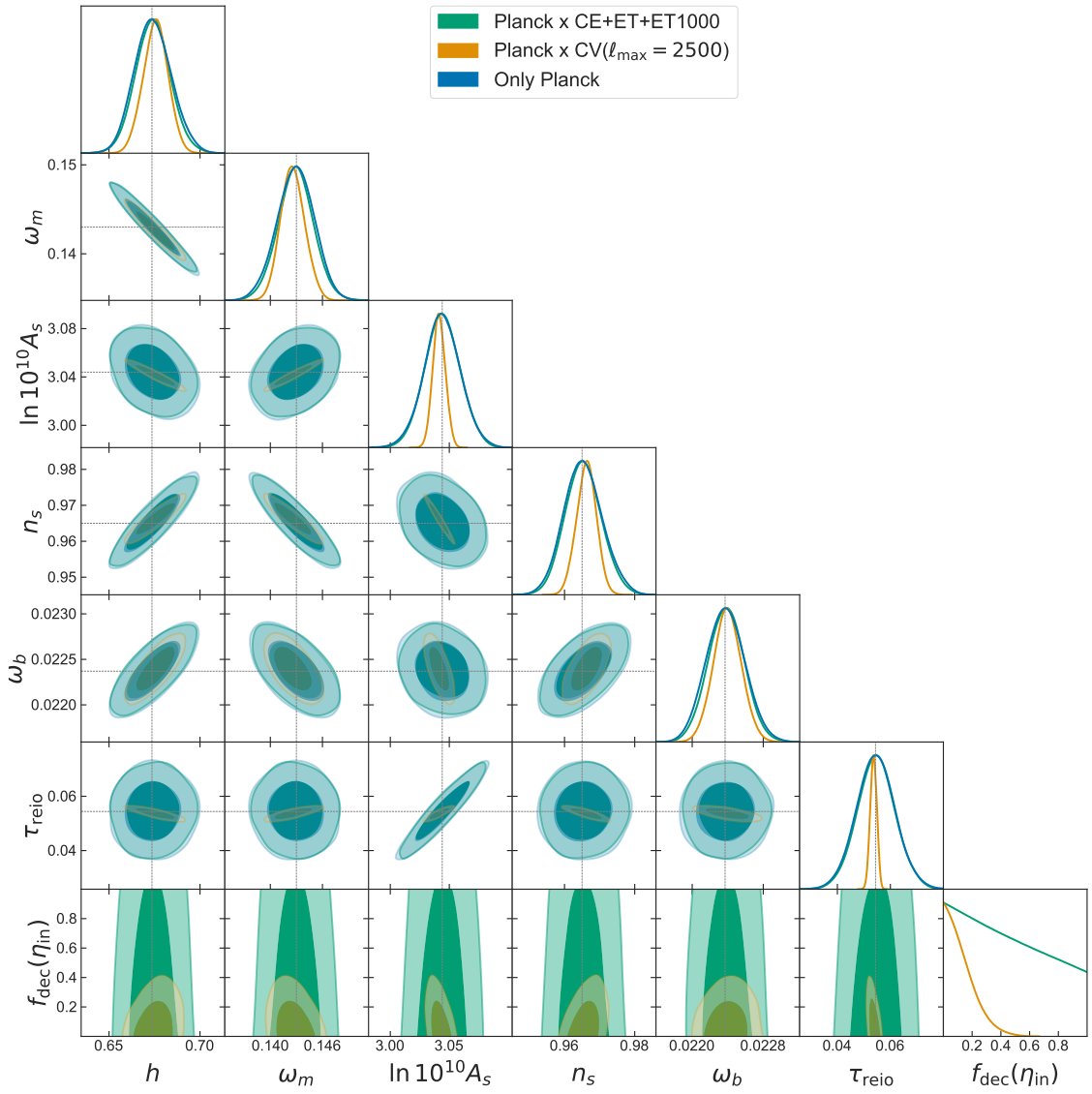

Figure 6.7: For the same forecast as in Table 6.1, one-dimensional posteriors and two-dimensional 68% / 95% confidence limits on the reconstructed cosmological parameters.

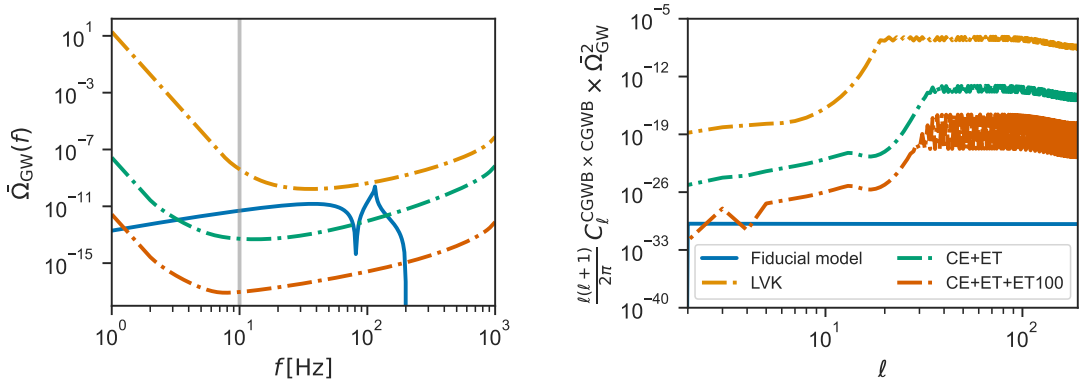

Figure 6.8: Left: plot of the fiducial monopole of the CGWB compared with the PLS of LVK, CE+ET, CE+ET+ET100, CE+ET+ET1000. Right: plot of the angular power spectrum of the CGWB and of the angular power spectrum of the noise of LVK, CE+ET, CE+ET+ET100, CE+ET+ET1000 for the fiducial monopole considered.

Parameter	Fiducial	[Prior]	CE+ET+ET100
$f_{\rm NL}$	1	[-11.1 - 9.3]	$1.17^{+0.23}_{-0.41}$, $-1.74^{+0.42}_{-0.23}$
$f_{\rm dec}(\eta_{\rm in})$	0	[0 - 1]	$- - -$

Table 6.2: Forecasted errors on the cosmological parameters affecting only the CGWB anisotropies, assumed to be measured by the GW detector combination CE+ET+ET100. We assume a CGWB produced by PBHs like in Figure 6.8.

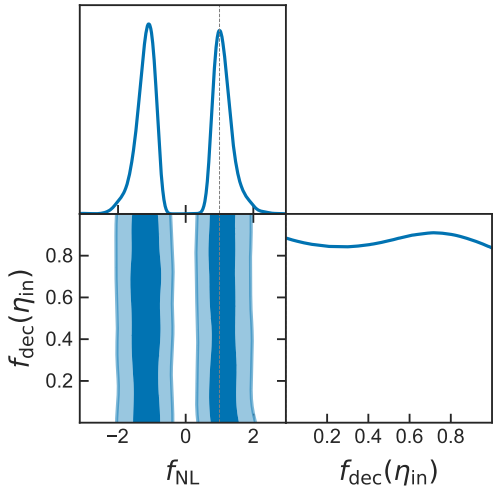

Figure 6.9: For the same forecast as in Table 6.2, one-dimensional posteriors and two-dimensional 68% / 95% confidence limits on the reconstructed cosmological parameters.

in Table 6.3 and Figure 6.11. The results make clear that for this kind of mechanisms, the anisotropies could be significantly detected just in case of a large NAD initial condition.

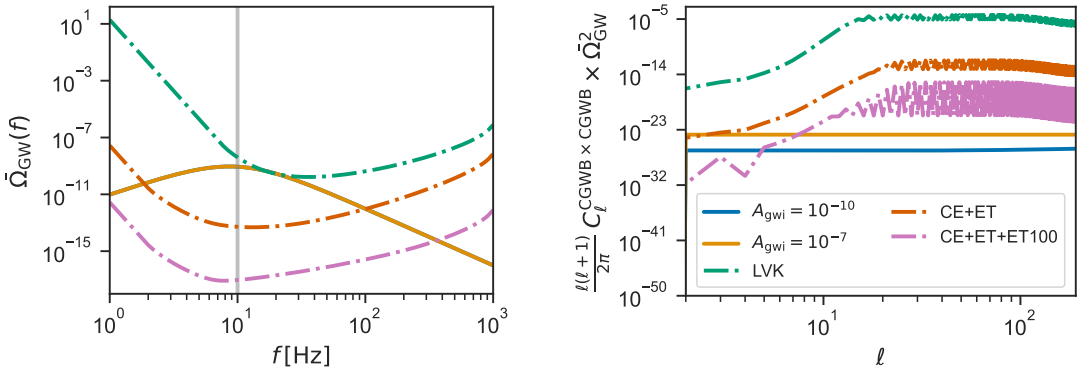

Figure 6.10: Left: plot of the fiducial monopole of the CGWB compared with the PLS of LVK, CE+ET, CE+ET+ET100, CE+ET+ET1000. Right: plot of the angular power spectrum of the CGWB and of the angular power spectrum of the noise of LVK, CE+ET, CE+ET+ET100, CE+ET+ET1000 for the fiducial monopole considered.

Parameter	Fiducial	[Prior]	CE+ET+ET100
$\ln 10^{10} A_{\rm gwi}$	0	[-10 - 10]	< 0.927
$n_{\rm gwi}$	0	[-2 - 2]	> 0.0344
$f_{\rm dec}(\eta_{\rm in})$	0	[0 - 1]	$- - -$
$\ln 10^{10} A_{\rm gwi}$	6.9	[-10 - 30]	6.6 ± 3.1
$n_{\rm gwi}$	0	[-2 - 2]	-0.06 ± 0.65
$f_{\rm dec}(\eta_{\rm in})$	0	[0 - 1]	$- - -$

Table 6.3: Forecasted errors on the cosmological parameters affecting only the CGWB anisotropy spectrum for the detector combination CE+ET+ET100.

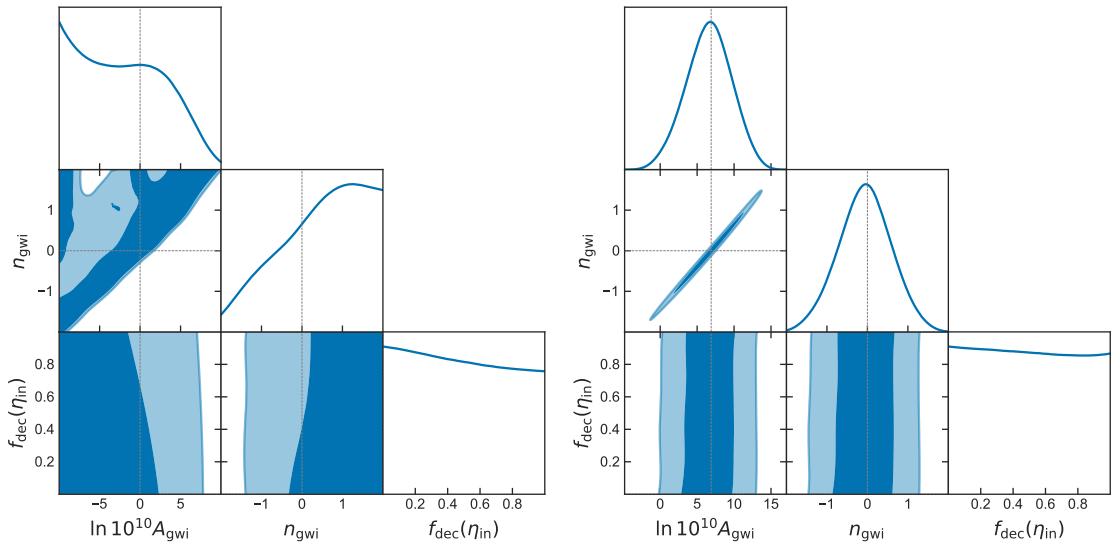

Figure 6.11: For the same forecasts as in Table 6.3 one-dimensional posteriors and two-dimensional 68% / 95% confidence limits on the reconstructed cosmological parameters.

Chapter 7

The Astrophysical Gravitational Wave Background

7.1 AGWB from unresolved sources

7.1.1 Threshold for the detection of a GW source

In Section 1.4.2, we have defined the astrophysical background as the superposition of many astrophysical sources that cannot be individually detected. Among many GW emitters, we consider here mainly the case of BBH of stellar masses, which are expected to give the dominant contribution to the AGWB at future ground-based interferometers like ET and CE [48, 8]. In some specific cases, we will show also some results for BNS and BHNS. In [197], it has been shown that the number of BBH is not large enough to produce an overlap in the individual waves to make them indistinguishable. Therefore, in our work we consider a BBH to be unresolved only when it produces a signal so small that its SNR at the detector is lower than a threshold $\mathrm{SNR}^{\mathrm{res}}_{\mathrm{thr}}$. If we define a source in terms of its intrinsic properties, $\boldsymbol{\theta}$, of the redshift at which emits GWs, z, and of its location in the celestial sphere, $\hat{n}$, it is possible to define the window function for a detection of the event and the efficiency of a network of interferometers by

$$w(\boldsymbol{\theta}, z) \equiv 1 - \epsilon(\boldsymbol{\theta}, z) \equiv \Theta_H \left(\mathrm{SNR}^{\mathrm{res}}_{\mathrm{thr}} - \mathrm{SNR}(\boldsymbol{\theta}, z)\right) . \tag{7.1}$$

In analogy with the procedure discussed in Section 1.3.2, it is possible to show that the SNR for the detection of a resolved source, obtained after matched filtering [99], is equal to

$$\langle \mathrm{SNR}\,(\hat{n}, \boldsymbol{\theta}, z\,)\rangle = \sqrt{4 \int_0^{+\infty} \mathrm{d}f \sum_A \frac{\left|h^2_A(\hat{n}, \boldsymbol{\theta}, z, f)\right|^2}{N_{AA}(f)}}\,, \tag{7.2}$$

where we have defined

$$h_A(\hat{n}, \boldsymbol{\theta}, z, f) \equiv \sum_\alpha F^\alpha_A(\hat{n}, f) h_\alpha(\hat{n}, f)\,, \tag{7.3}$$

with h_α the amplitude of the GW and F_A^α the detector pattern function for the polarization α defined in Eq. (1.54), while N_{AA} is the auto-spectrum of the noise of the interferometer A. The choice of the threshold strongly depends on the analysis that one is interested in. For instance, if one wants to look for a cosmological background and would like to remove the astrophysical sources, a large threshold is necessary, in order to not have a spurious contribution to the background due to the imperfect subtraction of the sources [282, 283, 284]. On the other hand, if the population of the binaries needs to be inferred, a slightly smaller threshold could be used. When a precise localisation of the source is necessary to combine GW and EM measurements, the threhsold could be even larger than 300 [285]. In this work, in order to avoid contaminations to the SGWB due to the subtraction of the BBH, we use the conservative value $\mathrm{SNR}_{\mathrm{thr}}^{\mathrm{res}} = 80$ in the network ET+CE, which corresponds to $\mathrm{SNR}_{\mathrm{thr}}^{\mathrm{res}} = 20$ in all the single interferometers. This choice is consistent with [286].

7.1.2 Superposition of unresolved sources

According to [47, 48], the energy density of the AGWB is computed by using

$$\Omega^{\alpha}_{\mathrm{AGWB}}(\hat{n}, f) = \frac{f}{\rho_{\mathrm{crit}} c^2} \sum_{t_d\,,\boldsymbol{\theta}\,,z} \frac{N^{\mathrm{unres}}_{\mathrm{GW}}(\hat{n}, t_d, \boldsymbol{\theta}, z) \frac{dE^{\alpha}}{df_e d\Omega_e}(\boldsymbol{\theta}, z, f)}{(1+z) H(z) T_{\mathrm{obs}} \frac{dV}{dz d\Omega_e}(z)}\,, \tag{7.4}$$

with $N^{\mathrm{unres}}_{\mathrm{GW}}$ the number of unresolved sources that emits GWs at redshift z, with intrinsic parameters $\boldsymbol{\theta}$ and that emit GWs after a time t_d from the production of the binary system. $\mathrm{d}E^{\alpha}/\mathrm{d}f_e \mathrm{d}\Omega_e$ is the energy spectrum of the individual binary, while T_{obs} is the observing time and $\mathrm{d}V/\mathrm{d}z\mathrm{d}\Omega_e$ is the volume element at the source. In this case α identifies the Stokes parameters introduced in Eqs. (1.43), (1.44). If the population of the sources is known, it is possible to estimate the spectrum of the AGWB by using the "direct integration" method given by Eq. (7.4). This expression is valid when the number of sources is large enough to represent faithfully the population of the GW emitters, characterized by $N^{\mathrm{unres}}_{\mathrm{GW}}$. In the case in which the number of sources is small or the energy spectrum of the binaries is rapidly oscillating, the low number of events would not reflect the entire population, therefore the poor sampling would generate an astrophysical background different to the one computed in Eq. (7.4). The astrophysical background generated by the population[1] in this case is computed by summing the many individual signals produced in a realization of $N^{\mathrm{unred}}_{\mathrm{GW}}$ in a time T_{obs},

$$\Omega_{\mathrm{AGWB}}(\hat{n}, f) = \frac{1}{T_{\mathrm{obs}}} \frac{f^3}{8 G \rho_c} \sum_{i=1}^{N^{T_{\mathrm{obs}}}_{\mathrm{GW}}} \left[|h_{+,i}(f)|^2 + |h_{\times,i}(f)|^2 \right]\,, \tag{7.5}$$

where we have defined

$$N^{T_{\mathrm{obs}}}_{\mathrm{GW}} \equiv \sum_{t_d\,,\boldsymbol{\theta}\,,z} N^{\mathrm{unres}}_{\mathrm{GW}}(\hat{n}, t_d, \boldsymbol{\theta}, z)\,. \tag{7.6}$$

[1] In this chapter we focus just on the intensity, while in Chapter 8 we will consider also the other Stokes parameters.

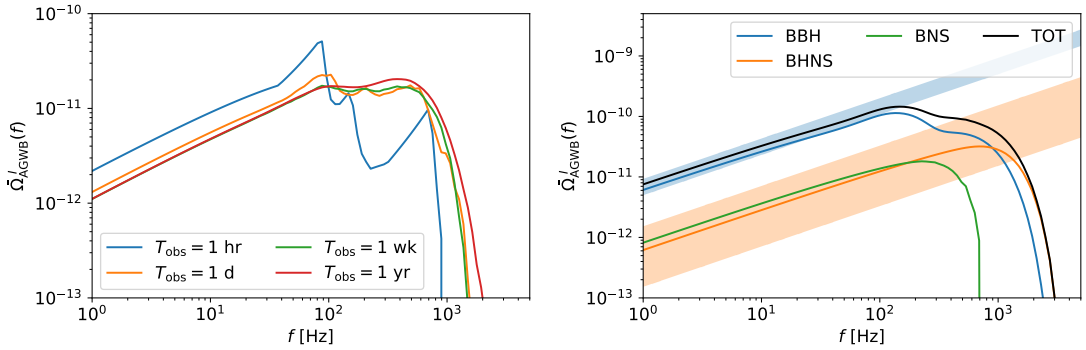

Figure 7.1: Left: plot of the monopole of the AGWB for different observing times and $\mathrm{SNR}^{\rm res}_{\rm thr} = 80$. Right: plot of the AGWB for different sources for $\mathrm{SNR}^{\rm res}_{\rm thr} \to \infty$. The blue and orange shaded regions correspond to the LVK bounds on the amplitude of the AGWB from BBH and BNS respectively.

When $N^{T_{\rm obs}}_{\rm GW} \to \infty$, Eqs. (7.4), (7.5) coincide, otherwise the background computed by summing the individual signals would fluctuate (presenting spikes and irregularities) w.r.t. the smooth contribution computed by considering the full population of emitters. In the case of the GWs emitted by BBH during the inspiral, the merger and the ringdown, the number of sources in one year is large enough and the background computed with Eq. (7.4) and (7.5) coincide. In the right panel of Figure 7.1, we plot the homogeneous and isotropic contribution to the monopole computed by using the two approaches, by considering different observing times, showing how the Poisson fluctuations due to the discrete number of sources would affect the shape of the background. For this background, we have used $\mathrm{SNR}^{\rm res}_{\rm thr} = 80$. In the right panel of figure 7.1, we show the monopole of the AGWB generated by BBH, BNS and BHNS, considering the populations described in the next section. In the same Figure, we plot also the LVK bound on the AGWB from BBH, Eq. (1.94), rescaled w.r.t. the local merger rate of the populations we have considered in this work, Eq. (7.21). In order to check that the AGWB we have computed is consistent with the LVK bounds, the window function introduced in Section 7.1.1 has been taken equal to one (which is equivalent to set $\mathrm{SNR}^{\rm res}_{\rm thr} \to \infty$). In the left panel of Figure 7.2, we plot the AGWB which is expected to be detected by the network ET+CE for different values of $\mathrm{SNR}^{\rm res}_{\rm thr}$.

7.2 Population of BBH

CBCs are characterized by their intrinsic properties $\boldsymbol{\theta}$, by the redshift of the merger z and by the time delay between the formation of the binary and the merger of the two objects[2]. In our work we assume that we can factorize the dependence of the binary parameters

[2]For practical purposes, here we include in the description of the populations the window function of the detector, thus the population discussed here are not the full BBH, BNS and BHNS populations, but the ones that contributes to the astrophysical background.

w.r.t. the redshift and the time delay,

$$\frac{\mathrm{d}N_{\mathrm{GW}}^{[i]}}{\mathrm{d}t_d\,\mathrm{d}\boldsymbol{\theta}\,\mathrm{d}z}(t_d,\boldsymbol{\theta},z)=p^{[i]}(\boldsymbol{\theta})\frac{\mathrm{d}R^{[i]}(t_d,z)}{\mathrm{d}t_d}T_{\mathrm{obs}}\frac{\mathrm{d}V}{\mathrm{d}z\mathrm{d}\Omega_e}(z_d)w^{[i]}(\boldsymbol{\theta},z)\,, \tag{7.7}$$

where i is the type of source considered (BBH, BNS, BHNS), T_{obs} is the observation time of the background, while $\mathrm{d}V/\mathrm{d}z\mathrm{d}\Omega_e$ is the comoving volume element. In our framework, we are considering binaries that emit GWs at z, which is the redshift at the time t, produced at z_d, which is the redshift at the time $t-t_d$. The expression of the number of events given by Eq. (7.7) is not the most general, since it could not be possible to factorize the dependences on z and $\boldsymbol{\theta}$. For instance, this happens for the posterior derived from observations of resolved sources at current interferometers [8]. Moreover, here we assume that the distribution of the astrophysical parameters that characterize the binary can be factorized in the following way,

$$p^{[i]}(\boldsymbol{\theta})=p^{[i]}(m_1,m_2)p^{[i]}(\chi_1,\chi_2)p(\iota)\,, \tag{7.8}$$

with m_1, m_2 the masses of the objects in the system, χ_1, χ_2 the spin and ι the inclination angle. Note that all the distributions we will consider in our work are affected by large uncertainties, because of the low number of CBC detections by the three runs of LVK [107, 108, 8]. In principle. each of the probability distribution should be marginalized w.r.t. its nuisance parameters, however, since in this Thesis we are considering the network of ET+CE, it is safe to assume that Eq. (7.8) is not affect by lack of knowledge in the population of the binaries, because of the large number of individual sources which will be detected by $3g$ interferometers. We will compute therefore the background by conditioning the values of the parameters of the distributions to the maximum a posteriori estimates of [8].

Mass Distribution

For BBH, we use the Power Law + Peak mass distribution [108, 8], which is favoured by the last GW observations,

$$p^{\mathrm{BBH}}(m_1,m_2)=p^{\mathrm{BBH}}(m_2|m_1)p^{\mathrm{BBH}}(m_1)\mathcal{S}(m_1)\,, \tag{7.9}$$

where we have

$$p^{[\mathrm{BBH}]}(m_1)=(1-\lambda_{\mathrm{BBH}})\frac{(1-\alpha_{\mathrm{BBH}})m_1^{-\alpha_{\mathrm{BBH}}}}{M_{\mathrm{max}}^{\mathrm{BBH}\,1-\alpha_{\mathrm{BBH}}}-M_{\mathrm{min}}^{\mathrm{BBH}\,1-\alpha_{\mathrm{BBH}}}}+\lambda_{\mathrm{BBH}}\frac{1}{\sqrt{2\pi}\sigma_{\mathrm{BBH}}}e^{-\frac{(m_1-\mu_{\mathrm{BBH}})^2}{2\sigma_{\mathrm{BBH}}^2}}\,, \tag{7.10}$$

with $\alpha_{\mathrm{BBH}}=3.4$, $M_{\mathrm{min}}^{\mathrm{BBH}}=2.5\,M_\odot$, $M_{\mathrm{max}}^{\mathrm{BBH}}=100\,M_\odot$, $\mu_{\mathrm{BBH}}=34\,M_\odot$, $\sigma_{\mathrm{BBH}}=5.09\,M_\odot$, $\lambda_{\mathrm{BBH}}=0.039$. We have also used a smoothing function for m_1,

$$\mathcal{S}(m_1)=\frac{\theta_H\left(m_1-M_{\mathrm{min}}^{\mathrm{BBH}}\right)\theta_H\left(M_{\mathrm{min}}^{\mathrm{BBH}}+\delta_M-m_1\right)}{\exp\left[\frac{\delta_M}{m_1-M_{\mathrm{min}}^{\mathrm{BBH}}}+\frac{\delta_M}{m_1-M_{\mathrm{min}}^{\mathrm{BBH}}-\delta_M}\right]}\,, \tag{7.11}$$

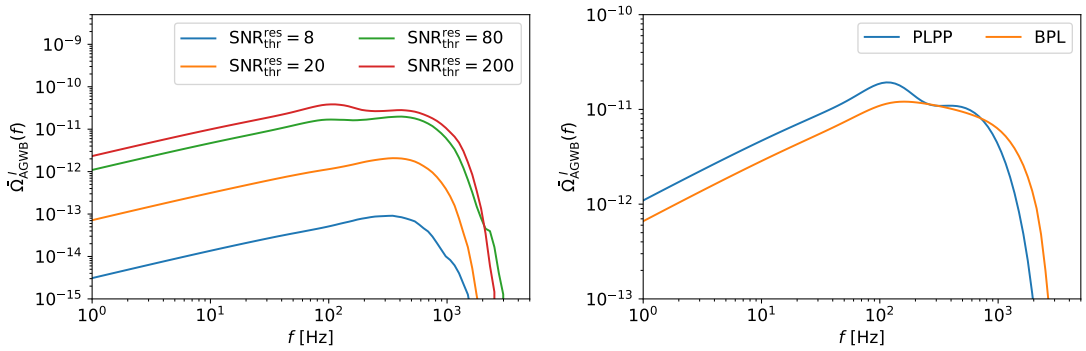

Figure 7.2: Left: plot of the monopole of the AGWB for different detection threshold of the resolved sources. Right: plot of the monopole of the AGWB for a BPL and PLPP mass distribution.

with θ_H the Heaviside theta function and $\delta_M = 7.8\,M_\odot$. We have considered them a uniform distribution in the mass ratio $q \equiv m_2/m_1$, with $q \leq 1$,

$$p^{[\mathrm{BBH}]}(m_2|m_1) = p^{\mathrm{BBH}}(q|m_1)\frac{dq}{dm_2} = \frac{1}{1-\frac{M^{\mathrm{BBH}}_{\mathrm{min}}}{m_1}}\frac{1}{m_1} = \frac{1}{m_1 - M^{\mathrm{BBH}}_{\mathrm{min}}}\,. \tag{7.12}$$

In the BNS case, we assume that the masses of NSs in merging binaries are uniformly distributed [8] between $M^{[\mathrm{BNS}]}_{\mathrm{min}} = 1\,M_\odot$ and $M^{[\mathrm{BNS}]}_{\mathrm{max}} = 2.5\,M_\odot$,

$$p^{[\mathrm{BNS}]}(m_1, m_2) = \frac{1}{\left(M^{\mathrm{BNS}}_{\mathrm{max}} - M^{\mathrm{BNS}}_{\mathrm{min}}\right)^2}\,. \tag{7.13}$$

For BHNS we use the MULTI SOURCE *model* adopted in [8], describing the distributions of the masses of the BH and of the NS as two Gaussians with mean $\mu_{\mathrm{BHNS\,BH}} = 7.5\,M_\odot$, $\mu_{\mathrm{BHNS\,NS}} = 1.33\,M_\odot$ and rms $\sigma_{\mathrm{BHNS\,BH}} = 0.75\,M_\odot$, $\sigma_{\mathrm{BHNS\,NS}} = 0.09\,M_\odot$ [287, 288].

Spin Distribution

We assume that the spin distribution of BBH

$$p^{\mathrm{BBH}}(\chi_1, \chi_2) = p(\chi_1)p(\chi_2) = \prod_{i=1}^{2}\frac{1}{\sqrt{2\pi}\sigma_\chi}e^{-\frac{\chi_i^2}{2\sigma_\chi^2}}\,, \tag{7.14}$$

where $\sigma_\chi = 0.1$ [8]. According to [288], assuming zero spin for both the objects in BNS systems seems to be a very good approximation. On the other hand, the spin of the objects in BHNS systems could be large in some cases, but we expect that on average it is close to zero; therefore, considering also the large amount of uncertainties in modelling the BHNS population, we neglect it.

Inclination Angle Distribution

The inclination angle of the binary is defined as the angle between the total angular momentum of the binary and the line of sight,

$$\cos\iota \equiv \hat{J}\cdot\hat{n}\,. \tag{7.15}$$

If the Universe is homogeneous and isotropic, the inclination of the binaries w.r.t. the line-of-sight is distributed isotropically. In this Thesis, we will assume an isotropic distribution of the sources, therefore $\cos\iota$ is drawn from a uniform PDF, thus iota is distributed according to

$$p(\iota) = p(\cos\iota)\frac{\mathrm{d}\cos\iota}{\mathrm{d}(-\iota)} = \frac{\sin\iota}{2}\,. \tag{7.16}$$

Merger Rate

In our work we characterize the merger rate of compact binaries in terms of the star-formation rate (SFR). The dependence of the SFR on the redshift is still debated, because different surveys provide different constraints, since it is sensitive to the distribution of the mass and metallicity of the host galaxies. We decide to evaluate the SFR by using Universe Machine [289, 75], in which it is shown that the SFR inside an halo of mass M_h ad redshift z is distributed according to a log-normal distribution,

$$p\left(\mathrm{SFR}|M_h,z\right) = \left[1-f_Q(M_h,z)\right]\frac{1}{\sqrt{2\pi}\sigma_{\mathrm{SF}}(M_h,z)\mathrm{SFR}}\exp\left\{-\frac{\left[\ln\mathrm{SFR}-\mathrm{SFR}_{\mathrm{SF}}(M_h,z)\right]^2}{2\sigma^2_{\mathrm{SF}}(M_h,z)}\right\}, \tag{7.17}$$

where f_Q is the fraction of quenched galaxies that produce no more stars at z. The expectation value and the covariance associated to the SFR per halo of mass M_h are

$$\begin{aligned}\langle\mathrm{SFR}\rangle(M_h,z) =& \mathrm{SFR}_{\mathrm{SF}}(M_h,z)\exp\left(\frac{\sigma^2_{\mathrm{SF}}}{2}\right),\\ \left\langle\left[\mathrm{SFR}-\langle\mathrm{SFR}\rangle(M_h,z)\right]^2\right\rangle =& \left[\exp\left(\sigma^2_{\mathrm{SF}}(M_h,z)\right)-1\right]\exp\left[2\mathrm{SFR}_{\mathrm{SF}}(M_h,z)+\sigma^2_{\mathrm{SF}}(M_h,z)\right].\end{aligned} \tag{7.18}$$

The average SFR at a given redshift is obtained therefore just by integrating the average SFR per halo of mass M_h times the number of halos with mass M_h over the halo mass M_h,

$$R_\star(z) = \int \mathrm{d}M_h\,\langle\mathrm{SFR}\rangle(M_h,z)\frac{d\bar{N}_h}{dM_h}(M_h,z) \quad \left[M_\odot\,\mathrm{yr}^{-1}\,\mathrm{Mpc}^{-3}\right], \tag{7.19}$$

where we use the halo mass function $\mathrm{d}\bar{N}/\mathrm{d}M_h$ of [290]. In the left panel of Figure 7.3 we compare the SFR obtained with the Universe Machine approach with the ones computed by Madau [291, 292], and Vangioni [293]. It can be easily seen that different approaches to compute the SFR lead to very different results. To connect the merger rate to the SFR we convolve the SFR distribution in redshift with a time delay distribution, keeping

into account for the formation time of the binary and for the early inspiral stage of the evolution of the system, normalizing this new SFR w.r.t. the local number of compact objects detected by LVK,

$$R^{[i]}(z) = R^{[i]}_{\rm LIGO}(z=0)\frac{\int {\rm d}t_d p^{[i]}(t_d) R_\star[z_d(z,t_d))]}{\int {\rm d}t_d p^{[i]}(t_d) R_\star[z_d(z=0,t_d))]}\,. \tag{7.20}$$

The LIGO normalization factors[3] have been taken from [8],

$$\begin{aligned} R^{\rm BBH}_{\rm LIGO}(z=0) =& 28.3^{+13.9}_{-9.1}\,{\rm Gpc}^{-3}\,{\rm yr}^{-1}\,,\\ R^{\rm BNS}_{\rm LIGO}(z=0) =& 105.5^{+190.2}_{-83.9}\,{\rm Gpc}^{-3}\,{\rm yr}^{-1}\,,\\ R^{\rm BHNS}_{\rm LIGO}(z=0) =& 45.0^{+75.0}_{-33.0}\,{\rm Gpc}^{-3}\,{\rm yr}^{-1}\,. \end{aligned} \tag{7.21}$$

The time delay distribution has been taken from [294, 295, 296], where PDF can be parametrized as an inverse power law,

$$p(t_d|n_{t_d}) \propto \frac{1}{t_d^{n_{t_d}}}\,. \tag{7.22}$$

In our work, we condition the time delay distribution to $n_{t_d} = 1$, although the uncertainties on this tilt would affect the shape in redshift of the merger rate. In this way $p(t_d)$ can be written by using

$$p^{[i]}(t_d) = \ln\left(\frac{t_d^{\rm max}}{t_d^{[i]\,\rm min}}\right)\frac{1}{t_d}\,, \tag{7.23}$$

with $t_d^{\rm max}$ equal to the age of the Universe at the redshift of the emission of the GWs, $t(z)$, while $t_d^{[\rm BBH],min} = t_d^{\rm BHNS,min} = 50\,{\rm Myr}$ and $t_d^{\rm BNS,min} = 20\,{\rm Myr}$ [297, 298]. In the above expression z is the redshift at which GWs are emitted, t is the time at redshift z and z_d is the redshift at[4] $t - t_d$. In the right panel of Figure 7.3, we plot the merger rate obtained with our approach, starting from Universe Machine, the merger rate of [288] (Iacovelli), obtained from the undelayed Madau SFR with a different choice of the local merger rate, and the one computed in [284], which differs from our prescription just because of a different choice of the SFR (the Vangioni model) and because of a rescaling in the SFR which depends on the metallicity of the stars. In [284], it is considered that BHs with masses larger than $30\,M_\odot$ can be produced in low-metallicity environments, therefore the SFR for large masses has been rescaled by the factor

$$f_{\rm met} \equiv \int_0^{+\infty} dZ_{\rm met}\, p\left(Z_{\rm met}\right)\, \theta_{\rm Heaviside}\left(\frac{1}{2}Z_\odot - 3\,Z_{\rm met}\right)\,, \tag{7.25}$$

[3] To be consistent, the local merger rates considered here are the ones obstained by assuming the mass distributions discussed in Section 7.2.

[4] To compute z_d we invert the relation

$$t_d = -\int_{z_d}^{z} d\tilde{z}\frac{1}{(1+\tilde{z})H(\tilde{z})}\,. \tag{7.24}$$

Note that for very high redshifts the SFR is zero, thus the imprint of very high z_d on the AGWB is zero too.

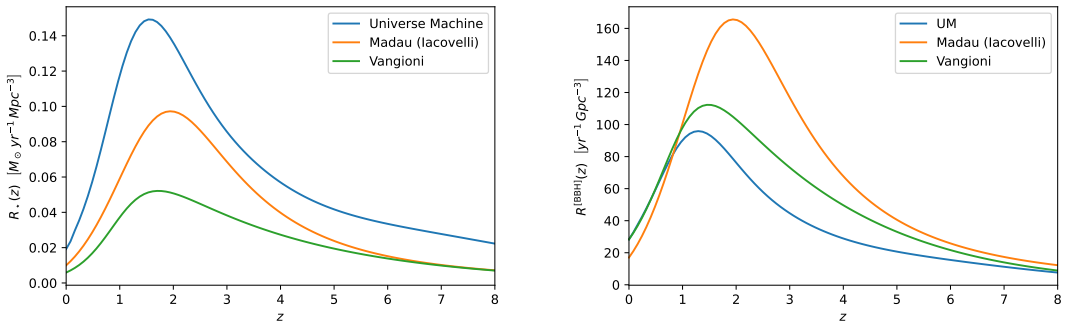

Figure 7.3: Left: plot of the SFR as a function of the redshift for three different parametrizations: Universe Machine (blue), Madau (orange), and Vangioni (green). Right: plot of the merger rate of BBH obtained from Universe Machine, Madau and Vangioni. For the Madau model a different local merger rate has been chosen.

where the metallicity distribution is a log10-normal distribution with $\sigma_{\rm met} = 0.5$ and mean $\bar{Z}_{\rm met}(z)$ [291],

$$p(Z_{\rm met}) = \frac{\log_{10}(e)}{\sqrt{2\pi}\sigma_{\rm met} Z_{\rm met}} \exp\left[-\frac{1}{2\sigma^2_{\rm met}}\left(\log_{10} Z_{\rm met} - \bar{Z}_{\rm met}(z)\right)^2\right] . \tag{7.26}$$

By looking at Eq. (7.20), it is therefore straightforward to see that the merger rate for a given time delay, introduced in Eq. (7.7), is

$$\frac{{\rm d}R^{[i]}(t_d, z)}{{\rm d}t_d} \equiv R^{[i]}_{\rm LIGO}(z=0) \frac{p^{[i]}(t_d) R_\star[z_d(z, t_d))]}{\int dt_d p^{[i]}(t_d) R_\star[z_d(z=0, t_d))]} . \tag{7.27}$$

Note that the merger rate defined in Eq. (7.20) is the comoving merger rate, therefore to compute the total number of events at $z = 0$ we use

$$N^{[i],{\rm obs}}_{\rm GW} = \int {\rm d}z \frac{1}{1+z} R^{[i]}(z) \frac{{\rm d}V}{{\rm d}z}(z) . \tag{7.28}$$

For the three models considered in this section we find $N^{[{\rm BBH}],{\rm obs}}_{\rm GW} = 4.1 \times 10^4 {\rm yr}^{-1}$ with the Universe Machine approach, $N^{[{\rm BBH}],{\rm obs}}_{\rm GW} = 7.5 \times 10^4 {\rm yr}^{-1}$ in the Iacovelli case [288] and $N^{[{\rm BBH}],{\rm obs}}_{\rm GW} = 5.0 \times 10^4 {\rm yr}^{-1}$ for the Vangioni model [284].

Bias of CBC

The bias of CBCs is computed with the approach used in [75], connecting the halo bias to the bias of GW emitters via

$$b^{[i]\,{\rm res}}_{\rm GW}(z) \equiv \frac{\int {\rm d}M_h \frac{{\rm d}\bar{N}^{[i]}_{\rm GW}}{{\rm d}M_h {\rm d}z}(M_h, z)\, b_h(M_h, z)}{\int {\rm d}M_h \frac{{\rm d}\bar{N}^{[i]}_{\rm GW}}{{\rm d}M_h {\rm d}z}(M_h, z)} , \tag{7.29}$$

where the halo bias has been computed in [299] and the number of resolved GW events is given by

$$\frac{\mathrm{d}\bar{N}^{[i]}_{\rm GW}}{\mathrm{d}M_h \mathrm{d}z}(M_h,z) = \int \mathrm{d}\boldsymbol{\theta}\, p^{[i]}(\boldsymbol{\theta}) T_{\rm obs} \left(1 - w^{[i]}(\boldsymbol{\theta},z)\right) R^{[i]}_{\rm LIGO}(z=0) \\ \frac{\int \mathrm{d}t_d\, p(t_d)\, \langle \mathrm{SFR}\rangle(M_h,z_d) \frac{\mathrm{d}\bar{N}_h}{\mathrm{d}M_h}(M_h,z_d) \frac{\mathrm{d}V}{\mathrm{d}z\mathrm{d}\Omega_e}(z_d)}{\int \mathrm{d}M_h \int \mathrm{d}t_d\, p(t_d)\, \langle \mathrm{SFR}\rangle(M_h,z_d) \frac{\mathrm{d}\bar{N}_h}{\mathrm{d}M_h}(M_h,z_d)\Big|_{z=0}} \,. \tag{7.30}$$

In the Universe Machine prescription, many terms simplifies and we get that the bias of the resolved sources is

$$b^{[i]\,\rm res}_{\rm GW}(z) = \frac{\int \mathrm{d}M_h \int \mathrm{d}t_d\, p(t_d)\, \langle \mathrm{SFR}\rangle(M_h,z_d) \frac{\mathrm{d}\bar{N}_h}{\mathrm{d}M_h}(M_h,z_d) \frac{\mathrm{d}V}{\mathrm{d}z\mathrm{d}\Omega_e}(z_d)\, b_h(M_h,z)}{\int \mathrm{d}M_h \int \mathrm{d}t_d\, p(t_d)\, \langle \mathrm{SFR}\rangle(M_h,z_d) \frac{\mathrm{d}\bar{N}_h}{\mathrm{d}M_h}(M_h,z_d) \frac{\mathrm{d}V}{\mathrm{d}z\mathrm{d}\Omega_e}(z_d)} \,. \tag{7.31}$$

Note that the bias does not depend on the window function related to the efficiency of the detector network considered w, which means that the bias for the resolved and unresolved GW events is the same. This is related to the fact that we discriminate between resolved and unresolved sources by some functions which depend on z, $\boldsymbol{\theta}$, which do not depend on M_h and t_d, therefore any contribution from these terms cancels in the computation of the bias. In the same way, we notice that the bias does not depend on the mass distribution or on other properties of the sources, therefore in our approximation in which $p(\boldsymbol{\theta})$ can be factorized in uncorrelated redshift and mass distribution, the bias is the same for BBH, BNS and BHNS. We conclude therefore that

$$b_{\rm GW}(z) \equiv b^{[i]\,\rm res}_{\rm GW}(z) = b^{[i]\,\rm unres}_{\rm GW}(z) \,. \tag{7.32}$$

The bias defined in Eq. (7.29) should not be confused with the "effective bias" introduced in [75], which is defined by

$$b^{[i]}_{\rm GW,eff}(f,z) \equiv \frac{\frac{\bar{\Omega}^{[i]}_{\rm AGWB}(f)}{\bar{\Omega}^{\rm tot}_{\rm AGWB}(f)} \tilde{W}^{[i]}_{\rm AGWB}(z,f) b^{[i]\,\rm unres}_{\rm GW}(z)}{\sum_i \frac{\bar{\Omega}^{[i]}_{\rm AGWB}(f)}{\bar{\Omega}^{\rm tot}_{\rm AGWB}(f)} \tilde{W}^{[i]}_{\rm AGWB}(z,f)} \,, \tag{7.33}$$

where the window function of the AGWB generated by the source i is simply defined by

$$\tilde{W}^{[i]}_{\alpha}(z,f) \equiv \frac{1}{\bar{\Omega}^{[i]}_{\rm AGWB}(f)} \frac{\mathrm{d}\bar{\Omega}^{[i]}_{\rm AGWB}}{\mathrm{d}z}(z,f) \,. \tag{7.34}$$

The effective bias in this case depends on the frequency, on the source considered and it is different for unresolved and resolved sources. In Figure 7.4 we plot the "true" bias, defined in Eq. (7.29) and the effective biases, defined in Eq. (7.33), for BBH, BNS and BHNS. We note that the GW bias we find is consistent with [300, 301]. The effective biases of BNS and BHNS are suppressed, because the monopole of the AGWB generated by BBH dominates the energy spectrum, according to the right plot of Fig. 7.1.

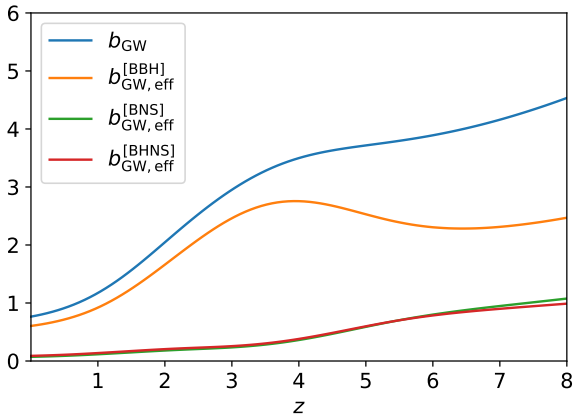

Figure 7.4: Plot of the bias of the GW events and of the effective bias of BBH, BNS and BHNS as a function of the redshift.

7.3 Energy spectrum of the binary system

We describe the Fourier transform of the chirp signal emitted by a binary system by using the parametrization of [99], which gives for the two polarizations

$$\begin{aligned} h_+(f_e) =& \frac{1}{\pi^{2/3}} \left(\frac{5}{24}\right)^{1/2} e^{i\Psi_+(f_e)} \frac{c}{r} \left(\frac{GM_c}{c^3}\right)^{5/6} \frac{1}{f_e^{7/6}} \frac{1+\cos^2\iota}{2}\,, \\ h_\times(f_e) =& \frac{1}{\pi^{2/3}} \left(\frac{5}{24}\right)^{1/2} e^{i\Psi_+(f_e)+i\pi/2} \frac{c}{r} \left(\frac{GM_c}{c^3}\right)^{5/6} \frac{1}{f_e^{7/6}} \cos\iota\,, \end{aligned} \tag{7.35}$$

with r the physical distance from the source, related to the luminosity distance by $D_L(z) = (1+z)r$. The chirp mass is defined by

$$M_c \equiv \frac{(m_1 m_2)^{3/5}}{(m_1+m_2)^{1/5}}\,. \tag{7.36}$$

The observed frequency and strain f are redshifted w.r.t. to the ones at the emitter, $f_e = (1+z)f$, $h(f) = (1+z)h(f_e)$, thus the observed waves at interferometers are

$$\begin{aligned} h_+(f) =& \frac{1}{\pi^{2/3}c^{3/2}} \sqrt{\frac{5}{24}} \frac{1}{D_L(z)} (GM_c)^{5/6} \frac{1}{f^{7/6}} e^{i\Psi_+(f_e)} \frac{1+\cos^2\iota}{2}\,, \\ h_\times(f) =& \frac{1}{\pi^{2/3}c^{3/2}} \sqrt{\frac{5}{24}} \frac{1}{D_L(z)} (GM_c)^{5/6} \frac{1}{f^{7/6}} e^{i\Psi_+(f_e)+i\pi/2} \cos\iota\,. \end{aligned} \tag{7.37}$$

This expression can be generalized to each stage of the evolution of the binary, including also the merger and ringdown, and by considering also post-Newtonian corrections in the inspiral stage. The Fourier transform of the GW signal for each polarization state is then

$$\begin{aligned} h_+(\boldsymbol{\theta}, f) =& \frac{1+\cos^2\iota}{2}\,\tilde{h}(\boldsymbol{\theta}, f)\,, \\ h_\times(\boldsymbol{\theta}, f) =& \cos\iota\, e^{i\pi/2}\tilde{h}(\boldsymbol{\theta}, f)\,, \end{aligned} \tag{7.38}$$

where the GW amplitude $\tilde{h}$ has been computed with the fit of [302, 303, 304],

$$\tilde{h}(f) = A(\boldsymbol{\theta}, f) e^{-i\Xi(\boldsymbol{\theta}, f)}\,, \tag{7.39}$$

where the phase plays no role in the AGWB. For the inspiral, merger and ringdown it is possible to parametrize A in the following way,

$$A(\boldsymbol{\theta}, f) = \sqrt{\frac{5}{24}} \frac{(GM_c)^{5/6}}{\pi^{2/3} c^{3/2}} \frac{(1+z)^{5/6}}{D_L(z)} f_1^{-7/6} \begin{cases} \left(\frac{f}{f_1}\right)^{-7/6} (1 + \alpha_2 v^2 + \alpha_3 v^3) & f < f_1 \\ \omega_m \left(\frac{f}{f_1}\right)^{-2/3} (1 + \epsilon_1 v + \epsilon_2 v^2) & f \in [f_1, f_2] \\ \frac{\omega_r}{2\pi} \frac{\sigma}{(f - f_2)^2 + \sigma^2/4} & f \in [f_2, f_3] \end{cases} \tag{7.40}$$

By evaluating all the frequency-dependent quantities at the emitter the amplitude becomes

$$A(\boldsymbol{\theta}, f) = \sqrt{\frac{5}{24}} \frac{(GM_c)^{5/6}}{\pi^{2/3} c^{3/2}} \frac{(1+z)^{2}}{D_L(z)} f_{1,e}^{-7/6} \begin{cases} \left(\frac{f_e}{f_{1,e}}\right)^{-7/6} (1 + \alpha_2 v^2 + \alpha_3 v^3) & f_e < f_{1,e} \\ \omega_m \left(\frac{f_e}{f_{1,e}}\right)^{-2/3} (1 + \epsilon_1 v + \epsilon_2 v^2) & f_e \in [f_{1,e}, f_{2,e}] \\ \frac{\omega_r}{2\pi} \frac{\sigma_e}{(f_e - f_{2,e})^2 + \sigma_e^2/4} & f_e \in [f_{2,e}, f_{3,e}] \end{cases} \tag{7.41}$$

For the inspiral stage, the GW strain is connected to the energy spectrum per frequency at the emitter [99, 61], by

$$\frac{dE}{df_e} = \frac{\pi^{2/3}}{3G} (GM_c)^{5/3} f_e^{-1/3}\,, \tag{7.42}$$

thus a generalization of this result to any stage of evolution of the binary gives

$$\frac{dE}{df_e d\Omega_e} = \frac{\pi c^3 D_L^2(z)}{2G(1+z)^2} f^2 \left[|h_+(f)|^2 + |h_\times(f)|^2\right]\,. \tag{7.43}$$

The waveform used in Eq. (7.40) is not the only possible choice. More recent waveforms, such as PhenomD [305, 306], have been proposed and provide a more accurate description of the GW signals during the merger and the ringdown. Nevertheless, the AGWB is expected to depend slightly on the choice of the waveform, thence these differences would not affect the validity of the result we will find for the anisotropies of the background. The extension of the energy spectrum given in Eq. (7.43) to any Stokes parameter is given by

$$\frac{\mathrm{d}E^\alpha}{\mathrm{d}f_e \mathrm{d}\Omega_e} = \frac{\pi c^3 D_L^2(z)}{2G(1+z)^2} f^2 S_\alpha(f)\,, \tag{7.44}$$

where the Stokes parameters are related to the expectation values of the strain by Eq. (1.43).

7.4 Intrinsic anisotropies of the AGWB

7.4.1 Contributions to the anisotropies

As other cosmological observables, like the CMB [42] and the galaxy number count [216], the energy density of the AGWB is expected to reflect the homogeneity and isotropy of

the Universe at leading order, showing tiny deviations from a uniform spectrum in the sky of the order of 10^{-2} or smaller. In the case of the CGWB, discussed in chapter 3, the fluctuations have been evaluated by using a Boltzmann approach, computing the evolution of the distribution function of graviton in space and time, assuming no external sources and collisions of GWs. In the case of the AGWB the situation is different, because at every time new binary systems emit GWs for a short duration, thus it could be difficult to solve the Boltzmann equation in presence of a source term which depends on space and time. In addition, different uncorrelated sources of anisotropies would impact the spectrum of astrophysical gravitons, therefore, for practical purposes, it is more convient to characterize them separately. The dominant contribution to the angular power spectrum of the AGWB is due to shot noise (SN), induced by Poisson fluctuations in the number of discrete events that contribute to the signal [65, 66, 64]. Another important effect is the kinetic dipole [307, 308, 67, 6, 68] produced by the peculiar motion of the observer w.r.t. the rest frame of the sources. Subdominant contributions are given by the intrinsic anisotropies, generated by cosmological perturbations of the metric and in the number density and velocity of the GW emitters [69, 309, 70, 71, 72, 73, 74]. In Chapters 8, 9 we will focus on the SN and the kinetic contribution to the anisotropies respectively, while in the remaining part of this section we will compute only the intrinsic anisotropies.

7.4.2 Cosmic rulers

The necessity of a gauge-invariant approach

The energy density of the AGWB along a direction of observation in the sky, at the frequency f is equal to

$$\Omega^{\alpha}_{\rm AGWB}(\hat{n},f)=\frac{f}{\rho_{\rm crit}c^2}\int \mathrm{d}z\int \mathrm{d}\boldsymbol{\theta}\int \mathrm{d}t_d\,\frac{N^{\rm unres}_{\rm GW}(\hat{n},t_d,\boldsymbol{\theta},z)\frac{\mathrm{d}E^{\alpha}}{\mathrm{d}f_e d\Omega_e}(\boldsymbol{\theta},z,f)}{(1+z)H(z)T_{\rm obs}\frac{\mathrm{d}V}{\mathrm{d}z\mathrm{d}\Omega_e}(z)}\,, \tag{7.45}$$

where we have taken the continuous limit of Eq. (7.4). It is useful to introduce the total physical energy density of the AGWB,

$$\mathfrak{n}^{[i]}_{\alpha}(t_d,\boldsymbol{\theta},z,\hat{n},f)\equiv\frac{1}{(1+z)^3}\frac{1}{T_{\rm obs}\frac{\mathrm{d}V}{\mathrm{d}z\mathrm{d}\Omega_e}(z)}\frac{\mathrm{d}N^{[i]}_{\rm GW}}{\mathrm{d}t_d\mathrm{d}\boldsymbol{\theta}\mathrm{d}z}(t_d,\boldsymbol{\theta},z)\frac{\mathrm{d}E^{\alpha}}{\mathrm{d}f_e d\Omega_e}(\boldsymbol{\theta},z,f)\,, \tag{7.46}$$

where the factor $(1+z)^3$ comes from the fact that $N^{[i]}_{\rm GW}$ is a comoving number density. We introduce also the comoving distance of the source from the observer, obtained by integrating the distance travelled by GWs at the speed of light from their production at t up to the time t_0

$$\chi\equiv\int_t^{t_0}\mathrm{d}\tilde{t}\,a(\tilde{t})=\int_a^{a_0}\mathrm{d}\tilde{a}\frac{\mathrm{d}t}{\mathrm{d}\tilde{a}}=\int_z^0\mathrm{d}\tilde{z}\frac{\mathrm{d}}{\mathrm{d}\tilde{z}}\left(\frac{a_0}{1+\tilde{z}}\right)\frac{1}{H(\tilde{z})}=\int_0^z\mathrm{d}\tilde{z}\frac{1}{(1+\tilde{z})^2H(\tilde{z})}\,. \tag{7.47}$$

By comparing the definition of comoving distance with the one of conformal time given in Eq. (2.3), it is immediate to see that $\chi=\eta_0-\eta$, with χ and η evaluated at the same time.

The energy density of the AGWB expressed as a function of the comoving distance is

$$\Omega^{\alpha\,[i]}_{\rm AGWB}(\hat{n},f)=\frac{f}{\rho_{\rm crit}c^2}\int \mathrm{d}\chi\int \mathrm{d}\boldsymbol{\theta}\int \mathrm{d}t_d\,\frac{\mathfrak{n}^{[i]}_\alpha(t_d,\boldsymbol{\theta},\chi,\hat{n},f)}{(1+z)^2}\,, \tag{7.48}$$

where z is function of χ. The homogeneous and isotropic contribution to $\mathfrak{n}^{[i]}_\alpha$, which is defined by

$$\bar{\mathfrak{n}}^{[i]}_\alpha(t_d,\boldsymbol{\theta},z,f)\equiv\frac{1}{4\pi}\int \mathrm{d}\hat{n}\,\mathfrak{n}^{[i]}_\alpha(t_d,\boldsymbol{\theta},z,\hat{n},f)\,, \tag{7.49}$$

is used to compute $\bar{\Omega}^{\alpha}_{\rm AGWB}$ defined in Eq. (1.47) and plotted in Figures 7.1, 7.2. The main issue associated to the computation of the perturbations of $\Omega^{\alpha}_{\rm AGWB}$ is that the quantities that induce the anisotropies, like the inhomogeneities in the matter distribution, are gauge dependent, therefore, in order to obtain the true physical information on the observer angular power spectrum, one should evaluate the fluctuations in terms of gauge-invariant variables. The approach we use is the *Cosmic Rulers* formalism, introduced in [276, 310] to study other kind of LSS effects, by using observed, thus gauge-independent, quantities to compute the anisotropies of the AGWB

Connection between the physical and observed frames

We denote with $x^\mu(\chi)$ the physical frame and with $\bar{x}^\mu(\bar{\chi})$ the observer's frame where we perform observations. The observed frame is associated to measured quantities, thence it is not affected by unphysical degrees of freedom due to the choice of the coordinates and it contains all the physical information we want to extract. In a generic gauge, the physical frame is characterized by the line element introduced in Eq. (2.74). In the observer's frame, geodesics are flattened along the past GW cone, therefore the trajectories of gravitons are parametrized by

$$\bar{\eta}=\eta_0-\bar{\chi}\,,\qquad \bar{\mathbf{x}}=\bar{\chi}\,\hat{n}\,, \tag{7.50}$$

where the comoving distance $\bar{\chi}$ can be written as a function of the conformal time by using $\bar{\chi}=\eta_0-\bar{\eta}$. Following the definition of the 4-momentum, Eq. (3.6), in the observer frame we have

$$\bar{p}^\mu\equiv\frac{\mathrm{d}\bar{x}^\mu}{\mathrm{d}\lambda}=-2\pi f_o\,\frac{\bar{k}^\mu}{\bar{a}_0^2}\,, \tag{7.51}$$

where we could set $\bar{a}_0=1$ by convention and we have defined the unit vector

$$\bar{k}^\mu\equiv\frac{\mathrm{d}\bar{x}^\mu}{\mathrm{d}\bar{\chi}}=\begin{pmatrix}-1 & \hat{n}\end{pmatrix}\,. \tag{7.52}$$

The transformation that connects the observed frame, where photon and graviton geodesics are straight lines, with the real frame, in which the GW trajectories are perturbed by the

inhomogeneities in the Universe, are defined by

$$\begin{aligned}\delta\chi(\bar{\chi}) \equiv& \chi - \bar{\chi}\,,\\ \delta x^{\mu}(\bar{\chi}) \equiv& x^{\mu}(\bar{\chi}) - \bar{x}^{\mu}(\bar{\chi})\,,\\ \Delta x^{\mu}(\bar{\chi}) \equiv& x^{\mu}(\chi) - \bar{x}^{\mu}(\bar{\chi}) = x^{\mu}(\bar{\chi}) + \frac{d}{d\bar{\chi}}x^{\mu}(\bar{\chi})\delta\chi - \bar{x}^{\mu}(\bar{\chi}) = \frac{d}{d\bar{\chi}}x^{\mu}(\bar{\chi})\delta\chi + \delta x^{\mu}(\bar{\chi})\,.\end{aligned} \tag{7.53}$$

In the physical frame the 4-momentum can still be written as a function of a unit vector and of the observed frequency, but it also depends on the scale factor at $\bar{\chi}$,

$$p^{\mu}_{\rm GW} = -2\pi f_o \frac{k^{\mu}}{a^2}\,, \tag{7.54}$$

where the relation between k^{μ} and $\bar{k}^{\mu}$ is given in terms of the transformations introduced in Eq. (7.53),

$$k^{\mu}(\bar{\chi}) \equiv \frac{dx^{\mu}}{d\bar{\chi}}(\bar{\chi}) = \frac{d}{d\bar{\chi}}\left(\bar{x}^{\mu} + \delta x^{\mu}\right)(\bar{\chi}) = \bar{k}^{\mu} + \frac{d}{d\bar{\chi}}\delta x^{\mu}(\bar{\chi})\,. \tag{7.55}$$

We define then the variation of the 4-vector k^{μ} as

$$\delta k^{\mu}(\bar{\chi}) \equiv k^{\mu}(\bar{\chi}) - \bar{k}^{\mu}(\bar{\chi}) = \begin{pmatrix}\delta f & \delta\hat{n}\end{pmatrix}\,. \tag{7.56}$$

Since $\delta k^{\mu}(\bar{\chi}) = {\rm d}\delta x^{\mu}(\bar{\chi})/{\rm d}\bar{\chi}$, the transformation law that maps the coordinates of the observer frame to the ones of the physical frame is

$$\delta x^{\mu}(\bar{\chi}) = \delta x^{\mu}_{o} + \int_0^{\bar{\chi}} d\bar{\chi}\,\delta k^{\mu}(\bar{\chi})\,. \tag{7.57}$$

By using the geodesic equation, Eq. (3.7), it is possible to show [74] that

$$\begin{aligned}\delta f =& -\delta a_o - A_o + v_{\parallel\, o} + 2A - B_{\parallel} - 2I\,,\\ \delta n_{\parallel} =& \delta a_o + A_o - v_{\parallel\, o} - A - \frac{1}{2}H_{\parallel} + 2I\,,\\ \delta n^{i}_{\perp} =& -v^{i}_{\perp\, o} + \frac{1}{2}\mathcal{P}^{i}_{k}H^{k}_{j\, o}n^{j} + B^{i}_{\perp\, o} - B^{i}_{\perp} - \mathcal{P}^{i}_{k}H^{k}_{j}n^{j} + 2S^{i}_{\perp}\,,\end{aligned} \tag{7.58}$$

where the velocity of the observer is

$$u^{\mu} = \frac{1}{a}\begin{pmatrix}1 - A & v^{i}\end{pmatrix} \tag{7.59}$$

and we have introduced the decomposition

$$X_{\parallel} \equiv \hat{n}^{i}\hat{n}^{j}X_{ij}\,, \qquad Y^{\perp}_{i} \equiv \mathcal{P}^{j}_{i}Y_{j} = Y_{i} - \hat{n}_{i}\hat{n}^{j}Y_{j}\,. \tag{7.60}$$

The solution of the geodesic equation depends also on the integrals

$$\begin{aligned}S^{i}_{\perp} \equiv& -\frac{1}{2}\int_0^{\bar{\chi}} d\chi\left[\partial^{i}_{\perp}\left(A - B_{\parallel} - \frac{1}{2}H_{\parallel}\right) + \frac{1}{\chi}\left(B^{i}_{\perp} + n^{k}H_{kj}\mathcal{P}^{ij}\right)\right]\,,\\ I \equiv& -\frac{1}{2}\int_0^{\bar{\chi}} d\chi\left(A' - B'_{\parallel} - \frac{1}{2}H'_{\parallel}\right)\,.\end{aligned} \tag{7.61}$$

Perturbation of the energy density

In the observer frame, the energy density given in Eq. (7.46), is characterized by the unperturbed value, $\bar{\mathfrak{n}}^{[i]}_{\alpha}(t_d, \boldsymbol{\theta}, \bar{\eta}, f)$. The relation between the perturbation of the energy density in the physical and observer frames is

$$\mathfrak{n}^{[i]}_{\alpha}(t_d, \boldsymbol{\theta}, x, f) = \bar{\mathfrak{n}}^{[i]}_{\alpha}(t_d, \boldsymbol{\theta}, \bar{\eta}) + \frac{\mathrm{d}}{\mathrm{d}\bar{\eta}}\bar{\mathfrak{n}}^{[i]}_{\alpha}(t_d, \boldsymbol{\theta}, \bar{\eta}, f)\Delta x^0 + \bar{\mathfrak{n}}^{[i]}_{\alpha}(t_d, \boldsymbol{\theta}, \bar{\eta}, f)\delta^{[i]}(x)\,, \tag{7.62}$$

with $\delta^{[i]}$ the intrinsic density perturbation. By introducing the comoving energy density,

$$\mathfrak{N}^{[i]}_{\alpha}(t_d, \boldsymbol{\theta}, x, f) \equiv (1+z)^3 \mathfrak{n}^{[i]}_{\alpha}(t_d, \boldsymbol{\theta}, x, f) \tag{7.63}$$

we get

$$\mathfrak{n}^{[i]}_{\alpha}(t_d, \boldsymbol{\theta}, x, f) = \bar{\mathfrak{N}}^{[i]}_{\alpha}(t_d, \boldsymbol{\theta}, \bar{\eta}, f)(1+z^3)\left[1 + \Delta\ln(a)\left(\frac{\mathrm{d}\ln\mathfrak{N}^{[i]}_{\alpha}(t_d, \boldsymbol{\theta}, \bar{\eta}, f)}{\mathrm{d}\ln\bar{a}} - 3\right) + \delta^{[i]}(x)\right], \tag{7.64}$$

where we have defined

$$\begin{aligned} \Delta\ln(a) \equiv& \frac{a(\chi)}{\bar{a}(\bar{\chi})} - 1 = -\delta f + A + v_{\parallel} - B_{\parallel} = \delta a_o + (A_o - v_{\parallel\, o}) - A + v_{\parallel} + 2I\,, \\ \frac{d}{d\bar{\chi}}\Delta\ln(a) =& -\frac{d}{d\bar{\chi}}A + \frac{d}{d\bar{\chi}}v_{\parallel} + 2\frac{d}{d\bar{\chi}}I\,. \end{aligned} \tag{7.65}$$

By expanding Eq. (7.48) at first order in the perturbations, by using Eqs. (7.58), (7.64) we get

$$\begin{aligned} \Omega^{\alpha\,[i]}_{\mathrm{AGWB}} = \frac{f_o}{\rho_{\mathrm{crit}}}\int \mathrm{d}\bar{\chi}\,\mathrm{d}\boldsymbol{\theta}\,\mathrm{d}t_d\,\frac{\bar{\mathfrak{N}}^{[i]}_{\alpha}}{1+z} \\ \left[1 + \delta^{[i]} + \delta f + \Delta\ln(a)\left(\frac{d\ln\bar{\mathfrak{N}}^{[i]}_{\alpha}}{d\ln(\bar{a})} - \frac{\mathcal{H}'}{\mathcal{H}^2} - 1\right) - \frac{1}{\mathcal{H}}\frac{d}{d\bar{\chi}}\Delta\ln(a)\right]. \end{aligned} \tag{7.66}$$

By using the solution of the geodesic equation we find

$$\begin{aligned} \Omega^{\alpha\,[i]}_{\mathrm{AGWB}} = \frac{f_o}{\rho_{\mathrm{crit}}}\int \mathrm{d}\bar{\chi}\,\mathrm{d}\boldsymbol{\theta}\,\mathrm{d}t_d\,\frac{\bar{\mathfrak{N}}^{[i]}_{\alpha}}{1+z} \\ \left[1 + \delta^{[i]} + A\left(3 - b^{[i]}_{e,\alpha} + \frac{\mathcal{H}'}{\mathcal{H}^2}\right) - B_{\parallel} + 2I\left(b^{[i]}_{e,\alpha} - \frac{\mathcal{H}'}{\mathcal{H}^2} - 2\right)\right. \\ + v_{\parallel}\left(b^{[i]}_{e,\alpha} - \frac{\mathcal{H}'}{\mathcal{H}^2} - 1\right) + \left[\delta a_o + A_o - v_{\parallel\, o}\right]\left(b^{[i]}_{e,\alpha} - \frac{\mathcal{H}'}{\mathcal{H}^2} - 2\right) \\ \left. + \frac{1}{\mathcal{H}}\left(\frac{d}{d\bar{\chi}}A - \frac{d}{d\bar{\chi}}v_{\parallel} + A' - B'_{\parallel} - \frac{1}{2}H'_{\parallel}\right)\right], \end{aligned} \tag{7.67}$$

where we have defined the evolution bias

$$b^{[i]}_{e,\alpha} \equiv \frac{\mathrm{d}\ln \mathfrak{N}^{[i]}_{\alpha}}{\mathrm{d}\ln a}\,. \tag{7.68}$$

Connection with CLASS - Poisson gauge

In Section 2.4.1, we have shown that the Poisson gauge is defined by $B = 0$, $F = 0$, $F^{\perp}_{j} = 0$, $\Phi = A$ and $\Psi = -D$. $B^{\perp}_{i} = 0$ is not a gauge choice, but a consequency of the expansion of the Universe that suppresses solenoidal vector fields. In the synchronous-comoving gauge, the density of binaries of type i are connected to the underlying density of matter through a bias,

$$\delta^{[i]\,(SC)} = b^{[i]}\delta^{(SC)}_{m}\,. \tag{7.69}$$

The bias has been computed by using Eq. (7.29) and the result is shown in Figure 7.4. As shown in [310], in the Poisson gauge, the density perturbation is connected to the perturbation of CDM by

$$\delta^{[i]\,(P)} = b^{[i]}\left(\delta_m - 3\mathcal{H}V\right) - \left(b^{[i]}_{e,\alpha} - 3\right)\mathcal{H}V\,, \tag{7.70}$$

where the velocity potential is defined as

$$\vec{v} \equiv \vec{\nabla}V\,. \tag{7.71}$$

The term proportional to the derivative w.r.t. the comoving distance of $v_{\parallel}$, which appears in Eq. (7.67), can be simplified by using the Euler equation of CDM,

$$\vec{v}' + \mathcal{H}\vec{v} + \vec{\nabla}\Psi = 0 \to \hat{n}\cdot\left(\vec{v}' + \mathcal{H}\vec{v} + \vec{\nabla}\Psi\right) = 0 \to -\frac{d}{d\bar{\chi}}v_{\parallel} + \partial_{\parallel}v_{\parallel} + \mathcal{H}v_{\parallel} + \partial_{\parallel}\Psi = 0\,. \tag{7.72}$$

The computation of the Fourier transform of the density contrast of the AGWB, defined in Eq. (1.49), gives

$$\begin{aligned}\delta^{[i]}_{\mathrm{AGWB}} = \int d\bar{\chi}\,\mathrm{d}\boldsymbol{\theta}\,\mathrm{d}t_d\,\frac{\tilde{\mathcal{W}}^{[i]}_{\alpha}}{(2\pi)^3}\Bigg[&b^{[i]}\left(\delta_m + 3\mathcal{H}\frac{\theta_m}{k^2}\right) - (3 - b^{[i]}_{e,\alpha})\mathcal{H}\frac{\theta_m}{k^2} + \Psi\left(3 - b^{[i]}_{e,\alpha} + \frac{\mathcal{H}'}{\mathcal{H}^2}\right)\\ &+ 2I\left(b^{[i]}_{e,\alpha} - \frac{\mathcal{H}'}{\mathcal{H}^2} - 2\right) - \frac{\hat{n}\cdot\hat{k}}{ik}\theta_m\left(-b^{[i]}_{e,\alpha} + \frac{\mathcal{H}'}{\mathcal{H}^2} + 2\right)\\ &+ e^{-ik\bar{\chi}\hat{k}\cdot\hat{n}}\left(\delta a_o + \Psi_o - \frac{\hat{n}\cdot\hat{k}}{ik}\theta_{m\,o}\right)\left(b^{[i]}_{e,\alpha} - \frac{\mathcal{H}'}{\mathcal{H}^2} - 2\right)\\ &- \frac{ik\left(\hat{k}\cdot\hat{n}\right)^2}{ik\mathcal{H}}\theta_m + \frac{1}{\mathcal{H}}\Phi' - \frac{1}{\mathcal{H}}\frac{1}{2}H^{\mathrm{TT}\,\prime}_{ij}n^i n^j\Bigg]e^{ik\bar{\chi}\hat{k}\cdot\hat{n}}\,,\end{aligned} \tag{7.73}$$

where we have defined

$$\theta_m \equiv \vec{\nabla}\cdot\vec{v}\,. \tag{7.74}$$

The total anisotropy of the AGWB is the sum of the anisotropies over many infinitesimal shells at different distances from the observer. The window function $\tilde{W}_\alpha^{[i]}$ represents the weight of the contribution given by the inhomogeneities at the comoving distance $\bar{\chi}$ w.r.t. the total,

$$\begin{aligned}\tilde{W}_\alpha^{[i]}(t_d,\boldsymbol{\theta},\eta,f) \equiv & \frac{1}{\bar{\Omega}^{\alpha\,[i]}_{\rm AGWB}(f)}\frac{\mathrm{d}\bar{\Omega}^{\alpha\,[i]}_{\rm AGWB}}{\mathrm{d}\bar{\chi}}(\bar{\chi},f) = \\ = & \frac{1}{\bar{\Omega}^{\alpha\,[i]}_{\rm AGWB}(f)}\frac{1}{(1+z)H(z)}\frac{1}{T_{\rm obs}\frac{\mathrm{d}V}{\mathrm{d}z\mathrm{d}\Omega_e}(z)}\frac{\mathrm{d}N^{[i]}_{\rm GW}}{\mathrm{d}t_d\mathrm{d}\boldsymbol{\theta}\mathrm{d}z}(t_d,\boldsymbol{\theta},z)\frac{\mathrm{d}E^\alpha}{\mathrm{d}f_e d\Omega_e}(\boldsymbol{\theta},z,f)\,.\end{aligned} \tag{7.75}$$

The window function selects the redshift that can be probed by observations of the AGWB and differences in its shape could change significantly the angular power spectrum of the AGWB. It is possible to note that the cosmological perturbations δ_m, θ_m, Ψ, Φ, H_{ij} that influence the evolution of the density contrast of the AGWB are insensitive to the parameters $\boldsymbol{\theta}$ and t_d that characterize the population of the sources. It is therefore natural to perform the integration over these parameters separately, introducing some effective function,

$$\begin{aligned}\tilde{W}_\alpha^{[i],\rm eff}(\eta,f) &\equiv \int \mathrm{d}\boldsymbol{\theta}\,\mathrm{d}t_d\,\tilde{W}_\alpha^{[i]}(t_d,\boldsymbol{\theta},\eta,f)\,,\\ \tilde{W}_\alpha^{[i],\rm eff}(\eta,f)b^{[i]\,\rm eff}(\eta) &\equiv \int \mathrm{d}\boldsymbol{\theta}\,\mathrm{d}t_d\,\tilde{W}_\alpha^{[i]}(t_d,\boldsymbol{\theta},\eta,f)\,b^{[i]}(\eta)\,,\\ \tilde{W}_\alpha^{[i],\rm eff}(\eta,f)\,b^{[i]\,\rm eff}_{e,\alpha}(\eta,f) &\equiv \int \mathrm{d}\boldsymbol{\theta}\,\mathrm{d}t_d\,\tilde{W}_\alpha^{[i]}(t_d,\boldsymbol{\theta},\eta,f)b^{[i]}_{e,\alpha}(t_d,\boldsymbol{\theta},\eta,f)\,.\end{aligned} \tag{7.76}$$

We will come back on the shape of the window functions and on their frequency dependence in Chapter 9, where the frequency scaling of these terms will play a crucial role to do the component separation of the anisotropies. By factorizing the integrals w.r.t. $\boldsymbol{\theta}$ and t_d, it is possible to compute the angular power spectrum of the AGWB as an integral over the conformal time/comoving distance. This allows to implement the computation in the Boltzmann solver CLASS in analogy to what has been done for LSS observables in CLASSgal [311]. Following [75], in analogy with Eq. (3.33), it is possible to expand the anisotropies of the AGWB in terms of source functions,

$$\begin{aligned}\delta^{[i]}_{{\rm AGWB},\ell m} = 4\pi(-i)^\ell\int\frac{d^3k}{(2\pi)^3}e^{i\mathbf{k}\cdot\mathbf{x}_0}\Big[Y^*_{\ell m}(\hat{k})\Big(&\Delta^{\rm den}_\ell+\Delta^{D1}_\ell+\Delta^{D2}_\ell+\Delta^{\rm rsd}_\ell+\\ &+\Delta^{G1}_\ell+\Delta^{G2}_\ell+\Delta^{G3}_\ell+\Delta^{G4}_\ell+\Delta^{G5-S}_\ell\\ &+\Delta^{o}_\ell\Big)\zeta(\mathbf{k})+\sum_\lambda {}_{-\lambda}Y^*_{\ell m}(\hat{k})H_\lambda(\mathbf{k})\Delta^{G5-T}_\ell\Big]\,,\end{aligned} \tag{7.77}$$

where ζ and H_λ are the same primordial scalar and tensor perturbations used to compute the CMB and the CGWB anisotropies in the previous chapters. The source functions have

been defined according to

$$
\begin{aligned}
\Delta_\ell^{\rm den} &= \int_0^{\eta_0} \mathrm{d}\eta\, \tilde{W}_\alpha^{[i]\,\rm eff} \left(b^{[i]\,\rm eff}\delta_m + 3\frac{aH}{k^2}\theta_m \right) j_\ell(k\bar{\chi})\,, \\
\Delta_\ell^{\rm D1} &= \int_0^{\eta_0} \mathrm{d}\eta\, \tilde{W}_\alpha^{[i]\,\rm eff} \frac{1}{k}\theta_m \left(-b_{e,\alpha}^{[i]\,\rm eff} + \frac{H'}{aH^2} + 3 \right) \frac{d}{d[k\bar{\chi}]} j_\ell(k\bar{\chi})\,, \\
\Delta_\ell^{\rm D2} &= \int_0^{\eta_0} \mathrm{d}\eta\, \tilde{W}_\alpha^{[i]\,\rm eff} (b_{e,\alpha}^{[i]\,\rm eff} - 3)\frac{aH}{k^2}\theta_m j_\ell(k\bar{\chi})\,, \\
\Delta_\ell^{\rm rsd} &= \int_0^{\eta_0} \mathrm{d}\eta\, \tilde{W}_\alpha^{[i]\,\rm eff} \frac{1}{aH}\theta_m \frac{d^2}{d[k\bar{\chi}]^2} j_\ell(k\bar{\chi})\,, \\
\Delta_\ell^{\rm G1} &= \int_0^{\eta_0} \mathrm{d}\eta\, \tilde{W}_\alpha^{[i]\,\rm eff} \Psi \left(4 - b_{e,\alpha}^{[i]\,\rm eff} + \frac{H'}{aH^2} \right) j_\ell(k\bar{\chi})\,, \\
\Delta_\ell^{\rm G2} &= 0\,, \\
\Delta_\ell^{\rm G3} &= \int_0^{\eta_0} \mathrm{d}\eta\, \tilde{W}_\alpha^{[i]\,\rm eff} \frac{1}{aH}\Phi' j_\ell(k\bar{\chi})\,, \\
\Delta_\ell^{\rm G4} &= 0\,, \\
\Delta_\ell^{\rm G5-S} &= \int_0^{\eta_0} \mathrm{d}\eta\, \tilde{W}_\alpha^{[i]\,\rm eff} \left(-b_{e,\alpha}^{[i]\,\rm eff} + \frac{H'}{aH^2} + 3 \right) \int_0^{\tilde{\eta}} \mathrm{d}\tilde{\eta}\, j_\ell(k\bar{\chi}) \left(\Phi'(\tilde{\eta}) + \Psi'(\tilde{\eta}) \right)\,, \\
\Delta_\ell^{\rm o\,mon} &= \int_0^{\eta_0} \mathrm{d}\eta\, \tilde{W}_\alpha^{[i]\,\rm eff} \left(\delta a_o + \Psi_o \right) \left(b_{e,\alpha}^{[i]\,\rm eff} - \frac{H'}{aH^2} - 3 \right) \frac{1}{2\ell+1}\delta_{\ell 0}\,, \\
\Delta_\ell^{\rm o\,dipole} &= \int_0^{\eta_0} \mathrm{d}\eta\, \tilde{W}_\alpha^{[i]\,\rm eff} \left(b_{e,\alpha}^{[i]\,\rm eff} - \frac{H'}{aH^2} - 3 \right) \frac{1}{k}\theta_{m\,o} \frac{1}{2\ell+1}\delta_{\ell 1}\,,
\end{aligned}
\tag{7.78}
$$

where we have connected the Hubble rate to the conformal Hubble rate by using Eq. (2.10) and we have neglected the ISW effect due to the tensor perturbations. The notation used for the different contributios is the same used in [311]. The density terms represents the anisotropies induced by the density perturbation of the matter field which traces the sources, while the D and the rsd contributions are the redshift space distorsion terms induced by the peculiar motion of the sources, while the G-source functions encode the information about the redshifting of gravitons induced by the metric perturbations, like the ISW. The last two terms represent the monopole and the dipole at the observer and contain information about the local perturbations of the metric and peculiar velocity respectively. The perturbation of the monopole can be reabsorbed in the definition of $\bar{\Omega}^{\alpha}_{\rm AGWB}$, therefore it is not observable, while the dipole plays an important role and will be discussed in Chapter 9. In Figure 7.5, we plot the different contributions to the angular power spectrum of the AGWB at the pivot frequency 25 Hz. As expected from the galaxy number count, the anisotropies of the AGWB are dominated by the overdensity of the CDM, while the RSD and the GR corrections play a negligible role.

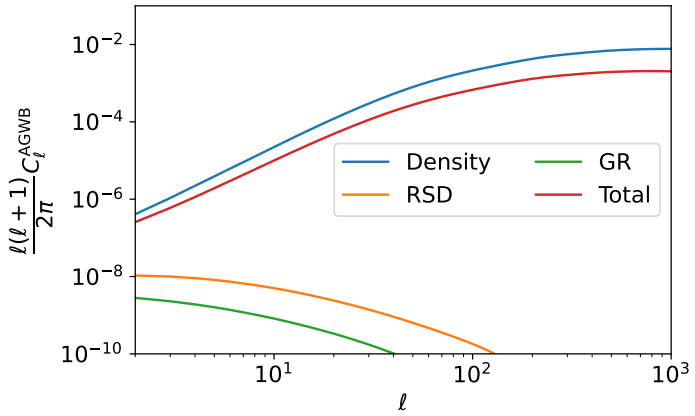

Figure 7.5: Plot of the different contributions to the angular power spectrum of the AGWB at $f_p = 25\,\mathrm{Hz}$.

Chapter 8

Circular polarization of the AGWB

In the discussion of the anisotropies of the CGWB we have mainly focused on the fluctuations in the intensity, neglecting the other Stokes parameters defined in Eq (1.43). However, many cosmological models, like axion-inflation [24, 76, 77, 78, 79] or Chern-Simons operators [80, 81, 82], could produce a circularly-polarized monopole of the CGWB. At the anisotropic level, it is expected that, in analogy with the CMB, the polarization of gravitons can be generated by the propagation of the signal through the scalar perturbations (E modes) or by weak lensing and large-scale tensor perturbations (B modes) [312, 313]. Because of the lower amplitudes of these two contributions compared to the intensity, in Chapter 3, we have focused just on the perturbations of the intensity, which have the highest chance to be detected, while we consider in this Thesis that any amount of circular polarization of primordial GWs is contained in the monopole. A parity-violating signature of a SGWB could be an important feature to exploit in order to distinguish between the astrophysical or cosmological origin of the signal, because, as we will show, the AGWB, for an isotropic distribution of the inclination angle of the binaries is expected to be unpolarized in GR. Nevertheless, anisotropies in the distribution of the GW emitters could induce a net amount of circular polarization which could be detected by future interferometers [5]. A proper characterization of these anisotropies and circularly-polarized background is necessary to subtract efficiently the astrophysical contaminations to the data, which could hid the more interesting GWs from the early Universe. In addition, the polarization of the AGWB could be used to study the statistical isotropy of the Universe and the population of the binaries. In this chapter we focus on the dominant contribution to the anisotropies of the AGWB, induced by the Poisson fluctuations in the number of sources, which is much larger compared to the intrinsic anisotropies computed in Section 7.4 and the kinetic dipole discussed in Chapter 9. The low number of BBH in the local Universe, Eq. (7.21), makes clear that the fluctuations of the sources would generate a large fluctuation of the order of $10^{-2} - 10^{-3}$.

8.1 Stokes parameters of the monopole of the AGWB

The definition of the Stokes parameters provided in Eq. (1.43), shows that the intensity, the circular and linear polarization of a single source can be written as the following combinations of h_+ and $h_\times$,

$$\begin{aligned}
S_I(\boldsymbol{\theta},\hat{n},f) =& |h_+(\boldsymbol{\theta},\hat{n},f)|^2 + |h_\times(\boldsymbol{\theta},\hat{n},f)|^2 = \left|\tilde{h}(\boldsymbol{\theta},f)\right|^2 \left[\left(\frac{1+\cos^2\iota}{2}\right)^2 + \cos^2\iota\right] ,\\
S_V(\boldsymbol{\theta},\hat{n},f) =& i\left(h_+(\boldsymbol{\theta},\hat{n},f)h_\times^*(\boldsymbol{\theta},\hat{n},f) - h_+^*(\boldsymbol{\theta},\hat{n},f)h_\times(\boldsymbol{\theta},\hat{n},f)\right) = \left|\tilde{h}(\boldsymbol{\theta},f)\right|^2 (1+\cos^2\iota)\cos\iota ,\\
S_U(\boldsymbol{\theta},\hat{n},f) =& h_+(\boldsymbol{\theta},\hat{n},f)h_\times^*(\boldsymbol{\theta},\hat{n},f) + h_+^*(\boldsymbol{\theta},\hat{n},f)h_\times(\boldsymbol{\theta},\hat{n},f) = -i\left|\tilde{h}(\boldsymbol{\theta},f)\right|^2 (1+\cos^2\iota)\cos\iota ,\\
S_Q(\boldsymbol{\theta},\hat{n},f) =& |h_+(\boldsymbol{\theta},\hat{n},f)|^2 - |h_\times(\boldsymbol{\theta},\hat{n},f)|^2 = \left|\tilde{h}(\boldsymbol{\theta},f)\right|^2 \left[\left(\frac{1+\cos^2\iota}{2}\right)^2 - \cos^2\iota\right] ,
\end{aligned} \tag{8.1}$$

where we have used the parametrization of the waveform given in Eqs. (7.37), (7.38), with $\tilde{h}$ computed for the inspiral, merger and ringwdown stages by using Eqs. (7.39), (7.40). In GR, the individual binary could emit circularly-polarized (V) and linearly-polarized GWs (Q), because of the inclination angle of the system. In some modified theories of gravity in which parity is violated, there is a mixing between the $+$ and $\times$ modes that generate a nontrivial dependence of the Stokes parameters on the inclination angle [314, 315]. In these models of birefringent GWs, the amount of circular polarization could be enhanced and used to constrain the alternative theories of gravity [316]. Moreover, higher-order multipoles could play a role in a different dependence of the waveform on the inclination angle [317, 8, 318]. From now on, we will consider the standard case of GR and we quantify the polarization of the AGWB by using the parameter

$$Q_\alpha(\iota) \equiv \begin{cases} \left(\frac{1+\cos^2\iota}{2}\right)^2 + \cos^2\iota & \alpha = I \\ (1+\cos^2\iota)\cos\iota & \alpha = V \\ -i\,(1+\cos^2\iota)\cos\iota & \alpha = U \\ \left(\frac{1+\cos^2\iota}{2}\right)^2 - \cos^2\iota & \alpha = Q \end{cases} \tag{8.2}$$

The Stokes parameters of the AGWB depend on the energy spectrum of the individual binaries, given by Eq. (7.44), which are related to the inclination angle of the binaries through the Q_α parameter defined in Eq. (8.2). The total energy spectrum can be computed by using Eq. (7.4), therefore the dependence on the inclination angle can be factorized and the AGWB is sensitive to the following integral

$$\bar{\Omega}^\alpha_{\rm AGWB} \sim \int \mathrm{d}\iota\, p(\iota)\, Q_\alpha(\iota) = \begin{cases} \frac{4}{5} & \alpha = I \\ 0 & \alpha = V \\ 0 & \alpha = U \\ \frac{2}{15} & \alpha = Q \end{cases} \tag{8.3}$$

where we have used the isotropic distribution of the inclination angle, Eq. (7.16). It is clear therefore that the amount of circular polarization is zero if the inclination angle of the binaries is distributed isotropically, while a tiny amount of linear polarization is produced, $\bar{\Omega}^{Q}_{\rm AGWB} = \bar{\Omega}^{I}_{\rm AGWB}/6$. Any deviation of the V and U modes from zero would indicate new aspects about GR of the population of the binaries that has not been completely understood.

8.2 Shot noise of the AGWB

In Eq. (7.4), we have introduced the number of sources which contribute to the AGWB and which emit GWs at redshift z, after a time delay t_d from their formation, with intrinsic parameters $\boldsymbol{\theta}$ and along the direction of observation $\hat{n}$. This number corresponds to the GW events which occur per unit time and around an infinitesimal volume centred at redshift z along the direction $\hat{n}$. Since the number of GW events that occur are independent and take place with constant rate, $N^{\rm unres}_{\rm GW}$ is a Poisson random variable, whose mean and covariance depend on the population of the sources. To see more explicitly this, we write the number of events in terms of a number density,

$$N^{\rm unres}_{\rm GW}(\hat{n}, t_d, \boldsymbol{\theta}, z) = \frac{{\rm d}N^{[i]}_{\rm GW}}{{\rm d}t_d\, {\rm d}\boldsymbol{\theta}\, {\rm d}z}(\hat{n}, t_d, \boldsymbol{\theta}, z)\, \Delta t_d\, \Delta\boldsymbol{\theta}\, \Delta z\,. \tag{8.4}$$

Consistently with Eqs. (7.19), (7.20), we trace the distribution of sources starting from the SFR per halo and convolving it with the halo mass function, for all the possible halo masses,

$$\frac{{\rm d}N_{\rm GW}}{{\rm d}t_d {\rm d}\boldsymbol{\theta} {\rm d}z}(\hat{n}, t_d, \boldsymbol{\theta}, z) = \sum_{M_h} \frac{{\rm d}N_{\rm GW}}{{\rm d}M_h {\rm d}t_d {\rm d}\boldsymbol{\theta} {\rm d}z}(\hat{n}, M_h, t_d, \boldsymbol{\theta}, z)\Delta M_h\,, \tag{8.5}$$

where we have defined the discrete summation in the following way,

$$\sum_{M_h} \frac{{\rm d}N_{\rm GW}(M_h)}{{\rm d}M_h {\rm d}t_d {\rm d}\boldsymbol{\theta} {\rm d}z}\Delta M_h \equiv \sum_{i=1}^{i_{\rm max}} \frac{{\rm d}N_{\rm GW|h}(M_h^{(i)})}{{\rm d}M_h {\rm d}t_d {\rm d}\boldsymbol{\theta} {\rm d}z}\Delta M_h^{(i)}\,, \tag{8.6}$$

and we have defined the number of GW events per each bin in all the halos of mass M_h as

$$\frac{{\rm d}N_{\rm GW}(M_h)}{{\rm d}M_h {\rm d}t_d {\rm d}\boldsymbol{\theta} {\rm d}z}\Delta M_h \equiv \sum_{i=1}^{N_h(\hat{n}, M_h, t_d, z)} \frac{{\rm d}N^{i}_{\rm GW|h}}{{\rm d}t_d {\rm d}\boldsymbol{\theta} {\rm d}z}(M_h)\,. \tag{8.7}$$

The number of GW events per halo and the number of halos are both Poisson random variables,

$$\begin{aligned} p(N^{i}_{\rm GW|h}, \bar{N}_{\rm GW|h}) =& \frac{\bar{N}^{N^{i}_{\rm GW|h}}_{\rm GW|h} e^{-\bar{N}_{\rm GW|h}}}{N^{i}_{\rm GW|h}!}\,, \\ p(N_h, \bar{N}_h) =& \frac{\bar{N}^{N_h}_{h} e^{-\bar{N}_{h}}}{N_h!}\,, \end{aligned} \tag{8.8}$$

whose mean and covariance are given by

$$\begin{aligned}\bar{N}_{\mathrm{GW}|h}(M_h,t_d,\boldsymbol{\theta},z) =& \frac{R_{\mathrm{LVK}}(0)\langle \mathrm{SFR}(M_h,t_d,z)\rangle}{\int dt_d p(t_d) R_\star[z_d(z=0,t_d))]} p(t_d)p(\boldsymbol{\theta})w(\boldsymbol{\theta},z)T_{\mathrm{obs}}\frac{\mathrm{d}V}{\mathrm{d}z\mathrm{d}\Omega_e}(z)\Delta t_d\,\Delta\boldsymbol{\theta}\,\Delta z\,,\\ \bar{N}_h(M_h,t_d,z) =& \frac{\mathrm{d}\bar{N}_h}{\mathrm{d}M_h}(M_h,t_d,z)\Delta M_h\,,\end{aligned} \tag{8.9}$$

with $\mathrm{d}\bar{N}_h/\mathrm{d}M_h$ the halo mass function. By looking at Eqs. (8.4), (8.5), it is clear that the number density of mergers is the combination of two Poisson variables and it follows a compound Poisson distribution [65, 66]. The expectation value of the CPD is the product of the expectation values of the two Poisson distributions,

$$\bar{N}^{\mathrm{unres}}_{\mathrm{GW}}(t_d,\vec{\theta},z) = \sum_{M_h}\bar{N}_h(M_h,t_d,z),\bar{N}_{\mathrm{GW|h}}(M_h,t_d,\vec{\theta},z)\,. \tag{8.10}$$

This result has been used to compute of the homogeneous and isotropic part of the AGWB, shown in Figures 7.1, 7.2 and whose Stokes parameters have been evaluated in Eq. (8.3). The covariance of the compound Poisson distribution then gives

$$\begin{aligned}\sigma^2_{N^{\mathrm{unres}}_{\mathrm{GW}}N^{\mathrm{unres}\,\prime}_{\mathrm{GW}}} \equiv& \mathrm{cov}\left[N^{\mathrm{unres}}_{\mathrm{GW}}(\hat{n},t_d,\vec{\theta},z),N^{\mathrm{unres}}_{\mathrm{GW}}(\hat{n}',t'_d,\vec{\theta}',z')\right]\\ =& \sum_{M_h}\bar{N}_h\left(\bar{N}_{\mathrm{GW|h}}+\bar{N}^2_{\mathrm{GW|h}}\right)\delta_{\hat{n}\hat{n}'}\delta_{\mathrm{t_d}\mathrm{t}'_\mathrm{d}}\delta_{\vec{\theta}\vec{\theta}'}\delta_{zz'}\,,\end{aligned} \tag{8.11}$$

where we have introduced the short notation for the Kronecker delta,

$$\begin{cases} X\equiv x_i\\ X'\equiv x_j\end{cases}\quad\rightarrow\delta_{XX'}\equiv\delta_{ij}\,. \tag{8.12}$$

The term proportional to the square of the number of GW events per halo is subdominant, because the number of BBH per halo is very low. The amount of polarization of the AGWB induced by the shot noise is then computed from the covariance of the Poisson fluctuations in the number of sources,

$$\begin{aligned}C^{\alpha\alpha'}_{ff',\hat{n}\hat{n}'} \equiv& \mathrm{cov}\left[\Omega^\alpha_{\mathrm{AGWB}}(\hat{n},f),\Omega^{\alpha'}_{\mathrm{AGWB}}(\hat{n}',f')\right] =\\ =& \sum_{t_d,\vec{\theta},z}\sum_{t'_d,\vec{\theta}',z'}\frac{1}{(1+z)H(z)}\frac{1}{(1+z')H(z')}\frac{ff'}{(\rho_{\mathrm{crit}}c^2)^2}\frac{\mathrm{d}E^V}{\mathrm{d}f_e\mathrm{d}\Omega_e}\left(\vec{\theta},z,f\right)\frac{\mathrm{d}E^V}{\mathrm{d}f_e\mathrm{d}\Omega_e}\left(\vec{\theta},z,f'\right)\\ &\frac{\sigma^2_{N_{\mathrm{GW}}N'_{\mathrm{GW}}}}{T^2_{\mathrm{obs}}\frac{\mathrm{d}V}{\mathrm{d}z\mathrm{d}\Omega_e}(z)\frac{\mathrm{d}V}{\mathrm{d}z\mathrm{d}\Omega_e}(z')} =\\ =& \sum_{t_d,\vec{\theta},z}\frac{1}{[(1+z)H(z)]^2}\frac{\frac{\mathrm{d}E^\alpha}{\mathrm{d}f_e\mathrm{d}\Omega_e}\left(\vec{\theta},z,f\right)\frac{\mathrm{d}E^{\alpha'}}{\mathrm{d}f_e\mathrm{d}\Omega_e}\left(\vec{\theta},z,f'\right)}{\left[T_{\mathrm{obs}}\frac{\mathrm{d}V}{\mathrm{d}z\mathrm{d}\Omega_e}(z)\right]^2}\frac{ff'}{(\rho_{\mathrm{crit}}c^2)^2}\\ &\bar{N}_h(M_h,t_d,z)\left[\bar{N}_{\mathrm{GW|h}}(M_h,t_d,\vec{\theta},z)+\bar{N}^2_{\mathrm{GW|h}}(M_h,t_d,\vec{\theta},z)\right]\delta_{\hat{n}\hat{n}'}\,.\end{aligned} \tag{8.13}$$

The interesting result is that the integral over the inclination angle which determines the Stokes parameters in this case depends on a different combination of the Q_α's, because the shot noise fluctuation is sensitive to the square of the energy spectrum,

$$C^{\alpha\alpha'}_{ff',\hat{n}\hat{n}'} \sim \int \mathrm{d}\iota \; p(\iota) Q_\alpha(\iota) Q_{\alpha'}(\iota) \,. \tag{8.14}$$

What emerges is that the covariance of the fluctuations of the V and U Stokes parameters is non-null, therefore a net amount of circular polarization is generated. More specifically, the covariance $C^{\alpha\alpha'}_{ff',\hat{n}\hat{n}'}$ is proportional to the factors

$$\begin{pmatrix} II & IV & IQ & IU \\ VI & VV & VQ & VU \\ QI & QV & QQ & QU \\ UI & UV & UQ & UU \end{pmatrix} = \begin{pmatrix} \frac{284}{315} & 0 & -\frac{183}{256}\pi & 0 \\ 0 & \frac{92}{105} & 0 & -i\frac{92}{105} \\ -\frac{183}{256}\pi & 0 & \frac{8}{315} & 0 \\ 0 & -i\frac{92}{105} & 0 & -\frac{92}{105} \end{pmatrix} . \tag{8.15}$$

This expression tells us that the I and Q parameters are slightly correlated, while the correlation between U and V is exactly one. When the number of sources is very large, the central limit theorem holds and the Poisson distribution is approximated by a Gaussian distribution, therefore the amount of circular polarization induced in the AGWB is a realization of a Gaussian random field of zero mean and covariance given by Eq. (8.13), where the covariance between different Stokes parameters is proportional to the factors given in Eq. (8.15). In Figure 8.1, we plot the intensity of the monopole of the AGWB and the amplitude of the circular polarization induced by the shot noise. At low frequencies, when all the binaries emit in the inspiral stage, there is an exact correlation between the shot noise fluctuations ar different frequencies,

$$C^{\alpha\alpha'}_{ff',\hat{n}\hat{n}'} = f^{2/3} f'^{2/3} \tilde{C}^{\alpha\alpha'}_{\hat{n}\hat{n}'} \,. \tag{8.16}$$

This happens because all the BBH emit in the inspiral stage, therefore any frequency dependence can be factor out and the amplitude of the fluctuations at one frequency univocally determine the others. The amplitude of the circular polarization has therefore the same scaling of the monopole,

$$\Omega^V_{\mathrm{AGWB}}(\hat{n}, f) \sim \sqrt{C^{VV}_{ff,\hat{n}\hat{n}}} \sim f^{2/3} \,. \tag{8.17}$$

At around 200 Hz, when binaries of different intrinsic parameters emit in different stages of evolution of the binary, the situation becomes more complicated and the correlation is no longer equal to one. We will consider in more detail this frequency dependence of the anisotropies of the AGWB (including the shot noise) in Section 9.3.

8.3 Detectability of the circular polarization of the AGWB

The detectability of homogeneous and isotropic SGWBs has been discussed in Section 1.3.2, where an optimal estimator for a uniform (in the sky) GW map has been defined. In this

section, we will go through the same procedure in order to build an estimator for $\Omega^{\alpha}_{\rm AGWB}$, in the case in which the Stokes parameter could depend on the direction of observation. The underlying assumption we make is that the correlation of the shot noise at different frequencies is exactly one, and we write the AGWB signal in a similar fashion of Eq. (1.55), by decomposing the background in terms of a function which encodes the frequency scaling and an amplitude evaluated at the pivot frequency f_p,

$$\Omega^{\alpha}_{\rm AGWB}(\hat{n}, f) = \bar{\Omega}^{I}_{\rm AGWB}(f) + \bar{\Omega}^{Q}_{\rm AGWB}(f) + A_{\alpha}(\hat{n})\mathcal{E}^{\alpha}_{p}(f)\,. \tag{8.18}$$

In this discussion, we neglect the monopole contributions $\bar{\Omega}^{I}_{\rm AGWB}$, $\bar{\Omega}^{Q}_{\rm AGWB}$, because it is a good approximation to assume that there is no leakage of the intensity map into the one of the circular polarization. A more detailed discussion of the component separation between different contributions to the SGWB will be done in Section 8.4 and in Chapter 9. The observed data in the interferometer A, defined in Eq. (1.53), have mean and covariance given by

$$\begin{aligned}
\langle d_A(f)\rangle =& 0\,,\\
\langle d_A(f)\, d^{*}_{B}(f')\rangle =& \frac{1}{2}\delta(f-f')\left(N_{AB}(f) + \sum_{\alpha}\int \mathrm{d}\hat{n}\, \tilde{B}^{\alpha}_{AB}(\hat{n}, f)\, A_{\alpha}(\hat{n})\, \mathcal{E}^{\alpha}_{p}(f)\right)\,,
\end{aligned} \tag{8.19}$$

where the tensors $\tilde{B}^{\alpha}_{AB}$ have been defined in terms of the detector pattern function defined in Eq. (1.54) according to

$$\begin{aligned}
\tilde{B}^{I}_{AB}(\hat{n}, f) \equiv& \frac{3H_0^2}{4\pi^2 f^3}\left(F^{+}_{A}(\hat{n}, f)F^{+\,*}_{B}(\hat{n}, f) + F^{\times}_{A}(\hat{n}, f)F^{\times\,*}_{B}(\hat{n}, f)\right)\,,\\
\tilde{B}^{V}_{AB}(\hat{n}, f) \equiv& \frac{3H_0^2}{4\pi^2 f^3}\left(F^{+}_{A}(\hat{n}, f)F^{\times\,*}_{B}(\hat{n}, f) - F^{\times}_{A}(\hat{n}, f)F^{+\,*}_{B}(\hat{n}, f)\right)\, i\,,\\
\tilde{B}^{U}_{AB}(\hat{n}, f) \equiv& \frac{3H_0^2}{4\pi^2 f^3}\left(F^{+}_{A}(\hat{n}, f)F^{\times\,*}_{B}(\hat{n}, f) + F^{\times}_{A}(\hat{n}, f)F^{+\,*}_{B}(\hat{n}, f)\right)\,,\\
\tilde{B}^{Q}_{AB}(\hat{n}, f) \equiv& \frac{3H_0^2}{4\pi^2 f^3}\left(F^{+}_{A}(\hat{n}, f)F^{+\,*}_{B}(\hat{n}, f) - F^{\times}_{A}(\hat{n}, f)F^{\times\,*}_{B}(\hat{n}, f)\right)\,.
\end{aligned} \tag{8.20}$$

As we have done for $\bar{\Omega}^{I/Q}_{\rm AGWB}$, we neglect any contamination of the shot noise of the Stokes parameters $\alpha \neq V$ to the reconstructed map of the circular polarization. We leave the joint estimate of all the Stokes parameters together for a future work. The optimal estimator of the map $A_{\alpha}(\hat{n})$ is a quadratic object in the data, which exploit the auto- and the cross-correlation channels of the detectors,

$$\hat{A}_{\alpha}(\hat{n}) = \sum_{A,B}\int \mathrm{d}f\, d_A(f)\, E^{\alpha}_{AB}(\hat{n}, f)\, d^{*}_{B}(f) - b^{\alpha}(\hat{n})\,. \tag{8.21}$$

The functions E and b have to be chosen to minimize the covariance and the bias of the estimator respectively. By imposing that $\left\langle \hat{A}_{\alpha}(\hat{n})\right\rangle = A_{\alpha}(\hat{n})$, we get the constraints on the

bias

$$b^{\alpha}(\hat{n}) = T_{\rm seg} \sum_{A,B} \int \mathrm{d}f \, \frac{E^{\alpha}_{AB}(\hat{n}, f)}{2} N_{AB}(f) \,, \tag{8.22}$$

and on the weights

$$\sum_{A,B} \int \mathrm{d}f \, \frac{T_{\rm seg}}{2} E^{\alpha}_{AB}(\hat{n}, f) \mathcal{E}^{\alpha}_{p}(f) \tilde{B}^{\alpha}_{AB}(\hat{m}, f) = \delta(\hat{n} - \hat{m}) \,. \tag{8.23}$$

The factor $T_{\rm seg}$ comes from the Dirac delta evaluated in zero. In a similar fashion of Eq. (1.62), the covariance of the estimator of the circular polarization depends on the four-point function of the data and by using Eq. (8.19), the covariance has the simple form

$$\begin{aligned} \hat{\mathcal{C}}^{\alpha\alpha'}(\hat{n}, \hat{n}') = \int \mathrm{d}f \sum_{A,B,C,D} & E^{\alpha}_{AB}(\hat{n}, f) E^{\alpha}_{CD}(\hat{n}') \, 2 \, T_{\rm seg} \\ & \int \mathrm{d}\hat{m} \, \mathrm{d}\hat{m}' \Big[\tilde{B}^{\alpha}_{AD}(\hat{m}, f) \tilde{B}^{\alpha}_{CD}(\hat{m}', f) \, (A_{\alpha})^2 \, \mathcal{E}^{\alpha}_{p}(f) \mathcal{E}^{\alpha'}_{p}(f) + \frac{1}{4} N_{AD}(f) N_{BC}(f) \Big] \,. \end{aligned} \tag{8.24}$$

The choice of the weights E can be done by minimizing the covariance, considering also the constraints provided by Eq. (8.23). The optimal way to do this is to introduce a Lagrangian function, as in Section 1.3.2,

$$\mathcal{L} = \hat{\mathcal{C}}^{\alpha\alpha'}(\hat{n}, \hat{m}) + \lambda \left[T_{\rm seg} \int \mathrm{d}\hat{n}' \sum_{A,B} \int \mathrm{d}f \, \frac{1}{2} E^{\alpha}_{AB}(f, f; \hat{n}) \mathcal{E}^{\alpha}_{p}(f) \tilde{B}^{\alpha}_{AB}(\hat{n}', f) - 1 \right] \,. \tag{8.25}$$

and minimize it w.r.t. the weights and the Lagrange multiplier,

$$\frac{\delta}{\delta E^{\alpha}_{AB}(\hat{n}, f)} \mathcal{L} = \frac{\delta}{\lambda} \mathcal{L} = 0 \,. \tag{8.26}$$

From now on, we work in the low signal regime, $A_{\alpha} \ll N_{AB}$, therefore we neglect any contribution induced by cosmic variance in the AGWB signal. The condition on the functional derivative w.r.t. E gives

$$\sum_{C,D} E^{\alpha}_{CD}(\hat{m}, f) N_{AD}(f) N_{CB}(f') + \lambda \, \tilde{B}^{\alpha}_{AB}(\hat{n}, f) \mathcal{E}_{p}(f) = 0 \,. \tag{8.27}$$

We can isolate in this expression the contribution coming from the weights, by using the inverse matrix of the noise PSD,

$$\mathcal{E}_{p}(f) E^{\alpha}_{AB}(\hat{m}, f) + \lambda \, [\mathcal{E}_{p}(f)]^2 \sum_{C,D} N^{-1}_{AC}(f) \tilde{B}^{\alpha}_{CD}(\hat{n}, f) N^{-1}_{DB}(f) = 0 \,. \tag{8.28}$$

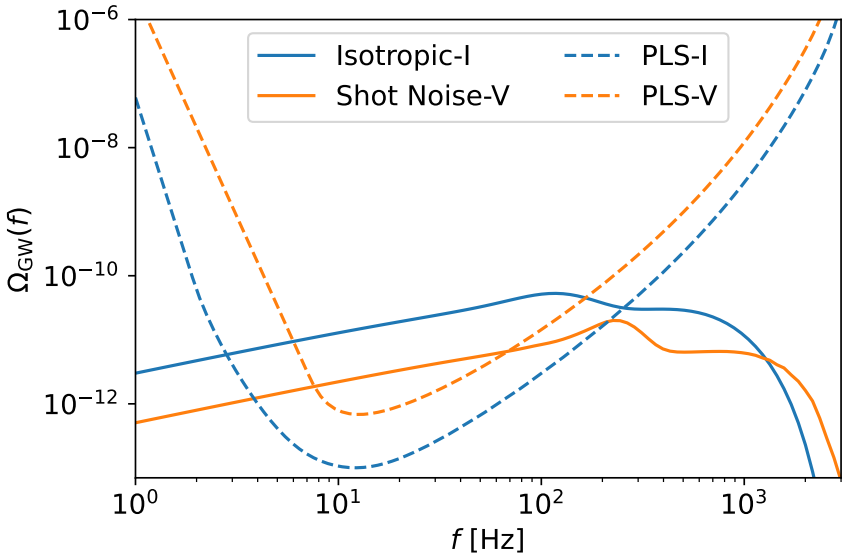

Figure 8.1: Plot ot the dominant contributions to the intensity and circular polarization of the AGWB and of the PLS curves for the network ET+CE for the intensity and circular polarization. The sensitivities of ET+CE have been computed for $T_{\rm obs} = 1\,\rm yr$.

By multiplying this equation by $T_{\rm seg}\,\tilde{B}^{\alpha}_{AB}(\hat{n}, f')$, summing over A, B and integrating over the frequency we get

$$\lambda = -\frac{1}{T_{\rm seg}} \frac{2}{\int \mathrm{d}f\, [\mathcal{E}_p(f)]^2 \sum_{A,B,C,D} \tilde{B}^{\alpha}_{AB}(\hat{n}, f) N^{-1}_{BC}(f) \tilde{B}^{\alpha}_{CD}(\hat{n}, f) N^{-1}_{DA}(f)}\,. \tag{8.29}$$

The weights are then given by

$$E^{\alpha}_{AB}(\hat{n}, f) = \frac{1}{T_{\rm seg}} \frac{2\,\mathcal{E}_p(f) \sum_{C,D} N^{-1}_{AC}(f) \tilde{B}^{\alpha}_{CD}(\hat{n}, f) N^{-1}_{DB}(f)}{\int \mathrm{d}f\, [\mathcal{E}_p(f)]^2 \sum_{A,B,C,D} \tilde{B}^{\alpha}_{AB}(\hat{n}, f) N^{-1}_{BC}(f) \tilde{B}^{\alpha}_{CD}(\hat{n}, f) N^{-1}_{DA}(f)}\,. \tag{8.30}$$

The covariance of the estimator can be computed by plugging (1.70) into (1.63), finding

$$\mathcal{C}_{\hat{A}_\alpha}(\hat{n}, \hat{m}) = \frac{1}{T_{\rm obs}} \frac{2\,\delta(\hat{n} - \hat{m})}{\int \mathrm{d}f\, [\mathcal{E}_p(f)]^2 \sum_{A,B,C,D} \tilde{B}^{\alpha}_{AB}(\hat{n}, f) N^{-1}_{BC}(f) \tilde{B}^{\alpha}_{CD}(\hat{n}, f) N^{-1}_{DA}(f)}\,, \tag{8.31}$$

where the factor $1/T_{\rm obs}$ comes from the fact that Eq. (1.63) describes the covariance in a single time segment of duration $T_{\rm seg}$, while the total information we get on the SGWB is obtained by integrating the information at different times for the total duration of our observations, $T_{\rm obs}$. In Figure 8.1, we plot the PLS for ET+CE for $T_{\rm obs} = 1\,\rm yr$ for the covariance matrix defined in Eq. (8.31) for $\alpha = V$. In the same Figure we plot the monopole of the AGWB for $\mathrm{SNR}^{\rm res}_{\rm thr} = 80$ with the associated PLS.

8.4 Foreground subtraction of the astrophysical signal

The circular polarization of the AGWB represents at the same time an interesting target for future ground- and space-based interferometers and a foreground for the detection of the Stokes parameters of primordial signals. For instance, if a CGWB is sourced by axion-inflation [24, 76, 77, 78, 79] or Chern-Simons operators [80, 81, 82], a non-negligible amount of circular polarization is produced. In this section, we would like to quantify the detectability of the Stokes parameters of the cosmological gravitons in presence of a circularly-polarized AGWB. To simplify the computations, we assume that the CGWB is homogeneous and isotropic and we characterize its frequency scaling by a power-law spectrum with a constant tensor tilt,

$$\bar{\Omega}^I_{\rm CGWB}(f) = \bar{A}^I_{\rm CGWB}\left(\frac{f}{1\,\rm Hz}\right)^{n_t^I}\,, \qquad \bar{\Omega}^V_{\rm CGWB}(f) = \bar{A}^V_{\rm CGWB}\left(\frac{f}{1\,\rm Hz}\right)^{n_t^V}\,, \tag{8.32}$$

with $\bar{A}^I_{\rm CGWB}$, $\bar{A}^V_{\rm CGWB}$ the amplitudes of the background at 1 Hz. In general, n_t^I and n_t^V can be different, but we assume here that they are equal, $n_t^I = n_t^V = n_t$. In this case, the total incoming signal at the interferometers is

$$h_p^{\rm tot}(f,\hat{n}) = h_p^{\rm AGWB}(f,\hat{n}) + \bar{h}_p^{\rm CGWB}(f)\,, \tag{8.33}$$

which corresponds to the following covariance matrix of the data,

$$\begin{aligned}\left\langle d_A(f)\, d_B^*(f')\right\rangle = \frac{\delta(f-f')}{2}\Bigg\{ & N_{AB}(f) + \\ & \int \mathrm{d}\hat{n}\, \tilde{B}^{\alpha}_{AB}(\hat{n},f)\Bigg[\Bigg(\bar{\Omega}^I_{\rm AGWB}(f_p) + \bar{\Omega}^Q_{\rm AGWB}(f_p) \\ & + \Omega^V_{\rm AGWB}(\hat{n},f_p) + \Omega^U_{\rm AGWB}(\hat{n},f_p)\Bigg)\left(\frac{f}{f_p}\right)^{2/3} + \\ & + \left(\bar{A}^I_{\rm CGWB} + \bar{A}^V_{\rm CGWB}\right)\left(\frac{f}{f_p}\right)^{n_t}\Bigg]\Bigg\}\,.\end{aligned} \tag{8.34}$$

In this chapter, we do not consider the propagation of errors on $\bar{A}^I_{\rm CGWB}$ and n_t on the estimate of $\bar{A}^V_{\rm CGWB}$. We build therefore the estimator for the amplitude of the circular polarization in a similar way to what has been done in Eq. (1.59), by considering as source of noise just the presence of the circular polarization of the AGWB. The estimator is

$$\hat{A}^V_{\rm CGWB} = \int \mathrm{d}f \sum_{A,B} d_A(f) E^V_{AB}(f) d^*_B(f) - b^V\,. \tag{8.35}$$

As seen in Section 1.3, it can be shown that the covariance of our estimator due to instrumental noise is given by Eq. (1.72),

$$\mathcal{C}^{\hat{A}_V}_{h^4} = \frac{1}{T_{\rm obs}} \frac{2}{\int \mathrm{d}f \left(\frac{f}{f_p}\right)^{2\,n_t} \sum_{A,B,C,D} \gamma^V_{AB}(f) N^{-1}_{BC}(f) \gamma^V_{CD}(f) N^{-1}_{DA}(f)}\,, \tag{8.36}$$

where h^4 means that the error is related to the four-point function of the data. The presence of a circularly-polarized AGWB generates an additional source of noise in the estimator we have provided, since the average (of the square of the strain h_{ij}) gives

$$\left\langle \hat{A}^V_{\rm CGWB} \right\rangle = \bar{A}^V_{\rm CGWB} + \int {\rm d}f \sum_{A,B} \frac{T_{\rm seg}}{2} E^V_{AB}(f) \int {\rm d}\hat{n}\, \tilde{B}^V_{AB}(\hat{n}, f) \Omega^V_{\rm AGWB}(\hat{n}, f_p) \left(\frac{f}{f_p}\right)^{2/3} , \tag{8.37}$$

where we have neglected contaminations from other Stokes parameters. On average, the shot noise fluctuation is zero, but its covariance is given by Eq. (8.13), therefore it is possible to estimate the impact of the astrophysical foreground on the error on the cosmological background by using

$$\mathcal{C}^{\hat{A}_V}_{\rm cs} \equiv \left\langle \left(\left\langle \hat{A}^V_{\rm CGWB} \right\rangle - \bar{A}^V_{\rm CGWB} \right)^2 \right\rangle , \tag{8.38}$$

where cs denotes that the contribution is related to the component separation of the signals, while the average is now taken w.r.t. the realizations of the shot noise. By using the weights to minimize the instrumental noise given by Eq. (1.70), it is possible to show that the noise due to the presence of the astrophysical foreground in this case is equal to

$$\mathcal{C}^{\hat{A}_V}_{\rm cs} = \frac{\int {\rm d}f {\rm d}f' {\rm d}\hat{n} {\rm Tr}\left[S^{-1}(f) \tilde{\gamma}^V(f) S^{-1}(f) \tilde{B}(\hat{n}, f) \right] {\rm Tr}\left[S^{-1}(f') \tilde{\gamma}^V(f') S^{-1}(f') \tilde{B}(\hat{n}, f') \right] C^{VV}_{ff'}}{\left[\int {\rm d}f'' \left(\frac{f''}{f_p}\right)^{2\,n_t} \sum_{A,B,C,D} \gamma^V_{AB}(f'') N^{-1}_{BC}(f'') \gamma^V_{CD}(f'') N^{-1}_{DA}(f'') \right]^2} , \tag{8.39}$$

where we have defined

$$C^{VV}_{ff'} \equiv \int {\rm d}\hat{n}'\, C^{VV}_{ff',\hat{n}\hat{n}'} , \tag{8.40}$$

with $C^{VV}_{ff',\hat{n}\hat{n}'}$ the covariance of the shot noise computed in Eq. (8.13). In Section 9.6, we will give additional details on this computation. Eq. (8.39) shows that, since $\bar{\Omega}^V_{\rm CGWB}$ and $\Omega^V_{\rm AGWB}$ have two very different angular dependences, the numerator is suppressed w.r.t. the denominator and the covariance goes to zero. This implies that it is possible, in principle, to exploit the angular dependence of the shot noise (whose angular power spectrum is constant in ℓ), to reconstruct faithfully a stochastic background of primordial origin. When the frequency scaling of the two signals is different, the component separation of the two terms becomes more efficient, in analogy with what has been done in Section 1.3.

Chapter 9

Kinetic dipole of the AGWB

9.1 Determination of our peculiar motion with different probes

As discussed in 2.1, the cosmological principle assumes that the Universe is homogeneous and isotropic when smoothed over sufficiently large scales. Observations of the CMB [93] and LSS probes, such as radio sources [85, 86, 87, 88, 89, 90] and quasars [91, 92], show that this assumption is true, when a dipole in the temperature anisotropies of the CMB and in the distribution of galaxies in the sky is subtracted. These dipoles are associated to the velocity of the observer w.r.t. the rest frame of the CMB and LSS respectively. The LSS measurements of the kinetic dipole are affected by contaminations due to shot noise fluctuations in the number of sources, which are enhanced in the case of partial sky coverage [86], furthermore contaminitions from intrinsic anisotropies in the distribution of the sources should be carefully considered too. In the case of the CMB, it is not clear if the CMB anomalies [138, 319, 320, 321, 322, 323, 324, 325, 326] at low multipoles could affect the estimate of our peculiar velocity. Current measurements of the kinetic dipole obtained by CMB and LSS measurements are in tension [94, 90], because the CMB dipole differ significantly w.r.t. the LSS one in amplitude and direction. In this chapter, we consider the AGWB as an additional source of information for our peculiar velocity [6], exploring the possibility of cleaning the total signal observed at inferferometers from the shot noise and the intrinsic contributions by exploiting the full-sky coverage of future GW interferometers and the frequency dependence of the AGWB anisotropies. The results we have found show that it is possible, in the limit of low instrumental noise or large monopoles, to reconstruct our peculiar velocity with observations of the AGWB with higher precision than with the other cosmological probes considered nowadays.

9.2 Kinetic dipole of the AGWB

The velocity of the observer w.r.t. the rest frame of the AGWB is the superposition of many, uncorrelated, contributions. We consider here the sum of the velocity of the Earth around the Sun, of the Sun w.r.t. the center of the Milky way (MW), of the MW w.r.t.

the Local Group (LG) and of the Local Group w.r.t. the LSS,

$$\mathbf{v}_o^{\rm tot} = \mathbf{v}_E + \mathbf{v}_\odot + \mathbf{v}_{\rm MW} + \mathbf{v}_{\rm LG}\,. \tag{9.1}$$

The motion of the Earth around the Sun, $v_E \approx 30\,\mathrm{km/s}$, is considered automatically in the analysis of the detector response at GW interferometers, since the detector pattern function defined in Eq. (1.54) keeps into account for the position of the interferometers in time. An extension of the standard pipeline which uses the prior knowledge of $\mathbf{v}_E$ has been presented in [68]. In this work we assume that the motion of the Sun w.r.t. the center of the MW, $v_\odot \approx 230\,\mathrm{km/s}$, and of the MW w.r.t. the LG, $v_{\rm MW} \approx 100\,\mathrm{km/s}$, have been already subtracted from the data stream. In this way it is possible to set $\mathbf{v}_o = \mathbf{v}_{\rm LG}$, which is the only unknown velocity we are interested in. From CMB observations [93], $v_{\rm LG} \approx 622\,\mathrm{km/s}$ and $v_o^{\rm tot} \approx 370\,\mathrm{km/s}$, because the LG and the Sun velocity have opposite directions.

The computation of the anisotropies of the AGWB done in Section 7.4 shows that local perturbations of the metric and our peculiar velocity generate a monopole and a dipole term respectively, see e.g., Eq. (7.73). The first term can be reabsorbed in the definition of $\bar{\Omega}^\alpha_{\rm AGWB}$, therefore the only local term which affects the angular power spectrum is the kinetic dipole,

$$\delta^{\alpha\,[i]\,\rm KD}_{\rm AGWB}(\hat{n}, f) = \int \mathrm{d}\bar{\chi}\, \tilde{W}^{[i]\,\rm eff}_\alpha(\bar{\chi}, f) \left(b^{[i]\,\rm eff}_{e,\alpha}(\bar{\chi}, f) - \frac{H'(\bar{\chi})}{a(\bar{\chi})H^2(\bar{\chi})} - 3 \right) \hat{n}\cdot\mathbf{v}_o = \mathcal{R}_\alpha(f)\,\hat{n}\cdot\mathbf{v}_o\,, \tag{9.2}$$

where v_o is our peculiar velocity, $b^{[i]\,\rm eff}_{e,\alpha}$ the evolution bias defined in Eq. (7.68) and $\mathcal{R}_\alpha$ is the Kaiser-Rocket factor, defined by

$$\mathcal{R}_\alpha(f) \equiv \int_0^{\eta_0} \mathrm{d}\eta\, \tilde{W}^{[i]\,\rm eff}_\alpha(\eta, f) \left(b^{[i]\,\rm eff}_{e,\alpha}(\eta, f) - \frac{H'(\eta)}{a(\eta)H^2(\eta)} - 3 \right). \tag{9.3}$$

From now on, we will focus just on the intensity of the AGWB and we will omit the index which specifies the Stokes parameter. The Kaiser-Rocket factor represents a Doppler boosting over many infinitesimal shells, accounting for the GWs emitted at different η (or, equivalently, $\bar{\chi}$). Eq. (9.2) refers to the kinetic dipole induced by non-statistical velocities, such as $\mathbf{v}_{\rm LG}$, while the subtraction of $\mathbf{v}_E$, $\mathbf{v}_\odot$ and $\mathbf{v}_{\rm MW}$ would generate a Doppler shift discussed for instance in [67]. In the *Cosmic Rulers* formalism used in Section 7.4, the peculiar velocities of the emitters are not included in the KD, but in the redshift-space-distorsion terms D1, D2 and rsd which appear in Eq. (7.78). In terms of the source functions, the kinetic dipole reads

$$\delta^{[i]\,\rm KD}_{{\rm AGWB},\ell m} = 4\pi(-i)^\ell \int \frac{\mathrm{d}^3k}{(2\pi)^3} Y^*_{\ell m}(\hat{k})\zeta(\mathbf{k})\,\Delta^{o,\rm dipole}_\ell(\eta, k)\,, \tag{9.4}$$

where we have introduced

$$\Delta^{\rm o\,dipole}_\ell(f) = \int_0^{\eta_0} \mathrm{d}\eta\, \tilde{W}^{[i]\,\rm eff}_\alpha \left(b^{[i]\,\rm eff}_{e,\alpha} - \frac{H'}{aH^2} - 3 \right) \frac{1}{k}\theta_{m\,o} \frac{1}{2\ell+1}\delta_{\ell 1}\,. \tag{9.5}$$

The magnitude of the kinetic dipole depends on the realization of the Gaussian random field $\delta^{[i]\,\mathrm{KD}}_{\mathrm{AGWB},\ell m}$, which is drawn from a Gaussian distribution with zero mean and covariance given by

$$C_\ell^{\mathrm{KD}}(f,f') = 4\pi \int \frac{\mathrm{d}k}{k} P(k) \Delta_\ell^{\mathrm{o\,dipole}}(f) \Delta_\ell^{\mathrm{o\,dipole}}(f') \,. \tag{9.6}$$

In this chapter, we prefer to characterize the anisotropies by using directly Eq. (9.2), because it is more intuitive to connect the KD to the peculiar velocity we want to estimate.

9.3 Frequency dependence of the anisotropies

The monopole of the angular power spectrum of the AGWB depends on the frequency, because of the energy spectrum of the individual binaries defined in Eq. (7.44). The scaling of the monopole with the frequency at low frequencies is $f^{2/3}$, because all the binaries emit in the inspiral stage and the frequency dependence can be factor out because of the coherence of the waves. As shown in the right panel of Figure 7.1, when the frequency increases, a fraction of the binaries start emitting GWs during the merger and ringdown, thus the scaling with the frequency cannot be written in a simple analytical form. Furthermore, the observed frequency at which some binaries end their inspiral stage, depends on the redshift and on the masses of the compact objects in the system, therefore it is not possible to factorize the energy density of the AGWB into a frequency-dependent and a redshift-dependent contributions. To see more explicitly this, we recall that the monopole of the AGWB depends on the integral

$$\bar{\Omega}_{\mathrm{AGWB}}(f) \sim f \int \mathrm{d}M_1 \, \mathrm{d}M_2 \, p(m_1,m_2) \frac{\mathrm{d}E_{\mathrm{GW}}}{\mathrm{d}f_e \mathrm{d}\Omega_e}(m_1,m_2,\chi_1,\chi_2,\iota,z,f) \,, \tag{9.7}$$

where $f_e = (1+z)f$. When all the binaries are in the inspiral,

$$\frac{\mathrm{d}E_{\mathrm{GW}}}{\mathrm{d}f_e \mathrm{d}\Omega_e} \sim f^{-1/3} \,, \tag{9.8}$$

while at higher frequencies we have a non-factorizable integral over the frequency. The interesting thing to notice is that at high frequencies the shape in frequency of the AGWB is sensitive to the distribution in mass and redshift of the sources, because the scaling with the frequency is generated by the superposition of binaries at different stages of the evolution with different intrinsic parameters and which emit GWs at different redshifts. The important consequence of this fact is that the evolution bias, defined in Eq. (7.68), and the window function, defined in Eq. (7.75), depends on the frequency and so anisotropies exhibit a non-trivial scaling in f. The physical interpretation of this result is that the weight of the sources that contribute to the background at redshift z could be different at two different frequencies, because at the two frequencies the number of objects in the inspiral, merger and ringdown stage of the evolution could be different. In Figure 9.1, we plot the effective window function and the evolution bias for the intensity of the AGWB generated by BBH of stellar masses at CE+ET. When $f \lesssim 80\,\mathrm{Hz}$, no huge differences could

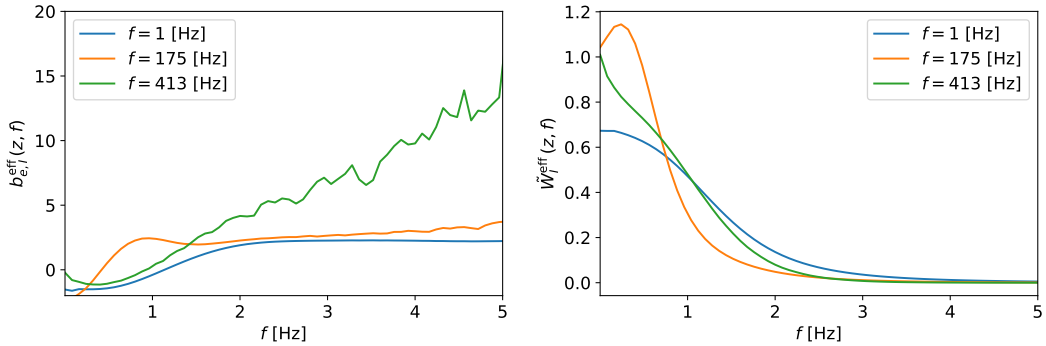

Figure 9.1: Plot of the evolution bias (left) and of the window function (right) of the intensity of the AGWB generated by the superposition of BBH of stellar mass.

be appreciated in the window function and in the effective bias, because the majority of the BBH emit in the inspiral stage. This non-trivial dependence on the frequencies implies that the intrinsic, the shot noise and the kinetic dipole scale in a different way, because they depend on different combinations of the window function and evolution bias. In Figure 9.3 we plot the three contributions to the dipole of the AGWB as a function of the frequency. We will show how this frequency-dependence could be used to disentangle these three terms in Section 9.5.

9.4 Measurement of the dipole with the standard technique

The standard approach used to evaluate the detectability of the anisotropies of the AGWB is analogous to the one discussed in Section 6.4.2. For instance, if we suppose to consider the auto- and the cross-correlation of the AGWB with a galaxy survey, the amount of information that can be extracted by the intrinsic and kinetic anisotropies is quantified by Eqs. (6.23), (6.24),

$$\mathrm{SNR}^2 \equiv \sum_{\ell=1}^{\ell_{\rm max}} \vec{C}_\ell^{\,\mathrm{T}} \Sigma_\ell^{-1} \vec{C}_\ell \,, \tag{9.9}$$

where $\ell_{\rm max}$ identifies the maximum multipole at which we have a non-negligible contribution to the SNR. The vector $\vec{C}_\ell$ in this case is

$$\vec{C}_\ell = \begin{pmatrix} C_\ell^{\rm AGWB,KD} + C_\ell^{\rm AGWB,int} \\ C_\ell^{g\times \rm AGWB} \end{pmatrix} . \tag{9.10}$$

The components of the covariance matrix in this case are

$$\begin{aligned}
\Sigma_{\ell,11} =& \frac{2}{2\ell+1}\left(C_\ell^{\rm AGWB,KD}+C_\ell^{\rm AGWB,int}+C_\ell^{\rm AGWB,SN}+N_\ell\right)^2\,,\\
\Sigma_{\ell,12} =& \frac{2}{2\ell+1}\left(C_\ell^{\rm AGWB,KD}+C_\ell^{\rm AGWB,int}+C_\ell^{\rm AGWB,SN}+N_\ell\right)\left(C_\ell^{g\times{\rm AGWB,int}}+C_\ell^{g\times{\rm AGWB,SN}}\right)\,,\\
\Sigma_{\ell,22} =& \frac{1}{2\ell+1}\Bigg[\left(C_\ell^{g\times{\rm AGWB,int}}+C_\ell^{g\times{\rm AGWB,SN}}\right)^2\\
&+\left(C_\ell^{\rm AGWB,KD}+C_\ell^{\rm AGWB,int}+C_\ell^{\rm AGWB,SN}+N_\ell\right)\left(C_\ell^{g,{\rm KD}}+C_\ell^{g,{\rm int}}+C_\ell^{g,{\rm SN}}\right)\Bigg]\,.
\end{aligned} \tag{9.11}$$

The angular power spectrum of the noise N_ℓ has been computed with `schNell` for the network CE+ET for five years of observations. A suitable survey that can be combined with the AGWB is SKAO2, which will be described in Appendix I. In Figure 9.2 we have depicted the cumulative SNR of the various contributions to the anisotropies as a function of the maximum multipole considered. We have also plotted the various contribution to the SNR up to $\ell_{\rm max}=200$ as a function of the monopole amplitude of the AGWB. Note that when instrumental noise is considered, different choices of $\ell_{\rm max}$ above a certain value do not change the SNR, since the instrumental noise automatically keeps into account for the angular resolution of the detector. We have computed the SNR in three different scenarios: with instrumental noise only, with SN only, and with SN plus instrumental noise. From the picture it is clear that with the standard estimator of the intrinsic and kinetic anisotropies, the SNR of the angular power spectra is always smaller than one, because the shot noise and the instrumental noise are always orders of magnitude larger than the interesting signals. In the next sections, we will illustrate a technique based on the frequency dependence of the anisotropies to clean measurements of the intrinsic and the kinetic dipole from the shot noise contaminations.

9.5 Component separation in the noiseless case

In Section 9.3 we have shown that at high frequencies, when it is not possible to factorize the redshift and the frequency dependence in the integral to compute the AGWB, the anisotropies scale in a non-trivial way. In Figure 9.3 we have plotted the shot noise, the kinetic and the intrinsic dipoles of the AGWB at different frequencies. In the left panel, we show the total magnitude of the three contributions, making clear that the shot noise dominates the other two terms of at least one order of magnitude. In the right plot, we show the three contributions, normalized w.r.t. their values at 1 Hz, in order to enlight the fact that at large frequencies the three scalings could be very different. In this section, we show how the different frequency scaling could be used to discriminate between the three contributions in the case in which there is no instrumental noise at the GW detector considered.

To do component separation between the contributions to the anisotropies we use Internal Linear Combination (ILC) [327, 138], or any other kind of component separation

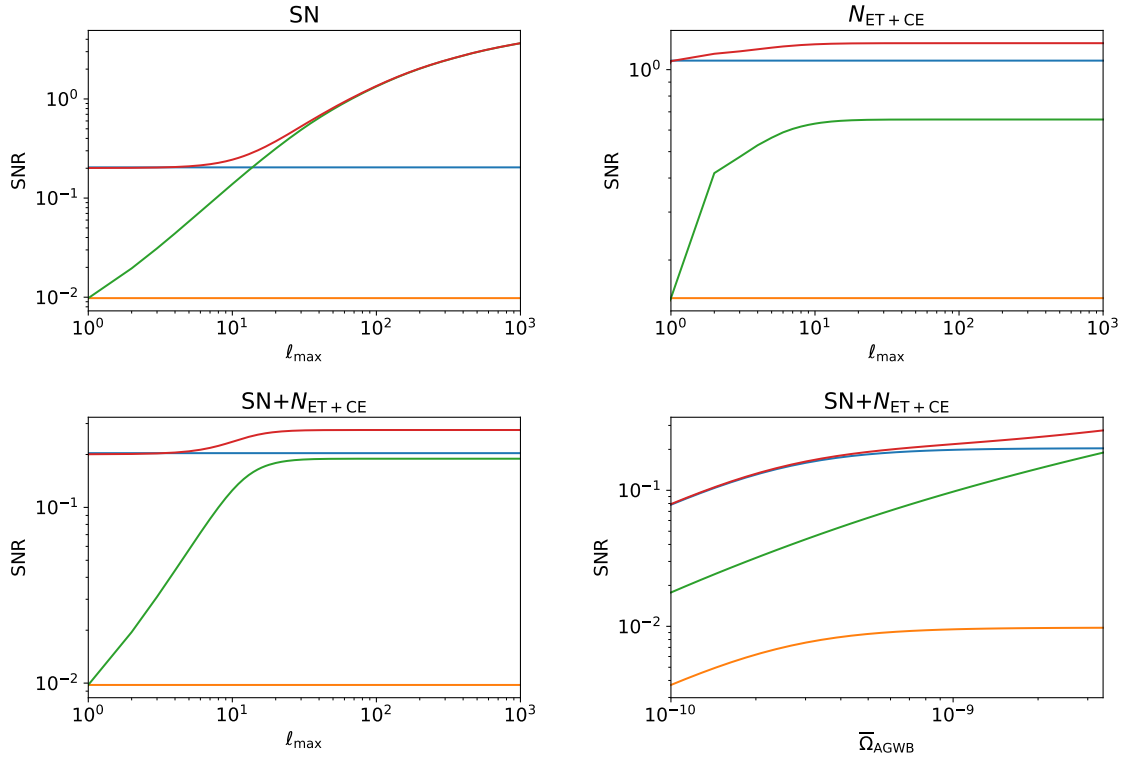

Figure 9.2: *Plot of the contributions to the cumulative SNR as a function of the maximum multipole, with SN only (upper left), with instrumental noise only (upper right), with instrumental noise plus SN (lower left). The blue line corresponds to the kinematic dipole, the orange one to the intrisic dipole, the green one to the intrinsic anisotropies and the red one to the total. When instrumental noise is considered, we have computed the cumulative SNR assuming the maximum monopole amplitude for the AGWB. Lower right: plot of the cumulative SNR for* $\ell_{\mathrm{max}} = 200$ *as a function of the monopole amplitude of the AGWB, considering both instrumental noise and SN. We have considered* $\ell_{\mathrm{max}} = 200$*, because, when we compute the SNR with instrumental noise, we automatically take into account the angular resolution of the detector, therefore higher multipoles give negligible contribution to the SNR. All the SNRs have been computed for the auto-correlation of the AGWB and for the cross-correlation between the AGWB with the galaxy survey SKAO2. The SNR computed here does not include the auto-correlation of the galaxy survey, because we want to quantify the amount of extra-information added by considering also the AGWB in the analysis.*

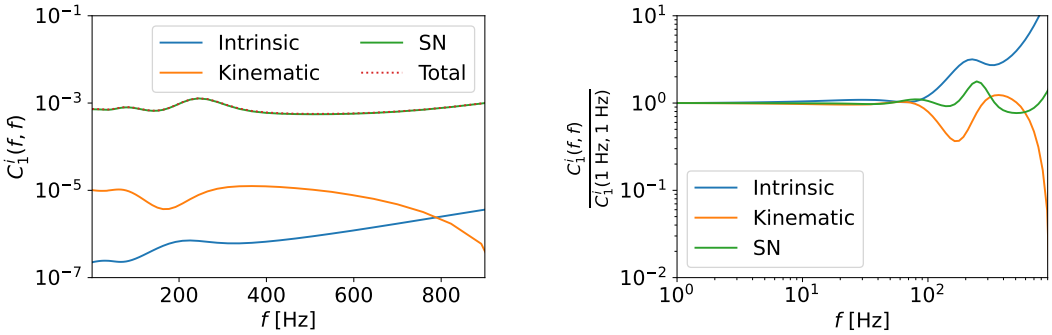

Figure 9.3: Left: plot of the intrinsic, SN, KD, and total contribution to the $\ell = 1$ term of the angular power spectrum of the AGWB at different frequencies. Right: plot of the intrinsic, SN, KD contributions to the auto-correlation spectra of the AGWB normalized w.r.t. their values at 1 Hz.

technique. We write the observed dipole in the vector form

$$\vec{d}_i^{\,\text{obs}} = \vec{d}_i^{\,\text{int}} + \vec{d}_i^{\,\text{KD}} + \vec{d}_i^{\,\text{SN}}\,, \tag{9.12}$$

where the vector symbol identifies the array of frequencies at the detector, while i the spatial direction in the sky. The kinetic dipole at a pivot frequency f_{piv} is connected to the velocity of the observer through the Kaiser-Rocket factor,

$$d_i^{\text{KD}}(f) = \mathcal{R}(f) v_{o,i}\,. \tag{9.13}$$

It is possible then to write the total signal by using

$$\vec{d}_i^{\,\text{obs}} = \vec{\mathcal{R}} v_{o,i} + \vec{d}_i^{\,\text{int}} + \vec{d}_i^{\,\text{SN}}\,. \tag{9.14}$$

The main idea of ILC is to combine the data at different frequency to build an estimator for $v_{o,i}$ with the minimum covarince possible. If we assume a knowledge of the frequency scaling of the three contributions to the angular power spectrum of the AGWB, it is possible to introduce a vector $\vec{w}$ in such a way that the estimator for our peculiar velocity is

$$\hat{v}_{o,i} \equiv \vec{w}^T \vec{d}_i^{\,\text{obs}}\,. \tag{9.15}$$

We assume that our estimator is unbiased,

$$\langle \hat{v}_{o,i} \rangle = v_{o,i} \to \vec{w}^T \vec{\mathcal{R}} = 1\,, \tag{9.16}$$

and that is covariance is minimized by a smart choice of the weights

$$\frac{\partial}{\partial \vec{w}} \left\langle (\hat{v}_{o,i} - v_{o,i})^2 \right\rangle = 0\,. \tag{9.17}$$

We notice that our strategy is similar to the one adopted in Sections 1.3.2 and 8.3 to evaluate the best unbiased estimator of the anisotropies of SGWB in presence of instrumental

noise. Also in this case, to minimize the differential equation with a constraint we use a Lagrange multiplier. The Lagrangian function is

$$\mathcal{L}(\vec{w},\lambda) = \left\langle (\hat{v}_{o,i} - v_{o,i})^2 \right\rangle - \lambda \left(\vec{w}^T \vec{\mathcal{R}} - 1 \right) = \vec{w}^T C \vec{w} - \lambda \left(\vec{w}^T \vec{\mathcal{R}} - 1 \right) , \tag{9.18}$$

where C is the covariance matrix of the total dipole, where its (α, β) entry is defined as,

$$C_{\alpha\beta} \equiv \mathrm{cov} \left[d_i^{\mathrm{obs}}(f_\alpha), d_i^{\mathrm{obs}}(f_\beta) \right] = C_1^{\mathrm{int}}(f_\alpha, f_\beta) + C_1^{\mathrm{SN}}(f_\alpha, f_\beta) \, . \tag{9.19}$$

By minimizing the Lagrangian function w.r.t. the two parameters we get

$$\begin{cases} \vec{w}^T \vec{\mathcal{R}} = 1 \\ 2\vec{w}^T C - \lambda \vec{\mathcal{R}}^T = 0 \end{cases} \rightarrow \begin{cases} \vec{w}^T = \frac{1}{2} \lambda \vec{\mathcal{R}}^T C^{-1} \\ \frac{1}{2} \lambda \vec{\mathcal{R}}^T C^{-1} \vec{\mathcal{R}} = 1 \end{cases} \rightarrow \begin{cases} \lambda = \frac{2}{\vec{\mathcal{R}}^T C^{-1} \vec{\mathcal{R}}} \\ \vec{w}^T = \frac{\vec{\mathcal{R}}^T C^{-1}}{\vec{\mathcal{R}}^T C^{-1} \vec{\mathcal{R}}} \end{cases} \tag{9.20}$$

The estimator of the kinetic dipole is

$$\hat{v}_{o,i} = \frac{\vec{\mathcal{R}}^T C^{-1} \vec{d}_i^{\,\mathrm{obs}}}{\vec{\mathcal{R}}^T C^{-1} \vec{\mathcal{R}}} \, . \tag{9.21}$$

The associated error to this estimate is

$$\sigma_{\hat{v}_{o,i}} = \sqrt{\left\langle (\hat{v}_{o,i} - v_{o,i})^2 \right\rangle} = \sqrt{\vec{w}^T C \vec{w}} = \frac{1}{\sqrt{\vec{\mathcal{R}}^T C^{-1} \vec{\mathcal{R}}}} \, . \tag{9.22}$$

In Figure 9.4, we plot one realization of the total map, Eq. (9.12) (left), the kinetic dipole map (middle), and of the reconstructed kinetic dipole map, Eq. (9.21). The maps have been evaluated at the pivot frequency $f_p = 30\,\mathrm{Hz}$ and we have used the value of the LG velocity $v_{\mathrm{LG}} = 600\,\mathrm{km/s}$. The pictorial representation of our result makes clear that, although the initial map does not allow to reconstruct the kinetic dipole, because of the contamination of the shot noise and of the intrinsic anisotropies, the reconstructed signal, which exploits the frequency dependence, is very good. In a more quantitative way, the SNR of the reconstruction of the dipole in all the directions is

$$\mathrm{SNR} \equiv \sqrt{\sum_{i,j} v_{o,i} \, \mathrm{cov}^{-1}_{\mathrm{ILC},ij} \, v_{o,j}} \approx 10 \, . \tag{9.23}$$

The key assumption we have done here is a perfect knowledge of the Kaiser-Rocket factor $\mathcal{R}(f)$ and the scaling of the theoretical angular power spectra of the SN and of the intrinsic anisotropies. This simplification is justified by the fact that the several uncertainties in the astrophysical models which describe the population of the emitters will be reduced by the large number of sources that will be detected by the network ET+CE [286].

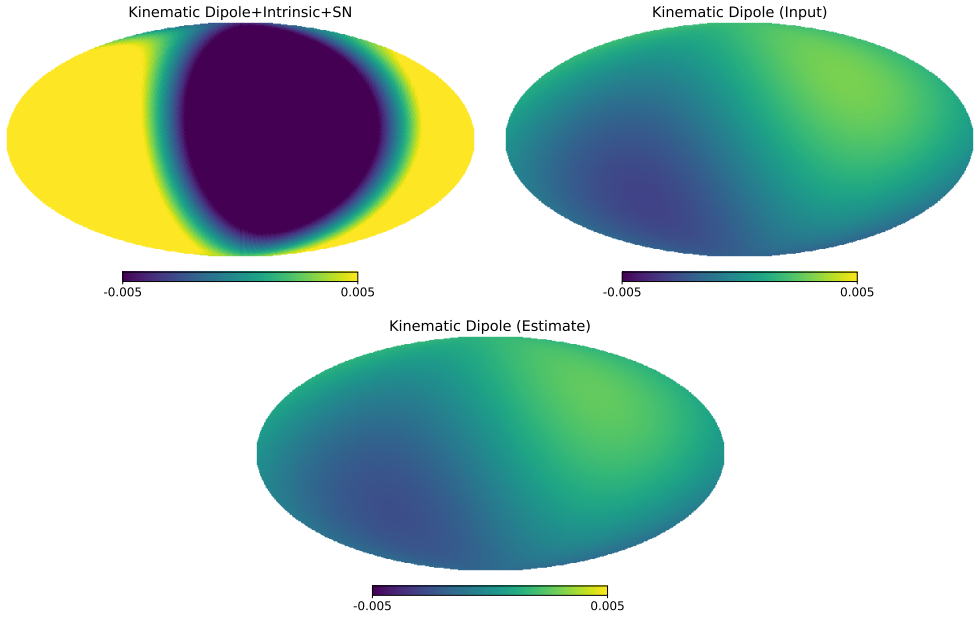

Figure 9.4: *Upper Left: AGWB density contrast map at* $f_o = 30\,\mathrm{Hz}$*; Upper Right : input velocity map* $\hat{n}\cdot\vec{v}_o$*; Bottom: reconstructed velocity map* $\hat{n}\cdot\vec{v}_o^{\,\mathrm{est}}$*.*

9.6 Component separation in presence of instrumental noise

The anisotropies of the AGWB are obtained by the superposition of the intrinsic, the kinematic and the shot noise fluctuations in the energy spectrum. In analogy with Eq. (8.19), the covariance of the data $d_A(f)$ measured at interferometers is proportional to

$$\langle d_A(f)\, d_B^*(f')\rangle = \frac{1}{2}\delta(f-f')\Big[N_{AB}(f) + \bar{\Omega}_{\mathrm{AGWB}}(f)\gamma^I_{AB}(f) + \bar{\Omega}_{\mathrm{AGWB}}(f)\int \mathrm{d}\hat{n}\,\tilde{B}^I_{AB}(\hat{n},f)\sum_c \delta^c_{\mathrm{AGWB}}(\hat{n},f)\,, \tag{9.24}$$

with $c \in \{\mathrm{int}, \mathrm{KD}, \mathrm{SN}\}$. In this case, we have neglected the circular polarization, since in this chapter we focus just on the intensity and we assume that there is no contamination in the AGWB maps from different Stokes parameters. In order to relax the notation, we write the AGWB as a map at a pivot frequency f_p, times a scaling function which describes the scaling with the frequency,

$$\Omega^c_{\mathrm{AGWB}}(\hat{n},f) = \mathcal{E}^c_p(f)\bar{\Omega}_{\mathrm{AGWB}}(f_p)\delta^c_{\mathrm{AGWB}}(\hat{n},f_p)\,. \tag{9.25}$$

In this section we assume that the scaling functions $\mathcal{E}^c_p(f)$, defined by

$$\mathcal{E}^c_p(f) \equiv \frac{\bar{\Omega}^c_{\mathrm{AGWB}}(f)\delta^c_{\mathrm{AGWB}}(\hat{n},f)}{\bar{\Omega}_{\mathrm{AGWB}}(f_p)\delta^c_{\mathrm{AGWB}}(\hat{n},f_p)}\,, \tag{9.26}$$

are known and we try to use differences in $\mathcal{E}^{\rm KD}$, $\mathcal{E}^{\rm SN}$ and $\mathcal{E}^{\rm int}$ to separate the three contributions to the AGWB anisotropies. We define an estimator quadratic in the data,

$$\hat{\Omega}_p^{\rm KD} = \sum_{A,B} \int {\rm d}f \, d_A(f) E_{AB}(\hat{n}, f) d_B^*(f) - b(\hat{n}) \,. \tag{9.27}$$

and we require that it is unbiased,

$$\left\langle \hat{\Omega}_p^{\rm KD} \right\rangle = \Omega_{\rm AGWB}^{\rm KD}(\hat{n}, f_p) \,. \tag{9.28}$$

In this case, the expectation value of the estimator is

$$\left\langle \hat{\Omega}_p^{\rm KD} \right\rangle = \sum_{A,B} \int {\rm d}f \frac{T_{\rm seg} \, E_{AB}(\hat{n}, f)}{2} \left[\sum_c \mathcal{E}_p^c(f) \int {\rm d}\hat{m} \, \tilde{B}_{AB}^I(\hat{m}, f) \Omega_{\rm AGWB}^c(\hat{m}, f_p) + N_{AB}(f) \right] - b(\hat{n}) \,. \tag{9.29}$$

Since the shot noise and the intrinsic map are realizations of Gaussian random fields, they cannot be subtracted a priori, thus we can only subtract the PSD of the noise,

$$b(\hat{n}) = T_{\rm seg} \sum_{A,B} \int {\rm d}f \frac{E_{AB}(\hat{n}, f)}{2} N_{AB}(f) \,. \tag{9.30}$$

At the same time, we impose that the contribution to the average of the estimator proportional to the kinetic dipole is unbiased,

$$T_{\rm seg} \sum_{A,B} \int {\rm d}f \frac{1}{2} E_{AB}(\hat{n}, f) \mathcal{E}_p^c(f) \tilde{B}_{AB}^I(\hat{m}, f) = \delta(\hat{n} - \hat{m}) \,. \tag{9.31}$$

The expectation value of our estimator is therefore

$$\left\langle \hat{\Omega}_p^{\rm KD}(\hat{n}) \right\rangle = \Omega_{\rm AGWB}^{\rm KD}(\hat{n}, f_p) + \int {\rm d}f \frac{T_{\rm seg} \, E_{AB}(\hat{n}, f)}{2} \sum_{c \neq {\rm KD}} \mathcal{E}_p^c(f) \int {\rm d}\hat{m} \, \tilde{B}_{AB}^I(\hat{m}, f) \Omega_{\rm AGWB}^c(\hat{m}, f_p) \,. \tag{9.32}$$

Over infinite realizations of the intrinsic and kinetic anisotropies (which are uncorrelated with the kinetic dipole), the bias is zero. However, in a single realization of the system, they introduce an error in the reconstruction of the dipole which can be quantified by

$$\begin{aligned} \hat{\mathcal{C}}_{\rm cs}^{\rm KD}(\hat{n}, \hat{n}') \equiv & {\rm cov} \left(\left\langle \hat{\Omega}_p^{\rm KD}(\hat{n}) \right\rangle, \left\langle \hat{\Omega}_p^{\rm KD}(\hat{n}') \right\rangle \right)_{cv} \\ = & \left\langle \left(\langle \hat{\Omega}_p^{\rm KD}(\hat{n}) \rangle - \hat{\Omega}_p^{\rm KD}(\hat{n}) \right) \left(\langle \hat{\Omega}_p^{\rm KD}(\hat{n}') \rangle - \hat{\Omega}_p^{\rm KD}(\hat{n}') \right) \right\rangle_{\rm cs} \\ = & \frac{T_{\rm seg}^2}{4} \int {\rm d}f {\rm d}f' {\rm d}\hat{m} {\rm d}\hat{m}' \, {\rm Tr} \left(E(\hat{n}, f) B^{\rm KD}(\hat{m}, f) \right) {\rm Tr} \left(E(\hat{n}', f') B^{\rm KD}(\hat{m}', f') \right) \\ & \sum_{c \neq {\rm KD}} \frac{C_c(f, f'; \hat{m}, \hat{m}')}{\mathcal{E}_p^{\rm KD}(f) \mathcal{E}_p^{\rm KD}(f')} \,, \end{aligned} \tag{9.33}$$

where the trace is computed w.r.t. the indices of the detectors in the newtork, while cs stands for "component separation" and $B^{\rm KD}(\hat{n},f) \equiv \tilde{B}^I_{AB}(\hat{n},f)\,\mathcal{E}^{\rm KD}_p(f)$. The covariance matrix in the last row is the covariance of the maps of the intrinsic and the shot noise and is related to the angular power spectrum by

$$C_c(f,f';\hat{m},\hat{m}') \equiv \sum_\ell (2\ell+1)\mathcal{P}_\ell(\hat{m}\cdot\hat{m}')C^c_\ell(f,f')\ . \tag{9.34}$$

This contribution represents the difficulty of detecting the kinetic dipole in presence of foregrounds. Another, independent, error is induced by the fact that the estimator is quadratic in the data and the four-point function of the data does not vanish. This source of noise is quantified by the following covariance matrix,

$$\begin{aligned}\hat{\mathcal{C}}^{\rm KD}_{h^4}(\hat{n},\hat{n}') = 2\,T_{\rm seg}\int {\rm d}f \sum_{A,B,C,D} & E_{AB}(\hat{n},f)E_{CD}(\hat{n}',f) \\ & \Big[\frac{1}{4}N_{AD}(f)N_{BC}(f) \\ & + \int {\rm d}\hat{m}\,{\rm d}\hat{m}' \sum_{c,c'} \tilde{B}^I_{AD}(\hat{m},f)\tilde{B}^I_{CD}(\hat{m}',f)\Omega^c_{\rm AGWB}(\hat{m},f)\Omega^{c'}_{\rm AGWB}(\hat{m}',f)\Big]\,.\end{aligned} \tag{9.35}$$

Note that in the noise dominated regime this contribution reduces to

$$\hat{\mathcal{C}}^{\rm KD}_{h^4}(\hat{n},\hat{n}') = 2\,T_{\rm seg}\int {\rm d}f \sum_{A,B,C,D} E_{AB}(\hat{n},f)E_{CD}(\hat{n}',f)\frac{1}{4}N_{AD}(f)N_{BC}(f)\,. \tag{9.36}$$

The total error on the estimator is therefore

$$\hat{\mathcal{C}}^{\rm KD}(\hat{n},\hat{n}') = \hat{\mathcal{C}}^{\rm KD}_{h^4}(\hat{n},\hat{n}') + \hat{\mathcal{C}}^{\rm KD}_{\rm cs}(\hat{n},\hat{n}')\,. \tag{9.37}$$

Also in this case, we introduce the Lagrangian function

$$\mathcal{L} = \hat{\mathcal{C}}^{\rm KD}(\hat{n},\hat{m}) + \lambda\left[T_{\rm seg}\int {\rm d}\hat{n}' \sum_{A,B}\int {\rm d}f\,\frac{1}{2}E^\alpha_{AB}(\hat{n},f)\mathcal{E}^\alpha_p(f)\tilde{B}^\alpha_{AB}(\hat{n}',f) - 1\right]\,. \tag{9.38}$$

and we choose the weights E by minimizing it w.r.t. the weights and the Lagrange multiplier,

$$\frac{\delta}{\delta E^\alpha_{AB}(\hat{n},f)}\mathcal{L} = \frac{\delta}{\lambda}\mathcal{L} = 0\,. \tag{9.39}$$

The condition on the function derivative w.r.t. E gives

$$\begin{aligned}&\sum_{C,D} E^\alpha_{CD}(\hat{m},f)N_{AD}(f)N_{CB}(f') + \lambda\,\tilde{B}^\alpha_{AB}(\hat{n},f)\mathcal{E}_p(f) \\ &\quad + \frac{T_{\rm seg}}{2}{\rm d}f'{\rm d}\hat{m}{\rm d}\hat{m}'\ B^{\rm KD}_B(\hat{m},f){\rm Tr}\left[E(\hat{n}',f')B^{\rm KD}(\hat{m}',f')\right]\sum_{c\neq{\rm KD}}\frac{C_c(f,f';\hat{m},\hat{m}')}{\mathcal{E}^{\rm KD}_p(f)\mathcal{E}^{\rm KD}_p(f')} = 0\,,\end{aligned} \tag{9.40}$$

where the trace is taken wr.t. the indices of the detectors in the network. At first order in C_c, the Lagrange multiplier is equal to

$$\lambda = \frac{1}{T_{\rm seg}} \frac{2}{\int \mathrm{d}f \mathcal{T}(f;\hat{n},\hat{n})} + T_{\rm seg} \int \mathrm{d}f \mathrm{d}f' \int \mathrm{d}\hat{m} \mathrm{d}\hat{m}' \frac{\mathcal{T}(f;\hat{n},\hat{m})\mathcal{T}(f';\hat{n}',\hat{m}')}{\left[\int \mathrm{d}f'' \mathcal{T}(f'';\hat{n},\hat{n})\right]^2} \frac{C^{\rm tot}_{ff',\varphi\varphi'}}{\mathcal{E}^{\rm KD}_f \mathcal{E}^{\rm KD}_{f''}} \,, \tag{9.41}$$

where we have defined

$$\mathcal{T}(f;\hat{n},\hat{m}) \equiv \mathrm{Tr}\left[N^{-1}(f) B^{\rm KD}(\hat{n},f) N^{-1}(f) B^{\rm KD}(\hat{m},f)\right] \,, \tag{9.42}$$

The weights are then equal to

$$E_{AB}(f,f;\hat{n}) = \frac{1}{T_{\rm seg}} \frac{2 S^{-1}_{AC}(f) B^{\rm KD}_{CD}(\hat{n},f) S^{-1}(f)}{\int \mathrm{d}f' \mathcal{T}(f';\hat{n},\hat{n})} \,. \tag{9.43}$$

The final expression of the covariance reduces to

$$\hat{\mathcal{C}}^{\rm KD}(\hat{n},\hat{n}') = \frac{1}{T_{\rm obs}} \frac{2\delta(\hat{n}-\hat{n}')}{\int \mathrm{d}f \mathcal{T}(f;\hat{n},\hat{n})} + \int \mathrm{d}f \mathrm{d}f' \int \mathrm{d}\hat{m} \mathrm{d}\hat{m}' \frac{\mathcal{T}(f;\hat{n},\hat{m})\mathcal{T}(f';\hat{n}',\hat{m}')}{\left[\int \mathrm{d}f'' \mathcal{T}(f'';\hat{n},\hat{n})\right]^2} \frac{C^{\rm tot}_{ff',\varphi\varphi'}}{\mathcal{E}^{\rm KD}_f \mathcal{E}^{\rm KD}_{f''}} \,, \tag{9.44}$$

where we have replace $T_{\rm seg}$ with $T_{\rm obs}$, because we want the estimate of the error over the whole duration of the experiment and not in a single time segment. Note that the error induced by the component separation does not depend on $T_{\rm obs}$. This is due to the fact that the error due to the component separation depends on the realization of the shot noise and of the intrinsic anisotropies, which do not depend on time, therefore in different time segments our knowledge on the different contributions to the overall anisotropies does not improve. However, the different frequency dependence of the kinetic, intrinsic and shot noise anisotropies can be used to dinstinguish between the different components. This can be seen as the fact that in the covariance given in Eq. 9.44, the numerator is a convolution of two integrals over the frequencies, weighted by the frequency dependence of the covariance matrices of the intrinsic and shot noise anisotropies. When $\mathcal{E}^{\rm KD}_p(f)$ is much different from $\mathcal{E}^{\rm SN}_p$ and $\mathcal{E}^{\rm int}_p$, the double integral is suppressed, by the incoherent superposition of the various terms, w.r.t. the denominator, proportional just to $\mathcal{E}^{\rm KD}_p(f)$. This is consistent with the efficient component separation in the noiseless case, discussed in Section 9.5. From the map of the kinetic dipole we can extract the estimator of the velocity by using

$$\hat{v}_i = \frac{1}{\mathcal{R}(f_p)} \int \mathrm{d}\hat{n}\, \hat{n}_i\, \delta^{\rm KD}_{\rm AGWB}(\hat{n},f_p) \,, \tag{9.45}$$

where we have used the relation between the kinetic dipole, the velocity and the Kaiser-Rocket factor given by Eq. (9.13). The covariance associated to the reconstruction of the velocity is

$$\hat{\mathcal{C}}^v_{ij} \equiv \mathrm{cov}\left[\hat{v}_i, \hat{v}_j\right] = \int \mathrm{d}\hat{n}\, \hat{n}_i \hat{n}_j \hat{\mathcal{C}}^{\rm KD}(\hat{n},\hat{n}) \,. \tag{9.46}$$

In analogy with Eq. (9.23), we have provided an estimate of the SNR of the dipole by using

$$\mathrm{SNR}^2 = \vec{v}_o^{\,T}\,\mathrm{cov}^{-1}\vec{v}_o\,. \tag{9.47}$$

The result is plotted in Figure 9.5 as a function of the monopole amplitude of the AGWB at $f = 25\,\mathrm{Hz}$. We can see that for values of the monopole of the AGWB within the upper bound of LIGO/Virgo, the estimator is able to reduce the instrumental noise and to give an SNR larger than one. In the figure we have also compared the SNR computed with this multi-frequency analysis to the standard one evaluated in Section 9.4, showing that in the limit of large monopoles/low instrumental noise, the technique we have used could increment the detectability by an order of magnitude.

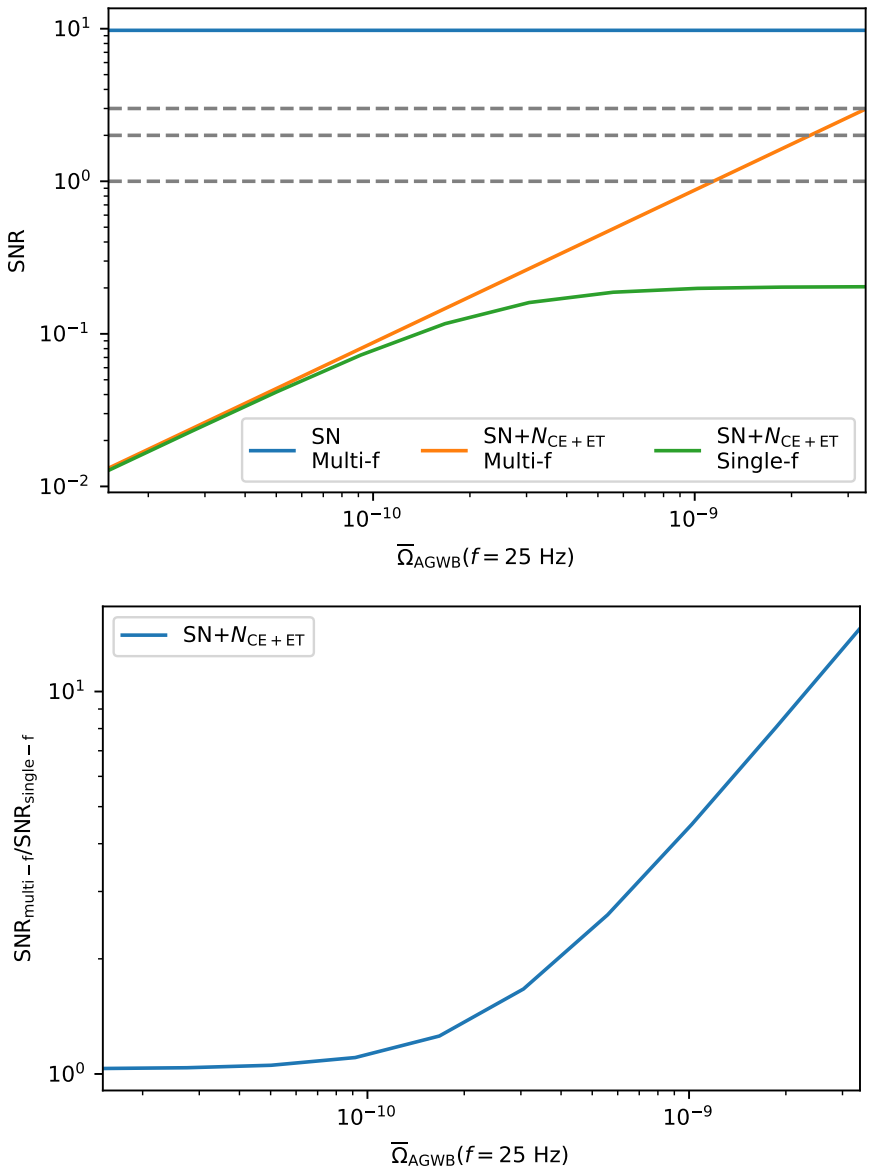

Figure 9.5: *Upper: plot of the SNR of the kinematic dipole as a function of the monopole amplitude of the AGWB by considering SN and SN plus instrumental noise (N_{ET+CE}). The horizontal lines show the SNR equal to 1, 2 and 3 respectively. Lower: Plot of the ratio of the SNR obtained by using the multi-frequency and the SNR computed by looking at a single frequency.*

Chapter 10

Conclusions

Summary

The work presented in this Thesis represents an extensive research about the anisotropies of stochastic backgrounds of cosmological and astrophysical origin. The increases in the sensitivity of current GW detectors, such as Advanced LIGO, Advanced Virgo and KAGRA [328], or the prospects of having more sensitive third-generation interferometers, like ET [13], CE [14], LISA [15], Taiji [16], BBO [17] and DECIGO [18], make clear the importance of being prepared from a theoretical point of view to the enormous amount of GW data available in the next decades. Furthermore, the recent detection of a SGWB by the IPTA collaboration [9, 10, 11, 12] made concrete the possibility of observing this kind of stochastic signals and to explore their features in the near future. Although a clear detection of the monopole and of its scaling with the frequency are the main targets of SGWB observations, it is reasonable to expect that as a second step the anisotropies will become the main objective of this research field. This is analogous to what happens in the CMB case, since its detection by Penzias and Wilson [25] until measurements of the angular power spectrum by *Planck* [26].

In Chapter 1 we reviewed the propagation of GWs in vacuum and in curved spacetimes, describing the shortwave approximation and the structure of the energy-momentum tensor of the gravitational field. Part of the chapter is devoted to a formal definition of stochastic signals, to a description of the statistical properties of SGWBs and to the strategies for their detection. In particular, we have illustrated the matched filtering technique used at GW interferometers, computing the PLS curves for ET, CE, LISA and BBO.

In Chapter 2 we overviewed the ΛCDM model, which is the main pillar of modern Cosmology. We summarized the geometrical properties of the Universe and of its particle content, at the homogeneous and isotropic level and by taking into account the small cosmological perturbations. More specifically, we have derived the set of Einstein and Boltzmann equations which control the evolution of the scalar and tensor perturbations of the metric Φ, Ψ and H_{ij}, which are responsible for the anisotropies of the CGWB.

In Chapter 3 we derived the Boltzmann equation for the distribution function of the cosmological gravitons. The solution of the Boltzmann equation shows that the anisotropies

are imprinted by the inhomogeneities encountered by gravitons along their geodesics and by fluctuations in the spectrum of the CGWB at its production. In this chapter we defined rigorously the production time of the CGWB and we introduced the three main sources of primordial GWs considered in this Thesis: inflation, PBH and PT.

In Chapter 4 we performed the first robust computation of the initial conditions on the anisotropies of an inflationary CGWB. In this calculation, we used an original approach in which which we did not evaluate the initial conditions by looking at the Einstein and Boltzmann equations, but we computed directly the energy-momentum tensor of the GWs in terms of the gravitational field h_{ij}. This new result leads to NAD initial conditions for the inflationary waves, which increase the angular power spectrum by an order of magnitude w.r.t. the adiabatic case. In this chapter we presented also the computation of the initial conditions in the case of PBH, stressing the importance of primordial non-Gaussianity to enhance the angular power spectrum.

In Chapter 5 we gave the first numerical prediction of the angular power spectrum of the CGWB, showing the importante of the SW, ISW and of the initial conditions. We furnished also a physical interpretation of the features of the spectra in terms of the scaling with the tensor tilt of the monopole and of the properties of the transfer functions of the perturbations of the metric. In addition, we illustrated that the angular power spectrum is sensitive to the fractional energy density of relativistic and decoupled species at the production of the background. Since cosmological backgrounds were produced at temperatures larger than $10^{12}\,\mathrm{GeV}$, $f_{\mathrm{dec}}(\eta_{\mathrm{in}})$ could be a crucial observable to probe Physics beyond the Standard Model.

In Chapter 6 we computed the angular power spectrum of the cross-correlation between the CMB and CGWB. We elucidated the features of the cross-correlation by mean of the projection effects of photons and gravitons which come from two close (but not identical) last-scattering surfaces. We found that at low multipoles the correlation between these two signals is close to one, mainly because at large angular scales photons and gravitons share the geodesics and are sensitive to the same perturbations of the metric. We stressed the importance of this interrelation between the CMB and the CGWB by showing how from the observed CMB map it is possible to build a precise constrained realization of the CGWB, which could be used in the future to test systematics or foreground contaminations in the data. In this chapter, we estimated also the detectability of the auto- and cross-correlation spectra with future detectors, by computing the SNR for ET+CE, LISA and BBO. We forecasted also the sensitivity of the network ET+CE to the fraction of relativistic and decoupled species introduced in Chapter 5, on f_{NL} and on isocurvature perturbations, finding that tight constraints could be put in the cosmic variance limit or in the case in which the sensitivity of ET is increased by three orders of magnitude. Even though a so large suppression of the instrumental noise of ET is unrealistic, BBO and DECIGO are expected to improve the sensitivity by orders of magnitude. Furthermore, in different frequency bands not constrained by LVK, the amplitudes of CGWBs could be larger than $10^{-10} - 10^{-9}$, giving rise to anisotropies detectable with SNRs large enough to do a precise parameter estimation.

In Chapter 7 we reviewed the AGWB produced by the coalescences of BBH, BNS and

BHNS. We listed the population of the astrophysical sources, describing the PDF of the intrinsic parameters and the number density of the objects in the sky. We computed the monopole for the three different kind of emitters, obtaining results consistent with the LVK bounds. We described then the computation of the intrinsic anisotropies of the AGWB by using the *Cosmic Rulers* formalism, plotting the angular power spectrum of the AGWB emitted by BBH.

In Chapter 8 we illustrated the first prediction of the circular polarization of the AGWB. In spite of the fact that the monopole of the AGWB is expected to be unpolarized in GR, because of the isotropic distribution of the inclination angle of the binaries, we presented the counterintuitive result that when the shot noise fluctuations in the number of sources is taken into account, a net amount of circular polarization is generated, because the average of the inclination angle of the binaries differs from zero. The angular power spectrum of the circular polarization of the shot noise is constant in the multipole space and it scales with the frequency as the square of the monopole, $C_\ell^{\rm SN}(f) \sim f^{4/3}$. Because of the low number of sources that contribute to the background, the shot noise fluctuation is very large and it could be detected with SNR larger than 2 in one year of observations by the network ET+CE. The circular polarization of the AGWB could be at the same time an interesting observable and a foreground for the detection of cosmological signals, like the polarized backgrounds produced during axion inflation. We showed that it is possible to disentangle a cosmological signal by exploiting the different frequency and angular dependence of the shot noise and of the cosmological backgrounds.

In Chapter 9 we gave an extensive description of the dipole of the AGWB sourced by BBH. We characterized the three contributions to the dipole, given by the cosmological perturbations (intrinsic anisotropies), by the shot noise, and by our peculiar motion w.r.t. the rest frame of the sources (kinetic dipole). In this dissertation, we illustrated that at high frequencies the dipole of the AGWB depends on the frequency in a different way compared to the monopole, because of the different contributions coming by binaries in different stages of their evolution. We paid a lot of attention on this frequency dependence, exploiting it to do the first component separation analysis in the context of GW anisotropies. More precisely, we used the different scaling with the frequency of the intrinsic, the kinetic and the shot noise anisotropies to reconstruct our peculiar velocity with high precision, even if the shot noise is orders of magnitude larger than the kinetic and the intrinsic terms.

The work conducted in this Thesis highlights the importance of the study of the anisotropies of SGWBs, which is crucial from the theoretical and observational point of view. Chapter 3, 4 and 5 emphasize the importance of a theoretical description of the Universe at early times, because its geometry, particle content and the initial conditions at early times could strongly affect the angular power spectrum of SGWBs. Chapter 6 points up the possibility of doing multimessenger cosmology with impressive results, because of the large correlation between the CMB and CGWB. Chapter 8 and 9 elucidate the nature of the anisotropies of the AGWB, which could be used to separate the astrophysical and cosmological components and to improve our knowledge of the Universe at late times.

Appendix A

Decomposition of the perturbations in GR

A.1 Gauge transformations in GR

We consider a gauge transformation of the form of Eq. (1.3), which maps the coordinate x^μ to new ones $x^{\mu\prime}$ by using the infinitesimal four-vector ξ^μ. According to [329], a generic tensor Y transforms under this map as

$$Y'(x') = Y(x) + \mathfrak{L}_\xi Y(x)\,, \tag{A.1}$$

where the Lie derivative of a tensor with covariant and contravariant indices along the vector field ξ is defined by

$$\mathfrak{L}_\xi Y^\mu_\nu \equiv \mathcal{D}_\lambda Y^\mu_\nu \xi^\lambda + Y^\mu_\lambda \mathcal{D}_\nu \xi^\lambda - Y^\lambda_\nu \mathcal{D}_\lambda \xi^\mu\,, \tag{A.2}$$

with $\mathcal{D}_\lambda$ the covariant derivative introduced in Eq. (1.22),

$$\mathcal{D}_\rho Y^\mu_\nu \equiv \partial_\rho Y^\mu_\nu + \Gamma^\mu_{\rho\sigma} Y^\sigma_\nu - \Gamma^\sigma_{\rho\nu} Y^\mu_\sigma\,. \tag{A.3}$$

If the tensor Y can be decomposed into a dominant contribution $\bar{Y}$ and a small fluctuation δY, the gauge transformations of the two terms at first order in ξ are

$$Y'(x') = \bar{Y}'(x') + \delta Y'(x') = \bar{Y}(x) + \delta Y(x) + \mathfrak{L}_\xi \bar{Y}(x) \to \begin{cases} \bar{Y}'(x') = \bar{Y}(x) \\ \delta Y'(x') = \delta Y(x) + \mathfrak{L}_\xi \bar{Y}(x) \end{cases} \tag{A.4}$$

A.2 Decomposition of the FLRW metric

As discussed in Chapter 2, the Cosmological Principle states that the Universe is mainly homogeneous and isotropic, thus the dominant contribution to the metric is given by the

FLRW line element given in Eq. (2.1). By adopting the conformal time introduced in Eq. (2.3) and assuming a flat spacetime, the FLRW line element is

$$ds^2 = a^2(\eta)\left[-\mathrm{d}\eta^2 + \delta_{ij}\mathrm{d}x^i\mathrm{d}x^j\right] . \tag{A.5}$$

This line element corresponds to the background metric

$$\bar{g}_{00}(\eta) = -a^2(\eta)\,, \qquad \bar{g}_{0i} = 0\,, \qquad \bar{g}_{ij} = a^2(\eta)\delta_{ij}\,. \tag{A.6}$$

However, tiny inhomogeneities and anisotropies are present in the Universe, therefore small perturbations of the metric should be considered,

$$g_{\mu\nu}(\eta, \mathbf{x}) = \bar{g}_{\mu\nu}(\eta) + \delta g_{\mu\nu}(\eta, \mathbf{x})\,. \tag{A.7}$$

In [235, 236], it has been realized that it is convenient to decompose the metric perturbations into irreducible representations of the group of spatial rotations in the background spacetime. The $(0,0)$ component is a scalar under SO(3), thus we can set

$$\delta g_{00}(\eta, \mathbf{x}) = -2a^2(\eta)A(\eta, \mathbf{x})\,. \tag{A.8}$$

The $(0,i)$ component transforms as a spatial vector, thence it can be decomposed, according to the Helmoltz's theorem, into an curl-free and longitudinal part plus a divergence-free and transverse term,

$$\delta g_{0i}(\eta, \mathbf{x}) = -a^2(\eta)\left[\partial_i B(\eta, \mathbf{x}) + B_i^{\perp}(\eta, \mathbf{x})\right] . \tag{A.9}$$

By definition, for the solenoidal field the divergence vanishes, $\partial^i B_i^{\perp}(\eta, \mathbf{x}) = 0$. The (i,j) component of the metric transforms as a 3×3 symmetric tensor, therefore it can be decomposed into two scalar fields, D and F, a solenoidal vector field, $F_i^{\perp}$, and a transverse-traceless tensor H_{ij},

$$\delta g_{ij}(\eta, \mathbf{x}) = a^2(\eta)\left\{\delta_{ij}\left[1 + 2D(\eta, \mathbf{x})\right] + \left(\partial_i\partial_j - \frac{1}{3}\delta_{ij}\nabla^2\right)F(\eta, \mathbf{x}) + \partial_{(i}F_{j)}^{\perp}(\eta, \mathbf{x}) + H_{ij}(\eta, \mathbf{x})\right\} . \tag{A.10}$$

A.3 Gauge transformations of the metric perturbations

Following Eq. (A.4), the gauge transformation of the perturbations of the metric is

$$\delta g'_{\mu\nu}(\eta', \mathbf{x}') = \delta g_{\mu\nu}(\eta, \mathbf{x}) + \mathfrak{L}_{\xi}\bar{g}_{\mu\nu}(\eta, \mathbf{x})\,. \tag{A.11}$$

Since the covariant derivative of the metric vanishes, the previous equation becomes

$$\delta g'_{\mu\nu}(\eta', \mathbf{x}') = \delta g_{\mu\nu}(\eta, \mathbf{x}) + \mathcal{D}_{\nu}\xi_{\mu}(\eta, \mathbf{x}) + \mathcal{D}_{\mu}\xi_{\nu}(\eta, \mathbf{x})\,. \tag{A.12}$$

In a similar fashion of what has been done for the perturbations of the metric, we decompose the vector field which characterizes the gauge transformations into two scalars and one solenoidal vector,

$$\xi^\mu = \begin{pmatrix} \alpha & \partial^i\beta + \beta^i_\perp \,, \end{pmatrix} \tag{A.13}$$

with $\partial_i \beta^i_\perp = 0$. The covariant derivative of ξ^μ is

$$\begin{aligned}
\mathcal{D}_0\xi^0 =&\partial_0\xi^0 + \Gamma^0_{0\rho}\xi^\rho = \partial_0\xi^0 + \Gamma^0_{00}\xi^0 = \partial_0\xi^0 + \mathcal{H}\xi^0 = \partial_0\alpha + \mathcal{H}\alpha \,, \\
\mathcal{D}_0\xi^i =&\partial_0\xi^i + \Gamma^i_{0\rho}\xi^\rho = \partial_0\xi^i + \Gamma^i_{0j}\xi^j = \partial_0\beta^i_\perp + \partial_0\partial^i\beta + \mathcal{H}\partial^i\beta + \mathcal{H}\beta^i_\perp \,, \\
\mathcal{D}_j\xi^0 =&\partial_j\xi^0 + \Gamma^0_{j\rho}\xi^\rho = \partial_j\xi^0 + \Gamma^0_{jk}\xi^k = \partial_j\alpha + \mathcal{H}\partial_j\beta + \mathcal{H}\beta_{\perp\, j} \,, \\
\mathcal{D}_j\xi^i =&\partial_j\xi^i + \Gamma^i_{j\rho}\xi^\rho = \partial_j\xi^i + \Gamma^i_{j0}\xi^0 = \partial_j\partial^i\beta + \partial_j\beta^i_\perp + \mathcal{H}\delta^i_j\alpha \,,
\end{aligned} \tag{A.14}$$

where to compute the affine connection we have used the terms of order zero in the perturbations which appear in Eq. (2.79). The transformation[1] of the $(0,0)$ perturbation of the metric is then

$$\delta g'_{00}(x') = \delta g_{00}(x) + 2\bar{g}_{0\lambda}(x)\mathcal{D}_0\xi^\lambda(x) = \delta g_{00}(x) + 2\bar{g}_{00}(x)\mathcal{D}_0\xi^0(x) \to A' = A + \partial_0\alpha + \mathcal{H}\alpha \,. \tag{A.15}$$

For the $(0,i)$ part we have

$$\delta g'_{0i}(x) = \delta g_{0i}(x) + \bar{g}_{0\lambda}\mathcal{D}_i\xi^\lambda(x) + \bar{g}_{i\lambda}\mathcal{D}_0\xi^\lambda(x) = \delta g_{0i}(x) + \bar{g}_{00}\mathcal{D}_i\xi^0(x) + \bar{g}_{ij}\mathcal{D}_0\xi^j(x) \,. \tag{A.16}$$

Since at linear order in the perturbations the gauge transformations of irrotational and solenoidal vector are decoupled [236], we disentangle also the gauge transformations of the perturbations of the $(0,i)$ perturbation of the metric,

$$\begin{aligned}
-\partial_i B' =& -\partial_i B - \partial_i\alpha - \mathcal{H}\partial_i\beta + \partial_i\partial_0\beta + \mathcal{H}\partial_i\beta \to B' = B + \alpha - \partial_0\beta \,, \\
-B_i^{\perp\,\prime} =& -B_i^\perp - \mathcal{H}\beta_{\perp\, i} + \partial_0\beta_{\perp\, i} + \mathcal{H}\beta_{\perp\, i} \to B_i^{\perp\,\prime} = B_i^\perp - \partial_0\beta_{\perp\, i} \,.
\end{aligned} \tag{A.17}$$

For the (i,j) component the computation is analogue,

$$\begin{aligned}
\delta g'_{ij}(x') =&\delta g_{ij}(x) + \bar{g}_{i\lambda}(x)\mathcal{D}_j\xi^\lambda + \bar{g}_{j\lambda}(x)\mathcal{D}_i\xi^\lambda = \delta g_{ij}(x) + \bar{g}_{ik}(x)\mathcal{D}_j\xi^k + \bar{g}_{jk}(x)\mathcal{D}_i\xi^k = \\
=&\delta g_{ij}(x) + \mathcal{D}_j\xi_i + \mathcal{D}_i\xi_j \,.
\end{aligned} \tag{A.18}$$

Also in this case we separate the scalar, one of the two proportional to δ_{ij} and the other to $\partial_i\partial_j - \frac{1}{3}\delta_{ij}$, vector and tensor contributions to δg_{ij}, finding

$$\begin{aligned}
2\delta_{ij}D' =&2\delta_{ij}D + 2\delta_{ij}\left(\mathcal{H}\alpha + \frac{1}{3}\nabla^2\beta\right) \to D' = D + \mathcal{H}\alpha + \frac{1}{3}\nabla^2\beta \,, \\
\left(\partial_i\partial_j - \frac{1}{3}\delta_{ij}\nabla^2\right)F' =& \left(\partial_i\partial_j - \frac{1}{3}\delta_{ij}\nabla^2\right)F + 2\left(\partial_j\partial_i - \frac{1}{3}\delta_{ij}\nabla^2\right)\beta \to F' = F + 2\beta \,, \\
\partial_{(i}F_{j)}^{\perp\,\prime} =&\partial_{(i}F_{j)}^\perp + \partial_{(i}\beta_{\perp\, j)} \to F_i^{\perp\,\prime} = F_i^\perp + \beta_{\perp\, i} \,, \\
H'_{ij} =&H_{ij} \,.
\end{aligned} \tag{A.19}$$

[1] To relax the notation, we use the four-vector x as argument of the perturbations and we do not write explicitly η, $\mathbf{x}$.

A.4 Gauge transformations of the perturbations of the energy-momentum tensor

Eq. (2.91) provides the expression for the energy-momentum tensor of a fluid in terms of its pressure, energy density and anisotropic stress,

$$T_{\mu\nu} = (\rho + P)\, u_\mu u_\nu + P\, g_{\mu\nu} + \pi_{\mu\nu}\,. \tag{A.20}$$

The velocity satisfies the conditions $u^\mu u_\mu = -1$ and, if we define $v^i \equiv u^i$, we get

$$u^\mu u^\nu g_{\mu\nu} = -1 \to -\left(u^0_{(0)}\right)^2 - 2u^0_{(1)} - 2Au^0_{(0)} = -\frac{1}{a^2} \to u^0 = \frac{1}{a}\left(1 - A\right)\,. \tag{A.21}$$

The covariant and the contravariant velocities are then

$$u^\mu = \frac{1}{a}\begin{pmatrix}1 - A & v^i\end{pmatrix} \qquad u_\mu = a\begin{pmatrix}-(1+A) & v_i\end{pmatrix}\,. \tag{A.22}$$

The energy momentum tensor is made by a homogeneous and isotropic contribution, $\bar{T}_{\mu\nu}$, whose components are

$$\bar{T}_{00}(\eta) = a^2(\eta)\bar{\rho}(\eta)\,, \qquad \bar{T}_{0i}(\eta) = 0\,, \qquad \bar{T}_{ij}(\eta) = a^2(\eta)\delta_{ij}\bar{P}(\eta)\,. \tag{A.23}$$

Note that the anisotropic stress is present just at first order in the perturbations and, by exploiting the conservation of the energy-momentum tensor, it can be recasted in the form π_{ij}, with vanishing temporal components. The perturbations of the energy-momentum tensor are therefore $\delta\rho$, δP, v^i and π_{ij} and their gauge transformations can be computed by using

$$\delta T'_{\mu\nu}(x') = \delta T_{\mu\nu}(x) + \mathfrak{L}_\xi \bar{T}_{\mu\nu}(x)\,. \tag{A.24}$$

The covariant derivatives of the unperturbed energy-momentum tensor are

$$\begin{aligned}
\mathcal{D}_0\bar{T}_{00} =& \partial_0\bar{T}_{00} - 2\Gamma^\lambda_{00}\bar{T}_{0\lambda} = \partial_0\bar{T}_{00} - 2\Gamma^0_{00}\bar{T}_{00} = a^2\partial_0\bar{\rho}\,,\\
\mathcal{D}_0\bar{T}_{ij} =& \partial_0\bar{T}_{ij} - \Gamma^0_{i\lambda}\bar{T}^\lambda_j - \Gamma^0_{j\lambda}\bar{T}^\lambda_i = \partial_0\bar{T}_{ij} - \Gamma^0_{ik}\bar{T}^k_j - \Gamma^0_{jk}\bar{T}^k_i = \partial_0\bar{T}_{ij} - 2\mathcal{H}\bar{T}_{ij} = a^2\delta_{ij}\partial_0\bar{P}\,,\\
\mathcal{D}_0\bar{T}_{0i} =& \partial_0\bar{T}_{0i} + \Gamma^\rho_{0i}\bar{T}_{0\rho} + \Gamma^\rho_{00}\bar{T}_{i\rho} = 0\,,\\
\mathcal{D}_i\bar{T}_{00} =& \partial_i\bar{T}_{00} - 2\Gamma^\lambda_{i0}\bar{T}_{\lambda 0} = -2\Gamma^0_i 0\bar{T}_{00} = 0\,,\\
\mathcal{D}_k\bar{T}_{ij} =& \partial_k\bar{T}_{ij} - \Gamma^\lambda_{ik}\bar{T}_{kj} - \Gamma^\lambda_{jk}\bar{T}_{\lambda i} = 0\,,\\
\mathcal{D}_j\bar{T}_{0i} =& \partial_j\bar{T}_{0i} + \Gamma^\rho_{ij}\bar{T}_{0\rho} + \Gamma^\rho_{0j}\bar{T}_{\rho i} = a^2\delta_{ij}\mathcal{H}\left(\bar{\rho} + \bar{P}\right)\,.
\end{aligned} \tag{A.25}$$

The energy-momentum tensor at first order is

$$\begin{aligned}
\delta T_{00} =& a^2\left[\bar{\rho}(1+2A) + \delta\rho\right]\,,\\
\delta T_{0i} =& -a^2\left[\left(\bar{\rho} + \bar{P}\right)v_i + \bar{P}\left(\partial_i B + B^\perp_i\right)\right]\,,\\
\delta T_{ij} =& a^2\,\delta_{ij}\,\delta P + a^2\left[(1+2D)\delta_{ij} + \left(\partial_i\partial_j - \frac{1}{3}\delta_{ij}\nabla^2\right)F + \partial_{(i}F^\perp_{j)} + H_{ij}\right]\bar{P} + \pi_{ij}\,.
\end{aligned} \tag{A.26}$$

The perturbation of the $(0,0)$ component is then equal to

$$\delta T'_{00} = \delta T_{00} + \mathcal{D}_\lambda \bar{T}_{00} \xi^\lambda + 2\bar{T}_{\lambda 0} \mathcal{D}_0 \xi^\lambda = \delta T_{00} + \mathcal{D}_0 \bar{T}_{00} \xi^0 + 2\bar{T}_{00} \mathcal{D}_0 \xi^0 \,, \tag{A.27}$$

which corresponds to

$$\delta\rho' + 2\bar{\rho}A' = \delta\rho + 2\bar{\rho}A + \partial_0\bar{\rho}\,\alpha + 2\bar{\rho}\partial_0\alpha + 2\bar{\rho}\mathcal{H}\alpha \to \delta\rho' = \delta\rho + \partial_0\bar{\rho}\alpha \,. \tag{A.28}$$

The perturbation of the (i,j) component is

$$\begin{aligned} \delta T'_{ij} =& \delta T_{ij} + \mathcal{D}_\lambda \bar{T}_{ij} \xi^\lambda + \bar{T}_{\lambda i} \mathcal{D}_j \xi^\lambda + \bar{T}_{\lambda j} \mathcal{D}_i \xi^\lambda = \delta T_{ij} + \mathcal{D}_0 \bar{T}_{ij} \xi^0 + \bar{T}_{ki} \mathcal{D}_j \xi^k + \bar{T}_{kj} \mathcal{D}_i \xi^k = \\ =& \delta T_{ij} + a^2 \delta_{ij}\, \partial_0 \bar{P}\, \alpha + a^2 \bar{P} \left[2\partial_i\partial_j\beta + \partial_i\beta_{\perp j} + \partial_j\beta_{\perp i} + 2\mathcal{H}\delta_{ij}\alpha \right] . \end{aligned} \tag{A.29}$$

From this relation it is straightforward to get

$$\begin{aligned} \pi'_{ij} =& \pi_{ij} \,, \\ \delta P' =& \delta P + \partial_0 \bar{P} \alpha \,. \end{aligned} \tag{A.30}$$

The perturbation of the $(0,i)$ component is

$$\begin{aligned} \delta T'_{0i} =& \delta T_{0i} + \mathcal{D}_\lambda \bar{T}_{0i} \xi^\lambda + \bar{T}_{\lambda 0} \mathcal{D}_i \xi^\lambda + \bar{T}_{\lambda i} \mathcal{D}_0 \xi^\lambda = \delta T_{0i} + \mathcal{D}_j \bar{T}_{0i} \xi^j + \bar{T}_{00} \mathcal{D}_i \xi^0 + \bar{T}_{ki} \mathcal{D}_0 \xi^k = \\ =& \delta T_{0i} + a^2 \left(\bar{\rho} + \bar{P}\right) \mathcal{H} \left(\partial_i\beta + \beta_{\perp i}\right) \\ & + a^2 \left[\bar{\rho} \left(\partial_i\alpha + \mathcal{H}\partial_i\beta + \mathcal{H}\beta_{\perp i}\right) + \bar{P} \left(\partial_0\beta_{i\perp} + \partial_0\partial_i\beta + \mathcal{H}\partial_i\beta + \mathcal{H}\beta_{\perp i}\right) \right] . \end{aligned} \tag{A.31}$$

From this relation we find

$$v'_i = v_i - \partial_i\alpha \tag{A.32}$$

Appendix B

Brill-Hartle Average

In Section 1.1.2 and 1.1.3 we have faced the problem of connecting the macroscopic description of the dynamics of the large-scale background to the microphysics involving directly the metric perturbations with small wavelengths. A similar problem appears in electromagnetism [330], when one would try to determine the electric field in a dielectric medium generated by the superposition of all the single electric charges present. In both cases, it is possible to focus separately on the large- and small-scale features of the system, therefore the most rational choice would be to simplify the complexity of the problem by doing a statistical treatment by averaging over the small scales the equations, avoiding cumbersome computations that keep into account for the microphysics. In analogy with EM, to perform the average it is necessary to rigorously define a scheme to smooth out the microscopic variations of the fields.

In this appendix, we will describe the averaging scheme introduced by Brill and Hartle [98] (BH average), developed also in [35, 36] and, more recently, in [331, 332, 333, 334, 335]. Considering a generic tensor $T_{\mu\nu}(x)$, we defined the Brill-Hartle average by using

$$\langle T_{\mu\nu}(x)\rangle \equiv \int d^4y\, f(x,y)\, \mathcal{B}^{\tilde{\alpha}}_{\mu}(x,y)\, \mathcal{B}^{\tilde{\beta}}_{\nu}(x,y)\, T_{\tilde{\alpha}\tilde{\beta}}(y)\,, \tag{B.1}$$

with $f(x,y)$ a smooth weighting function which falls to zero when $1/q \ll |\vec{x}-\vec{y}| \ll 1/k$, where q and k have been defined in Sec. 1.1.2 and represent the scales over which the background and the GWs vary. The quantity $\mathcal{B}^{\tilde{\alpha}}_{\mu}$ is the bi-vector of geodesic parallel displacement used in [336, 37] and it is the nonlocal generalization of an ordinay tensor field. In our convention, $\mathcal{B}^{\tilde{\alpha}}_{\mu}$ transforms as a covariant vector w.r.t. x for the index μ and as contravariant vector w.r.t. y for the index $\tilde{\alpha}$. In this appendix, we will explicitly show that the BH average satifies the following rules [35, 36]:

1. it is possible to neglect the average of terms of the form $\mathcal{D}_\rho S^\rho_{\mu\nu}$, where $S^\rho_{\mu\nu}$ is an object quadratic in $\gamma^{(\mathrm{GW})}_{\mu\nu}$, because they are suppressed w.r.t. the unaveraged terms by a factor k/q,

$$\left\langle \mathcal{D}_\rho S^\rho_{\mu\nu}\right\rangle_{\mathrm{BH}} \ll \mathcal{D}_\rho S^\rho_{\mu\nu}\,; \tag{B.2}$$

2. it is possible to "integrate by parts" averages,

$$\left\langle \mathcal{D}^{\rho}\gamma_{\mu}^{(\mathrm{GW})\,\sigma}\mathcal{D}_{\sigma}\gamma_{\rho\nu}^{(\mathrm{GW})}\right\rangle = -\left\langle \gamma_{\mu}^{(\mathrm{GW})\,\sigma}\mathcal{D}^{\rho}\mathcal{D}_{\sigma}\gamma_{\rho\nu}^{(\mathrm{GW})}\right\rangle ; \tag{B.3}$$

3. covariant derivatives inside the averages commute when they act on the GWs.

To prove the first point, we make use of the Gauss theorem on curved manifolds,

$$\left\langle \mathcal{D}_{\rho}S_{\mu\nu}^{\rho}\right\rangle = \int_{V} d^{4}y\, f\, \mathcal{B}_{\mu}^{\tilde{\alpha}}\,\mathcal{B}_{\nu}^{\tilde{\beta}}\,\mathcal{D}_{\tilde{\rho}}S_{\tilde{\alpha}\tilde{\beta}}^{\tilde{\rho}} = \int_{\Sigma} d\Sigma_{\tilde{\rho}}\; f\,\mathcal{B}_{\mu}^{\tilde{\alpha}}\,\mathcal{B}_{\nu}^{\tilde{\beta}}S_{\tilde{\alpha}\tilde{\beta}}^{\tilde{\rho}} - \int_{V} d^{4}y\,\mathcal{D}_{\tilde{\rho}}\left[f\,\mathcal{B}_{\mu}^{\tilde{\alpha}}\,\mathcal{B}_{\nu}^{\tilde{\beta}}\right]S_{\tilde{\alpha}\tilde{\beta}}^{\tilde{\rho}} . \tag{B.4}$$

The boundary term is zero, because the smoothing function f vanishes at spatial infinity, while the second terms contain derivatives of tensors and bi-tensors that vary just on large-scales, therefore they are negligible compared to derivatives of $S_{\mu\nu}^{\rho}$, which are proportional to the GWs of high frequency,

$$\left\langle \mathcal{D}_{\rho}S_{\mu\nu}^{\rho}\right\rangle \sim \mathcal{D}_{\rho}S_{\mu\nu}^{\rho}\frac{k}{q} \ll \mathcal{D}_{\rho}S_{\mu\nu}^{\rho} . \tag{B.5}$$

The second property is a corollary of the first rule, since we have shown in our proof for rule 1. that the boundary terms of the average of objects quadratic in the GWs is negligible. In a very trivial way, by exploiting the first two rules, it is also possible to show that the covariant derivates commute when the small scales are smoothed out.

Appendix C

Detectability of the CGWB anisotropies

C.1 Polarization basis

Given a direction of observation $\hat{n}$ and a coordinate system $\{\hat{x}, \hat{y}, \hat{z}\}$ arbitrarily oriented, it is possible to define an orthonormal basis $\{\hat{n}, \hat{u}, \hat{v}\}$ according to

$$\hat{u} \equiv \frac{\hat{n} \times \hat{z}}{|\hat{n} \times \hat{z}|}\,, \qquad \hat{v} \equiv \hat{n} \times \hat{u}\,, \tag{C.1}$$

where $\hat{u}$ and $\hat{v}$ stay in the $\hat{x} - \hat{y}$ plane when $\hat{n} \parallel \hat{z}$. By introducing the spherical coordinates in the $\{\hat{x}, \hat{y}, \hat{z}\}$ basis, it is possible to write

$$\begin{aligned} \hat{n} &= \begin{pmatrix} \sin\theta\cos\phi & \sin\theta\sin\phi & \cos\theta \end{pmatrix}\,, \\ \hat{u} &= \begin{pmatrix} \sin\phi, & -\cos\phi, & 0 \end{pmatrix}\,, \\ \hat{v} &= \begin{pmatrix} \cos\theta\cos\phi, & \cos\theta\sin\phi, & -\sin\theta \end{pmatrix}\,. \end{aligned} \tag{C.2}$$

We define then the $+$, $\times$ polarization tensors by using

$$e_{ij,+}(\hat{n}) \equiv \frac{u_i u_j - v_i v_j}{\sqrt{2}} \qquad e_{ij,\times}(\hat{n}) \equiv \frac{u_i v_j + u_j v_i}{\sqrt{2}}\,. \tag{C.3}$$

This basis is related to the chiral basis L, R by

$$e_{ij,L}(\hat{n}) \equiv \frac{e_{ij,+}(\hat{n}) - i e_{ij,\times}(\hat{n})}{\sqrt{2}} \qquad e_{ij,R}(\hat{n}) \equiv \frac{e_{ij,+}(\hat{n}) + i e_{ij,\times}(\hat{n})}{\sqrt{2}}\,. \tag{C.4}$$

Since the overall amplitude of a stochastic background is independent on the basis used, we can related the amplitudes in the two bases through

$$h_+(\hat{n}, f) e_{ij,+}(\hat{n}) + h_\times(\hat{n}, f) e_{ij,\times}(\hat{n}) = h_L(\hat{n}, f) e_{ij,L}(\hat{n}) + h_R(\hat{n}, f) e_{ij,R}(\hat{n})\,, \tag{C.5}$$

which gives the relations

$$h_L(\hat{n}, f) = \frac{h_+(\hat{n}, f) + i h_\times(\hat{n}, f)}{\sqrt{2}}\,, \qquad h_R(\hat{n}, f) = \frac{h_+(\hat{n}, f) - i h_\times(\hat{n}, f)}{\sqrt{2}}\,. \tag{C.6}$$

C.2 Detector tensor for ground-based interferometers

We consider a detector network whose interferometers are labelled by A and each of them has two arms oriented along the directions $\mathbf{x}_{A,\omega} - \mathbf{x}_{A,1}$ with ω equal to 2 or 3. In our discussion, we assume here that the arms of the interferometers have the same length L. The observable in this case is the time for light to travel from $\mathbf{x}_{A,1}$ to $\mathbf{x}_{A,\omega}$ and to come back[1], looking for gravitational signatures in the time delay between the two measurements. When a GW is crossing the detector, the metric can be written according to

$$\mathrm{d}s^2 = -\mathrm{d}t^2 + \mathrm{d}x^i \mathrm{d}x^j \left[\delta_{ij} + h_{ij}\left(t, \mathbf{x}\right)\right] . \tag{C.7}$$

The geodesics of the photons in the two arms going from $\mathbf{x}_{A,1}$ to $\mathbf{x}_{A,\omega}$ can be written in terms of an affine parameter λ,

$$\mathbf{r}_{A,1\omega}(\lambda) = \mathbf{x}_{A,1} + \lambda\, L\, \hat{l}_{A,\omega} \,, \tag{C.8}$$

where we have defined

$$\hat{l}_{A,\omega} \equiv \frac{\mathbf{x}_{A,\omega} - \mathbf{x}_{A,1}}{|\mathbf{x}_{A,\omega} - \mathbf{x}_{A,1}|} \,. \tag{C.9}$$

By solving the equation of motion for massless particles we get

$$ds^2 = 0 \rightarrow dt^2 = d\mathbf{x}^2 + \mathrm{d}x^i \mathrm{d}x^j \, h_{ij}(t, \mathbf{x}) \rightarrow t_{1\omega}(\lambda) = \lambda\, L + \int_{\Gamma_{1\omega}} \frac{\mathrm{d}x^i \mathrm{d}x^j}{2} h_{ij}\left(t(\tilde{\lambda}), \mathbf{x}(\tilde{\lambda})\right) \,, \tag{C.10}$$

where $\Gamma_{1\omega}$ means that the second integral is evaluated along the trajectories given by Eqs. (C.8) from $\tilde{\lambda} = 0$ to $\tilde{\lambda} = \lambda$. Since h_{ij} is a small perturbation, it is possible to write the argument of the GWs in the previous expression at zero order in h_{ij}, avoiding terms quadratic in the tensor modes, which are subdominant,

$$t_{1\omega}(\lambda) = \lambda\, L + \frac{L}{2} \int_0^\lambda \mathrm{d}\tilde{\lambda}\, \frac{\hat{l}^i_{A,1\omega}\, \hat{l}^j_{A,1\omega}}{2}\, h_{ij}\left(\bar{t} - L + \tilde{\lambda}\, L, \mathbf{x}_{A,1} + \tilde{\lambda}\, L\, \hat{l}_{A,1\omega}\right) \,, \tag{C.11}$$

where $\bar{t} - L$ is the time at which photons start propagating from $\mathbf{x}_{A,1}$. If we write the SGWB in the plane wave expansion defined in Eq. (1.38), we get that the time delay to cross one arm is

$$T_{A,1\omega} = L + L \frac{\hat{l}^i_{A,1\omega}\, \hat{l}^j_{A,1\omega}}{2} \int_0^1 \mathrm{d}\tilde{\lambda} \int \mathrm{d}\hat{n} \int_{-\infty}^{+\infty} \mathrm{d}f \sum_\alpha h_\alpha(\hat{n}, f)\, e^\alpha_{ij}(\hat{n}) \, e^{-2\pi i f \tilde{\lambda} L (1 - \hat{n}\cdot\hat{l}_{A,1\omega})} e^{-2\pi i f (\bar{t} - L - \hat{n}\cdot\mathbf{x}_{A,1})} \,. \tag{C.12}$$

It is possible to perform the integration over λ, finding

$$T_{A,1\omega} = L + L \frac{\hat{l}^i_{A,1\omega}\, \hat{l}^j_{A,1\omega}}{2} \int \mathrm{d}\hat{n} \int_{-\infty}^{+\infty} \mathrm{d}f \sum_\alpha h_\alpha(\hat{n}, f)\, e^\alpha_{ij}(\hat{n}) \, \frac{e^{-2\pi i f L (1 - \hat{n}\cdot\hat{l}_{A,1\omega})} - 1}{-2\pi i f L (1 - \hat{n}\cdot\hat{l}_{A,1\omega})} \, e^{-2\pi i f (\bar{t} - L - \hat{n}\cdot\mathbf{x}_{A,1})} \,. \tag{C.13}$$

[1] This result can be easily generalized to the case of TDI 1.5 variables, in which more complicated paths are considered.

We can re-write the time delays as

$$T_{A,1\omega} = L + L \int \mathrm{d}\hat{n} \int_{-\infty}^{+\infty} \mathrm{d}f \sum_{\alpha} h_\alpha(\hat{n}, f)\, \mathcal{G}_\alpha\left(\hat{n}, \hat{l}_{A,1\omega}\right) \mathcal{M}\left(f\,\hat{n}, \hat{l}_{A,1\omega}\right) e^{-2\pi i f(\bar{t} - L - \hat{n}\cdot\mathbf{x}_{A,1})}\,, \tag{C.14}$$

where we have defined

$$\begin{aligned} \mathcal{G}_\alpha\left(\hat{n}, \hat{l}_{A,1\omega}\right) \equiv & \frac{\hat{l}^i_{A,1\omega}\,\hat{l}^j_{A,1\omega}}{2} e^\alpha_{ij}(\hat{n})\,, \\ \mathcal{M}\left(f\,\hat{n}, \hat{l}_{A,1\omega}\right) \equiv & e^{-i\pi f L(1-\hat{n}\cdot\hat{l}_{A,1\omega})}\,\mathrm{sinc}\left(\pi f L\left(1 - \hat{n}\cdot\hat{l}_{A,1\omega}\right)\right)\,, \end{aligned} \tag{C.15}$$

with the normalization for the sinc function given by

$$\mathrm{sinc}(x) \equiv \frac{\sin x}{x}\,. \tag{C.16}$$

The geodesic of photons in a return flight is parametrized by

$$\mathbf{r}_{A,\omega 1}(\lambda) = \mathbf{x}_{A,1} + (1-\lambda)\, L\, \hat{l}_{A,\omega}\,, \tag{C.17}$$

and we can write at first order $t = \bar{t} + \lambda\, L$. The time to return from $\mathbf{x}_{A,\omega}$ to $\mathbf{x}_{A,1}$ is therefore equal to

$$\begin{aligned} T_{A,\omega 1} = L + L \int \mathrm{d}\hat{n} \int_{-\infty}^{+\infty} \mathrm{d}f \sum_{\alpha} & h_\alpha(\hat{n}, f)\, \mathcal{G}_\alpha\left(\hat{n}, \hat{l}_{A,1\omega}\right) \mathcal{M}\left(f\,\hat{n}, \hat{l}_{A,\omega 1}\right) e^{-2\pi i f(\bar{t} - L - \hat{n}\cdot\mathbf{x}_{A,1})} \\ & e^{2\pi i f L(1-\hat{n}\cdot\hat{l}_{A,1\omega})}\,, \end{aligned} \tag{C.18}$$

where $\hat{l}_{A,\omega 1} = -\hat{l}_{A,1\omega}$. The total time for a round trip in the two arms is given by the combination

$$\begin{aligned} \Delta T_{A,1} \equiv & T_{A,1\omega} + T_{A,\omega 1} = \\ = & 2L + L \int \mathrm{d}\hat{n} \int_{-\infty}^{+\infty} \mathrm{d}f \sum_{\alpha} h_\alpha(\hat{n}, f)\, \mathcal{G}_\alpha\left(\hat{n}, \hat{l}_{A,1\omega}\right) e^{-2\pi i f(\bar{t} - L - \hat{n}\cdot\mathbf{x}_{A,1})} \\ & \left[\mathcal{M}\left(f\,\hat{n}, \hat{l}_{A,1\omega}\right) + \mathcal{M}\left(f\,\hat{n}, \hat{l}_{A,\omega 1}\right) e^{2\pi i f L(1-\hat{n}\cdot\hat{l}_{A,1\omega})}\right]\,. \end{aligned} \tag{C.19}$$

This expression is consistent[2] with [148, 149].

[2]The exponential in their results depend on the quantity we call $\mathbf{x}_{A,2}$ and not on $\mathbf{x}_{A,1}$.

Appendix D

Computation of the source functions of the CGWB

Eq. (3.32) describes the decomposition of the CGWB map at the present time in spherical harmonics. In this appendix, we will derive analytic expressions for the coefficients of the spherical harmonics decomposition for the scalar, tensor and initial contributions to the anisotropies.

Scalar term

The scalar contribution to the angular power spectrum is given by the contributions to the solution of the Boltzmann equation in Eq. (3.31) which depends just on Φ and Ψ,

$$\frac{\delta^S_{\rm CGWB}(\eta_0,\mathbf{q})}{4-n_{\rm gwb}(q)} \equiv \int \frac{{\rm d}^3k}{(2\pi)^3}\left\{\Phi(\eta_{\rm in},\mathbf{k})e^{ik\mu(\eta_{\rm in}-\eta_0)} + \int_{\eta_{\rm in}}^{\eta_0}{\rm d}\tilde{\eta}\left[\Psi'(\tilde{\eta},\mathbf{k})+\Phi'(\tilde{\eta},\mathbf{k})\right]e^{ik\mu(\tilde{\eta}-\eta_0)}\right\}. \tag{D.1}$$

In order to find the coefficient of the expansion in spherical harmonics it is useful to write the exponential in terms of spherical harmonics and spherical Bessel functions,

$$e^{i\mathbf{k}\cdot\mathbf{r}} = 4\pi\sum_{\ell=0}^{\infty}\sum_{m=-\ell}^{\ell} i^\ell\, j_\ell(kr)\, Y^*_{\ell m}(\hat{k})\, Y_{\ell m}(\hat{r}) = , \tag{D.2}$$

therefore we have

$$\begin{aligned}\frac{\delta_{{\rm GW},\ell m,S}(q)}{4-n_{\rm gwb}(q)} =& \int {\rm d}\hat{n}\, Y^*_{\ell m}(\hat{n})\frac{\delta^S_{\rm CGWB}(\eta_0,\mathbf{q})}{4-n_{\rm gwb}(q)}\\ =&4\pi\sum_{L=0}^{\infty}\sum_{M=-L}^{L}(-i)^L\int\frac{{\rm d}^3k}{(2\pi)^3}\,\zeta(\mathbf{k})\,Y^*_{LM}(\hat{k})\Delta^S_L(k,\eta_0,\eta_{\rm in})\int{\rm d}\hat{n}Y^*_{\ell m}(\hat{n})Y_{LM}(\hat{n})\\ =&4\pi(-i)^\ell\int\frac{{\rm d}^3k}{(2\pi)^3}\,\zeta(\mathbf{k})\,Y^*_{\ell m}(\hat{k})\Delta^S_\ell(k,\eta_0,\eta_{\rm in}),\end{aligned} \tag{D.3}$$

where we have used the transformation property of the spherical Bessel function under parity, $j_\ell(x) = (-1)^\ell j_\ell(-x)$, the definitions of the scalar source function, Eq. (3.34), and of the transfer functions of the scalar perturbations of the metric, Eq. (3.35), and the normalization of the spherical harmonics,

$$\int \mathrm{d}\hat{n} Y^*_{\ell m}(\hat{n}) Y_{LM}(\hat{n}) = \delta_{\ell L}\delta_{mM} \,. \tag{D.4}$$

Tensor term

The computation of the coefficients of the spherical harmonics expansion associated to the tensor contribution is more complicated, since it involves a less trivial integration over the direction of observation $\hat{n}$. According to Eq. (3.31), the tensor contribution can be written as

$$\frac{\delta^T_{\mathrm{CGWB}}(\eta_0, \mathbf{q})}{4 - n_{\mathrm{gwb}}(q)} \equiv -\frac{1}{2}\int \frac{\mathrm{d}^3k}{(2\pi)^3} \int_{\eta_{\mathrm{in}}}^{\eta_0} \mathrm{d}\tilde{\eta}\, \hat{n}^i \hat{n}^j H'_{ij}(\tilde{\eta}, \mathbf{k})\, e^{ik\mu(\tilde{\eta}-\eta_0)} \,. \tag{D.5}$$

The coefficient of the expansion in spherical harmonics is compute by using

$$\begin{aligned} \frac{\delta_{\mathrm{GW},\ell m,T}(q)}{4 - n_{\mathrm{gwb}}(q)} &= \int \mathrm{d}\hat{n}\, Y^*_{\ell m}(\hat{n}) \frac{\delta^T_{\mathrm{CGWB}}(\eta_0, \mathbf{q})}{4 - n_{\mathrm{gwb}}(q)} \\ &= -\frac{1}{2}\int \frac{\mathrm{d}^3k}{(2\pi)^3} \int \mathrm{d}\hat{n}\, Y^*_{\ell m}(\hat{n})\, \hat{n}^i \hat{n}^j \int \mathrm{d}\tilde{\eta}\, H'_{ij}(\tilde{\eta}, \mathbf{k}) e^{ik\mu(\tilde{\eta}-\eta_0)} \,. \end{aligned} \tag{D.6}$$

In order to perform the integration over the solid angle, it is convenient to express H_{ij} in terms of its polarization tensors $e_{ij,\lambda}$ in a basis in which the polarization has a simple form. We call $\{\hat{x}, \hat{y}, \hat{z}\}$ the canonical basis in which the direction of observation is expressed according to Eq. (C.2). We introduce then the basis $\{\hat{r}, \hat{s}, \hat{k}\}$ orthonormal to the vector $\hat{k}$, following Appendix C.1. This new basis is expressed in the canonical basis by using

$$\begin{aligned} \hat{k} &= \begin{pmatrix} \sin\theta_k \cos\phi_k & \sin\theta_k \sin\phi_k & \cos\theta_k \end{pmatrix} , \\ \hat{r} &= \begin{pmatrix} \sin\phi_k, & -\cos\phi_k, & 0 \end{pmatrix} , \\ \hat{s} &= \begin{pmatrix} \cos\theta_k \cos\phi_k, & \cos\theta_k \sin\phi_k, & -\sin\theta_k \end{pmatrix} . \end{aligned} \tag{D.7}$$

Note that the direction of observation in the canonical basis is just given by

$$\hat{n} = \begin{pmatrix} \sin\theta\cos\phi & \sin\theta\sin\phi & \cos\theta \end{pmatrix} , \tag{D.8}$$

while in the $\{\hat{r}, \hat{s}, \hat{k}\}$ basis is

$$\hat{n}_\mu = \begin{pmatrix} \sin\theta_\mu\cos\phi_\mu & \sin\theta_\mu\sin\phi_\mu & \cos\theta_\mu \end{pmatrix} , \tag{D.9}$$

where $\mu = \cos\theta_\mu$. Eqs. (C.3), (C.4) show that the polarization tensors in the L, R basis are

$$\begin{aligned} e_{ij,R} = e_{ij,+2} &= \frac{1}{2}[(r_i r_j - s_i s_j) + i(r_i s_j + r_j s_i)] \,, \\ e_{ij,L} = e_{ij,-2} &= \frac{1}{2}[(r_i r_j - s_i s_j) - i(r_i s_j + r_j s_i)] \,. \end{aligned} \tag{D.10}$$

In this basis, the contraction between $\hat{n}_\mu$ and the polarization tensors which appear in the solution of the Boltzmann equation is simple,

$$\begin{aligned}
\hat{n}^i_\mu \hat{n}^j_\mu e_{ij,L}(\hat{k}) =& \frac{1}{2}\left\{\left[(\sin\theta_\mu\cos\phi_\mu)^2 - (\sin\theta_\mu\sin\phi_\mu)^2\right] + i\,2\,(\sin\theta_\mu\cos\phi_\mu)\,(\sin\theta_\mu\sin\phi_\mu)\right\} = \\
=& \frac{1}{2}\sin^2\theta_\mu\, e^{i\,2\phi_\mu}\,, \\
\hat{n}^i_\mu \hat{n}^j_\mu e_{ij,L}(\hat{k}) =& \frac{1}{2}\left\{\left[(\sin\theta_\mu\cos\phi_\mu)^2 - (\sin\theta_\mu\sin\phi_\mu)^2\right] - i\,2\,(\sin\theta_\mu\cos\phi_\mu)\,(\sin\theta_\mu\sin\phi_\mu)\right\} = \\
=& \frac{1}{2}\sin^2\theta_\mu\, e^{-i\,2\phi_\mu}\,.
\end{aligned} \tag{D.11}$$

By recalling the functional form of the tensor transfer function introduced in Eq. (3.35), we have

$$\frac{1}{2}\hat{n}^i_\mu \hat{n}^j_\mu\, H_{ij}(\eta,\mathbf{k}) = \frac{1}{4}(1-\mu^2)T_H(\eta,k)\left[e^{2i\phi_\mu}\, H_L(\mathbf{k}) + e^{-2i\phi_\mu}\, H_R(\mathbf{k})\right]\,, \tag{D.12}$$

where we have assumed that the transfer function for the two polarization states of the tensor perturbations are identical. The only change in Eq. (D.15) due to the change of basis from $\hat{n}$ to $\hat{n}_\mu$ is given by the transformation of the spherical harmonics, which transforms according to the Wigner D-matrix,

$$Y^*_{\ell m}(\hat{n}) = \sum_{m'=-\ell}^{+\ell} D^{(\ell)}_{mm'}(\hat{k}) Y^*_{\ell m}(\hat{n}_\mu). \tag{D.13}$$

The Wigner matrices can be computed in terms of the spin-weighted spherical harmonics,

$$D^{(\ell)}_{ms}(\hat{k}) = \sqrt{\frac{4\pi}{2\ell+1}}(-1)^s\, {}_sY^*_{\ell m}(\hat{k})\,. \tag{D.14}$$

Eq. (D.15) becomes now

$$\begin{aligned}
\frac{\delta_{\mathrm{GW},\ell m,T}(q)}{4-n_{\mathrm{gwb}}(q)} =& -\frac{1}{2}\int\frac{\mathrm{d}^3k}{(2\pi)^3}\int \mathrm{d}\hat{n}_\mu \sum_{s=-\ell}^{+\ell}\sqrt{\frac{4\pi}{2\ell+1}}(-1)^s\, {}_sY^*_{\ell m}(\hat{k})\, Y^*_{\ell m}(\hat{n}_\mu) \\
& \int \mathrm{d}\tilde{\eta}\, e^{ik\mu(\tilde{\eta}-\eta_0)}\, \hat{n}^i_\mu \hat{n}^j_\mu H'_{ij}(\tilde{\eta},\mathbf{k}) \\
=& -\frac{1}{4}\int\frac{\mathrm{d}^3k}{(2\pi)^3}\sum_{se=-\ell}^{+\ell}\sqrt{\frac{4\pi}{2\ell+1}}(-1)^s\, {}_sY^*_{\ell m}(\hat{k})\int \mathrm{d}\tilde{\eta}\, e^{ik\mu(\tilde{\eta}-\eta_0)}\, T'_H(\tilde{\eta},k) \\
& \int \mathrm{d}\hat{n}_\mu Y^*_{\ell m}(\hat{n}_\mu)(1-\mu^2)\left[e^{2i\phi_\mu}\, H_L(\mathbf{k}) + e^{-2i\phi_\mu}\, H_R(\mathbf{k})\right]
\end{aligned} \tag{D.15}$$

The spherical harmonics can be written in terms of the Legendre polynomials according to

$$Y^*_{\ell m}(\hat{n}_\mu) = (-1)^m\left[\frac{2\ell+1}{4\pi}\frac{(\ell-m)!}{(\ell+m)!}\right]^{\frac{1}{2}}\mathcal{P}_{\ell m}(cos\theta_\mu)e^{-im\phi_\mu}\,. \tag{D.16}$$

It is possible therefore to split the integral over $\hat{n}_\mu$ can be splitted in two integrals over ϕ_μ and θ_μ. The integration over the anomaly angle gives a condition of the form

$$\int_0^{2\pi} \mathrm{d}\phi_\mu e^{i\alpha\phi_\mu} = 2\pi\,\delta_{\alpha 0}\,, \tag{D.17}$$

which corresponds to a term proportional to $\delta_{2-m\,0}$ and $\delta_{2+m\,0}$ for the contributions proportional to H_L and H_R respectively. The integral over θ_μ is done by exploiting the definition of the associated Legendre polynomials introduced in Eq. (D.16),

$$\begin{aligned}
\mathcal{P}_{\ell|m|}(x) =& (-1)^{|m|}(1-x^2)^{\frac{|m|}{2}}\frac{d^{|m|}\mathcal{P}_\ell(x)}{dx^{|m|}}\,,\\
\mathcal{P}_{\ell-|m|}(x) =& (-1)^{|m|}\frac{(\ell-|m|)!}{(\ell+|m|)!}\mathcal{P}_{\ell|m|}(x)\,,
\end{aligned} \tag{D.18}$$

where the Legendre polynomials are defined by the differential equation

$$\frac{d}{dx}\Big[(1-x^2)\frac{d\mathcal{P}_\ell(x)}{dx}\Big] = -\ell(\ell+1)\mathcal{P}_\ell(x)\,. \tag{D.19}$$

In order to compute the integral over θ_μ we use

$$\int_{-1}^{+1}\frac{d\mu}{2}\mathcal{P}_\ell(\mu)e^{ik\mu(\eta-\eta_0)} = \frac{1}{(-i)^\ell}j_\ell[k(\eta-\eta_0)]\,. \tag{D.20}$$

The integration by parts of the integral w.r.t. θ_μ gives

$$\begin{aligned}
I =& \int_{-1}^{+1}\frac{d\mu}{4}e^{ik\mu(\eta-\eta_0)}(1-\mu^2)^2\frac{d^2\mathcal{P}_\ell}{d\mu^2} = \int_{-1}^{+1}\frac{d\mu}{4}e^{ik\mu(\eta-\eta_0)}(1-\mu^2)\Big[2\mu\frac{d\mathcal{P}_\ell}{d\mu}-\ell(\ell+1)\mathcal{P}_\ell\Big] =\\
=& \int_{-1}^{+1}\frac{d\mu}{4}e^{ik\mu(\eta-\eta_0)}\Big\{-\frac{2}{ik(\eta-\eta_0)}\Big[\mu\frac{d}{d\mu}\Big((1-\mu^2)\frac{d\mathcal{P}_\ell}{d\mu}\Big)+(1-\mu^2)\frac{d\mathcal{P}_\ell}{d\mu}\Big]\\
&\qquad -\ell(\ell+1)(1-\mu^2)\mathcal{P}_\ell\Big\} =\\
=& \int_{-1}^{+1}\frac{d\mu}{4}e^{ik\mu(\eta-\eta_0)}\Big\{+\frac{2\mu}{ik(\eta-\eta_0)}\ell(\ell+1)\mathcal{P}_\ell+\frac{2}{k^2(\eta-\eta_0)^2}\ell(\ell+1)\mathcal{P}_\ell-\frac{2\ell(\ell+1)}{ik(\eta-\eta_0)}\mu\mathcal{P}_\ell+\\
&\qquad +\frac{\ell(\ell+1)}{ik(\eta-\eta_0)}(1-\mu^2)\frac{d\mathcal{P}_\ell}{d\mu}\Big\} =\\
=& \int_{-1}^{+1}\frac{d\mu}{4}\frac{e^{ik\mu(\eta-\eta_0)}}{k^2(\eta-\eta_0)^2}\mathcal{P}_\ell\ell(\ell+1)(2-\ell^2-\ell) =\\
=& -\frac{1}{2}(-i)^\ell\frac{j_\ell[k(\eta_0-\eta)]}{k^2(\eta_0-\eta)^2}\ell(\ell+1)(\ell+2)(\ell-1).
\end{aligned} \tag{D.21}$$

By plugging these results in Eq. (D.15) we get

$$\begin{aligned}\frac{\delta_{\mathrm{GW},\ell m,T}(q)}{4-n_{\mathrm{gwb}}(q)} &= \int \frac{d^3k}{(2\pi)^3}\sum_{\lambda}\sqrt{\frac{(\ell-\lambda)!}{(\ell+\lambda)!}}{}_{-\lambda}Y^*_{\ell m}(\Omega_k)2\pi(\delta_{\lambda,2}\xi_R+\delta_{\lambda,-2}\xi_L)\frac{1}{2}(-i)^l\times \\ &\qquad \int_{\eta_i}^{\eta_0} d\eta T'_H(\eta,k)\frac{j_\ell[k(\eta_0-\eta)]}{k^2(\eta_0-\eta)2}(\ell-1)\ell(\ell+1)(\ell+2)\Big[\delta_{2,\lambda}+\frac{(\ell-|\lambda|)!}{(\ell+|\lambda|)!}\delta_{\lambda,-2}\Big] \\ &= \int \frac{d^3k}{(2\pi)^3}4\pi(-i)^\ell\sum_{\lambda=\pm2}\xi_\lambda(\vec{k}){}_{-\lambda}Y^*_{\ell m}(\Omega_k)\int_{\eta_i}^{\eta_0}d\eta h'(\eta,k)\frac{j_\ell[k(\eta_0-\eta)]}{k^2(\eta_0-\eta)^2}\frac{1}{4}\sqrt{\frac{(\ell+2)!}{(\ell-2)!}}.\end{aligned} \tag{D.22}$$

Appendix E

Einstein tensor at second and third order in the perturbations

E.1 Energy-momentum tensor of the GWs at third order

The energy-momentum tensor of the CGWB produced by the quantum fluctuations of the metric during inflation has been computed by using the expression provided by [35, 36, 37] in the shortwave approximation, Eq. (1.29). We would like to check the consistency of this expression with the definition of stress-energy tensor of the gravitational field given by [101],

$$T_{\mu\nu}^{(\mathrm{GW})}(x) \equiv -\frac{1}{8\pi G}\, G_{\mu\nu}^{h}(x)\,. \tag{E.1}$$

$G_{\mu\nu}^{(2)}$ is part of the Einstein tensor which is quadratic in the GWs of the CGWB, i.e. the small-scale tensor perturbations of the metric h_{ij} introduced in Eq. (3.3). In our case, the Einstein tensor has to be quadratic in h_{ij}, but it could also contains terms linear in the perturbations of the metric Φ, Ψ and H_{ij}, because we would like to compute the large-scale perturbations of an object proportional to $\left\langle h'_{ij} h^{ij\,\prime} \right\rangle$. The Einstein tensor at third-order can therefore be computed with xPand [337], an algorithm to perturb homogeneous cosmologies. The computation of the Einstein tensor at order zero and one in the large-scale perturbation of the metric gives

$$\begin{aligned}
a^2 G_0^{0\,(2)} =& \frac{1}{8} h^{ij\,\prime} h'_{ij} + \mathcal{H} h^{ij} h'_{ij} + \frac{1}{2} h^{ij} \partial_i \partial_j \Psi - \frac{1}{2} h^{ij} \nabla^2 h_{ij} + \frac{1}{4} \partial^i h^{jk} \partial_k h_{ji} - \frac{3}{8} \partial^k h^{ij} \partial_k h_{ij}\,, \\
a^2 G_0^{0\,(3)} =& \frac{1}{4} \Big(-\Phi h^{ij\,\prime} h'_{ij} + 2\Psi h^{ij\,\prime} h'_{ij} - 2 h^{ij} h'_{ij} \Psi' \\
& - 12 \Psi h^{ij} \nabla^2 h_{ij} + 6 \Psi \partial^k h^{ij} \partial_j h_{ik} - 9 \Psi \partial^k h^{ij} \partial_k h_{ij} + \\
& - 2 H^{ij} h_i^{k\,\prime} h'_{jk} - 8 H^{ij} h^{kl} \partial_j \partial_l h_{ik} + 3 H^{ij} \partial_i h^{kl} \partial_j h_{kl} + 4 h^{ij} H^{kl} \partial_k \partial_l h_{ij} + \\
& + 8 h_i^j H^{ik} \nabla^2 h_{jk} - 4 H^{ij} \partial_j h_{kl} \partial^l h_i^k - 2 H^{ij} \partial_k h_{jl} \partial^l h_i^k + 6 H^{ij} \partial_k h_{jl} \partial^k h_i^l \Big)\,.
\end{aligned} \tag{E.2}$$

In these expressions we have neglected the friction terms $\mathcal{H}h_{ij} \ll h'_{ij}$ and spatial derivatives of the potentials, $\partial_k \Phi h_{ij} \ll \Phi \partial_k h_{ij}$, because we want to compute the energy density of the CGWB in the shortwave approximation, when $q\eta \gg 1$ and $q \gg k$. As proved in Appendix B, these expressions can be simplified by recalling that in the shortwave approximation it is possible to neglect contributions of the form of $\mathcal{D}_\rho S^\rho_{\mu\nu}$, with $S^\rho_{\mu\nu}$ quadratic in h_{ij}. It is possible to show that, neglecting for simplicity the tensor perturbations, that

$$\begin{aligned}
a^2 G_0^{0\,(2)} =& \frac{1}{4} h^{ij\,\prime} h'_{ij} + \frac{1}{8} h^{ij} \mathcal{E}^{(0)}_{ij} + \frac{1}{8} \mathcal{T}^{(0)} - \frac{1}{4} \mathcal{M}^{(0)} + \frac{3}{8} \mathcal{S}^{(0)} \,, \\
a^2 G_0^{0\,(3)} =& \frac{1}{4} \Big(-2\Phi h^{ij\,\prime} h'_{ij} + 4\Psi h^{ij\,\prime} h'_{ij} \\
& - 12 S^{(0)} + \frac{1}{2} \mathcal{G}^{(1)} \\
& - 4 H^{ij} \mathcal{A}^{(0)}_{ij} + 4 H^{ik} \mathcal{P}^{(0)}_{ik} + 4 H^{ik} \mathcal{B}^{(0)}_{ik} - 2 H^{ij} \mathcal{D}^{(0)}_{ij} - H^{ij} \mathcal{F}^{(0)}_{ij} - 3 H^{ij} B^{(0)}_{ij} \Big) \,,
\end{aligned} \tag{E.3}$$

where the negligible terms have been defined in Appendices E.2, E.3. This expressions coincides with the energy density of the CGWB found in Eq. (4.22), obtained from the definition of the energy-momentum tensor given in Eq. (1.29).

E.2 Equation of motion of GWs in a perturbed Universe

The GWs of small frequencies, denoted by h_{ij}, propagate through the large-scale perturbations of the Universe, identified with Φ, Ψ and H_{ij}, therefore by the computation of the Einstein tensor at second order in the perturbations it is possible to understand how the geodesics of the GWs are affected by the presence of the perturbations. The perturbed equation of motion of the GWs is defined by

$$\mathcal{E}^i_j \equiv G^{i\,(\mathrm{TT})}_j = 0 \,, \tag{E.4}$$

where TT identifies the transverse-traceless part of the Einstein tensor. The computation with xPand of this contribution gives

$$h''_{ij} + h'_{ij} \left(2\mathcal{H} - \Phi' + \Psi' \right) + h_{ij} \left(4\mathcal{H}\Psi' + 2\Psi'' \right) - \nabla^2 h_{ij} \left(1 + 2\Phi + 2\Psi \right) + 2 H^{kl} \partial_k \partial_l h_{ij} = 0 \,. \tag{E.5}$$

E.3 Negligible terms in the Brill-Hartle average in the Poisson gauge

Following Appendix B, in the shortwave approximations it is possible to neglect terms of the form

$$\mathcal{D}_\rho S^\rho_{\mu\nu} \,, \tag{E.6}$$

with $S^\rho_{\mu\nu}$ quadratic in the GW degrees of freedom of the metric. These degrees of freedom have been defined in Eq. 4.19 in terms of h_{ij} and of the metric perturbations in the

Poisson gauge. Note that the covariant derivative introduced here has to be computed w.r.t. the metric containing only the large-scale perturbations Φ, Ψ, and not w.r.t. h_{ij}. It is possible to build some negligible quantities starting from total derivative of time covariant derivatives of objects quadratic in the GWs,

$$\begin{aligned}
\mathcal{T} \equiv& \mathcal{D}_0 \left(\gamma^{\mathrm{GW}\,\mathrm{ij}} \mathcal{D}_0 \gamma_{ij}^{\mathrm{GW}}\right) = \\
=& -\left\{h^{ij\,\prime} h'_{ij}(1+4\Psi) + h^{ij} h''_{ij}(1+4\Psi) - h^{ij} h'_{ij}\left[\mathcal{H}(1+4\Psi) + \Phi' - 8\Psi'\right] + 2\left(\Psi'' - \mathcal{H}\Psi'\right) h^{ij} h_{ij}\right\}, \\
\mathcal{S}_{kl} \equiv& \mathcal{D}_k \left(\gamma^{\mathrm{GW}\,\mathrm{ij}}\, \mathcal{D}_l \gamma_{ij}^{\mathrm{GW}}\right) \\
S_{kk} =& -\left\{(1+4\Psi)\left[\partial_k h^{ij} \partial_k h_{ij} + h^{ij} \nabla^2 h_{ij}\right] - 3 h^{ij} h'_{ij}\left[\mathcal{H}(1-2\Phi+2\Psi) - \Psi'\right] - 6\mathcal{H}\Psi' h^{ij} h_{ij}\right\}, \\
\mathcal{M} \equiv& \mathcal{D}^\rho \left(\gamma^{\mathrm{GW}\,\mathrm{jk}} \mathcal{D}_k \gamma_{j\rho}^{\mathrm{GW}}\right) = \\
=& -\frac{1}{a^2}(1+4\Psi)\partial^i h^{jk} \partial_k h_{ij}\,.
\end{aligned} \tag{E.7}$$

The previous terms can be recasted in a four-divergence,

$$\begin{aligned}
\mathcal{G} \equiv& -\mathcal{D}^\mu \left(\gamma^{\mathrm{GW}\,\mathrm{ij}} \mathcal{D}_\mu \gamma_{ij}^{\mathrm{GW}}\right) = \\
=& -h^{ij\,\prime} h'_{ij}(1-2\Phi+4\Psi) - 4\Psi' h^{ij} h'_{ij} + (1+6\Psi)\partial^k h^{ij} \partial_k h_{ij} + h^{ij} \mathcal{E}_{ij}^{(1)} = \\
=& -h^{ij\,\prime} h'_{ij}(1-2\Phi+4\Psi) + (1+6\Psi)\partial^k h^{ij} \partial_k h_{ij}\,,
\end{aligned} \tag{E.8}$$

where we have used the fact that $\mathcal{E}_{ij}^{(1)} = 0$ and that Ψ' is negligible, because the evolution of the large-scale perturbations is zero. Other negligible quantities can be built from total derivatives of covariant derivatives with spatial indices,

$$\begin{aligned}
\mathcal{A}_{ij}^{(0)} \equiv& \mathcal{D}_\rho \left(\gamma^{\mathrm{GW}\,\rho\mathrm{k}} \mathcal{D}_j \gamma_{ik}^{\mathrm{GW}}\right) = h^{lk} \partial_l \partial_j h_{ik}\,, \\
\mathcal{B}_j^{i\,(0)} \equiv& \mathcal{D}_\rho \left(\gamma^{\mathrm{GW}\,\mathrm{ik}} \mathcal{D}^\rho \gamma_{jk}\right) = -\frac{1}{a^2}\left(\partial_l h^{ik} \partial^l h_{jk} - h^{ik\,\prime} h'_{jk}\right), \\
\mathcal{C}_{ij}^{(0)} \equiv& \mathcal{D}_\rho \left(\delta_j^\rho \gamma_{kl}^{\mathrm{GW}} \mathcal{D}^l \gamma_i^{\mathrm{GW}\,\mathrm{k}}\right) = \partial_j h_{kl} \partial^l h_i^k + h_{kl} \partial_j \partial^l h_i^k\,, \\
\mathcal{D}_{ij}^{(0)} \equiv& \mathcal{D}^\rho \left(\delta_\rho^l \mathcal{D}_j h_{kl} h_i^k\right) = \partial_j h_{kl} \partial^l h_i^k\,, \\
\mathcal{F}_{ij}^{(0)} \equiv& \mathcal{D}_\rho \left(h_{jl} \mathcal{D}^l h_i^\rho\right) = \partial_k h_{jl} \partial^l h_i^k\,, \\
\mathcal{P}_{ik}^{(0)} \equiv& \mathcal{D}^l \left(h_i^j \mathcal{D}^l h_{jk}\right) = \partial^l h_i^j \partial_l h_{jk} + h_i^j \nabla^2 h_{jk}\,.
\end{aligned} \tag{E.9}$$

Appendix F

Computation of the transfer functions of the metric perturbations

F.1 Transfer function of scalar perturbations

The transfer functions of scalar perturbations have analytic solutions in the case in which the perturbations re-enter the horizon far from the equality epoch. We compute the evolution of the scalar perturbations in the regimes $k \ll k_{\rm eq}$ and $k \gg k_{\rm eq}$, where the scale of equality has been defined in Eq. (5.21). For the scalar perturbations, we do not consider in this appendix the presence of neutrinos in the computation of the transfer function, because the solutions would not be analytic. The correct transfer functions, which includes also the presence of neutrinos, have been depicted in Figure 5.1.

F.1.1 Super-horizon perturbations during the radiation epoch

We compute the dynamics of the scalar perturbations of wavelength larger the causal horizon during the whole duration of the radiation dominated epoch. We divide the discussion in super-horizon dynamics, in which $k \ll \mathcal{H}$ and in sub-horizon dynamics, for which $k \gg \mathcal{H}$.

Super-horizon dynamics

By looking at the system of Boltzmann equations, Eq. (2.107), we see that the velocity of CDM is suppressed by the expansion of the Universe,

$$v_c' + \mathcal{H} v_c = -ik\Phi \rightarrow v_c' + \mathcal{H} v_c = 0 \rightarrow v \sim \frac{1}{a}\,. \tag{F.1}$$

It is therefore possible to neglect for these scale the effect of v_c in the Einstein and Boltzmann equations. The equations for the distribution function of photons is

$$\Theta_{r,0}' + k\Theta_1 = \Psi' \rightarrow \Theta_0' = \Psi'\,, \tag{F.2}$$

which gives a result also for the CDM density,

$$\delta_c' + ikv_c = 3\Psi' \rightarrow \delta_c' = 3\Psi' \rightarrow \delta' = 3\Theta_{r,0}' \rightarrow \delta_c = 3\Theta_{r,0}\,, \tag{F.3}$$

where in the last step we have used the fact that the initial conditions satisfy exactly $\delta_c(\eta_{\rm in}, k) = \Theta_{r,0}(\eta_{\rm in}, k)/3$. In absence of neutrinos, which provide a quadrupole moment, we have $\Phi = \Psi$ and the Einstein longitudinal scalar part of the Einstein equation, see Eq. (2.108), for super-horizon perturbation becomes

$$3\mathcal{H}(\Psi' + \mathcal{H}\Psi) = -4\pi G a^2 \bar{\rho}_c \delta_c \left(1 + \frac{4}{3}\frac{\bar{\rho}_r}{\bar{\rho}_c}\right) . \tag{F.4}$$

To solve this equation, we choose a convenient parametrization for the time variable,

$$y \equiv \frac{a}{a_{\rm eq}} = \frac{\bar{\rho}_c}{\bar{\rho}_r} \to \frac{\mathrm{d}}{\mathrm{d}\eta} = \frac{\mathrm{d}y}{\mathrm{d}\eta}\frac{\mathrm{d}}{\mathrm{d}y} = \frac{a'}{a}\frac{a}{a_{\rm eq}}\frac{\mathrm{d}}{\mathrm{d}y} = \mathcal{H} y \frac{\mathrm{d}}{\mathrm{d}y} . \tag{F.5}$$

In this way the equation assumes the simpler form

$$3\mathcal{H}^2 y \frac{d}{dy}\Psi + 3\mathcal{H}^2\Psi = -\frac{3}{2}\mathcal{H}^2 \frac{1}{\frac{1}{y}+1}\delta_c\Big(1 + \frac{4}{3y}\Big) . \tag{F.6}$$

In order to express δ_c as a function of Ψ, we derive the equation w.r.t. y, finding

$$\begin{aligned} 0 =& \frac{\mathrm{d}}{\mathrm{d}y}\Big[\frac{6(y+1)}{3y+4}\Big(y\frac{\mathrm{d}\Psi}{\mathrm{d}y} + \Psi\Big)\Big] + 3\frac{\mathrm{d}}{\mathrm{d}y}\Psi = \\ =& \frac{6(y+1)}{3y+4}\Big[2\frac{\mathrm{d}\Psi}{\mathrm{d}y} + y\frac{\mathrm{d}^2\Psi}{\mathrm{d}y^2}\Big] + \frac{6}{(3y+4)^2}\Big(y\frac{\mathrm{d}\Psi}{\mathrm{d}y} + \Psi\Big) + 3\frac{\mathrm{d}\Psi}{\mathrm{d}y} = \\ =& \frac{6(y+1)y}{3y+4}\frac{\mathrm{d}^2\psi}{\mathrm{d}y^2} + \Big[2(y+1)(3y+4) + \frac{(3y+4)^2}{2} + y\Big]\frac{6}{(3y+4)^2}\frac{\mathrm{d}\psi}{\mathrm{d}y} + 6\Psi . \end{aligned} \tag{F.7}$$

The equation we have to solve is then

$$\frac{d^2\Psi}{dy^2} + \frac{21y^2 + 54y + 32}{2y(3y+4)(y+1)}\frac{d\Psi}{dy} + \frac{1}{y(y+1)(3y+4)}\Psi = 0 , \tag{F.8}$$

which has as solution

$$\Psi(\eta, k) = \frac{1}{10y^3}\Big(16\sqrt{1+y} + 9y^3 + 2y^2 - 8y - 16\Big)\Psi(\eta_{\rm in}, k) . \tag{F.9}$$

When $y \ll 1$, i.e., long before $z_{\rm eq}$, $\Psi(\eta, k) = \Psi(\eta_{\rm in}, k)$, while for $y \gg 1$, we get $\Psi(\eta, k) = \frac{9}{10}\Psi(\eta_{\rm in}, k)$. In the absence of neutrinos, Φ and Ψ experience a transition from their initial value, which reduces their amplitudes by a factor 9/10.

Sub-horizon dynamics

After the transition of the potentials around the equality epoch, the potentials are frozen until they are super-horizon, because of the solution given by Eq. (F.9). We discuss now what happens to the metric perturbations when $k \gg \mathcal{H}$ in the matter-dominated epoch. In this stages, the equation for the CDM velocity is

$$v_c' + \mathcal{H} v_c = k\Phi \to (a v_c)' = ka\Phi , \tag{F.10}$$

which admits the solution

$$v(\eta,k)=v(\eta_*,k)\frac{\eta_*^2}{\eta^2}+\frac{k}{\eta^2}\int_{\eta_*}^{\eta}\mathrm{d}\tilde{\eta}\,\tilde{\eta}^2\Phi(\tilde{\eta},k)\,, \tag{F.11}$$

where we have used the expression of the conformal time as a function of the scale factor in the matter-dominated era computed in Eq. (2.13). By using the Einstein equation

$$k^2\Psi=-\frac{3}{2}\mathcal{H}^2\left(\delta_c+\frac{3\mathcal{H}v_c}{k}\right)\,, \tag{F.12}$$

it is possible to find the perturbation of the CDM density,

$$\delta(\eta,k)=-\frac{6}{\eta^3}\left(\frac{v(\eta_{\rm eq},k)\eta_{\rm eq}^2}{k}+\int_{\eta_*}^{\eta}\mathrm{d}\tilde{\eta}\,\tilde{\eta}^2\Phi(\tilde{\eta},k)\right)-\frac{k^2\eta^2}{6}\Psi(\eta,k)\,. \tag{F.13}$$

By using the Boltzmann equation for CDM,

$$\delta_c'+kv_c=3\Psi'\,, \tag{F.14}$$

it is possible to get an integro-differential equation for the dynamics of Ψ in absence of neutrinos,

$$\frac{18+k^2\eta^2}{\eta^4}\left(\int_{\eta_*}^{\eta}\mathrm{d}\tilde{\eta}\tilde{\eta}^2\Psi(\tilde{\eta},k)+\frac{v(\eta_*,k)\eta_*^2}{k}\right)-\frac{k^2\eta^2+18}{6}\Psi'-\frac{k^2\eta^2+18}{3\eta}\Psi=0\,. \tag{F.15}$$

We can derive with respect to the conformal time this expression and we obtain a second-order differential equation for ψ,

$$\frac{\eta^4}{6}\psi''+\eta^3\psi'=0\,. \tag{F.16}$$

This equation admits a solution which decreases with η and another one which is constant, $\psi''=\psi'=0$, thus we get the final solution

$$\Phi(\eta,k)=\Psi(\eta,k)=\frac{9}{10}\Phi(\eta_{\rm in},k). \tag{F.17}$$

F.1.2 Sub-horizon perturbations during the radiation epoch

When $k\gg k_{\rm eq}$ the dynamics of the perturbations is very different. When these modes are super-horizon, the dynamics is identical to the case $k\ll k_{\rm eq}$ during radiation domination. Around the horizon-crossing time, $\eta_{\rm h.c.}=1/k$, the perturbations however start oscillating. To see explicitly, we solve analytically the system of Einstein and Boltzmann equations, neglecting the impact of CDM, since its contribution is subdominant during the radiation dominated epoch. The Einstein equations give

$$k^2\Psi=-6\mathcal{H}^2\left(\Theta_{r,0}+\frac{3\mathcal{H}}{k}\Theta_{r,1}\right)\rightarrow\Theta_{r,0}=-\frac{k^2\eta^2}{6}\Psi-\frac{3}{k\eta}\Theta_{r,1}\,. \tag{F.18}$$

By plugging this expression in the Boltzmann equation for $\Theta_{r,0}$,

$$\Theta'_{r,0} + k\Theta_{r,1} = \Psi' \,, \tag{F.19}$$

we get

$$-\frac{k^2\eta}{3}\Psi - \frac{k^2\eta^2}{6}\Psi' + \frac{3}{k\eta^2}\Theta_{r,1} - \frac{3}{k\eta}\Theta'_{r,1} + k\Theta_{r,1} - \Psi' = 0 \,. \tag{F.20}$$

This equation can be combined with the Boltzmann equation for $\Theta_{r,1}$,

$$\Theta'_{r,1} + \frac{k}{3}\Theta_{r,0} = \frac{k}{3}\Phi \,, \tag{F.21}$$

finding

$$\Theta'_{r,1} + \frac{1}{\eta}\Theta_{r,1} - \frac{k}{3}\Psi\left(1 - \frac{k^2\eta^2}{6}\right) = 0 \,. \tag{F.22}$$

By combining Eqs. (F.20), (F.22) we get

$$\Theta_{r,1} = \frac{k\eta^2}{6}\left(\Psi' + \frac{1}{\eta}\Psi\right) \,. \tag{F.23}$$

It is easy to get then the equation of motion for the scalar perturbations of the metric,

$$\Psi'' + \frac{4}{\eta}\Psi' + \frac{k^2}{3}\Psi = 0 \,. \tag{F.24}$$

The solution of this equation is the spherical bessel function of order one, which can be expressed in terms of trigonometric functions as

$$\Psi(\eta, k) = 3\frac{\sin\frac{k\eta}{\sqrt{3}} - \frac{k\eta}{\sqrt{3}}\cos\frac{k\eta}{\sqrt{3}}}{\left(\frac{k\eta}{\sqrt{3}}\right)^3}\Psi(\eta_{\rm in}, k) \,. \tag{F.25}$$

The dynamics of the perturbations for these perturbations when $\eta \gg \eta_{\rm eq}$ is not important, since these modes are suppressed by the damping which occurred during the radiation epoch.

F.2 Transfer function of tensor perturbations

In the absence of a source of tensor perturbations, the equation of motion of the tensor perturbations is given by the tensor, transverse-traceless part of the Einstein equations,

$$H''_{ij}(\eta, \mathbf{k}) + 2\mathcal{H}(\eta)H'_{ij}(\eta, \mathbf{k}) + k^2 H_{ij}(\eta, \mathbf{k}) = 0 \,. \tag{F.26}$$

In this Thesis, we assume that the two polarizations propagates in an identical way, consistently with GR, therefore we write

$$T''_H(\eta, k) + 2\mathcal{H}(\eta)T'_H(\eta, k) + k^2 T_H(\eta, k) = 0 \,. \tag{F.27}$$

When $k \ll \mathcal{H}$, the equation of motion reduces to

$$T_H''(\eta,k)+2\mathcal{H}(\eta)T_H'(\eta,k)=0 \rightarrow \frac{\mathrm{d}\ln T_H'(\eta,k)}{\mathrm{d}\eta}=-2\frac{\mathrm{d}\ln a(\eta)}{\mathrm{d}\eta} \rightarrow T_H(\eta,k)=A+B\int_0^\eta \frac{\mathrm{d}\tilde{\eta}}{a^2(\tilde{\eta})}\,, \tag{F.28}$$

thus the tensor perturbations are constant for super-horizon scales, because the solution which evolves in time is suppressed by the expansion of the Universe. In the case $k \ll k_{\rm eq}$, the transfer function of the tensor perturbations can be therefore computed during the matter-dominated epoch,

$$T_H''(\eta,k)+\frac{4}{\eta}T_H'(\eta,k)+k^2T_H(\eta,k)=0\,. \tag{F.29}$$

The solution of this equation is simply given in terms of the spherical Bessel function of order one,

$$T_H(\eta,k\ll k_{\rm eq})=\frac{3j_1(k\eta)}{k\eta}\,. \tag{F.30}$$

For $k \gg k_{\rm eq}$, the computation of the transfer function of the tensor perturbations should keep into account for the transition between the radiation- and the matter-dominated eras. In the radiation dominated epoch, the equation of motion is

$$T_H''(\eta,k)+\frac{2}{\eta}T_H'(\eta,k)+k^2T_H(\eta,k)=0\,, \tag{F.31}$$

therefore the transfer function is just

$$T_H(\eta\ll\eta_{\rm eq},k\gg k_{\rm eq})=j_0(k\eta)\,. \tag{F.32}$$

In order to match the solution in the matter- and radiation- dominated epoch we get

$$\begin{aligned} T_H(\eta<\eta_{\rm eq},k>k_{\rm eq}) =& j_0(k\eta)\,,\\ T_H(\eta>\eta_{\rm eq},k>k_{\rm eq}) =& \frac{\eta_{\rm eq}}{\eta}\left[A(k)j_1(k\eta)+B(k)y_1(k\eta)\right]\,,\\ T_H(\eta,k<k_{\rm eq}) =& \frac{j_1(k\eta)}{k\eta}\,, \end{aligned} \tag{F.33}$$

where j_ℓ and y_ℓ are the spherical Bessel function of the first and the second kind, while the coefficients A and B comes from the matching of the solution during the radiation dominated era with the one evaluated during the matter dominated era at the equality,

$$\begin{aligned} A(k) \equiv& \frac{3}{2k\eta_{\rm eq}}-\frac{\cos(2k\eta_{\rm eq})}{2k\eta_{\rm eq}}+\frac{\sin(2k\eta_{\rm eq})}{(k\eta_{\rm eq})^2}\,,\\ B(k) \equiv& -1+\frac{1}{(k\eta_{\rm eq})^2}-\frac{\cos(2k\eta_{\rm eq})}{(k\eta_{\rm eq})^2}-\frac{\sin(2k\eta_{\rm eq})}{2k\eta_{\rm eq}}\,. \end{aligned} \tag{F.34}$$

Appendix G

Table of integrals

The integral of two Bessel functions with different arguments, multiplied by a generic polynomial, has been given in [338] in the form

$$\int \frac{\mathrm{d}x}{x^\lambda} J_\nu(\alpha x) J_\mu(\beta x) = \alpha^\nu \frac{\Gamma\left(\frac{\nu+\mu-\lambda+1}{2}\right)}{2^\lambda \beta^{\nu-\lambda+1} \Gamma\left(\frac{-\nu+\mu+\lambda+1}{2}\right) \Gamma(\nu+1)} F\left(\frac{\nu+\mu-\lambda+1}{2}, \frac{\nu-\mu-\lambda+1}{2}; \nu+1; \frac{\alpha^2}{\beta^2}\right), \tag{G.1}$$

with $0 < \alpha < \beta$, $\mathrm{Re}(\lambda) > -1$, $\mathrm{Re}(\nu+\mu-\lambda+1) > 0$ and F the hypergeometric series.

When the argument of the two Bessel is the same, the integral has also been computed in [338] and it is equal to

$$\int \frac{\mathrm{d}x}{x^\lambda} J_\nu(\alpha x) J_\mu(\alpha x) = \frac{\alpha^{\lambda-1} \Gamma(\lambda) \Gamma\left(\frac{\nu+\mu-\lambda+1}{2}\right)}{2^\lambda \Gamma\left(\frac{-\nu+\mu+\lambda+1}{2}\right) \Gamma\left(\frac{\nu+\mu+\lambda+1}{2}\right) \Gamma\left(\frac{\nu-\mu+\lambda+1}{2}\right)}, \tag{G.2}$$

with $\mathrm{Re}(\nu+\mu+1) > 0$ and $\mathrm{Re}(\lambda) > 0$. When $\nu = \mu = \ell + 1/2$, $\alpha = 1$ and $\lambda = 3 - n_s$, the integral becomes

$$\int \frac{\mathrm{d}x}{x^{3-n_s}} J^2_{\ell+1/2}(x) = \frac{1}{2^{3-n_s}} \frac{\Gamma(3-n_s) \Gamma\left(\frac{2\ell-1+n_s}{2}\right)}{\Gamma^2\left(\frac{4-n_s}{2}\right) \Gamma\left(\frac{2\ell+5-n_s}{2}\right)}. \tag{G.3}$$

Appendix H

Estimator of the angular power spectrum

H.1 Error on the angular power spectrum

We consider $2(2\ell+1)$ Gaussian independent random variables, $x_{\ell m}$, $y_{\ell m}$, one for each value of m at a fixed ℓ. The angular power spectra we are interested in are

$$\frac{1}{2}\langle x_{\ell m} y^*_{\ell' m'} + x^*_{\ell m} y_{\ell' m'}\rangle \equiv \delta_{\ell\ell'}\delta_{mm'} C_\ell^{XY} \,, \tag{H.1}$$

with x, y that could be $\delta_{\mathrm{GW},\,\ell\mathrm{m}}$ and $a_{\ell m}$. Note that, if we include the noise in the analysis, the observed maps are

$$s^x_{\ell m} = x_{\ell m} + n^X_{\ell m} \,. \tag{H.2}$$

In this thesis, we assume that the noise is a Gaussian random variable of zero mean and that the covariance of the map can be written as an angular power spectrum[1] The expectation value and the covariance of the noise are defined as

$$\begin{aligned} \langle n^X_{\ell m}\rangle \equiv& 0 \,, \\ \langle n^X_{\ell m} n^{Y\,*}_{\ell' m'}\rangle \equiv& N_\ell^{XY} \,. \end{aligned} \tag{H.3}$$

In our discussion, we assume that the noise is uncorrelated w.r.t. the signal we want to measure, although this could not be the most general case[2]. The statistical estimator of the the angular power spectrum C_ℓ^{XY} is the "Pseudo-C_ℓ", obtained by averaging over all the directions in the sky of the square of the maps at a given multipole, minus[3] the bias induced by instrumental noise,

$$\hat{C}_\ell^{XY} \equiv \frac{1}{2\ell+1}\sum_{m=-\ell}^{\ell} \frac{s^X_{\ell m} s^{Y\,*}_{\ell m} + s^{X\,*}_{\ell m} s^Y_{\ell m}}{2} - N_\ell^{XY} \,. \tag{H.4}$$

[1] This is not always true for GW interferometers.

[2] Think for example at the case in which the signal is a cosmological GW background and the noise/-foreground is the astrophysical GW background.

[3] This definition implies that it is possible to characterize in a very precise way the covariance of the noise.

It is immediate to see that, since the signal and the noise are uncorrelated, the estimator we have defined is unbiased,

$$\langle \hat{C}_\ell^{XY} \rangle = C_\ell^{XY} \,. \tag{H.5}$$

In the case in which both surveys are full-sky, the covariance matrix of the estimator of the angular power spectra is diagonal in multipole space. On the contrary, one should take into account for the mode coupling of the spectra due to the break of statistical isotropy in the experiments. As a first approximation, this mode coupling could be included in the factor $f_{\rm sky}$ in the likelihood and, consequently, in the SNR. The covariance at a given multipole is given by

$$\mathfrak{C}_\ell \equiv \begin{pmatrix} \mathfrak{C}_\ell^{XX-XX} & \mathfrak{C}_\ell^{XX-XY} & \mathfrak{C}_\ell^{XX-YY} \\ \mathfrak{C}_\ell^{XX-XY} & \mathfrak{C}_\ell^{XY-XY} & \mathfrak{C}_\ell^{XY-YY} \\ \mathfrak{C}_\ell^{XX-YY} & \mathfrak{C}_\ell^{XY-YY} & \mathfrak{C}_\ell^{YY-YY} \end{pmatrix} \tag{H.6}$$

where the covariance matrix of two angular power spectra is given by

$$\mathfrak{C}_\ell^{\alpha-\beta} \equiv \left\langle \left(C_\ell^\alpha - \hat{C}_\ell^\alpha \right) \left(C_\ell^\beta - \hat{C}_\ell^\beta \right) \right\rangle \,, \tag{H.7}$$

with α and β that could be equal to XX, XY, YY. To compute $\mathfrak{C}_\ell^{\alpha-\beta}$ we exploit the definition of the "Pseudo-C_ℓ" given in Eq. (H.4) and the Wick theorem for Gaussian random variables with zero mean, see e.g. Eq. (A1) of [339], and a procedure analogue to the one used in [340]. We note that $\mathfrak{C}_\ell$ contains four different kind of contributions: the covariance of the same auto-correlation spectrum, the covariance of two different auto-correlation spectra, the covariance of the auto-correlation and the cross-correlation and the covariance of two cross-correlation. To compute it in a general way we write the covariance for $\alpha = AB$ and $\beta = CD$, with A, B, C, D that could be X or Y,

$$\begin{aligned} \mathfrak{C}_\ell^{\alpha-\beta} =& \left\langle \left(C_\ell^{AB} - \hat{C}_\ell^{AB} \right) \left(C_\ell^{CD} - \hat{C}_\ell^{CD} \right) \right\rangle = \left\langle \hat{C}_\ell^{AB} \hat{C}_\ell^{CD} \right\rangle - C_\ell^{AB} C_\ell^{CD} = \\ =& \frac{1}{4} \frac{1}{(2\ell+1)^2} \sum_{m,m'} \left\langle \left(s_{\ell m}^a s_{\ell m}^{b\,*} + s_{\ell m}^{a\,*} s_{\ell m}^b \right) \left(s_{\ell m'}^c s_{\ell m'}^{d\,*} + s_{\ell m'}^{c\,*} s_{\ell m'}^d \right) \right\rangle \\ & - \left(C_\ell^{AB} + N_\ell^{AB} \right) \left(C_\ell^{CD} + N_\ell^{CD} \right) = \\ =& \frac{1}{(2\ell+1)^2} \sum_{m,m'} \left\langle s_{\ell m}^a s_{\ell m}^{b\,*} s_{\ell m'}^c s_{\ell m'}^{d\,*} \right\rangle - \left(C_\ell^{AB} + N_\ell^{AB} \right) \left(C_\ell^{CD} + N_\ell^{CD} \right) \,, \end{aligned} \tag{H.8}$$

where the last term has been obtained by considering the possible combinations of the second terms in the r.h.s. of Eq. (H.4). In the above computation we have simplified the complex-conjugate terms of the a, b, c and d maps, because they would produce the same

result to the final map. By using the Wick theorem as in [340, 339], we get

$$\begin{aligned}
\mathfrak{C}_\ell^{\alpha-\beta} =& \frac{1}{(2\ell+1)^2}\sum_{m,m'}\left\langle (a_{\ell m}+n^a_{\ell m})(b^*_{\ell m}+n^{b*}_{\ell m})(c_{\ell m'}+n^c_{\ell m'})(d^*_{\ell m'}+n^{d*}_{\ell m'})\right\rangle \\
&-\left(C_\ell^{AB}+N_\ell^{AB}\right)\left(C_\ell^{CD}+N_\ell^{CD}\right) = \\
=& \frac{1}{(2\ell+1)^2}\sum_{m,m'}\Big\{\left(C_\ell^{AB}+N_\ell^{AB}\right)\left(C_\ell^{CD}+N_\ell^{CD}\right) \\
&\qquad +\delta_{mm'}\left(C_\ell^{AC}+N_\ell^{AC}\right)\left(C_\ell^{BD}+N_\ell^{BD}\right) \\
&\qquad +\delta_{mm'}\left(C_\ell^{AD}+N_\ell^{AD}\right)\left(C_\ell^{BC}+N_\ell^{BC}\right)\Big\} \\
&-\left(C_\ell^{AB}+N_\ell^{AB}\right)\left(C_\ell^{CD}+N_\ell^{CD}\right) = \\
=& \frac{1}{2\ell+1}\left[\left(C_\ell^{AC}+N_\ell^{AC}\right)\left(C_\ell^{BD}+N_\ell^{BD}\right)+\left(C_\ell^{AD}+N_\ell^{AD}\right)\left(C_\ell^{BC}+N_\ell^{BC}\right)\right] .
\end{aligned} \tag{H.9}$$

It is straightforward to show then that

$$\begin{aligned}
\mathfrak{C}_\ell^{XX-XX} =& \frac{2}{2\ell+1}\left(C_\ell^{XX}+N_\ell^{XX}\right)^2 , \\
\mathfrak{C}_\ell^{XY-XY} =& \frac{1}{2\ell+1}\left[\left(C_\ell^{XY}+N_\ell^{XY}\right)^2+\left(C_\ell^{XX}+N_\ell^{XX}\right)\left(C_\ell^{YY}+N_\ell^{YY}\right)\right] , \\
\mathfrak{C}_\ell^{XX-YY} =& \frac{2}{2\ell+1}\left(C_\ell^{XY}+N_\ell^{XY}\right)^2 , \\
\mathfrak{C}_\ell^{XX-XY} =& \frac{2}{2\ell+1}\left(C_\ell^{XX}+N_\ell^{XX}\right)\left(C_\ell^{XY}+N_\ell^{XY}\right) .
\end{aligned} \tag{H.10}$$

H.2 Likelihood of the angular power spectrum

The likelihood for the Gaussian random variables $x_{\ell m}$ and $y_{\ell m}$ is

$$\mathcal{L}\left(x_{\ell m}, y_{\ell m}\middle| C_\ell^{XX}, C_\ell^{XY}, C_\ell^{YY}\right) = \prod_{\ell,m}\frac{1}{\sqrt{2\pi\det\Sigma_\ell}}\exp\left[-\frac{1}{2}\begin{pmatrix}x_{\ell m} & y_{\ell m}\end{pmatrix}\Sigma_\ell^{-1}\begin{pmatrix}x_{\ell m}\\ y_{\ell m}\end{pmatrix}\right] , \tag{H.11}$$

where the covariance matrix of the data is given by

$$\Sigma_\ell = \begin{pmatrix}C_\ell^{XX}+N_\ell^{XX} & C_\ell^{XY}+N_\ell^{XY}\\ C_\ell^{XY}+N_\ell^{XY} & C_\ell^{YY}+N_\ell^{YY}\end{pmatrix} . \tag{H.12}$$

In the case of full-sky measurements and isotropic noise, the likelihood for the angular power spectra, obtained by using the quadratic estimator in the maps defined in Eq. (H.4), is a Wishart distribution [275]. At high multipoles, the central limit theorem ensures that a Gaussian distribution in the power spectra is a good approximation of the true distribution. However, since the GW experiments are limited by instrumental noise to large angular scales, we cannot use the Gaussian approximation for the likelihood, thus we

use the same likelihood of [1], which is a Wishart distribution obtained starting from two Gaussian random variables,

$$-2\ln\mathcal{L}\left(\hat{C}_\ell^{XX},\hat{C}_\ell^{XY},\hat{C}_\ell^{YY}\middle|C_\ell^{XX},C_\ell^{XY},C_\ell^{YY}\right)=\sum_\ell(2\ell+1)\left[\frac{|D_\ell|}{|C_\ell|}+\ln\frac{|C_\ell|}{|\hat{C}_\ell|}-2\right], \quad \text{(H.13)}$$

where we have defined the following determinants,

$$\begin{aligned}
|D_\ell| &\equiv \left(C_\ell^{XX}+N_\ell^{XX}\right)\left(\hat{C}_\ell^{YY}+N_\ell^{YY}\right)+\left(\hat{C}_\ell^{XX}+N_\ell^{XX}\right)\left(C_\ell^{YY}+N_\ell^{YY}\right)\\
&\quad -2\left(C_\ell^{XY}+N_\ell^{XY}\right)\left(\hat{C}_\ell^{XY}+N_\ell^{XY}\right),\\
|C_\ell| &\equiv \left(C_\ell^{XX}+N_\ell^{XX}\right)\left(C_\ell^{YY}+N_\ell^{YY}\right)-\left(C_\ell^{XY}+N_\ell^{XY}\right)^2,\\
|\hat{C}_\ell| &\equiv \left(\hat{C}_\ell^{XX}+N_\ell^{XX}\right)\left(\hat{C}_\ell^{YY}+N_\ell^{YY}\right)-\left(\hat{C}_\ell^{XY}+N_\ell^{XY}\right)^2.
\end{aligned} \quad \text{(H.14)}$$

Although the likelihood is not Gaussian, it is always possible to quantify the detectability of the angular power spectra by computing the signal-to-noise ratio (SNR), defined by

$$\mathrm{SNR}\equiv\left[\sum_\ell\begin{pmatrix}C_\ell^{XX} & C_\ell^{XY} & C_\ell^{YY}\end{pmatrix}\mathfrak{C}_\ell^{-1}\begin{pmatrix}C_\ell^{XX}\\ C_\ell^{XY}\\ C_\ell^{YY}\end{pmatrix}\right]^{1/2}, \quad \text{(H.15)}$$

where the covariance matrix is the one defined in Eq. (H.6). In the limit in which we consider just the auto- or the cross-correlation of one of the two signals, marginalizing w.r.t. the other spectra, the SNRs are equal to

$$\begin{aligned}
\mathrm{SNR}_{\mathrm{auto}} &= \left[\sum_\ell\frac{C_\ell^{XX}}{\mathfrak{C}_\ell^{XX-XX}}\right]^{1/2}=\left[\sum_\ell\frac{2\ell+1}{2}\frac{\left(C_\ell^{XX}\right)^2}{\left(C_\ell^{XX}+N_\ell^{XX}\right)^2}\right]^{1/2},\\
\mathrm{SNR}_{\mathrm{cross}} &= \left[\sum_\ell\frac{C_\ell^{XY}}{\mathfrak{C}_\ell^{XY-XY}}\right]^{1/2}=\left[\sum_\ell\frac{(2\ell+1)\left(C_\ell^{XY}\right)^2}{\left(C_\ell^{XY}+N_\ell^{XY}\right)^2+\left(C_\ell^{XX}+N_\ell^{XX}\right)\left(C_\ell^{YY}+N_\ell^{YY}\right)}\right]^{1/2}.
\end{aligned} \quad \text{(H.16)}$$

Appendix I

SKAO2

The parametrization of the futuristic SKAO "phase two" (SKAO2) is described in [341],

$$\begin{aligned}
\frac{\mathrm{d}N}{\mathrm{d}\Omega_e \mathrm{d}z} =& 10^{c_1(S_c)} z^{c_2(S_c)} \exp\left[-c_3(S_c) z\right] \deg^{-2}, \\
c_1 =& 6.55\,,\ c_2 = 1.93\,,\ c_3 = 6.12\,, \\
Q(z) =& 0.28z^4 - 1.18z^3 + 1.76z^2 + 1.367z\,, \\
b_e^g(z) =& 0.08z^5 - 5.47z^4 + 16.4z^3 - 19.6z^2 + 7.35z + 0.22e^{89.2z^4 - 169.2z^3 - 102.5z^2 + 15.5z + 0.24}\,.
\end{aligned} \tag{I.1}$$

There are basically two reasons why we have chosen SKAO2. The first one is that this survey has an high sky coverage, $f_{\mathrm{sky}}^{\mathrm{SKAO}} \approx 72\%$. In addition, the SKAO2 window function peaks in a similar redshift range of the window function of the AGWB $\tilde{W}$. This means that the cross-correlation is very high and this increases the SNR.

Bibliography

[1] F. Schulze, L. Valbusa Dall'Armi, J. Lesgourgues, A. Ricciardone, N. Bartolo, D. Bertacca, C. Fidler, and S. Matarrese, "GW_CLASS: Cosmological Gravitational Wave Background in the Cosmic Linear Anisotropy Solving System," 5 2023.

[2] L. Valbusa Dall'Armi, A. Mierna, S. Matarrese, and A. Ricciardone, "Adiabatic or Non-Adiabatic? Unraveling the Nature of Initial Conditions in the Cosmological Gravitational Wave Background," 7 2023.

[3] L. Valbusa Dall'Armi, A. Ricciardone, N. Bartolo, D. Bertacca, and S. Matarrese, "Imprint of relativistic particles on the anisotropies of the stochastic gravitational-wave background," *Phys. Rev. D*, vol. 103, no. 2, p. 023522, 2021.

[4] A. Ricciardone, L. V. Dall'Armi, N. Bartolo, D. Bertacca, M. Liguori, and S. Matarrese, "Cross-Correlating Astrophysical and Cosmological Gravitational Wave Backgrounds with the Cosmic Microwave Background," *Phys. Rev. Lett.*, vol. 127, no. 27, p. 271301, 2021.

[5] L. Valbusa Dall'Armi, A. Nishizawa, A. Ricciardone, and S. Matarrese, "Circular Polarization of the Astrophysical Gravitational Wave Background," *Phys. Rev. Lett.*, vol. 131, no. 4, p. 041401, 2023.

[6] L. Valbusa Dall'Armi, A. Ricciardone, and D. Bertacca, "The dipole of the astrophysical gravitational-wave background," *JCAP*, vol. 11, p. 040, 2022.

[7] B. P. Abbott *et al.*, "Observation of Gravitational Waves from a Binary Black Hole Merger," *Phys. Rev. Lett.*, vol. 116, no. 6, p. 061102, 2016.

[8] R. Abbott *et al.*, "GWTC-3: Compact Binary Coalescences Observed by LIGO and Virgo During the Second Part of the Third Observing Run," 11 2021.

[9] G. Agazie *et al.*, "The NANOGrav 15 yr Data Set: Evidence for a Gravitational-wave Background," *Astrophys. J. Lett.*, vol. 951, no. 1, p. L8, 2023.

[10] J. Antoniadis *et al.*, "The second data release from the European Pulsar Timing Array III. Search for gravitational wave signals," 6 2023.

[11] D. J. Reardon *et al.*, "Search for an Isotropic Gravitational-wave Background with the Parkes Pulsar Timing Array," *Astrophys. J. Lett.*, vol. 951, no. 1, p. L6, 2023.

[12] H. Xu *et al.*, "Searching for the Nano-Hertz Stochastic Gravitational Wave Background with the Chinese Pulsar Timing Array Data Release I," *Res. Astron. Astrophys.*, vol. 23, no. 7, p. 075024, 2023.

[13] M. "Punturo and others", "The einstein telescope: a third-generation gravitational wave observatory," *Classical and Quantum Gravity*, vol. 27, p. 194002, sep 2010.

[14] D. Reitze *et al.*, "Cosmic Explorer: The U.S. Contribution to Gravitational-Wave Astronomy beyond LIGO," *Bull. Am. Astron. Soc.*, vol. 51, no. 7, p. 035, 2019.

[15] P. "Amaro-Seoane and others", "Laser interferometer space antenna," 2017.

[16] W.-R. Hu and Y.-L. Wu, "The Taiji Program in Space for gravitational wave physics and the nature of gravity," *Natl. Sci. Rev.*, vol. 4, no. 5, pp. 685–686, 2017.

[17] G. M. Harry, P. Fritschel, D. A. Shaddock, W. Folkner, and E. S. Phinney, "Laser interferometry for the big bang observer," *Class. Quant. Grav.*, vol. 23, pp. 4887–4894, 2006. [Erratum: Class.Quant.Grav. 23, 7361 (2006)].

[18] S. Kawamura *et al.*, "The Japanese space gravitational wave antenna: DECIGO," *Class. Quant. Grav.*, vol. 28, p. 094011, 2011.

[19] A. R. Liddle and D. H. Lyth, *Cosmological inflation and large scale structure*. 2000.

[20] C. J. Hogan, "Gravitational radiation from cosmological phase transitions," *Mon. Not. Roy. Astron. Soc.*, vol. 218, pp. 629–636, 1986.

[21] T. Damour and A. Vilenkin, "Gravitational wave bursts from cosmic strings," *Phys. Rev. Lett.*, vol. 85, pp. 3761–3764, 2000.

[22] T. Damour and A. Vilenkin, "Gravitational wave bursts from cusps and kinks on cosmic strings," *Phys. Rev. D*, vol. 64, p. 064008, 2001.

[23] N. Bartolo, D. Bertacca, V. De Luca, G. Franciolini, S. Matarrese, M. Peloso, A. Ricciardone, A. Riotto, and G. Tasinato, "Gravitational wave anisotropies from primordial black holes," *JCAP*, vol. 02, p. 028, 2020.

[24] M. M. Anber and L. Sorbo, "N-flationary magnetic fields," *JCAP*, vol. 10, p. 018, 2006.

[25] A. A. Penzias and R. W. Wilson, "A Measurement of excess antenna temperature at 4080-Mc/s," *Astrophys. J.*, vol. 142, pp. 419–421, 1965.

[26] N. Aghanim *et al.*, "Planck 2018 results. VI. Cosmological parameters," *Astron. Astrophys.*, vol. 641, p. A6, 2020. [Erratum: Astron.Astrophys. 652, C4 (2021)].

[27] C. L. Bennett, A. Banday, K. M. Gorski, G. Hinshaw, P. Jackson, P. Keegstra, A. Kogut, G. F. Smoot, D. T. Wilkinson, and E. L. Wright, "Four year COBE DMR cosmic microwave background observations: Maps and basic results," *Astrophys. J. Lett.*, vol. 464, pp. L1–L4, 1996.

[28] Y. Akrami *et al.*, "Planck 2018 results. VII. Isotropy and Statistics of the CMB," *Astron. Astrophys.*, vol. 641, p. A7, 2020.

[29] P. Coles and F. Lucchin, *Cosmology: The Origin and evolution of cosmic structure.* 1995.

[30] A. H. Guth, "The Inflationary Universe: A Possible Solution to the Horizon and Flatness Problems," *Phys. Rev. D*, vol. 23, pp. 347–356, 1981.

[31] S. W. Hawking, "The Development of Irregularities in a Single Bubble Inflationary Universe," *Phys. Lett. B*, vol. 115, p. 295, 1982.

[32] A. H. Guth and S. Y. Pi, "Fluctuations in the New Inflationary Universe," *Phys. Rev. Lett.*, vol. 49, pp. 1110–1113, 1982.

[33] A. A. Starobinsky, "Dynamics of Phase Transition in the New Inflationary Universe Scenario and Generation of Perturbations," *Phys. Lett. B*, vol. 117, pp. 175–178, 1982.

[34] Y. Akrami *et al.*, "Planck 2018 results. X. Constraints on inflation," *Astron. Astrophys.*, vol. 641, p. A10, 2020.

[35] R. A. Isaacson, "Gravitational Radiation in the Limit of High Frequency. I. The Linear Approximation and Geometrical Optics," *Phys. Rev.*, vol. 166, pp. 1263–1271, 1968.

[36] R. A. Isaacson, "Gravitational Radiation in the Limit of High Frequency. II. Nonlinear Terms and the Ef fective Stress Tensor," *Phys. Rev.*, vol. 166, pp. 1272–1279, 1968.

[37] C. W. Misner, K. S. Thorne, and J. A. Wheeler, *Gravitation.* San Francisco: W. H. Freeman, 1973.

[38] C. R. Contaldi, "Anisotropies of Gravitational Wave Backgrounds: A Line Of Sight Approach," *Phys. Lett. B*, vol. 771, pp. 9–12, 2017.

[39] N. Bartolo, D. Bertacca, S. Matarrese, M. Peloso, A. Ricciardone, A. Riotto, and G. Tasinato, "Anisotropies and non-Gaussianity of the Cosmological Gravitational Wave Background," *Phys. Rev. D*, vol. 100, no. 12, p. 121501, 2019.

[40] N. Bartolo, D. Bertacca, S. Matarrese, M. Peloso, A. Ricciardone, A. Riotto, and G. Tasinato, "Characterizing the cosmological gravitational wave background: Anisotropies and non-Gaussianity," *Phys. Rev. D*, vol. 102, no. 2, p. 023527, 2020.

[41] W. Hu, D. N. Spergel, and M. J. White, "Distinguishing causal seeds from inflation," *Phys. Rev. D*, vol. 55, pp. 3288–3302, 1997.

[42] S. Dodelson, *Modern Cosmology.* Amsterdam: Academic Press, 2003.

[43] R. K. Sachs and A. M. Wolfe, "Perturbations of a cosmological model and angular variations of the microwave background," *Astrophys. J.*, vol. 147, pp. 73–90, 1967.

[44] J. Lesgourgues, "The Cosmic Linear Anisotropy Solving System (CLASS) I: Overview," 4 2011.

[45] D. Blas, J. Lesgourgues, and T. Tram, "The Cosmic Linear Anisotropy Solving System (CLASS) II: Approximation schemes," *JCAP*, vol. 07, p. 034, 2011.

[46] A. Malhotra, E. Dimastrogiovanni, G. Domènech, M. Fasiello, and G. Tasinato, "New universal property of cosmological gravitational wave anisotropies," *Phys. Rev. D*, vol. 107, no. 10, p. 103502, 2023.

[47] E. S. Phinney, "A Practical theorem on gravitational wave backgrounds," 7 2001.

[48] T. Regimbau, "The astrophysical gravitational wave stochastic background," *Res. Astron. Astrophys.*, vol. 11, pp. 369–390, 2011.

[49] V. Ferrari, S. Matarrese, and R. Schneider, "Stochastic background of gravitational waves generated by a cosmological population of young, rapidly rotating neutron stars," *Mon. Not. Roy. Astron. Soc.*, vol. 303, p. 258, 1999.

[50] T. Regimbau and J. A. de Freitas Pacheco, "Cosmic background of gravitational waves from rotating neutron stars," *Astron. Astrophys.*, vol. 376, p. 381, 2001.

[51] V. Ferrari, S. Matarrese, and R. Schneider, "Gravitational wave background from a cosmological population of core collapse supernovae," *Mon. Not. Roy. Astron. Soc.*, vol. 303, p. 247, 1999.

[52] A. Buonanno, G. Sigl, G. G. Raffelt, H.-T. Janka, and E. Muller, "Stochastic gravitational wave background from cosmological supernovae," *Phys. Rev. D*, vol. 72, p. 084001, 2005.

[53] R. Schneider, A. Ferrara, B. Ciardi, V. Ferrari, and S. Matarrese, "Gravitational waves signals from the collapse of the first stars," *Mon. Not. Roy. Astron. Soc.*, vol. 317, p. 385, 2000.

[54] K. C. B. New, "Gravitational waves from gravitational collapse," *Living Rev. Rel.*, vol. 6, p. 2, 2003.

[55] S. Marassi, R. Ciolfi, R. Schneider, L. Stella, and V. Ferrari, "Stochastic background of gravitational waves emitted by magnetars," *Mon. Not. Roy. Astron. Soc.*, vol. 411, p. 2549, 2011.

[56] T. Regimbau and J. A. de Freitas Pacheco, "Gravitational wave background from magnetars," *Astron. Astrophys.*, vol. 447, p. 1, 2006.

[57] R. Schneider, V. Ferrari, S. Matarrese, and S. F. Portegies Zwart, "Gravitational waves from cosmological compact binaries," *Mon. Not. Roy. Astron. Soc.*, vol. 324, p. 797, 2001.

[58] A. J. Farmer and E. S. Phinney, "The gravitational wave background from cosmological compact binaries," *Mon. Not. Roy. Astron. Soc.*, vol. 346, p. 1197, 2003.

[59] T. Regimbau and J. A. de Freitas Pacheco, "Stochastic background from coalescences of NS-NS binaries," *Astrophys. J.*, vol. 642, pp. 455–461, 2006.

[60] A. Sesana, A. Vecchio, and C. N. Colacino, "The stochastic gravitational-wave background from massive black hole binary systems: implications for observations with Pulsar Timing Arrays," *Mon. Not. Roy. Astron. Soc.*, vol. 390, p. 192, 2008.

[61] X.-J. Zhu, E. Howell, T. Regimbau, D. Blair, and Z.-H. Zhu, "Stochastic Gravitational Wave Background from Coalescing Binary Black Holes," *Astrophys. J.*, vol. 739, p. 86, 2011.

[62] T. Regimbau, M. Evans, N. Christensen, E. Katsavounidis, B. Sathyaprakash, and S. Vitale, "Digging deeper: Observing primordial gravitational waves below the binary black hole produced stochastic background," *Phys. Rev. Lett.*, vol. 118, no. 15, p. 151105, 2017.

[63] C. Wu, V. Mandic, and T. Regimbau, "Accessibility of the Gravitational-Wave Background due to Binary Coalescences to Second and Third Generation Gravitational-Wave Detectors," *Phys. Rev. D*, vol. 85, p. 104024, 2012.

[64] D. Alonso, G. Cusin, P. G. Ferreira, and C. Pitrou, "Detecting the anisotropic astrophysical gravitational wave background in the presence of shot noise through cross-correlations," *Phys. Rev. D*, vol. 102, no. 2, p. 023002, 2020.

[65] A. C. Jenkins, J. D. Romano, and M. Sakellariadou, "Estimating the angular power spectrum of the gravitational-wave background in the presence of shot noise," *Phys. Rev. D*, vol. 100, no. 8, p. 083501, 2019.

[66] A. C. Jenkins and M. Sakellariadou, "Shot noise in the astrophysical gravitational-wave background," *Phys. Rev. D*, vol. 100, no. 6, p. 063508, 2019.

[67] G. Cusin and G. Tasinato, "Doppler boosting the stochastic gravitational wave background," *JCAP*, vol. 08, no. 08, p. 036, 2022.

[68] A. K.-W. Chung, A. C. Jenkins, J. D. Romano, and M. Sakellariadou, "Targeted search for the kinematic dipole of the gravitational-wave background," *Phys. Rev. D*, vol. 106, no. 8, p. 082005, 2022.

[69] G. Cusin, C. Pitrou, and J.-P. Uzan, "Anisotropy of the astrophysical gravitational wave background: Analytic expression of the angular power spectrum and correlation with cosmological observations," *Phys. Rev. D*, vol. 96, no. 10, p. 103019, 2017.

[70] G. Cusin, I. Dvorkin, C. Pitrou, and J.-P. Uzan, "First predictions of the angular power spectrum of the astrophysical gravitational wave background," *Phys. Rev. Lett.*, vol. 120, p. 231101, 2018.

[71] A. C. Jenkins, R. O'Shaughnessy, M. Sakellariadou, and D. Wysocki, "Anisotropies in the astrophysical gravitational-wave background: The impact of black hole distributions," *Phys. Rev. Lett.*, vol. 122, no. 11, p. 111101, 2019.

[72] A. C. Jenkins, M. Sakellariadou, T. Regimbau, and E. Slezak, "Anisotropies in the astrophysical gravitational-wave background: Predictions for the detection of compact binaries by LIGO and Virgo," *Phys. Rev. D*, vol. 98, no. 6, p. 063501, 2018.

[73] C. Pitrou, G. Cusin, and J.-P. Uzan, "Unified view of anisotropies in the astrophysical gravitational-wave background," *Phys. Rev. D*, vol. 101, no. 8, p. 081301, 2020.

[74] D. Bertacca, A. Ricciardone, N. Bellomo, A. C. Jenkins, S. Matarrese, A. Raccanelli, T. Regimbau, and M. Sakellariadou, "Projection effects on the observed angular spectrum of the astrophysical stochastic gravitational wave background," *Phys. Rev. D*, vol. 101, no. 10, p. 103513, 2020.

[75] N. Bellomo, D. Bertacca, A. C. Jenkins, S. Matarrese, A. Raccanelli, T. Regimbau, A. Ricciardone, and M. Sakellariadou, "CLASS_GWB: robust modeling of the astrophysical gravitational wave background anisotropies," *JCAP*, vol. 06, no. 06, p. 030, 2022.

[76] N. Barnaby and M. Peloso, "Large Nongaussianity in Axion Inflation," *Phys. Rev. Lett.*, vol. 106, p. 181301, 2011.

[77] L. Sorbo, "Parity violation in the Cosmic Microwave Background from a pseudoscalar inflaton," *JCAP*, vol. 06, p. 003, 2011.

[78] N. Barnaby, R. Namba, and M. Peloso, "Phenomenology of a Pseudo-Scalar Inflaton: Naturally Large Nongaussianity," *JCAP*, vol. 04, p. 009, 2011.

[79] N. Barnaby, E. Pajer, and M. Peloso, "Gauge Field Production in Axion Inflation: Consequences for Monodromy, non-Gaussianity in the CMB, and Gravitational Waves at Interferometers," *Phys. Rev. D*, vol. 85, p. 023525, 2012.

[80] N. Bartolo and G. Orlando, "Parity breaking signatures from a Chern-Simons coupling during inflation: the case of non-Gaussian gravitational waves," *JCAP*, vol. 07, p. 034, 2017.

[81] N. Bartolo, G. Orlando, and M. Shiraishi, "Measuring chiral gravitational waves in Chern-Simons gravity with CMB bispectra," *JCAP*, vol. 01, p. 050, 2019.

[82] N. Bartolo, L. Caloni, G. Orlando, and A. Ricciardone, "Tensor non-Gaussianity in chiral scalar-tensor theories of gravity," *JCAP*, vol. 03, p. 073, 2021.

[83] J. Ellis, M. Fairbairn, G. Hütsi, M. Raidal, J. Urrutia, V. Vaskonen, and H. Veermäe, "Prospects for Future Binary Black Hole GW Studies in Light of PTA Measurements," *Astron. Astrophys.*, vol. 676, p. A38, 2023.

[84] G. Sato-Polito and M. Kamionkowski, "Exploring the spectrum of stochastic gravitational-wave anisotropies with pulsar timing arrays," 5 2023.

[85] A. K. Singal, "LARGE PECULIAR MOTION OF THE SOLAR SYSTEM FROM THE DIPOLE ANISOTROPY IN SKY BRIGHTNESS DUE TO DISTANT RADIO SOURCES," *The Astrophysical Journal*, vol. 742, p. L23, nov 2011.

[86] M. Rubart and D. J. Schwarz, "Cosmic radio dipole from NVSS and WENSS," *Astron. Astrophys.*, vol. 555, p. A117, 2013.

[87] P. Tiwari and A. Nusser, "Revisiting the NVSS number count dipole," *JCAP*, vol. 03, p. 062, 2016.

[88] J. Colin, R. Mohayaee, M. Rameez, and S. Sarkar, "High redshift radio galaxies and divergence from the CMB dipole," *Mon. Not. Roy. Astron. Soc.*, vol. 471, no. 1, pp. 1045–1055, 2017.

[89] T. M. Siewert, M. Schmidt-Rubart, and D. J. Schwarz, "Cosmic radio dipole: Estimators and frequency dependence," *Astron. Astrophys.*, vol. 653, p. A9, 2021.

[90] A. K. Singal, "Discordance of dipole asymmetries seen in recent large radio surveys with the Cosmological Principle," 3 2023.

[91] N. J. Secrest, S. von Hausegger, M. Rameez, R. Mohayaee, S. Sarkar, and J. Colin, "A Test of the Cosmological Principle with Quasars," *Astrophys. J. Lett.*, vol. 908, no. 2, p. L51, 2021.

[92] N. J. Secrest, S. von Hausegger, M. Rameez, R. Mohayaee, and S. Sarkar, "A Challenge to the Standard Cosmological Model," *Astrophys. J. Lett.*, vol. 937, no. 2, p. L31, 2022.

[93] N. Aghanim *et al.*, "Planck 2013 results. XXVII. Doppler boosting of the CMB: Eppur si muove," *Astron. Astrophys.*, vol. 571, p. A27, 2014.

[94] C. Gibelyou and D. Huterer, "Dipoles in the Sky," *Mon. Not. Roy. Astron. Soc.*, vol. 427, pp. 1994–2021, 2012.

[95] A. Einstein, "Über Gravitationswellen," *Sitzungsber. Preuss. Akad. Wiss. Berlin (Math. Phys.)*, vol. 1918, pp. 154–167, 1918.

[96] A. S. Eddington, "The propagation of gravitational waves," *Proc. Roy. Soc. Lond. A*, vol. 102, pp. 268–282, 1922.

[97] H. Weyl and J. Ehlers, *Raum, Zeit, Materie: Vorlesungen über allgemeine Relativitätstheorie*. Springer, 1993.

[98] D. R. Brill and J. B. Hartle, "Method of the Self-Consistent Field in General Relativity and its Application to the Gravitational Geon," *Phys. Rev.*, vol. 135, pp. B271–B278, 1964.

[99] M. Maggiore, *Gravitational Waves. Vol. 1: Theory and Experiments*. Oxford University Press, 2007.

[100] M. Giovannini, "Effective energy density of relic gravitons," *Phys. Rev. D*, vol. 100, no. 8, p. 083531, 2019.

[101] L. D. Landau and E. M. Lifschits, *The Classical Theory of Fields*, vol. Volume 2 of *Course of Theoretical Physics*. Oxford: Pergamon Press, 1975.

[102] L. H. Ford and L. Parker, "Quantized Gravitational Wave Perturbations in Robertson-Walker Universes," *Phys. Rev. D*, vol. 16, pp. 1601–1608, 1977.

[103] L. H. Ford and L. Parker, "Infrared Divergences in a Class of Robertson-Walker Universes," *Phys. Rev. D*, vol. 16, pp. 245–250, 1977.

[104] S. V. Babak and L. P. Grishchuk, "The Energy momentum tensor for the gravitational field," *Phys. Rev. D*, vol. 61, p. 024038, 2000.

[105] B. P. Abbott *et al.*, "GW170817: Observation of Gravitational Waves from a Binary Neutron Star Inspiral," *Phys. Rev. Lett.*, vol. 119, no. 16, p. 161101, 2017.

[106] B. P. Abbott *et al.*, "GW151226: Observation of Gravitational Waves from a 22-Solar-Mass Binary Black Hole Coalescence," *Phys. Rev. Lett.*, vol. 116, no. 24, p. 241103, 2016.

[107] B. P. Abbott *et al.*, "GWTC-1: A Gravitational-Wave Transient Catalog of Compact Binary Mergers Observed by LIGO and Virgo during the First and Second Observing Runs," *Phys. Rev. X*, vol. 9, no. 3, p. 031040, 2019.

[108] R. Abbott *et al.*, "GWTC-2: Compact Binary Coalescences Observed by LIGO and Virgo During the First Half of the Third Observing Run," *Phys. Rev. X*, vol. 11, p. 021053, 2021.

[109] N. J. Cornish and J. D. Romano, "When is a gravitational-wave signal stochastic?," *Phys. Rev. D*, vol. 92, no. 4, p. 042001, 2015.

[110] J. D. Romano and N. J. Cornish, "Detection methods for stochastic gravitational-wave backgrounds: a unified treatment," *Living Rev. Rel.*, vol. 20, no. 1, p. 2, 2017.

[111] D. S. Sivia and J. Skilling, *Data Analysis - A Bayesian Tutorial*. Oxford Science Publications, Oxford University Press, 2nd ed., 2006.

[112] M. Maggiore, *Gravitational Waves. Vol. 2: Astrophysics and Cosmology*. Oxford University Press, 3 2018.

[113] M. C. Guzzetti, N. Bartolo, M. Liguori, and S. Matarrese, "Gravitational waves from inflation," *Riv. Nuovo Cim.*, vol. 39, no. 9, pp. 399–495, 2016.

[114] C. Caprini and D. G. Figueroa, "Cosmological Backgrounds of Gravitational Waves," *Class. Quant. Grav.*, vol. 35, no. 16, p. 163001, 2018.

[115] P. Auclair *et al.*, "Cosmology with the Laser Interferometer Space Antenna," 4 2022.

[116] M. Kamionkowski, A. Kosowsky, and A. Stebbins, "Statistics of cosmic microwave background polarization," *Phys. Rev. D*, vol. 55, pp. 7368–7388, 1997.

[117] V. Alba and J. Maldacena, "Primordial gravity wave background anisotropies," *JHEP*, vol. 03, p. 115, 2016.

[118] G. Nelemans, L. R. Yungelson, and S. F. Portegies Zwart, "The gravitational wave signal from the galactic disk population of binaries containing two compact objects," *Astron. Astrophys.*, vol. 375, pp. 890–898, 2001.

[119] S. Nissanke, M. Vallisneri, G. Nelemans, and T. A. Prince, "Gravitational-wave emission from compact Galactic binaries," *Astrophys. J.*, vol. 758, p. 131, 2012.

[120] S. Banagiri, A. Criswell, T. Kuan, V. Mandic, J. D. Romano, and S. R. Taylor, "Mapping the gravitational-wave sky with LISA: a bayesian spherical harmonic approach," *Monthly Notices of the Royal Astronomical Society*, vol. 507, pp. 5451–5462, sep 2021.

[121] K. Huang, *Statistical Mechanics, 2nd Edition*. 1987.

[122] P. A. R. Ade *et al.*, "Planck 2013 results. XXII. Constraints on inflation," *Astron. Astrophys.*, vol. 571, p. A22, 2014.

[123] P. A. R. Ade *et al.*, "Planck 2015 results. XX. Constraints on inflation," *Astron. Astrophys.*, vol. 594, p. A20, 2016.

[124] M. Tristram *et al.*, "Planck constraints on the tensor-to-scalar ratio," *Astron. Astrophys.*, vol. 647, p. A128, 2021.

[125] U. Seljak, "Measuring polarization in cosmic microwave background," *Astrophys. J.*, vol. 482, p. 6, 1997.

[126] U. Seljak and M. Zaldarriaga, "Signature of gravity waves in polarization of the microwave background," *Phys. Rev. Lett.*, vol. 78, pp. 2054–2057, 1997.

[127] P. A. R. Ade *et al.*, "BICEP2 II: Experiment and Three-Year Data Set," *Astrophys. J.*, vol. 792, no. 1, p. 62, 2014.

[128] M. Tristram *et al.*, "Improved limits on the tensor-to-scalar ratio using BICEP and Planck data," *Phys. Rev. D*, vol. 105, no. 8, p. 083524, 2022.

[129] F. B. Estabrook and H. D. Wahlquist, "Response of Doppler spacecraft tracking to gravitational radiation.," *General Relativity and Gravitation*, vol. 6, pp. 439–447, Oct. 1975.

[130] M. V. Sazhin, "Opportunities for detecting ultralong gravitational waves," *Soviet Astronomy*, vol. 22, pp. 36–38, Feb. 1978.

[131] S. Detweiler, "Pulsar timing measurements and the search for gravitational waves," *Astrophys. J*, vol. 234, pp. 1100–1104, Dec. 1979.

[132] M. A. McLaughlin, "The North American Nanohertz Observatory for Gravitational Waves," *Class. Quant. Grav.*, vol. 30, p. 224008, 2013.

[133] Z. Arzoumanian *et al.*, "The NANOGrav 12.5 yr Data Set: Search for an Isotropic Stochastic Gravitational-wave Background," *Astrophys. J. Lett.*, vol. 905, no. 2, p. L34, 2020.

[134] R. Abbott *et al.*, "Search for anisotropic gravitational-wave backgrounds using data from Advanced LIGO and Advanced Virgo's first three observing runs," *Phys. Rev. D*, vol. 104, no. 2, p. 022005, 2021.

[135] G. Agazie *et al.*, "The NANOGrav 15-year Data Set: Search for Anisotropy in the Gravitational-Wave Background," 6 2023.

[136] G. Mentasti, C. R. Contaldi, and M. Peloso, "Intrinsic limits on the detection of the anisotropies of the Stochastic Gravitational Wave Background," 1 2023.

[137] G. Mentasti, C. Contaldi, and M. Peloso, "Prospects for detecting anisotropies and polarization of the stochastic gravitational wave background with ground-based detectors," 4 2023.

[138] M. Tegmark, A. de Oliveira-Costa, and A. Hamilton, "A high resolution foreground cleaned CMB map from WMAP," *Phys. Rev. D*, vol. 68, p. 123523, 2003.

[139] H. K. Eriksen, A. J. Banday, K. M. Gorski, and P. B. Lilje, "Foreground removal by an internal linear combination method: Limitations and implications," *Astrophys. J.*, vol. 612, pp. 633–646, 2004.

[140] E. Thrane and J. D. Romano, "Sensitivity curves for searches for gravitational-wave backgrounds," *Phys. Rev. D*, vol. 88, no. 12, p. 124032, 2013.

[141] L. J. Rubbo, N. J. Cornish, and O. Poujade, "Forward modeling of space borne gravitational wave detectors," *Phys. Rev. D*, vol. 69, p. 082003, 2004.

[142] C. Leinert, S. Bowyer, L. K. Haikala, M. S. Hanner, M. G. Hauser, A. C. Levasseur-Regourd, I. Mann, K. Mattila, W. T. Reach, W. Schlosser, H. J. Staude, G. N. Toller, J. L. Weiland, J. L. Weinberg, and A. N. Witt, "The 1997 reference of diffuse night sky brightness," *Astron. Astrophys. Suppl. Ser*, vol. 127, pp. 1–99, Jan. 1998.

[143] S. Hild, S. Chelkowski, and A. Freise, "Pushing towards the ET sensitivity using 'conventional' technology," 10 2008.

[144] S. Hild *et al.*, "Sensitivity Studies for Third-Generation Gravitational Wave Observatories," *Class. Quant. Grav.*, vol. 28, p. 094013, 2011.

[145] M. Branchesi *et al.*, "Science with the Einstein Telescope: a comparison of different designs," 3 2023.

[146]

[147] M. Evans *et al.*, "A Horizon Study for Cosmic Explorer: Science, Observatories, and Community," 9 2021.

[148] G. Orlando, M. Pieroni, and A. Ricciardone, "Measuring Parity Violation in the Stochastic Gravitational Wave Background with the LISA-Taiji network," *JCAP*, vol. 03, p. 069, 2021.

[149] N. Bartolo *et al.*, "Probing anisotropies of the Stochastic Gravitational Wave Background with LISA," *JCAP*, vol. 11, p. 009, 2022.

[150] F. B. Estabrook, M. Tinto, and J. W. Armstrong, "Time delay analysis of LISA gravitational wave data: Elimination of spacecraft motion effects," *Phys. Rev. D*, vol. 62, p. 042002, 2000.

[151] M. Tinto and S. V. Dhurandhar, "Time-delay interferometry," *Living Rev. Rel.*, vol. 24, no. 1, p. 1, 2021.

[152] R. Flauger, N. Karnesis, G. Nardini, M. Pieroni, A. Ricciardone, and J. Torrado, "Improved reconstruction of a stochastic gravitational wave background with LISA," *JCAP*, vol. 01, p. 059, 2021.

[153] N. Seto, S. Kawamura, and T. Nakamura, "Possibility of direct measurement of the acceleration of the universe using 0.1-Hz band laser interferometer gravitational wave antenna in space," *Phys. Rev. Lett.*, vol. 87, p. 221103, 2001.

[154] S. Kawamura *et al.*, "Current status of space gravitational wave antenna DECIGO and B-DECIGO," *PTEP*, vol. 2021, no. 5, p. 05A105, 2021.

[155] H. Kudoh, A. Taruya, T. Hiramatsu, and Y. Himemoto, "Detecting a gravitational-wave background with next-generation space interferometers," *Phys. Rev. D*, vol. 73, p. 064006, 2006.

[156] K. Yagi and N. Seto, "Detector configuration of DECIGO/BBO and identification of cosmological neutron-star binaries," *Phys. Rev. D*, vol. 83, p. 044011, 2011. [Erratum: Phys.Rev.D 95, 109901 (2017)].

[157] W.-T. Ni, "Gravitational wave detection in space," *Int. J. Mod. Phys. D*, vol. 25, no. 14, p. 1630001, 2016.

[158] J. Crowder and N. J. Cornish, "Beyond LISA: Exploring future gravitational wave missions," *Phys. Rev. D*, vol. 72, p. 083005, 2005.

[159] C. Cutler and J. Harms, "BBO and the neutron-star-binary subtraction problem," *Phys. Rev. D*, vol. 73, p. 042001, 2006.

[160] A. R. Liddle, "The Inflationary energy scale," *Phys. Rev. D*, vol. 49, pp. 739–747, 1994.

[161] J. E. Lidsey, A. R. Liddle, E. W. Kolb, E. J. Copeland, T. Barreiro, and M. Abney, "Reconstructing the inflation potential : An overview," *Rev. Mod. Phys.*, vol. 69, pp. 373–410, 1997.

[162] N. Bartolo *et al.*, "Science with the space-based interferometer LISA. IV: Probing inflation with gravitational waves," *JCAP*, vol. 12, p. 026, 2016.

[163] R.-G. Cai, Z. Cao, Z.-K. Guo, S.-J. Wang, and T. Yang, "The Gravitational-Wave Physics," *Natl. Sci. Rev.*, vol. 4, no. 5, pp. 687–706, 2017.

[164] B. Allen, "The Stochastic gravity wave background: Sources and detection," in *Les Houches School of Physics: Astrophysical Sources of Gravitational Radiation*, pp. 373–417, 4 1996.

[165] C. J. Hogan, "Cosmological gravitational wave backgrounds," *AIP Conf. Proc.*, vol. 456, no. 1, pp. 79–86, 1998.

[166] C. J. Hogan, "Gravitational Wave Sources from New Physics," *AIP Conf. Proc.*, vol. 873, no. 1, pp. 30–40, 2006.

[167] E. W. Kolb and M. S. Turner, *The Early Universe*, vol. 69. 1990.

[168] K. Tomita, "Non-Linear Theory of Gravitational Instability in the Expanding Universe. II," *Progress of Theoretical Physics*, vol. 45, pp. 1747–1762, June 1971.

[169] S. Matarrese, O. Pantano, and D. Saez, "A General relativistic approach to the nonlinear evolution of collisionless matter," *Phys. Rev. D*, vol. 47, pp. 1311–1323, 1993.

[170] S. Matarrese, O. Pantano, and D. Saez, "General relativistic dynamics of irrotational dust: Cosmological implications," *Phys. Rev. Lett.*, vol. 72, pp. 320–323, 1994.

[171] S. Matarrese, S. Mollerach, and M. Bruni, "Second order perturbations of the Einstein-de Sitter universe," *Phys. Rev. D*, vol. 58, p. 043504, 1998.

[172] S. Mollerach, D. Harari, and S. Matarrese, "CMB polarization from secondary vector and tensor modes," *Phys. Rev. D*, vol. 69, p. 063002, 2004.

[173] R. Saito and J. Yokoyama, "Gravitational-Wave Constraints on the Abundance of Primordial Black Holes," *Prog. Theor. Phys.*, vol. 123, pp. 867–886, 2010. [Erratum: Prog.Theor.Phys. 126, 351–352 (2011)].

[174] K. N. Ananda, C. Clarkson, and D. Wands, "The Cosmological gravitational wave background from primordial density perturbations," *Phys. Rev. D*, vol. 75, p. 123518, 2007.

[175] K. Enqvist and M. S. Sloth, "Adiabatic CMB perturbations in pre - big bang string cosmology," *Nucl. Phys. B*, vol. 626, pp. 395–409, 2002.

[176] N. Bartolo, S. Matarrese, A. Riotto, and A. Vaihkonen, "The Maximal Amount of Gravitational Waves in the Curvaton Scenario," *Phys. Rev. D*, vol. 76, p. 061302, 2007.

[177] K. Enqvist, S. Nurmi, and G. I. Rigopoulos, "Parametric Decay of the Curvaton," *JCAP*, vol. 10, p. 013, 2008.

[178] M. Kawasaki, N. Kitajima, and S. Yokoyama, "Gravitational waves from a curvaton model with blue spectrum," *JCAP*, vol. 08, p. 042, 2013.

[179] M. Biagetti, M. Fasiello, and A. Riotto, "Enhancing Inflationary Tensor Modes through Spectator Fields," *Phys. Rev. D*, vol. 88, p. 103518, 2013.

[180] M. Biagetti, E. Dimastrogiovanni, M. Fasiello, and M. Peloso, "Gravitational Waves and Scalar Perturbations from Spectator Fields," *JCAP*, vol. 04, p. 011, 2015.

[181] T. Fujita, J. Yokoyama, and S. Yokoyama, "Can a spectator scalar field enhance inflationary tensor mode?," *PTEP*, vol. 2015, p. 043E01, 2015.

[182] J. L. Cook and L. Sorbo, "Particle production during inflation and gravitational waves detectable by ground-based interferometers," *Phys. Rev. D*, vol. 85, p. 023534, 2012. [Erratum: Phys.Rev.D 86, 069901 (2012)].

[183] E. Witten, "Cosmic Separation of Phases," *Phys. Rev. D*, vol. 30, pp. 272–285, 1984.

[184] C. Caprini *et al.*, "Science with the space-based interferometer eLISA. II: Gravitational waves from cosmological phase transitions," *JCAP*, vol. 04, p. 001, 2016.

[185] A. Kosowsky and M. S. Turner, "Gravitational radiation from colliding vacuum bubbles: envelope approximation to many bubble collisions," *Phys. Rev. D*, vol. 47, pp. 4372–4391, 1993.

[186] M. Kamionkowski, A. Kosowsky, and M. S. Turner, "Gravitational radiation from first order phase transitions," *Phys. Rev. D*, vol. 49, pp. 2837–2851, 1994.

[187] C. Caprini, R. Durrer, T. Konstandin, and G. Servant, "General Properties of the Gravitational Wave Spectrum from Phase Transitions," *Phys. Rev. D*, vol. 79, p. 083519, 2009.

[188] S. J. Huber and T. Konstandin, "Gravitational Wave Production by Collisions: More Bubbles," *JCAP*, vol. 09, p. 022, 2008.

[189] D. J. Weir, "Revisiting the envelope approximation: gravitational waves from bubble collisions," *Phys. Rev. D*, vol. 93, no. 12, p. 124037, 2016.

[190] M. Hindmarsh, S. J. Huber, K. Rummukainen, and D. J. Weir, "Gravitational waves from the sound of a first order phase transition," *Phys. Rev. Lett.*, vol. 112, p. 041301, 2014.

[191] M. Hindmarsh, S. J. Huber, K. Rummukainen, and D. J. Weir, "Numerical simulations of acoustically generated gravitational waves at a first order phase transition," *Phys. Rev. D*, vol. 92, no. 12, p. 123009, 2015.

[192] M. Hindmarsh, "Sound shell model for acoustic gravitational wave production at a first-order phase transition in the early Universe," *Phys. Rev. Lett.*, vol. 120, no. 7, p. 071301, 2018.

[193] C. Caprini, R. Durrer, and G. Servant, "The stochastic gravitational wave background from turbulence and magnetic fields generated by a first-order phase transition," *JCAP*, vol. 12, p. 024, 2009.

[194] P. Binetruy, A. Bohe, C. Caprini, and J.-F. Dufaux, "Cosmological Backgrounds of Gravitational Waves and eLISA/NGO: Phase Transitions, Cosmic Strings and Other Sources," *JCAP*, vol. 06, p. 027, 2012.

[195] A. Samajdar, J. Janquart, C. Van Den Broeck, and T. Dietrich, "Biases in parameter estimation from overlapping gravitational-wave signals in the third-generation detector era," *Phys. Rev. D*, vol. 104, no. 4, p. 044003, 2021.

[196] E. Pizzati, S. Sachdev, A. Gupta, and B. Sathyaprakash, "Toward inference of overlapping gravitational-wave signals," *Phys. Rev. D*, vol. 105, no. 10, p. 104016, 2022.

[197] Y. Himemoto, A. Nishizawa, and A. Taruya, "Impacts of overlapping gravitational-wave signals on the parameter estimation: Toward the search for cosmological backgrounds," *Phys. Rev. D*, vol. 104, no. 4, p. 044010, 2021.

[198] H. E. Bond, "Where is population III ?," 1981.

[199] T. Abel, G. L. Bryan, and M. L. Norman, "The formation of the first star in the Universe," *Science*, vol. 295, p. 93, 2002.

[200] V. Bromm and R. B. Larson, "The First stars," *Ann. Rev. Astron. Astrophys.*, vol. 42, pp. 79–118, 2004.

[201] B. S. Sathyaprakash and B. F. Schutz, "Physics, Astrophysics and Cosmology with Gravitational Waves," *Living Rev. Rel.*, vol. 12, p. 2, 2009.

[202] M. Sasaki, T. Suyama, T. Tanaka, and S. Yokoyama, "Primordial black holes—perspectives in gravitational wave astronomy," *Class. Quant. Grav.*, vol. 35, no. 6, p. 063001, 2018.

[203] M. Raidal, C. Spethmann, V. Vaskonen, and H. Veermäe, "Formation and Evolution of Primordial Black Hole Binaries in the Early Universe," *JCAP*, vol. 02, p. 018, 2019.

[204] S. Bird, I. Cholis, J. B. Muñoz, Y. Ali-Haïmoud, M. Kamionkowski, E. D. Kovetz, A. Raccanelli, and A. G. Riess, "Did LIGO detect dark matter?," *Phys. Rev. Lett.*, vol. 116, no. 20, p. 201301, 2016.

[205] K. Kritos, V. De Luca, G. Franciolini, A. Kehagias, and A. Riotto, "The Astro-Primordial Black Hole Merger Rates: a Reappraisal," *JCAP*, vol. 05, p. 039, 2021.

[206] G. Agazie *et al.*, "The NANOGrav 15-year Data Set: Constraints on Supermassive Black Hole Binaries from the Gravitational Wave Background," 6 2023.

[207] A. Afzal *et al.*, "The NANOGrav 15 yr Data Set: Search for Signals from New Physics," *Astrophys. J. Lett.*, vol. 951, no. 1, p. L11, 2023.

[208] D. G. Figueroa, M. Pieroni, A. Ricciardone, and P. Simakachorn, "Cosmological Background Interpretation of Pulsar Timing Array Data," 7 2023.

[209] R. Abbott *et al.*, "Upper limits on the isotropic gravitational-wave background from Advanced LIGO and Advanced Virgo's third observing run," *Phys. Rev. D*, vol. 104, no. 2, p. 022004, 2021.

[210] G. Galloni, N. Bartolo, S. Matarrese, M. Migliaccio, A. Ricciardone, and N. Vittorio, "Updated constraints on amplitude and tilt of the tensor primordial spectrum," *JCAP*, vol. 04, p. 062, 2023.

[211] M. Cerdonio *et al.*, "The Ultracryogenic gravitational wave detector AURIGA," *Class. Quant. Grav.*, vol. 14, pp. 1491–1494, 1997.

[212] P. Astone *et al.*, "EXPLORER and NAUTILUS gravitational wave detectors: A status report," *Class. Quant. Grav.*, vol. 25, p. 114048, 2008.

[213] S. Weinberg, *Gravitation and Cosmology: Principles and Applications of the General Theory of Relativity.* New York: John Wiley and Sons, 1972.

[214] V. Mukhanov, *Physical Foundations of Cosmology.* Oxford: Cambridge University Press, 2005.

[215] S. Weinberg, *Cosmology.* 2008.

[216] P. J. E. Peebles, *The large-scale structure of the universe.* 1980.

[217] G. F. Smoot *et al.*, "Structure in the COBE differential microwave radiometer first year maps," *Astrophys. J. Lett.*, vol. 396, pp. L1–L5, 1992.

[218] D. N. Spergel *et al.*, "First year Wilkinson Microwave Anisotropy Probe (WMAP) observations: Determination of cosmological parameters," *Astrophys. J. Suppl.*, vol. 148, pp. 175–194, 2003.

[219] E. Komatsu *et al.*, "Seven-Year Wilkinson Microwave Anisotropy Probe (WMAP) Observations: Cosmological Interpretation," *Astrophys. J. Suppl.*, vol. 192, p. 18, 2011.

[220] P. A. R. Ade *et al.*, "Planck 2015 results. XIII. Cosmological parameters," *Astron. Astrophys.*, vol. 594, p. A13, 2016.

[221] "The fractal galaxy distribution," *Physica D: Nonlinear Phenomena*, vol. 38, no. 1, pp. 273–278, 1989.

[222] J. Einasto and M. Gramann, "Transition Scale to a Homogeneous Universe," *Astrophys. J*, vol. 407, p. 443, Apr. 1993.

[223] V. J. Martinez, M.-J. Pons-Borderia, R. A. Moyeed, and M. J. Graham, "Searching for the scale of homogeneity," *Mon. Not. Roy. Astron. Soc.*, vol. 298, p. 1212, 1998.

[224] J. K. Yadav, J. S. Bagla, and N. Khandai, "Fractal dimension as a measure of the scale of homogeneity," *Monthly Notices of the Royal Astronomical Society*, pp. no–no, apr 2010.

[225] F. S. Labini, N. L. Vasilyev, L. Pietronero, and Y. V. Baryshev, "Absence of self-averaging and of homogeneity in the large scale galaxy distribution," *EPL*, vol. 86, no. 4, p. 49001, 2009.

[226] S. Alam *et al.*, "The clustering of galaxies in the completed SDSS-III Baryon Oscillation Spectroscopic Survey: cosmological analysis of the DR12 galaxy sample," *Mon. Not. Roy. Astron. Soc.*, vol. 470, no. 3, pp. 2617–2652, 2017.

[227] Y. Watanabe and E. Komatsu, "Improved Calculation of the Primordial Gravitational Wave Spectrum in the Standard Model," *Phys. Rev. D*, vol. 73, p. 123515, 2006.

[228] A. D. Dolgov, S. H. Hansen, and D. V. Semikoz, "Nonequilibrium corrections to the spectra of massless neutrinos in the early universe," *Nucl. Phys. B*, vol. 503, pp. 426–444, 1997.

[229] A. D. Dolgov, S. H. Hansen, and D. V. Semikoz, "Nonequilibrium corrections to the spectra of massless neutrinos in the early universe: Addendum," *Nucl. Phys. B*, vol. 543, pp. 269–274, 1999.

[230] A. F. Heckler, "Astrophysical applications of quantum corrections to the equation of state of a plasma," *Phys. Rev. D*, vol. 49, pp. 611–617, 1994.

[231] G. Mangano, G. Miele, S. Pastor, and M. Peloso, "A Precision calculation of the effective number of cosmological neutrinos," *Phys. Lett. B*, vol. 534, pp. 8–16, 2002.

[232] G. Mangano and P. D. Serpico *Physics Letters B*, vol. 701, pp. 296–299, jul 2011.

[233] B. D. Fields, K. A. Olive, T.-H. Yeh, and C. Young, "Big-Bang Nucleosynthesis after Planck," *JCAP*, vol. 03, p. 010, 2020. [Erratum: JCAP 11, E02 (2020)].

[234] T.-H. Yeh, J. Shelton, K. A. Olive, and B. D. Fields, "Probing physics beyond the standard model: limits from BBN and the CMB independently and combined," *JCAP*, vol. 10, p. 046, 2022.

[235] J. M. Bardeen, "Gauge Invariant Cosmological Perturbations," *Phys. Rev. D*, vol. 22, pp. 1882–1905, 1980.

[236] H. Kodama and M. Sasaki, "Cosmological Perturbation Theory," *Prog. Theor. Phys. Suppl.*, vol. 78, pp. 1–166, 1984.

[237] V. Acquaviva, N. Bartolo, S. Matarrese, and A. Riotto, "Second order cosmological perturbations from inflation," *Nucl. Phys. B*, vol. 667, pp. 119–148, 2003.

[238] N. Bartolo, S. Matarrese, and A. Riotto, "Cosmic Microwave Background Anisotropies up to Second Order," in *Les Houches Summer School - Session 86: Particle Physics and Cosmology: The Fabric of Spacetime*, 3 2007.

[239] N. Bartolo, S. Matarrese, and A. Riotto, "CMB Anisotropies at Second-Order. 2. Analytical Approach," *JCAP*, vol. 01, p. 019, 2007.

[240] A. Mangilli, N. Bartolo, S. Matarrese, and A. Riotto, "The impact of cosmic neutrinos on the gravitational-wave background," *Phys. Rev. D*, vol. 78, p. 083517, 2008.

[241] F. Bernardeau, S. Colombi, E. Gaztanaga, and R. Scoccimarro, "Large scale structure of the universe and cosmological perturbation theory," *Phys. Rept.*, vol. 367, pp. 1–248, 2002.

[242] L. D. Landau and E. M. Lifshitz, *Statistical Physics, Part 1*, vol. 5 of *Course of Theoretical Physics*. Oxford: Butterworth-Heinemann, 1980.

[243] K. Huang, *Statistical Mechanics*. John Wiley & Sons, 2 ed., 1987.

[244] J. Lesgourgues and S. Pastor, "Massive neutrinos and cosmology," *Phys. Rept.*, vol. 429, pp. 307–379, 2006.

[245] C. Dvorkin, H. V. Peiris, and W. Hu, "Testable polarization predictions for models of CMB isotropy anomalies," *Phys. Rev. D*, vol. 77, p. 063008, 2008.

[246] C. T. Byrnes and E. R. M. Tarrant, "Scale-dependent non-Gaussianity and the CMB Power Asymmetry," *JCAP*, vol. 07, p. 007, 2015.

[247] G. Galloni, N. Bartolo, S. Matarrese, M. Migliaccio, A. Ricciardone, and N. Vittorio, "Test of the statistical isotropy of the universe using gravitational waves," *JCAP*, vol. 09, p. 046, 2022.

[248] M. Bucher, K. Moodley, and N. Turok, "The General primordial cosmic perturbation," *Phys. Rev. D*, vol. 62, p. 083508, 2000.

[249] K. A. Malik and D. Wands, "Adiabatic and entropy perturbations with interacting fluids and fields," *JCAP*, vol. 02, p. 007, 2005.

[250] N. Aghanim *et al.*, "Planck 2018 results. V. CMB power spectra and likelihoods," *Astron. Astrophys.*, vol. 641, p. A5, 2020.

[251] P. A. R. Ade *et al.*, "Improved Constraints on Primordial Gravitational Waves using Planck, WMAP, and BICEP/Keck Observations through the 2018 Observing Season," *Phys. Rev. Lett.*, vol. 127, no. 15, p. 151301, 2021.

[252] S. Weinberg, "Damping of tensor modes in cosmology," *Phys. Rev. D*, vol. 69, p. 023503, 2004.

[253] D. A. Dicus and W. W. Repko, "Comment on damping of tensor modes in cosmology," *Phys. Rev. D*, vol. 72, p. 088302, 2005.

[254] B. A. Stefanek and W. W. Repko, "Analytic description of the damping of gravitational waves by free streaming neutrinos," *Phys. Rev. D*, vol. 88, no. 8, p. 083536, 2013.

[255] A. Garoffolo, "Wave-optics limit of the stochastic gravitational wave background," 10 2022.

[256] G. Domènech, S. Pi, and M. Sasaki, "Induced gravitational waves as a probe of thermal history of the universe," *JCAP*, vol. 08, p. 017, 2020.

[257] Y. B. Zel'dovich and I. D. Novikov, "The Hypothesis of Cores Retarded during Expansion and the Hot Cosmological Model," *Soviet Astron. AJ (Engl. Transl.)*,, vol. 10, p. 602, 1967.

[258] J. Kristiano and J. Yokoyama, "Ruling Out Primordial Black Hole Formation From Single-Field Inflation," 11 2022.

[259] A. Riotto, "The Primordial Black Hole Formation from Single-Field Inflation is Still Not Ruled Out," 3 2023.

[260] H. Firouzjahi and A. Riotto, "Primordial Black Holes and Loops in Single-Field Inflation," 4 2023.

[261] J. Garcia-Bellido, M. Peloso, and C. Unal, "Gravitational waves at interferometer scales and primordial black holes in axion inflation," *JCAP*, vol. 12, p. 031, 2016.

[262] V. Domcke, F. Muia, M. Pieroni, and L. T. Witkowski, "PBH dark matter from axion inflation," *JCAP*, vol. 07, p. 048, 2017.

[263] J. Fumagalli, S. Renaux-Petel, J. W. Ronayne, and L. T. Witkowski, "Turning in the landscape: A new mechanism for generating primordial black holes," *Phys. Lett. B*, vol. 841, p. 137921, 2023.

[264] B. J. Carr, "The Primordial black hole mass spectrum," *Astrophys. J.*, vol. 201, pp. 1–19, 1975.

[265] J. Yokoyama, "Formation of MACHO primordial black holes in inflationary cosmology," *Astron. Astrophys.*, vol. 318, p. 673, 1997.

[266] K. Kohri and T. Terada, "Semianalytic calculation of gravitational wave spectrum nonlinearly induced from primordial curvature perturbations," *Phys. Rev. D*, vol. 97, no. 12, p. 123532, 2018.

[267] J. R. Espinosa, D. Racco, and A. Riotto, "A Cosmological Signature of the SM Higgs Instability: Gravitational Waves," *JCAP*, vol. 09, p. 012, 2018.

[268] A. Romero, K. Martinovic, T. A. Callister, H.-K. Guo, M. Martínez, M. Sakellariadou, F.-W. Yang, and Y. Zhao, "Implications for First-Order Cosmological Phase Transitions from the Third LIGO-Virgo Observing Run," *Phys. Rev. Lett.*, vol. 126, no. 15, p. 151301, 2021.

[269] S. Weinberg, "Can non-adiabatic perturbations arise after single-field inflation?," *Phys. Rev. D*, vol. 70, p. 043541, 2004.

[270] C.-P. Ma and E. Bertschinger, "Cosmological perturbation theory in the synchronous and conformal Newtonian gauges," *Astrophys. J.*, vol. 455, pp. 7–25, 1995.

[271] S. Bashinsky and U. Seljak, "Neutrino perturbations in CMB anisotropy and matter clustering," *Phys. Rev. D*, vol. 69, p. 083002, 2004.

[272] K. M. Nollett and G. Steigman, "BBN And The CMB Constrain Neutrino Coupled Light WIMPs," *Phys. Rev. D*, vol. 91, no. 8, p. 083505, 2015.

[273] Y. Akrami *et al.*, "Planck 2018 results. IV. Diffuse component separation," *Astron. Astrophys.*, vol. 641, p. A4, 2020.

[274] D. Alonso, C. R. Contaldi, G. Cusin, P. G. Ferreira, and A. I. Renzini, "Noise angular power spectrum of gravitational wave background experiments," *Phys. Rev. D*, vol. 101, no. 12, p. 124048, 2020.

[275] M. Gerbino, M. Lattanzi, M. Migliaccio, L. Pagano, L. Salvati, L. Colombo, A. Gruppuso, P. Natoli, and G. Polenta, "Likelihood methods for CMB experiments," *Front. in Phys.*, vol. 8, p. 15, 2020.

[276] F. Schmidt and D. Jeong, "Cosmic Rulers," *Phys. Rev. D*, vol. 86, p. 083527, 2012.

[277] B. Audren, J. Lesgourgues, K. Benabed, and S. Prunet, "Conservative Constraints on Early Cosmology: an illustration of the Monte Python cosmological parameter inference code," *JCAP*, vol. 02, p. 001, 2013.

[278] T. Brinckmann and J. Lesgourgues, "MontePython 3: boosted MCMC sampler and other features," *Phys. Dark Univ.*, vol. 24, p. 100260, 2019.

[279] R. Allison, P. Caucal, E. Calabrese, J. Dunkley, and T. Louis, "Towards a cosmological neutrino mass detection," *Phys. Rev. D*, vol. 92, no. 12, p. 123535, 2015.

[280] T. Brinckmann, D. C. Hooper, M. Archidiacono, J. Lesgourgues, and T. Sprenger, "The promising future of a robust cosmological neutrino mass measurement," *JCAP*, vol. 01, p. 059, 2019.

[281] G. Perna, A. Ricciardone, D. Bertacca, and S. Matarrese, "Non-Gaussianity from the Cross-correlation of the Astrophysical Gravitational Wave Background and the Cosmic Microwave Background," 2 2023.

[282] S. Sachdev, T. Regimbau, and B. S. Sathyaprakash, "Subtracting compact binary foreground sources to reveal primordial gravitational-wave backgrounds," *Phys. Rev. D*, vol. 102, no. 2, p. 024051, 2020.

[283] B. Zhou, L. Reali, E. Berti, M. Çalışkan, C. Creque-Sarbinowski, M. Kamionkowski, and B. S. Sathyaprakash, "Compact Binary Foreground Subtraction in Next-Generation Ground-Based Observatories," 9 2022.

[284] B. Zhou, L. Reali, E. Berti, M. Çalışkan, C. Creque-Sarbinowski, M. Kamionkowski, and B. S. Sathyaprakash, "Subtracting Compact Binary Foregrounds to Search for Subdominant Gravitational-Wave Backgrounds in Next-Generation Ground-Based Observatories," 9 2022.

[285] N. Muttoni, D. Laghi, N. Tamanini, S. Marsat, and D. Izquierdo-Villalba, "Dark siren cosmology with binary black holes in the era of third-generation gravitational wave detectors," 3 2023.

[286] M. Pieroni, A. Ricciardone, and E. Barausse, "Detectability and parameter estimation of stellar origin black hole binaries with next generation gravitational wave detectors," *Sci. Rep.*, vol. 12, no. 1, p. 17940, 2022.

[287] J.-P. Zhu *et al.*, "Kilonova Emission from Black Hole–Neutron Star Mergers. II. Luminosity Function and Implications for Target-of-opportunity Observations of Gravitational-wave Triggers and Blind Searches," *Astrophys. J.*, vol. 917, no. 1, p. 24, 2021.

[288] F. Iacovelli, M. Mancarella, S. Foffa, and M. Maggiore, "Forecasting the Detection Capabilities of Third-generation Gravitational-wave Detectors Using GWFAST," *Astrophys. J.*, vol. 941, no. 2, p. 208, 2022.

[289] P. Behroozi, R. H. Wechsler, A. P. Hearin, and C. Conroy, "UniverseMachine: The correlation between galaxy growth and dark matter halo assembly from z = 0-10," *Monthly Notices of the Royal Astronomical Society*, vol. 488, pp. 3143–3194, may 2019.

[290] J. L. Tinker, A. V. Kravtsov, A. Klypin, K. Abazajian, M. S. Warren, G. Yepes, S. Gottlober, and D. E. Holz, "Toward a halo mass function for precision cosmology: The Limits of universality," *Astrophys. J.*, vol. 688, pp. 709–728, 2008.

[291] P. Madau and M. Dickinson, "Cosmic Star Formation History," *Ann. Rev. Astron. Astrophys.*, vol. 52, pp. 415–486, 2014.

[292] P. Madau and T. Fragos, "Radiation Backgrounds at Cosmic Dawn: X-Rays from Compact Binaries," *Astrophys. J.*, vol. 840, no. 1, p. 39, 2017.

[293] I. Dvorkin, E. Vangioni, J. Silk, J.-P. Uzan, and K. A. Olive, "Metallicity-constrained merger rates of binary black holes and the stochastic gravitational wave background," *Mon. Not. Roy. Astron. Soc.*, vol. 461, no. 4, pp. 3877–3885, 2016.

[294] E. Vangioni, S. Goriely, F. Daigne, P. François, and K. Belczynski, "Cosmic Neutron Star Merger Rate and Gravitational Waves constrained by the R Process Nucleosynthesis," *Mon. Not. Roy. Astron. Soc.*, vol. 455, no. 1, pp. 17–34, 2016.

[295] M. Mapelli, N. Giacobbo, E. Ripamonti, and M. Spera, "The cosmic merger rate of stellar black hole binaries from the Illustris simulation," *Mon. Not. Roy. Astron. Soc.*, vol. 472, no. 2, pp. 2422–2435, 2017.

[296] M. Mapelli, N. Giacobbo, F. Santoliquido, and M. C. Artale, "The properties of merging black holes and neutron stars across cosmic time," *Mon. Not. Roy. Astron. Soc.*, vol. 487, no. 1, pp. 2–13, 2019.

[297] C. J. Neijssel, A. Vigna-Gó mez, S. Stevenson, J. W. Barrett, S. M. Gaebel, F. S. Broekgaarden, S. E. de Mink, D. Szécsi, S. Vinciguerra, and I. Mandel, "The effect of the metallicity-specific star formation history on double compact object mergers," *Monthly Notices of the Royal Astronomical Society*, vol. 490, pp. 3740–3759, oct 2019.

[298] M. Dominik, K. Belczynski, C. Fryer, D. Holz, E. Berti, T. Bulik, I. Mandel, and R. O'Shaughnessy, "Double Compact Objects I: The Significance of the Common Envelope on Merger Rates," *Astrophys. J.*, vol. 759, p. 52, 2012.

[299] J. L. Tinker, B. E. Robertson, A. V. Kravtsov, A. Klypin, M. S. Warren, G. Yepes, and S. Gottlöber, "THE LARGE-SCALE BIAS OF DARK MATTER HALOS: NUMERICAL CALIBRATION AND MODEL TESTS," *The Astrophysical Journal*, vol. 724, pp. 878–886, nov 2010.

[300] G. Scelfo, N. Bellomo, A. Raccanelli, S. Matarrese, and L. Verde, "GW×LSS: chasing the progenitors of merging binary black holes," *JCAP*, vol. 09, p. 039, 2018.

[301] G. Scelfo, L. Boco, A. Lapi, and M. Viel, "Exploring galaxies-gravitational waves cross-correlations as an astrophysical probe," *JCAP*, vol. 10, p. 045, 2020.

[302] P. Ajith *et al.*, "A Template bank for gravitational waveforms from coalescing binary black holes. I. Non-spinning binaries," *Phys. Rev. D*, vol. 77, p. 104017, 2008. [Erratum: Phys.Rev.D 79, 129901 (2009)].

[303] P. Ajith *et al.*, "Inspiral-merger-ringdown waveforms for black-hole binaries with non-precessing spins," *Phys. Rev. Lett.*, vol. 106, p. 241101, 2011.

[304] P. Ajith, N. Fotopoulos, S. Privitera, A. Neunzert, and A. J. Weinstein, "Effectual template bank for the detection of gravitational waves from inspiralling compact binaries with generic spins," *Phys. Rev. D*, vol. 89, no. 8, p. 084041, 2014.

[305] S. Husa, S. Khan, M. Hannam, M. Pürrer, F. Ohme, X. Jiménez Forteza, and A. Bohé, "Frequency-domain gravitational waves from nonprecessing black-hole binaries. I. New numerical waveforms and anatomy of the signal," *Phys. Rev. D*, vol. 93, no. 4, p. 044006, 2016.

[306] S. Khan, S. Husa, M. Hannam, F. Ohme, M. Pürrer, X. Jiménez Forteza, and A. Bohé, "Frequency-domain gravitational waves from nonprecessing black-hole binaries. II. A phenomenological model for the advanced detector era," *Phys. Rev. D*, vol. 93, no. 4, p. 044007, 2016.

[307] B. Allen and A. C. Ottewill, "Detection of anisotropies in the gravitational wave stochastic background," *Phys. Rev. D*, vol. 56, pp. 545–563, 1997.

[308] A. C. Jenkins and M. Sakellariadou, "Anisotropies in the stochastic gravitational-wave background: Formalism and the cosmic string case," *Phys. Rev. D*, vol. 98, no. 6, p. 063509, 2018.

[309] G. Cusin, C. Pitrou, and J.-P. Uzan, "The signal of the gravitational wave background and the angular correlation of its energy density," *Phys. Rev. D*, vol. 97, no. 12, p. 123527, 2018.

[310] D. Jeong, F. Schmidt, and C. M. Hirata, "Large-scale clustering of galaxies in general relativity," *Physical Review D*, vol. 85, jan 2012.

[311] E. Di Dio, F. Montanari, J. Lesgourgues, and R. Durrer, "The CLASSgal code for Relativistic Cosmological Large Scale Structure," *JCAP*, vol. 11, p. 044, 2013.

[312] M. Zaldarriaga and U. Seljak, "An all sky analysis of polarization in the microwave background," *Phys. Rev. D*, vol. 55, pp. 1830–1840, 1997.

[313] A. Lewis and A. Challinor, "Weak gravitational lensing of the CMB," *Phys. Rept.*, vol. 429, pp. 1–65, 2006.

[314] S. Alexander and N. Yunes, "Chern-Simons Modified General Relativity," *Phys. Rept.*, vol. 480, pp. 1–55, 2009.

[315] W. Zhao, T. Zhu, J. Qiao, and A. Wang, "Waveform of gravitational waves in the general parity-violating gravities," *Phys. Rev. D*, vol. 101, no. 2, p. 024002, 2020.

[316] M. Okounkova, W. M. Farr, M. Isi, and L. C. Stein, "Constraining gravitational wave amplitude birefringence and Chern-Simons gravity with GWTC-2," *Phys. Rev. D*, vol. 106, no. 4, p. 044067, 2022.

[317] T. Islam, S. E. Field, C.-J. Haster, and R. Smith, "High precision source characterization of intermediate mass-ratio black hole coalescences with gravitational waves: The importance of higher order multipoles," *Phys. Rev. D*, vol. 104, no. 8, p. 084068, 2021.

[318] S. Vitale, S. Biscoveanu, and C. Talbot, "The orientations of the binary black holes in GWTC-3," 4 2022.

[319] A. de Oliveira-Costa, M. Tegmark, M. Zaldarriaga, and A. Hamilton, "The Significance of the largest scale CMB fluctuations in WMAP," *Phys. Rev. D*, vol. 69, p. 063516, 2004.

[320] C. J. Copi, D. Huterer, and G. D. Starkman, "Multipole vectors - A New representation of the CMB sky and evidence for statistical anisotropy or non-Gaussianity at $2 <= l <= 8$," *Phys. Rev. D*, vol. 70, p. 043515, 2004.

[321] C. Monteserin, R. B. B. Barreiro, P. Vielva, E. Martinez-Gonzalez, M. P. Hobson, and A. N. Lasenby, "A low CMB variance in the WMAP data," *Mon. Not. Roy. Astron. Soc.*, vol. 387, pp. 209–219, 2008.

[322] K. Land and J. Magueijo, "Is the Universe odd?," *Phys. Rev. D*, vol. 72, p. 101302, 2005.

[323] J. Kim and P. Naselsky *The Astrophysical Journal*, vol. 714, pp. L265–L267, apr 2010.

[324] A. Gruppuso, F. Finelli, P. Natoli, F. Paci, P. Cabella, A. D. Rosa, and N. Mandolesi, "New constraints on parity symmetry from a re-analysis of the WMAP-7 low-resolution power spectra," *Monthly Notices of the Royal Astronomical Society*, vol. 411, pp. 1445–1452, nov 2010.

[325] M. Cruz, E. Martinez-Gonzalez, P. Vielva, and L. Cayon, "Detection of a non-gaussian spot in wmap," *Mon. Not. Roy. Astron. Soc.*, vol. 356, pp. 29–40, 2005.

[326] P. Vielva, E. Martinez-Gonzalez, R. B. Barreiro, J. L. Sanz, and L. Cayon, "Detection of non-Gaussianity in the WMAP 1 - year data using spherical wavelets," *Astrophys. J.*, vol. 609, pp. 22–34, 2004.

[327] M. Tegmark, D. J. Eisenstein, W. Hu, and A. de Oliveira-Costa, "Foregrounds and forecasts for the cosmic microwave background," *Astrophys. J.*, vol. 530, pp. 133–165, 2000.

[328] B. P. Abbott *et al.*, "Prospects for observing and localizing gravitational-wave transients with Advanced LIGO, Advanced Virgo and KAGRA," *Living Rev. Rel.*, vol. 21, no. 1, p. 3, 2018.

[329] M. Bruni, S. Matarrese, S. Mollerach, and S. Sonego, "Perturbations of space-time: Gauge transformations and gauge invariance at second order and beyond," *Class. Quant. Grav.*, vol. 14, pp. 2585–2606, 1997.

[330] J. D. Jackson, *Classical Electrodynamics*. Wiley, 1998.

[331] T. W. Noonan, "The gravitational contribution to the stress-energy tensor of a medium in general relativity," *General relativity and gravitation*, vol. 16, pp. 1103–1118, 1984.

[332] R. M. Zalaletdinov, "Averaging out the Einstein equations and macroscopic space-time geometry," *Gen. Rel. Grav.*, vol. 24, pp. 1015–1031, 1992.

[333] N. V. Zotov and W. R. Stoeger, "Averaging einstein's equations," *Class. Quant. Grav.*, vol. 9, p. 1023, apr 1992.

[334] R. M. Zalaletdinov, "Averaging problem in general relativity, macroscopic gravity and using Einstein's equations in cosmology," *Bull. Astron. Soc. India*, vol. 25, pp. 401–416, 1997.

[335] W. R. Stoeger, S. J., A. Helmi, and D. F. Torres, "Averaging Einstein's equations: The Linearized case," *Int. J. Mod. Phys. D*, vol. 16, pp. 1001–1026, 2007.

[336] B. S. DeWitt and R. W. Brehme, "Radiation damping in a gravitational field," *Annals Phys.*, vol. 9, pp. 220–259, 1960.

[337] C. Pitrou, X. Roy, and O. Umeh, "xPand: An algorithm for perturbing homogeneous cosmologies," *Class. Quant. Grav.*, vol. 30, p. 165002, 2013.

[338] I. S. Gradshteyn, I. M. Ryzhik, D. Zwillinger, and V. Moll, *Table of integrals, series, and products; 8th ed.* Amsterdam: Academic Press, 2015.

[339] J. K. Bloomfield, S. H. P. Face, A. H. Guth, S. Kalia, and Z. Moss, "Statistics of Peaks in Chi-Squared Fields," 10 2018.

[340] L. Knox and M. S. Turner, "Detectability of tensor perturbations through CBR anisotropy," *Phys. Rev. Lett.*, vol. 73, pp. 3347–3350, 1994.

[341] R. Maartens, J. Fonseca, S. Camera, S. Jolicoeur, J.-A. Viljoen, and C. Clarkson, "Magnification and evolution biases in large-scale structure surveys," *JCAP*, vol. 12, no. 12, p. 009, 2021.